Acoustofluidic preparation of whole blood components

Urbansky, Anke

2019

Document Version:
Version created as part of publication process; publisher's layout; not normally made publicly available

Acoustofluidic preparation of whole blood components

Anke Urbansky

LUND
UNIVERSITY

DOCTORAL DISSERTATION
by due permission of the Faculty of Engineering, Lund University, Sweden.
To be defended in Segerfalksalen A10 BMC, Sölvegatan 17, Lund.
April 12th 2019 at 09:15

Faculty opponent
Professor Mehmet Toner

Organization LUND UNIVERSITY Department of Biomedical Engineering P.O. Box 118, SE-221 00 Lund, Sweden	**Document name** DOCTORAL DISSERTATION **Date of issue** March 13, 2019
Author: Anke Urbansky	**Sponsoring organizations** People Programme (Marie Curie Actions) of the European Union's Seventh Frame-work Programme FP7/2007–2013 under REA grant agreement No. 607350

Title: Acoustofluidic preparation of whole blood components

Abstract

Whole blood is rich in information about the physical state of an individual and is routinely used in a variety of clinical and research applications. In this thesis, the use of a microfluidic technique called acoustophoresis for separation of different blood components is explored. Acoustophoresis uses an ultrasonic standing wave field to manipulate cells in a microfluidic device. Cells within the standing wave field will experience forces which move the cells either to the place of minimum pressure, the node, or to the place of maximum pressure, the anti-node. The strength of the acoustic force is dependent on the cells' properties such as size, density, and compressibility in relation to its surrounding medium. In the first two papers a method is described to use affinity-bead-mediated acoustophoresis to separate cells which otherwise cannot be acoustically discriminated. Cells of interest were labeled with spherical particles creating large and dense bead-cell complexes which moved faster in the acoustic field compared to unbound cells. The performance was comparable to standard magnetic separation and no effect of the acoustic separation method on viability, cell proliferation or clonogenic stem cell capacity was observed. The third paper investigates the possibility to separate blood cells with similar acoustic mobilities. By changing the properties of the surrounding medium mononuclear cells reduced their mobility in relation to red blood cells and could be successfully separated. The outcomes in terms of efficiency and purity were comparable to conventional separation methods. Next, the possibility to enrich tumor cells from patients undergoing stem cell transplantation was explored. Tumor cells spiked into apheresis products were acoustically separated based on their size differences without interfering with the cells' viability, T cell activation, and tumor cell proliferation capacity. For the separation outcome a stable temperature is crucial. In the fifth paper a new chip holder was designed to employ an air-cooling unit in order to remove excessive heat and allow better heat distribution during the separation process. The system allowed high-throughput multiplex separation of particles at flow rates up to 500 µL/min and concurrent separation of the different white blood cell subgroups, i.e. lymphocytes, monocytes, and granulocytes, was achieved for flow rates up to 300 µL/min. Last, to predict the possibility to separate cells in an acoustic standing wave field it is crucial to know the cells properties. Therefore, a method to statistically estimate the cells biomechanical properties based on acoustophoretic separation data was developed. The work presented here shows the diversity, capability and usability of acoustophoresis for whole blood fractionation.

Key words: acoustophoresis, ultrasound, microfluidics, cell separation, blood, blood fractionation

Classification system and/or index terms (if any)

Supplementary bibliographic information ISRN: LUTEDX/TEEM - 1117 - SE Report Nr: 2/19		**Language:** English
ISSN and key title		ISBN: 978-91-7895-054-6 (print) ISBN: 978-91-7895-055-3 (pdf)
Recipient's notes	**Number of pages:** 188	**Price**
	Security classification	

To my family and friends

Das ist die perfekte Welle
Das ist der perfekte Tag
Lass dich einfach von ihr tragen
Denk am besten gar nicht nach
-Juli

Public defence
April 12th 2019, 09:15 in Segerfalksalen A10 BMC, Sölvegatan 17, 223 62 Lund, Sweden

Advisors
Prof. Thomas Laurell and Dr. Andreas Lenshof
Department of Biomedical Engineering, Lund University, Sweden
MD Stefan Scheding
Division of Molecular Hematology, Lund University, Sweden

Faculty opponent
Professor Mehmet Toner
Helen Andrus Benedict Professor of Biomedical Engineering, Harvard Medical School, Boston, MA, USA

Examination board
Professor Jenny Emneus
Department of Micro- and Nanotechnology, DTU, Lyngby, Denmark
Associate senior lecturer Edith Hammer
Department of Biology, Lund University, Sweden
Professor Aman Russom
Department of Protein Science, KTH Royal Institute of Technology, Stockholm, Sweden
Deputy member: Docent Patrik Önnerfjord
Department of Clinical Sciences, Lund University, Sweden

Chairman
Associate Professor Johan Nilsson
Department of Biomedical Engineering, Lund University, Sweden

Cover illustration
Illustration of acoustofluidic blood cell fractionation. Illustration by Anke Urbansky.

ISBN: 978-91-7895-054-6 (print)
ISBN: 978-91-7895-055-3 (pdf)
Report-nr: 2/19
ISRN: LUTEDX/TEEM - 1117 - SE
Printed in March 2019 by Tryckeriet i E-huset, Lund, Sweden

List of papers

I. Efficient Purification of CD4+ Lymphocytes from Peripheral Blood Progenitor Cell Products Using Affinity Bead Acoustophoresis
A. Lenshof†, A. Jamal†, J. Dykes, **A. Urbansky**, I. Åstrand-Grundström , T. Laurell, and S. Scheding
Cytometry Part A, 2014, 85(11), 933–941.

The author planned, performed and analysed the T cell proliferation assay experiment and helped editing the manuscript.

II. Affinity-Bead-Mediated Enrichment of CD8+ Lymphocytes from Peripheral Blood Progenitor Cell Products Using Acoustophoresis
A. Urbansky, A. Lenshof, J. Dykes, T. Laurell, and S. Scheding
Micromachines, 2016, 7(6), 101.

The author partly conceived the idea, planned and performed the experiments, analysed the data and did the major part of writing.

III. Rapid and effective enrichment of mononuclear cells from blood using acoustophoresis
A. Urbansky, P. Ohlsson, A. Lenshof, F. Garofalo, T. Laurell, and S. Scheding
Scientific Reports, 2017, 7, 17161.

The author partly conceived the idea, planned and performed the experiments, analysed

the data and did the major part of writing.

IV. Label-free neuroblastoma cell separation from hematopoietic progenitor cell products using acoustophoresis - towards cell processing of complex biological samples

F. Olm, **A. Urbansky**, J. Dykes, T. Laurell, and S. Scheding
Submitted

The author planned and performed inital experiments, was part of planning the experiments and edited the manuscript.

V. Separation of leukocyte subpopulations using high throughput multiplex acoustophoresis

A. Urbansky, F. Olm, S. Scheding, T. Laurell, and A. Lenshof
Lab on a Chip, 2019, DOI: 10.1039/C9LC00181F

The author planned and performed major parts of the experiments, analysed the data and did a major part of writing.

VI. Statistic Estimation of Biomechanical Cell Compressibility Based on Acoustophoretic Separation Data

F. Garofalo, A. Lenshof, **A. Urbansky**, F. Olm, A.C. Bonestroo, L. Ekblad, and T. Laurell
Manuscript

The author planned and performend major parts of the experiments, did part of analysing the data and wrote parts of the manuscript.

† Authors 1 and 2 share first authorship

Contents

Abbreviations

ACF	Acoustic contrast factor
ATPS	Aqueous two-phase system
BAW	Bulk acoustic wave
CD	Cluster of differentiation
CAR T cell	Chimeric antigen receptor T cell
CTC	Circulating tumor cell
DEP	Dielectrophoresis
DLD	Deterministic lateral displacement
FACS	Fluorescence activated cell sorting
HCT	Hematocrit
HSC	Hematopoietic stem cell
IDT	Interdigitated transducer
MACS	Magnetic activated cell sorting
MNC	Mononuclear cell
NBC	Neuroblastoma cell
nDEP	Negative dielectrophoresis
NK	Natural killer cell

ODEP	Optical induced dielectrophoresis
PBMC	Peripheral blood mononuclear cell
PBPC	Peripheral blood and progenitor cell
PZT	Piezoceramic transducer
RBC	Red blood cell
Re	Reynolds number
SAW	Surface acoustic wave
SIP	Stock isotonic Percoll
SSAW	Standing surface acoustic wave
TSAW	Traveling surface acoustic wave
WBC	White blood cell

1

Introduction

Whole blood holds various important information about the physical state and wellbeing of an individual. Cellular components within the blood play an important part of the immune system, are responsible for the oxygen transport, and are involved in the bloods self-repair function to prevent blood loss. Plasma, the liquid medium of blood, carries nutrients to the body cells and removes waste products.

Whole blood is routinely fractionated into its components for various clinical and research related applications, such as in diagnostics, blood transfusion, stem cell transplantation, and immunotherapy. Many separation methods are available both at the macroscale and microscale, all having their advantages and disadvantages. Microfluidic cell separation is a fast developing area within life science. It takes advantages of the controlled fluid behaviour in small volumes where liquids are flowing in parallel without mixing, i.e. laminar flow. The laminar flow domain in microfluidics allows to predict flow patterns and cells within liquids can be precisely controlled by external forces such as electric, magnetic, or acoustic forces.

This thesis investigates the use of acoustophoresis, a microfluidic technology using acoustic forces in an ultrasonic standing wave field, for fractionating whole blood. The aim was to explore ways of using acoustophoresis to separate different blood components and to deepen the understanding of practical aspects in acoustophoresis. The thesis describes the basic composition of human whole blood and brings it into context in clinical and research applications. The following chapter covers conventional separation methods at the macroscale routinely used for blood cell fractionation. Next, basic physical understanding about microfluidic and different microfluidic separation methods are described before going into detail about acoustophoresis and how it can be used in blood cell fractionation.

2

Blood

An average human adult has around 6-8 L of blood in the circulation, accounting for ~7% of the body weight. Within approximately one minute, blood recirculates through the entire body transporting oxygen, hormones and nutrients to the cells and removing waste products such as carbon dioxide and metabolites from the cells. Blood plays a major part in the immune response to protect the body from pathogens and has a self-repair function by forming blood clots to prevent blood loss at injuries. Blood contains a wealth of information about the physiological state of an individual, making it a central component in various clinical and research applications. This chapter gives an overview about blood in general, such as its' composition and origin, and introduces some common applications for blood cell fractionation.

2.1 Blood composition

Blood is composed to ~55% of plasma, the liquid medium of the blood, and to ~45% of blood cells (Figure 2.1). Plasma consists mainly of water (~90%) but also carries dissolved components (~10%) such as carbohydrates, proteins, lipids, electrolytes, vitamins, and minerals. Blood cells are divided into red blood cells, white blood cells, and platelets. Table 2.1 gives an overview about the different blood cells, their abundancy within blood and their characteristics such as cell size and density.

Red blood cells

The most abundant cell type in blood are the red blood cells (RBC), also called erythrocytes. The volume fraction of RBC in blood is termed hematocrit (HCT) and is in the range of 40-52% for men and 36-48% for woman.[5] Their main function is to transport oxygen from the lungs to the cells and to return carbon dioxide to the lungs. RBC have a very distinguishable biconcave shape

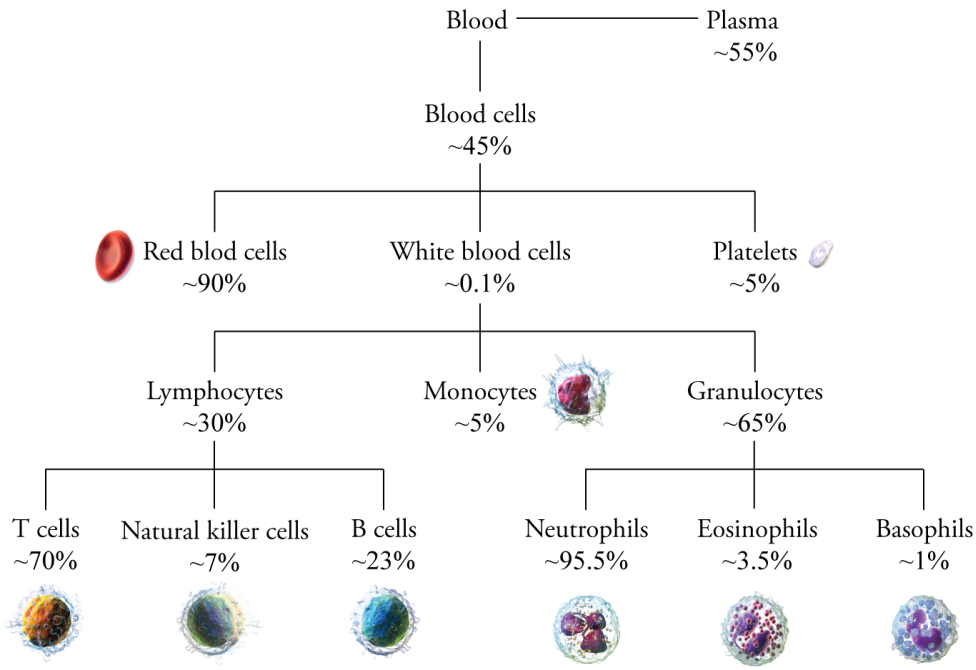

Figure 2.1: Human blood composition. An overview of the composition of human blood and the further subdivision of human blood cells with typical percentages within the subgroups.[1–3] Pictures are taken and adapted with permission from Blausen.com.[4]

giving them a large surface area to volume ratio for gas exchange. They do not have a nucleus and they are highly deformable to be able to squeeze through small capillaries within the vascular system.[1]

White blood cells

White blood cells (WBC), also called leukocytes, are part of the immune system and play an important role in the protection of the body against microorganism and foreign matter. Compared to RBC the WBC amount in blood is much lower, accounting for only ~0.1% of all blood cells (Figure 2.1, Table 2.1). They are further classified into lymphocytes, monocytes, and granulocytes, all with different functions within the immune response.

Lymphocytes

Lymphocytes have the ability to recognize specific molecules (antigens) on pathogens invading the body. Upon lymphocyte activation they generate a specific immune response to eliminate pathogens or pathogen-infected cells. *B cells*, which are lymphocytes maturing in the bone mar-

Table 2.1: Human blood cell properties.[3]

Cell type	Concentration [cells/mL]	Diameter [µm]	Volume [µm^3]	Density [g/cm^3]	Compressibility [T/Pa]
RBC	4.2-5.4x10^9	6-9	80-100	1.089-1.100	334 **
WBC	0.4-1.1x10^7	5.5-12 *	160-450	1.055-1.085	393 **
Lymphocytes	1-4.8x10^6	5.5-10 *	161-207	1.055-1.070	
Monocytes	1-8x10^5	7.5-12 *	382-449	1.055-1.070	
Granulocytes	2.1-6.6x10^6	8.5-11 *	239-382	1.075-1.085	
Platelets	2.1-5x10^8	2-4	5-10	1.04-1.06	

* **values are taken from Paper V**

** **values are taken from Cushing et al.**[6]

row, secrete antibodies targeting bacteria and viruses. Antibody binding to pathogens will initiate their destruction. *T cells* on the other hand mature in the thymus and produce either cytokines that direct the immune response (T helper cells) or produce toxic substances (cytotoxic T cells) which induces death of pathogen-infected cells. A small subgroup of lymphocytes, the *natural killer cells* (NK cells), recognizes altered features of surface molecules of tumor or virally infected cells and can induce cell death of these abnormal cells. NK cells present an early defense against abnormal cells.

Monocytes

Monocytes are produced in the bone marrow and circulate only for a short time in the bloodstream before migrating into various tissues where they differentiate into macrophages and dendritic cells. Macrophages play an important role in the nonspecific immune response by engulfing and removing dying or dead cells and cellular debris, a process known as phagocytosis, but also act as antigen-presenting cells to T cells. Dendritic cells are antigen-presenting cells which upon contact with pathogens such as viruses and bacteria activate T and B cells.

Granulocytes

Granulocytes have a characteristic morphology with a varying shape of their nucleus and are characterized by granules present in their cytoplasm. As part of the immune response, granulocytes play an important role in the protection against infection by producing substances toxic to many microorganisms. Granulocytes are further divided into neutrophils, eosinophils, and basophils. *Neutrophils* are involved in the defense of small inflammatory processes and against bacterial and fungal infection. They are typically one of the first cells attracted to an infected or inflamed site where they phagocytize invading organisms, dead cells, and debris, before they die and are phagocytized by macrophages. *Eosinophils* are mainly dealing with parasitic infections and are also predominant in allergic reactions. The least common type of granulocytes, the *basophils*, mainly release heparin which is an anticoagulant preventing blood clotting in areas of foreign invasion.[1,7]

Platelets

Platelets, also called thrombocytes, are essential in forming blood clots at the site of a vascular injury to prevent blood loss. They are discoid shaped cells without a nucleus and their surface is covered with proteins important for cell adhesion and aggregation.[1,8] In the event of a vascular injury, molecules are released into the blood vessels triggering platelet activation. Activated platelets change their shape and adhere to each other as well as to the area of the injury, forming a platelet plug. Upon platelet activation, coagulation of blood is initiated by clotting factors sealing the break in the blood vessel.

Plasma

All blood cells are suspended in plasma, the liquid medium of blood, which takes up ~55% of the blood volume. Plasma consists to ~90% of water and to ~10% of solutes such as proteins, carbohydrates, lipids, electrolytes, vitamins, minerals, and hormones. Plasma proteins have a variety of different tasks. Some proteins transport molecules which are not water soluble such as vitamins, hormones, and fatty acids. Others are involved in the repair of cellular damage as part of the blood clotting process, and yet other proteins help to maintain the osmotic pressure and blood volume. Antibodies as part of the plasma proteins are involved in the immune response to protect the body from foreign matter. Plasma proteins together with electrolytes help maintaining the pH of the blood while a balanced concentration of electrolytes is essential to perform physiological processes. The term 'serum' often used in context with blood refers to plasma where all the clotting factors, such as fibrinogen, are removed.

2.2 Origin of blood

All blood cells develop from hematopoietic stem cells (HSC) in a process called hematopoiesis (Figure 2.2). HSC have the ability of self-renewal, i.e. generate more HSC, and to differentiate into the different blood cells. Hematopoiesis takes place in the bone marrow and ~one trillion (10^{12}) blood cells are produced every day.[1]

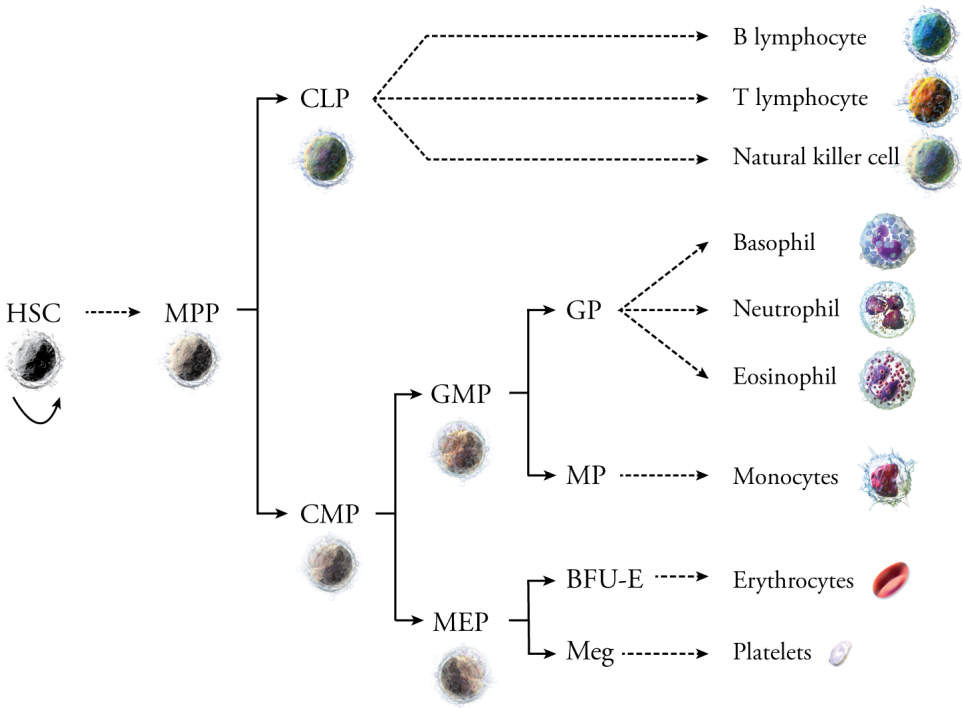

Figure 2.2: Hematopoiesis. The schematic gives an overview of the classical model of hematopoietic development where hematopoietic stem cells (HSC) give rise to all mature blood cells. The further down the tree, the more specialized the cells become. Abbreviations: MPP, multipotent progenitor; CLP, common lymphoid progenitor; CMP, common myeloid progenitor; GMP, granulocytes/ monocyte progenitor; MEP, megakaryocyte/ erythrocyte progenitor; GP, granulocyte progenitor; MP, monocyte progenitor; BFU-E, erythroid burst-forming unit; Meg, megakaryocyte. Pictures are taken and adapted with permission from Blausen.com.[4]

2.3 Applications for whole blood fractionation

For clinical diagnoses, it is often sufficient to look at the blood cell count of the various components. A higher WBC count, called leukocytosis, is a typical sign for infection or inflammation within the body but can also be a sign of cancer such as leukemia (increased count of immature WBC).[1,9] Individuals infected with the human immunodeficiency virus (HIV) will have a reduced WBC count, especially in the number of T helper cells which are part of the lymphocytes.[9] A low RBC count on the other hand could be the sign of anemia caused for example by shortage of vitamin B12 or iron deficiency.[10] Detection of circulating tumor cells (CTC) in blood is used in guiding prognosis in cancer patient and isolation of CTC further helps to characterize the cancer cells.[11]

Clinical applications and cell-based therapy often rely on a specific cell population. Patients with

certain blood cancers will undergo hematopoietic stem cell transplantation in order to restore the patient's hematopoietic system after chemotherapy or radiation.[7] In cell immunotherapies, cells are isolated from the blood, modified/engineered and retransfused into the patient. Monocytes are for example used to generate dendritic cells which can induce an immune response in healthy donors and cancer patients.[12] Patients with a reduced immune response, e.g. after chemotherapy, can benefit from granulocyte transfusion therapy in case of bacterial or fungal infections.[13] Another powerful tool is the chimeric antigen receptor (CAR) T cell therapy where a patient's T cells are programmed to specifically target tumor cells.[14]

In order to study and deepen the understanding about the different blood cells or to use them in clinical applications one needs to fractionate the blood. The next chapters will introduce and compare both conventional and microfluidic cell separation methods with focus on microfluidic acoustophoresis and the papers presented in this thesis (Figure 2.3).

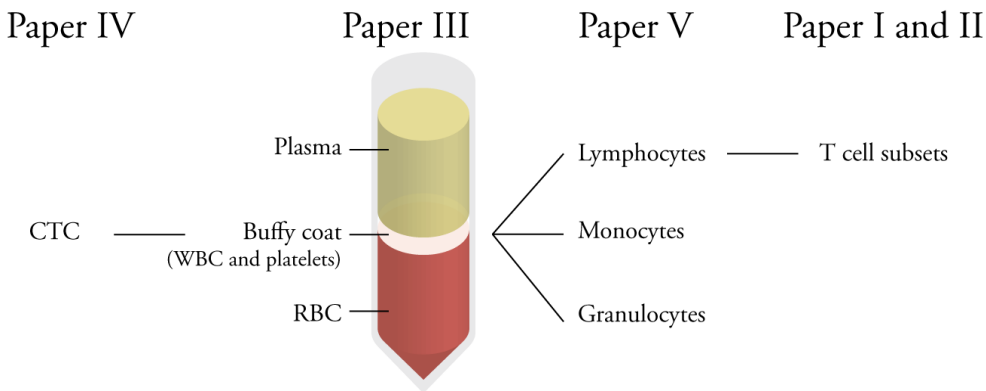

Figure 2.3: Blood fractionation presented in the papers of this thesis. A summary of the papers with the different approaches for blood cell fractionation can be found in chapter 7.

3

Conventional cell separation methods

Whole blood is a complex biofluid with hundreds of million cells in one drop of blood. It is rich in information about the physical state of a human being and blood cells are often used in diagnostic tests and for therapeutics. In order to fractionate blood into various cell populations or to isolate a specific cell type, different cell manipulation and sorting techniques are required. Depending on the downstream application after cell separation, the separation process should be as mild as possible, and the isolated cells should retain their viability and biological function. Typically, conventional cell separation methods at the macroscale are categorized into label-free and label-based methods (Figure 3.1). This chapter introduces the most common blood cell separation methods at the macroscale and shows their use in the clinic.

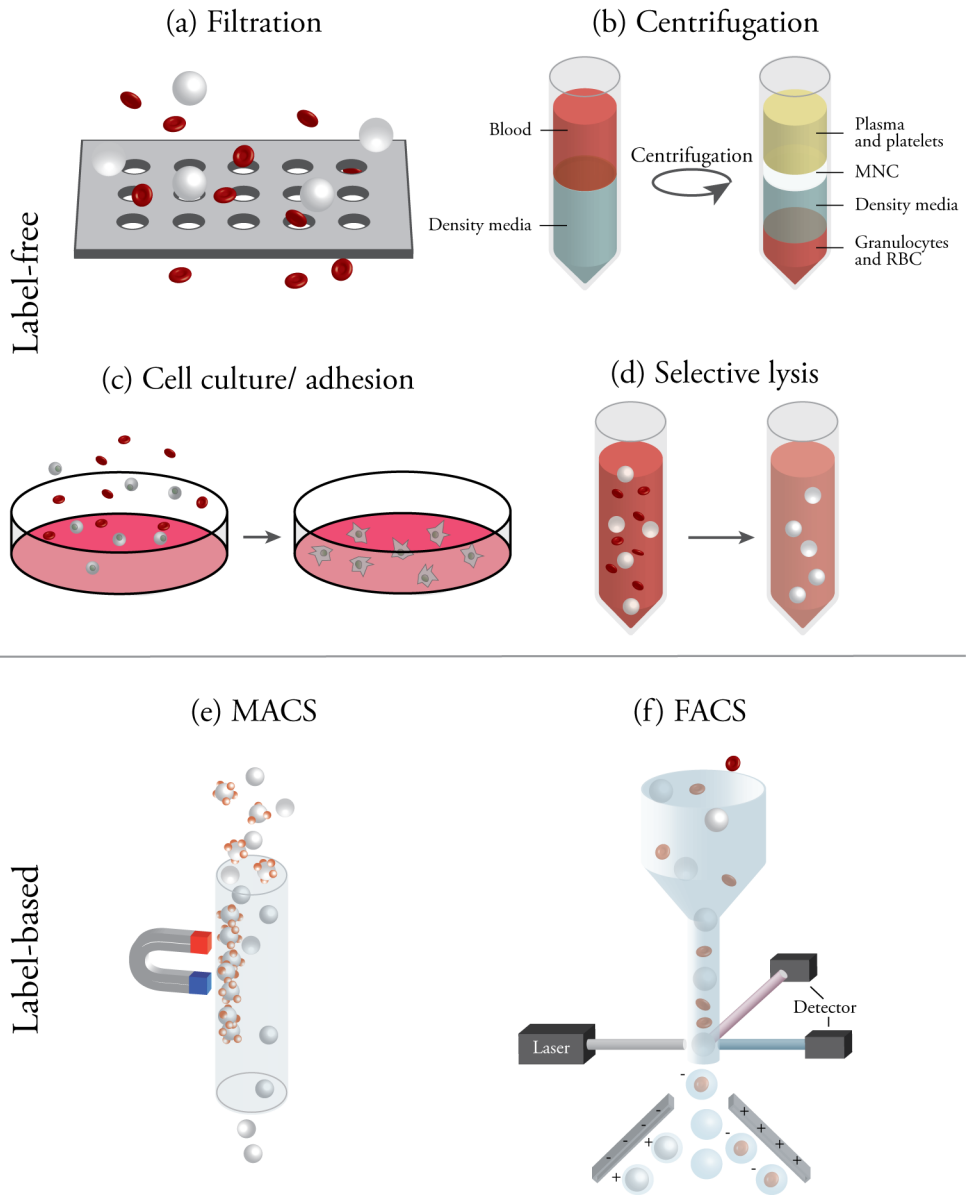

Figure 3.1: Overview of conventional cell separation methods. Biofluids such as blood are very heterogenous and need to be separated into specific cell populations in order to be useful in diagnostic tests and therapeutic applications. Commonly, separation methods are divided into label-free and label-based methods. Each technique is explained in more detail within this chapter.

3.1 Label-free separation methods

Different cell populations vary in their physical properties such as size, density, shape, and deformability. Label-free separation methods use these physical differences to fractionate heterogenous biofluids such as blood. Typically, label-free methods are simple to use, relatively cheap and have a high throughput, however, often with the drawback of lower purity and recovery.

Filtration

Cells in suspension passing through a filter with uniform microscale meshes or pores will be separated based on their size and deformability. Only cells smaller than a specific cut-off size will be able to pass through the filter while bigger cells are retained. Filtration methods are often used as pre-enrichment step or to prepare single cell suspension by removing cell aggregates. Within clinical applications, such as blood transfusion, filtration methods are routinely used for leukocyte reduction[7](Figure 3.1a). Remaining leukocytes in the blood for blood transfusions have been associated with a higher risk of post-transfusion infection. Modern filters remove >99% of leukocytes while recovering 90-95% of RBC.[7,15] Besides relying on the pore size, filters also use adhesion of leukocytes to negatively charged surfaces in the filter to improve the separation outcome.[16] Filtration is a very simple and straightforward method; however, significant amount of cell loss is a common disadvantage as well as clogging of the filter unit. Also leukocyte and platelet activation[17] and changes in platelet function have been reported for leukocyte filters.[18]

Centrifugation

Centrifugation is one of the most common separation methods used in laboratories. The principle of centrifugation is based on the sedimentation rate of particles in a centrifugal force field. The sedimentation rate is proportional to the particles size and to the density difference between a particle and its' surrounding medium. Centrifugation allows separation and concentration of large cell numbers in a simple and inexpensive way. Most blood component preparations use centrifugation techniques. Typically, blood can be divided into platelet-rich plasma, WBC, and RBC by centrifugation. In order to prepare RBC products, most of the plasma fraction is removed after centrifugation. By serial washing and centrifugation steps the RBC can be further purified, removing ~99% of the plasma proteins and 70-90% of leukocytes, however also accounting for ~20% RBC loss.[7] The term *differential centrifugation* describes the process of several centrifugal steps, every step performed at a higher velocity and longer time than the previous step and is for example used in platelet preparation.[19] First, a low-speed centrifugation separates RBC from platelet-rich plasma, which is further spun down at higher velocity to allow platelet sedimentation on the bottom of the centrifugal tube. Higher resolution of a separation can be achieved using *density gradient centrifugation*. This is commonly done for the isolation of mononuclear cells (MNC), i.e. monocytes and lymphocytes, by layering whole blood on top of a density media.[20] A density gradient is formed during centrifugation and cells will move to their isopycnic point, where the density of the media is equal to the cell's density. MNC can be collected by carefully removing the layer between the density media and the platelet-rich plasma

(Figure 3.1b).

The outcome, such as cell loss and purity of a sample after centrifugation, is highly depended on the application but also on the person handling the process. Furthermore, activation of cells after centrifugation has been reported in some applications.[21–24]

Cell adherence and cell culture

In cell culture, cells can be separated based on their adherence ability to a culture plate or by using certain culture media that stimulates or inhibits the growth of specific cell types[25] (Figure 3.1c). An example combining both adherence and cell culture is the generation of dendritic cells.[12] Here, monocytes are enriched from MNCs by plastic adherence and the removal of non-adherent cells by repeatably rinsing the culture plate. Dendritic cells are then generated by culturing the enriched monocytes in specific culture medium for several days. Using cell culture approaches to isolate cell populations are often time consuming and not very specific.

Selective lysis

A common method to isolate leukocytes from whole blood is using selective RBC lysis (Figure 3.1d). Whole blood is diluted in solutions, such as water or ammonium chloride, which lead to swelling and destruction of RBC via changes in the osmolality. Selective lysis is a simple and fast process but often includes several washing steps to remove cell debris. Depending on the lysing solution used, WBC cell loss and alteration in cell function can occur.[26–28]

3.2 Label-based separation methods

In contrast to label-free methods, which rely solely on the physical characteristics of cells, label-based methods target the characteristic biochemical surface of different cell types. Cells can be classified by cell membrane integrated proteins, so called cluster of differentiation (CD). By using antibodies directed against surface proteins on the cell membrane (CD molecules), specific cell subpopulations can be targeted which otherwise do not differ in their physical characteristics. In this way it is possible to achieve high purity cell separation, however, the procedure is often time consuming, labor intensive, costly, and importantly may affect the cells' function.

Magnetic activated cell sorting (MACS)

Affinity based magnetic separations, utilizing differential expressed cell-surface antigens, has become one of the golden standards in research and clinical laboratories when aiming for high separation efficiency and purity. Antibodies coupled with magnetic beads bind antigens on the cell surface of a target cell. When the sample is exposed to a magnetic field gradient, unbound cells can be washed away while bead-bound cells are retained in the magnetic field (Figure 3.1e). The technique can be used for positive selection, i.e. labeling the desired cell type, as well as for negative selection, i.e. labeling all the unwanted cells and collect the target cells in the flow

through fraction. Nowadays, a wide range of commercial kits are available and specific cells can be isolated from whole blood based on their antigen expression. MACS is routinely applied in the clinic to isolate hematopoietic stem cells (HSC) used for stem cell transplantation.[29,30] HSC are released from the bone marrow after hormone mobilization treatment and can be collected from the peripheral blood by leukapheresis, i.e. the enrichment of WBC from blood commonly done by centrifugation. This is followed by magnetic bead selection with antibodies targeting CD34+ cells, i.e. HSC, to further enrich the stem cells from the leukapheresis product.

The disadvantage of MACS is the reliance on a specific cell marker and that only one surface marker can be targeted per separation. Influences of the magnetic separation method on the cells' properties has been studied extensively and in some cases showed decreased cell viability, reduced proliferation, reduced metabolic activity, and changes in gene expression.[31,32]

Fluorescence activated cell sorting (FACS)

Flow cytometry identifies cells based on their relative size, scatter properties, their differential expression of specific biomarkers, and the intensity of fluorescent-labeled antibodies bound to a cell's membrane and/or internal structure. Cells in suspension are hydrodynamically focused before entering a flow cell where they pass laser beams one by one (Figure 3.1f) and scattered light as well as emitted fluorescence is measured by several detectors. The light scattering is depending on the cell's size, the granular material inside the cell, the cell membrane, and cell shape. At the end of the flow cell the stream of cells passes through a vibrating nozzle, causing the stream to break into droplets, ideally containing one cell each. Based on the information obtained from the scattered light a sorting decision is made for each individual cell/droplet and an electrical charge is placed on the droplet. Based on their electrical charge, droplets are then deflected in an electromagnetic field into separate collection tubes. Flow cytometers have often sorting capacities of ~10.000 events/s and in comparison with MACS, several antibodies targeting different CD molecules can be used to isolate specific subpopulations in the blood with high purities.[33] FACS requires expensive instrumentation, costly antibodies and trained staff. Depending on the sorting criteria, the input sample and the purity required, preparation and sorting can take several hours, limiting the number of clinical applications. Furthermore, viability and recovery of FACS sorted cells has been reported to be an issue depending on the sorting conditions.[34]

4

Microfluidic cell handling

The term microfluidics refers to the manipulation and control of fluids confined to small volumes in the microliter range. At the microscale, the flow pattern becomes predictable and external forces acting on particles in solution can be precisely controlled. Over the last decades various microfluidic technologies for cell and particle handling have emerged employing the advantages of microfluidics. This chapter will focus on the characteristic microfluidic phenomena relevant for this thesis and the introduction of microfluidic cell manipulation technologies.

4.1 Fluid dynamics at the microscale

Laminar Flow

In microfluidic channels the surface to volume ratio is increased, in contrast to the macro scale, and viscosity forces start to dominate over inertia. The dimensionless Reynolds number is used to predict whether the flow behavior of a system is dominated by viscous or inertial forces:

$$Re = \frac{\rho u L}{\mu}$$

where ρ is the fluid density, u the average flow speed, L the characteristic length and μ the dynamic viscosity of the fluid. For a circular tube the characteristic length equals the diameter of the tube. In microfluidic channels with a rectangular cross-section it can be calculated by the hydraulic diameter $D_h = 2ab/(a+b)$, with a and b are the channel width and height, respectively. Turbulent flow occurs at Re >2000 and becomes laminar for Re <2000 which is typically the case for microfluidic devices.[35] Laminar flow is characterized by fluid streams flowing in parallel (Figure 4.1) and mixing in the system only occurs through diffusion.

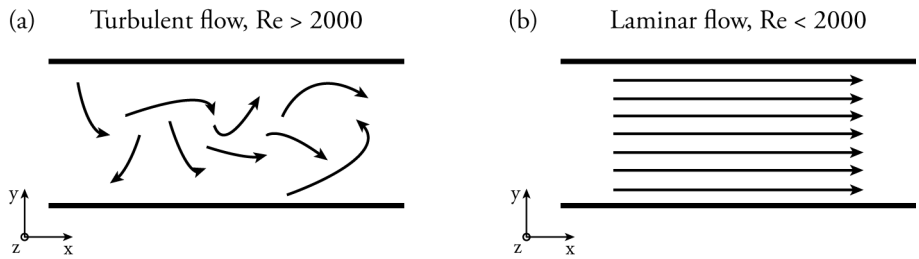

Figure 4.1: Turbulent and laminar flow. (a) For Reynolds numbers >2000 flow is turbulent, i.e. velocities in time and space are random, (b) while laminar flow with fluid streams flowing in parallel occurs for Re <2000.

Parabolic flow profile

In the laminar flow condition of a straight microfluidic channel with a pressure-driven, steady-state flow the velocity at the channel wall approaches zero. This so-called no-slip boundary condition leads to the formation of Poiseuille flow with a parabolic flow profile having the maximum velocity at the channel center (Figure 4.2). Cells or particles in solution will have different retention times in the microchannel depending on their positioning, with cells close to the side walls, top or bottom will be slower as compared to cells in the channel center.

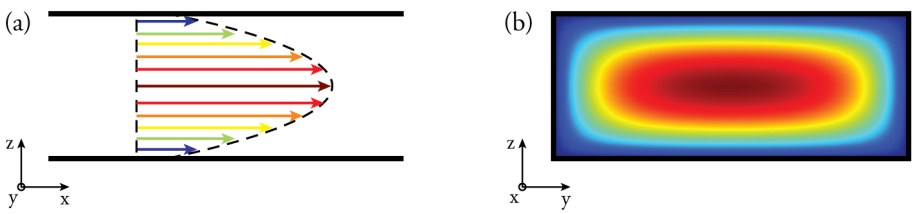

Figure 4.2: Parabolic flow profile. Due to the no-slip boundary conditions in the microchannel the fluid flow at the channel wall is zero (dark blue) and the maximum velocity (red) is observed in the channel center. The typical parabolic flow profile is shown for (a) the side view and (b) for the cross-section of a microchannel.

Stokes' law

If a particle is moved by an external force through a fluid it will experience a drag force, known as Stokes' drag, in the opposite direction (Figure 4.3). The drag force F_d on a spherical particle in laminar flow with Re < 1, assuming no interactions between particles, is described by the Stokes' law:

$$F_d = 6\pi\eta a u$$

where η is the dynamic viscosity, a is the particle radius and u is the flow velocity of the particle. Externally applied forces (e.g. acoustic, magnetic, electrical forces) commonly scale with the volume of the particle while the drag force scales with the particle radius. For small particles the drag force becomes more dominant making it challenging to manipulate smaller particles with external forces.

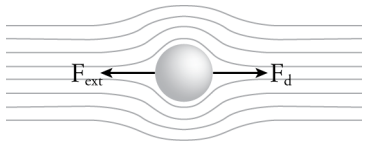

Figure 4.3: Stokes' drag. If a particle in laminar flow with low Reynolds number is moved by an external force F_{ext}, it will experience a drag force F_d (Stoke's drag) in the opposite direction of the movement.

4.2 Microfluidic cell manipulation

Cell manipulation at the microscale refers in general to the control of a cells' position within a fluid or its position relative to other cells. This includes techniques for washing, buffer exchange, focusing, separation, sorting, and trapping. The applications presented in paper I-V fall under the definition of 'separation' which refers to a process where a physical property of a cell is used to accumulate this specific cell type. In contrast, 'sorting' typically refers to a process where for each cell a sort decision is made based on specific identification of that cell.

Table 4.1: Classification of microfluidic separation techniques.

	Separation technique	**Separation criteria**
Passive	Filtration	Size, shape, deformability
	Hydrodynamic filtration	Size, shape, deformability
	Deterministic lateral displacement (DLD)	Size, shape, deformability
	Inertia	Size, shape, deformability
	Biomimetic	Intrinsic properties of blood
	Microstructures	Size, density, deformability
Active	Dielectrophoresis (DEP)	Polarizability, size
	Magnetophoresis	Intrinsic magnetic susceptibility
	Optical methods	Refractive index, size
	Acoustophoresis	Size, density, compressibility

Microfluidic separation methods can be classified into passive and active methods. Table 4.1 summarizes the most common techniques, which will be described in more detail in the following section with focus on blood fractionation applications. Cells can be manipulated in a variety of different modes such as kinetic, equilibrium, and elution mode (Figure 4.4). Kinetic modes use the rate of cell deflection perpendicular to a primary channel flow for cell separation.

In equilibrium mode cells migrate to their property-dependent equilibrium position, while in elution mode a force counteracting the force of the fluid flow creates differential retention time of cells.[36]

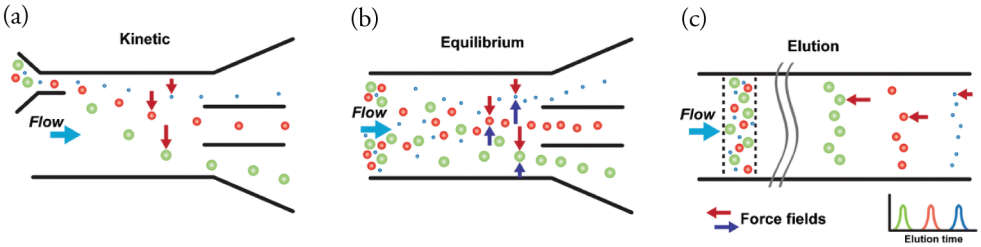

Figure 4.4: Microfluidic separation modes. Microfluidic systems can manipulate cells in a variety of ways. (a) In a continous kinetic mode cells are deflected perpendicular to the primary channel flow. (b) In an equilibrium mode cells migrate to their property-dependent equilibrium position, e.g. their isopycnic point in a density gradient, while in (c) elution mode forces are acting in the opposite direction of the primary flow creating differential retention of the cells. Adopted and reprinted with permission from © Gossett et al. (2010).[36]

A more detailed description of whole blood fractionation into WBC and RBC is given for each microfluidic separation method and are summarized in relation to their performance metrics at the end of this chapter in Table 4.2.

Performance metrics

In order to enable comparison between different microfluidic separation methods the most comment performance metrics are introduced. In this thesis, *purity* is the percentage of target cells in a sample divided by the total number of cells in that fraction.

$$Purity = \frac{\#target\ cells}{\#all\ cells} \cdot 100\%$$

Recovery describes the ratio between the number of target cells in the target outlet and the number of target cells in the input sample. It is used to describe the loss of target cells within the device and tubing.

$$Recovery = \frac{\#target\ cells_{target\ outlet}}{\#target\ cells_{input}} \cdot 100\%$$

Separation efficiency looks at the ratio of target cells in one outlet versus the number of target cells in all outlets after separation. It shows the efficiency of the separation method.

$$Separation\ efficiency = \frac{\#target\ cells_{target\ outlet}}{\#target\ cells_{all\ outlets}} \cdot 100\%$$

Enrichment is defined as the ratio of target cells divided by all cells in one outlet and the number of target cells divided by all cells in the input.

$$Enrichment = \frac{\left(\frac{\#target\ cells}{\#all\ cells}\right)_{target\ outlet}}{\left(\frac{\#target\ cells}{\#all\ cells}\right)_{input}}$$

Throughput defines either the volume per time unit (sample throughput) or the number of processed cells or events per second (cell throughput).

4.2.1 Passive cell separation methods

Microfluidic methods such as filtration, hydrodynamic focusing, deterministic lateral displacement (DLD), and inertia achieve cell manipulation without the use of an external force field and are classified as passive separation methods. Cells are separated based on their size, shape, and deformability.

Filtration

Microscale filters employ different obstacles such as membranes, pillars, and weirs to separate different sized cells. Based on the direction of the flow they are classified into dead-end filters with flow perpendicular to the filter plane, and cross-flow filters with flow along the filter plane (Figure 4.5). As in the microscale, microfiltration has been widely employed in whole blood fractionation[37] mainly for WBC depletion,[3,38] RBC depletion,[39–41] and plasma generation.[42–45]

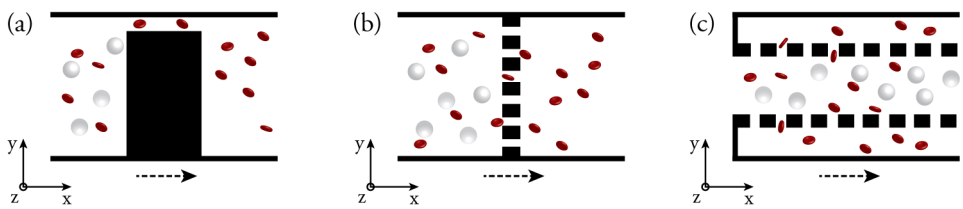

Figure 4.5: Microfiltration. The different types of filter used in microfluidics are (a) weir, (b) pillar, and (c) cross-flow filters. Both (a) and (b) are shown as dead-end filters. As an example, the principle of WBC depletion from blood due to the size difference of WBC and RBC is shown. RBC can, due to their biconcave shape, squeeze through the gaps in the filters while WBC cannot pass due to their bigger size. The dashed arrows indicate the flow dirction through the microchannel.

Leukapheresis, i.e. the removal of WBC from blood, is routinely done in clinical applications using filters at the macroscale.[7] Sethu et al.[3] designed a microfluidic diffuse filter for leukapheresis where RBCs were able to pass through sieves due to their biconcave shape, while larger spherical leukocytes could not pass through the structure. With flow rates of 5 µL/min whole blood the filter depleted >97% leukocytes but only recovered ~50% of the RBC.

Ji et al.[38] analyzed the efficiency of weir, pillar, crossflow and membrane microfilters to isolate WBC from RBC. A cut-off size of 3.5 µm was chosen for the different designs in the assumption that RBCs can pass through gaps as small as 3 µm due to their biconcave discoid shape, while WBC can only be deformed and squeezed through 7 µm gaps. Using 200x diluted blood it was found that membrane and weir types had a higher clogging risk while crossflow filtration with pillars achieved the best results with a recovery of 60-95% of RBC while removing 70-95% of WBC.

A similar comparison of two different crossflow filters for RBC removal was done by Chen et al.[40] comparing pillar- vs. weir-type filtration. Here, the weir-type worked better removing 91.2% of the RBC, which could be enhanced to >95% by rerunning the sample. In contrast, only 82.3% of RBC were removed with the pillar-type. Also, the WBC isolation was higher in the weir-type (27.4%) as compared to the pillar-type (8%). Cell concentration tests showed that the initial blood sample should have less than 10^4 cells/µL in order to maximize the separation efficiency.

In general, microfilters are easy to handle and are especially useful for label-free separation of blood components from microliter volumes of blood. They can be used as a first step within blood cell or plasma analysis and as low cost devices for point-of-care applications.[44] However, microfilters are often associated with the risk of clogging, especially when operated as dead-end filters. Cells and particles at the filter obstacles accumulate over time which reduces the separation efficiency. By vibrating the filter unit, pulsating the fluid flow or using a back flow, the risk of clogging has been reduced.[46,47] Another challenge is the heterogeneity of the cell size within a population which can lead to overlapping cell sizes between target cells and unwanted cells. As in macroscale filtration, platelet activation at the microscale occurs due to high shear stress[48,49] as well as interaction with the surface material of the filter unit.[50,51] Furthermore, hemolysis, i.e. the rupturing of RBC, can occur in the microfilter device if operated under high pressure or high shear rate.[42,45,52]

Hydrodynamic filtration

Hydrodynamic filtration explores the physical laws of laminar flow at low Reynolds numbers to separate cells. In laminar flow, cells will follow the streamline passing through its center of mass and thereby allowing for cell separation based on size and deformability. Typically, cells are positioned in stream lines controlled by the flow rates through the inlets, the channel geometry and the outlet configuration.

Yamada et al.[53] designed a microfluidic device with two inlets, a pinched segment and a broadened segment. Particles from one inlet are pinched against the wall using a high flow velocity of a particle free fluid from the second inlet. Smaller particles are positioned closer to the wall and follow different streamlines as compared to larger particles. In the broadened segment, the flow profile expands and particles following their streamline are separated according to their size (Figure 4.6a). Takagi et al.[54] added several outlets to the design and varied the flow resistance of the outlets by either making them shorter and/or broader. In this way they achieved an asymmetric flow profile in the broadened segment which allowed to improve the size dependent separation

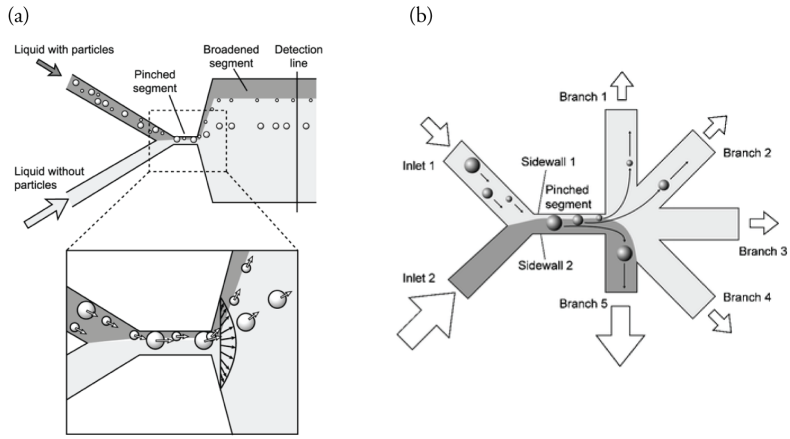

Figure 4.6: Principle of hydrodynamic filtration in pinched flow fractionation. (a) Particles in suspension are pinched against the wall using a high flow velocity of a particle free solution. Smaller particles are focused closer to the wall and exit the pinched segment at different streamlines as compared to bigger particles. (b) Having outlets with different flow resistance will create an asymmetric flow profile in the broadened segment, pulling the streamlines further apart and increasing separation performance. Adapted and reprinted with permisson from Yamada et al.[53] ©American Chemical Society (2004); and Takagi et al.[54] ©Royal Society for Chemistry (2005).

by pulling the streamlines further apart (Figure 4.6b). Separation of RBC from diluted whole blood was shown with ~80% separation efficiency at sample flow rates of 20 µL/h, equivalent to 0.001 µL/min whole blood. Further enhancement of pinched flow fractionation was shown by introducing an enhancing segment to the broadening segment[55] and by adding a sedimentation force for both size and density based sorting.[56] However, the applicability of these designs in cell separation was not shown.

A similar approach using hydrodynamic filtration was demonstrated by Yamada and Seki.[57] Their device consisted of one sample inlet and a straight channel with perpendicular branched side channels (Figure 4.7). By continuously removing liquid from the side branches, particles in the main channel are concentrated and aligned at the side wall. Increasing the flow at the side branches over time allows small particles being closer to the wall to follow their streamlines to the side branches and thereby separating them from bigger cells. Separation of RBC from WBC was shown at 20 µL/min sample flow for 10x diluted whole blood with a ~29-fold increase of the WBC to RBC ratio after two rounds of filtration, corresponding to a net-flow of 2 µL/min whole blood equivalent.

VanDelinder and Groisman[59] used a microfluidic cross-flow filter combined with medium exchange to separate WBC from blood. Medium was infused at the branches at one side of the main channel and thereby focusing the cells to the other side wall of the main channel. Similar to Yamada and Seki,[57] smaller particles will follow their streamlines to the side branches earlier within the device and can be separated. The device was able to deplete 99.975% of the RBC and

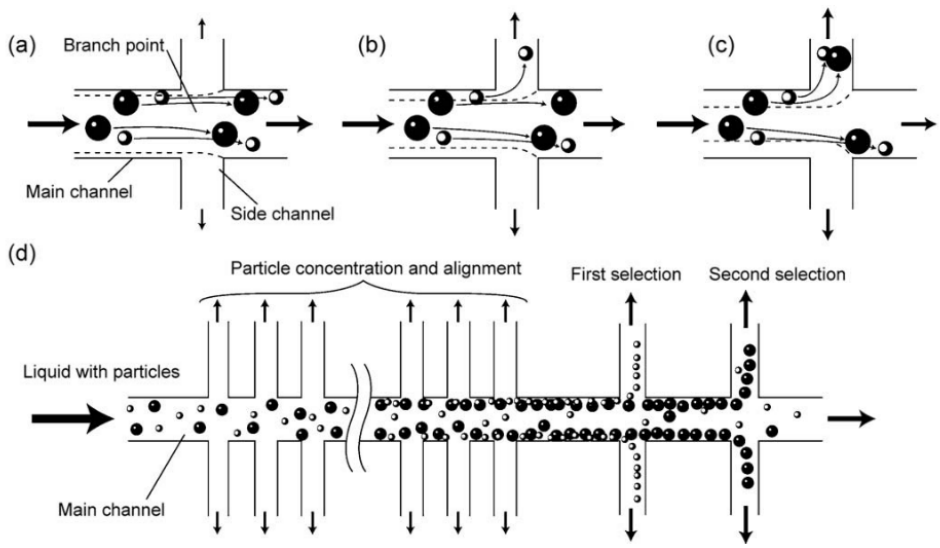

Figure 4.7: Hydrodynamic filtration. Particles in supsension are flowing through a main channel. By continuously removing liquid to side branches, particles will be concentrated and aligned close to the wall. Increasing the flow in the side channels will allow small particles closer to the wall to follow their streamlines and thereby be separated from larger particle. Reprinted with permission from Yamada et al.[57] ©Royal Society of Chemistry (2005).

achieve WBC purities of ~70% using undiluted whole blood. Besides the impressive outcome the sample throughput was as low as 0.06 µL/min and 50% of the cells were lost at the device inlet.

Yamada et al.[58] further improved the sized based separation using a slanted, asymmetric microfluidic lattices (Figure 4.8). Leukocytes were separated from RBC with ~80% WBC purity and a separation efficiency of ~80% at a sample flow rate of 40 µL/min, equivalent to 2 µL/min whole blood. Micrographs showing the cells before and after separation suggest a high shear stress on the cells showing deformed RBC.

Hydrodynamic filtration offers a label-free, simple and continuous microfluidic separation without the use of an external force. However, data on cell viability, cell activation, and hemolysis is underrepresented and would be desirable to show the usability of hydrodynamic focusing for blood cell fractionation in clinical and research applications.

Deterministic lateral displacement

Cells flowing through an array of pillars can be separated based on their size, shape, and deformability.[60–65] Each row of pillars is shifted laterally creating predictable streamlines around the pillar in a zig-zag mode. Particles below a critical diameter will follow their original streamline through the array of pillars without displacement. If the particle size is about the critical

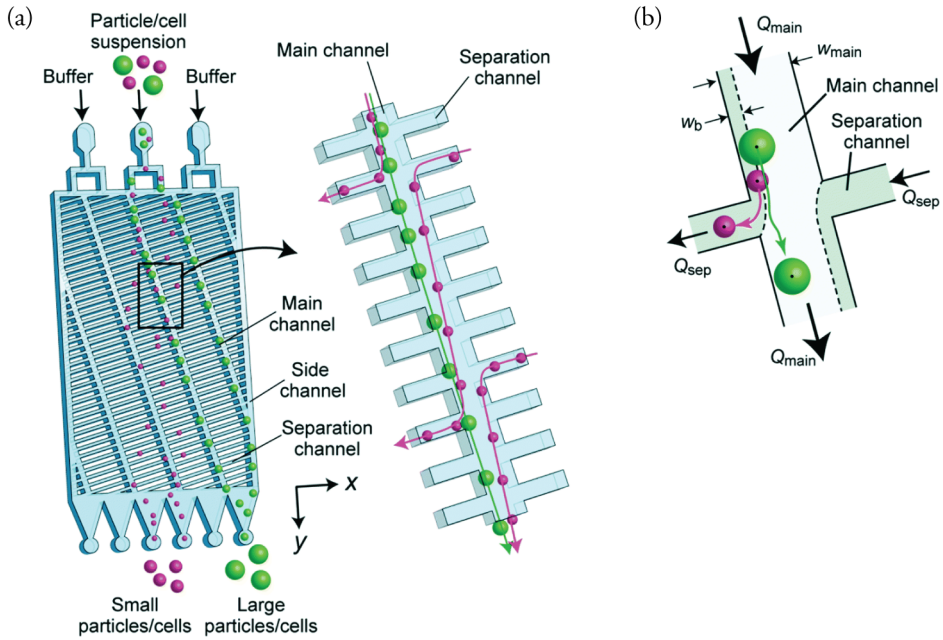

Figure 4.8: Hydrodynamic filtration in slanted, asymmetric microfluidic lattices. (a) Cells in suspension are flowing through a main channel while buffer is introduced in parallel channels. The fluid flow from the buffers in the separation channels pushes cells towards the side wall of the main channel. (b) Smaller cells closer to the wall will follow their streamlines to the separation channels and are thereby separated from larger cells. Adapted and reprinted with permission from Yamada et al.,[58] ©Royal Society of Chemistry (2017).

diameter, the particle will "bump" into the pillar pushing its center of mass to the next streamline. With each row of pillars, the particle will travel at an angle predetermined by the post offset distance away from its original streamline in a displacement mode (Figure 4.9).

Huang et al.[60] was one of the first to show the principle of deterministic lateral displacement (DLD) in a microfluidic device. DLD demonstrated to have a very good size resolution by separating particles with 10 nm size difference (0.8 µm, 0.9 µm, and 1.03 µm). Davis et al.[66] designed a DLD device with 13 functional regions of post arrays to fractionate undiluted whole blood. Separation of WBC from RBC was possible with ~99.6% WBC separation efficiency while depleting ~99% of the RBCs. The purity of WBC in outlet 2 reached ~9% with ~110-fold enrichment compared to the original sample. The device operated at a throughput of 1 µL/h blood (~0.017 µL/min).

Inglis et al.[67] used six parallel DLD channels to increase the sample throughput, fractionating the sample into three different outlets (small, medium, and large). An average flow rate of 23 µL/min of undiluted whole blood was achieved, with ~3.8 µL/min sample flow per chan-

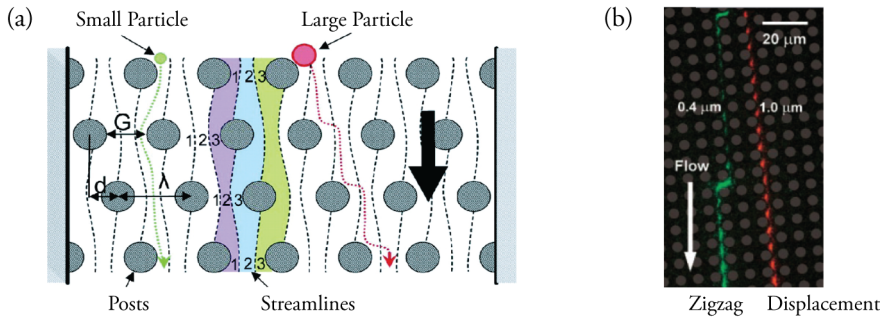

Figure 4.9: Deterministic lateral displacement. Particles flowing through an array of pillars can be separated based on their critical diameter. Particles below a critical diameter will follow their original streamline around the post in a zigzag mode. Larger particles will bump into the post and be deflected into neighboring streamlines, flowing through the array in displacement mode. Adopted and reprinted from Davis et al.,[66] ©National Academy of Sciences (2006); and Huang et al.,[60] ©American Association for the Advancement of Science (2004).

nel. The average leukocyte depletion in the small outlet for all tested conditions was 98.7%. For undiluted blood the enrichment in WBC concentration in the medium outlet was ~6.6-fold and in the larger outlet ~7.6-fold. Furthermore, separation of the different WBC subpopulation showed an enrichment in concentration for lymphocytes in the medium outlet while monocytes and granulocytes were enriched in the large outlet.

In general, DLD offers the benefit of being able to process whole blood, something most microfluidic separation techniques struggle with. Sample flow rates are typically very low, however, upscaling of sample throughput for clinical scales has been shown successfully.[68] As in other microfluidic separation methods shear stress on cells can be a limiting factor.[69,70] No alterations in viability and cell proliferation after DLD separation has been shown for CTCs,[71–73] however blood clot formation due to platelet activation has been observed.[74] Furthermore, as in filtration, clogging of the device running biological samples can be an issue due to the small gap between the posts and the heterogeneity in the cell sizes.[75,76]

Inertia

Typically, inertial effects are negligible in the microfluidic world. However, when employing high flow velocities (Re 1-100) inertial effects become significant.[36] Already in 1961, Segré & Silberberg[77] observed that randomly distributed particles flowing through a circular pipe will concentrate to a narrow band at ~0.6 times the pipe radius. The fundamentals of inertial focusing has been described extensively.[78–81] In brief, focusing occurs as a balance of shear-gradient-induced lift forces (F_{SG}) and wall-effect-induced lift forces (F_{WI}) (Figure 4.10a). Particles experience F_{SG} in the direction of the channel wall due to the velocity gradient in the parabolic flow profile in microfluidic channels with no-slip boundary conditions. On the other hand, F_{WI} is moving particles away from the channel wall due to a pressure build up between the wall and the particle.

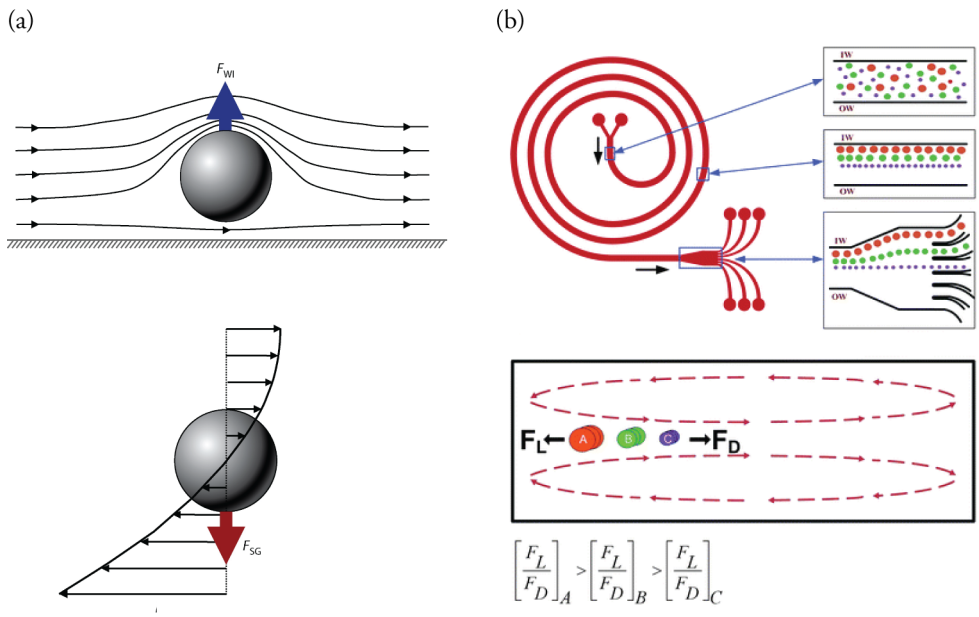

Figure 4.10: Interatial lift forces and dean vortices. (a) In straight microchannels, particles in suspension flowing at high Reynolds number will experience both wall-induced lift forces (F_{WI}) and shear-gradient-induced lift forces (F_{SG}). (b) In curved channels, particles will experience an additional force (F_D) due to dean vortices as a result of centrifugal forces. Based on a balance of the lift forces in the direction of the inner channel wall (IW) and dean forces in the direction of the outer wall (OW), particles can be separated according to their size. Adapted and reprinted with permisson from Martel and Toner,[80] ©Annual Reviews (2014); and Kuntaegowdanahalli et al.,[82] ©Royal Society of Chemistry (2009).

In curved channels a second inertial effect arises due to centrifugal effects. Two counter-rotating vortices perpendicular to the channel flow, called dean vortices, arise when the fluid at the center of the curvature with a higher momentum displaces lower momentum fluid near the channel walls[83] (Figure 4.10b). For small particles, the dean forces (F_D) is larger than the lift forces (F_L), moving smaller particles further away from the inner channel wall of the curvature. Taken the different inertial forces into account, cells and particles can be separated based on size,[82,84] shape,[85,86] and deformability.[87] Inertial microfluidic devices have been employed, amongst others, for plasma separation,[88] blood cell fractionation,[88–91] fractionation of WBC subtypes,[92,93] as well as separation of CTC from blood.[87,93,94]

Fractionation of WBC and RBC from 80x diluted whole blood using a spiral channel with trapezoid cross-section was shown by Wu et al.[89] The device was able to remove ~95% of RBC and recover 98.4% of WBC at flow rates of 800 µL/min, equivalent to 10 µL/min whole blood.

Nivedita and Papautsky[88] increased the sample flow for blood cell fractionation using a spiral channel with rectangular cross-section. The device was able to process sample at 1.8 mL/min at

similar efficiencies as Wu et al.,[89] however high dilution (500x) reduced the processing time of whole blood to 3.6 µL/min.

Using eight channels in parallel, Zhang et al.[91] managed to increase the sample throughput to 4.6 mL/min using a serpentine microchannel for inertial focusing and separation of WBC from 20x diluted whole blood. This corresponds to an impressive throughput of 240 µL/min whole blood (30 µL/min per channel). Fractionation data shows 48% WBC purity after two separation processes, however, the choice of analysing the sample with flow cytometer without any labelling of the WBC seems questionable.

Ramachandraiah et al.[93] combined selective RBC lysis with inertial microfluidics to fractionate WBC. High purities of 86%, 43%, and 91% for granulocytes, monocytes, and lymphocytes, respectively, were achieved. However, separation efficiencies in the corresponding outlets of 27%, 90%, and 47% of granulocytes, monocytes, and lymphocytes, respectively, indicates cell loss in their system.

Microfluidic separations employing inertial effects surpass most other microfluidic technologies in their volumetric flow rate. However, dilution of the sample is usually necessary to avoid defocusing of particles due to interparticle interactions.[79,88] Inertial separation does not show indication of neutrophil activation or changes in viability[89,93] and makes it a promising tool for blood cell fractionation.

Biomimetic

Biomimetic systems take advantages of the intrinsic properties of blood for blood cell fractionation at the microscale. As the diameter in blood vessels decreases <0.3 mm the blood starts to show unique flow characteristics. In small blood vessels, RBCs are focused towards the highest fluid velocity at the center of the blood vessel, which leads to an overall decrease in RBC concentration, an effect known as Fåhræus effect. Due to the decreasing RBC concentration, the viscosity in the small vessel also decreases, known as the Fåhræus-Lindqvist effect.[95]

Shevkoplyas et al.[96] used the Fåhræus effect to enrich leukocytes from whole blood in a microfluidic device. RBCs migrating towards the channel center will force leukocytes to move towards the channel wall, a process named leukocyte margination (Figure 4.11). WBC close to the channel wall are concentrated and separated from RBC in a cascade of bifurcation channels. With this simple principle, WBC were concentrated by a factor of 10 from 4300 WBC/µL in the whole blood sample to 42300 WBC/µL at the leukocyte outlet. The WBC to RBC ratio was 1:32 at the extraction channel showing a 34-fold enrichment as compared to the input sample. Extraction of cells at the WBC outlet was performed at a flow rate of 16 pL/s ($9.6x10^{-4}$ µL/min).

The effect has also been employed for blood filtration to separate pathogens from whole blood.[98,99] Similar to leukocyte margination, pathogens are pushed towards the channel wall when RBC move to the center and can be collected at the side fraction.

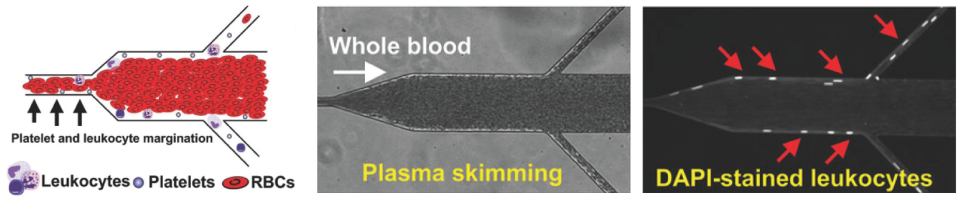

Figure 4.11: Leukocyte margination. RBCs in small channels will move towards the channel center with the highest velocity pushing WBC towards the channel wall. WBC close to the channel wall can be separated from RBC using a bifurication. Adopted and reprinted with permisson from Tay et al.,[97] ©WILEY-VCH Verlag GmbH & Co. KGaA, Weinheim (2018).

Other label-free methods

Besides the above-mentioned passive microfluidic separation methods, microstructures and aqueous two-phase systems (ATPS) have been used for blood cell fractionation to some extent. Typically, microstructures such as grooves, chevrons, and herringbones have been used for mixing within microfluidic devices.[100–102] Besides mixing, the use of microstructures for size-, density-, and deformability-based particle separation has been employed[103–105] and demonstrated for plasma separation and blood cell fractionation.[106,107]

Choi et al.[106] used slanted obstacles to focus blood cells before introducing them in a filtration area with filtration obstacles. Sized based separation was shown for rat blood at 1 µL/min sample flow (0.05 µL/min whole blood) with 58% WBC purity and 210-fold enrichment. Kang et al.[108] used slanted microstructures at the bottom of a microfluidic channel to focus blood cells towards one side while cell free plasma could be extracted from the opposite channel wall.

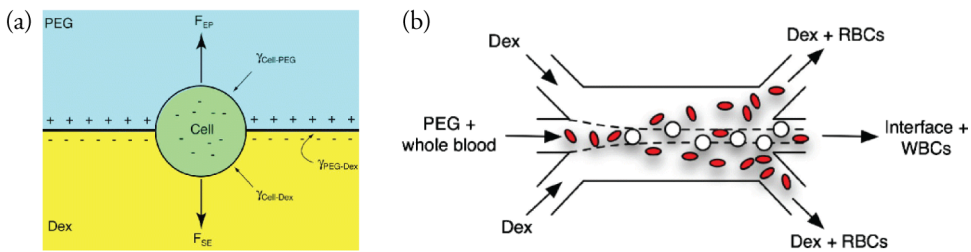

Figure 4.12: Aqeuous two-phase systems (ATPS). (a) Cells within a two-phase system will experience forces based on their particular surface properties and net charge. (b) WBC and RBC display different equilibrium positions within a two-phase system and can be separated from each other. Adopted an reprinted with permission from SooHoo et al.,[109] ©2009, Springer Science Business Media, LLC.

Aqueous two-phase systems (ATPS) use the differential affinity of cells based on their surface properties and net charge to separate cells. A cell placed between two liquids, each with a unique surface energy and charge, will experience both forces from the electrostatic potential as well as the surface energy of the phases (Figure 4.12a). This has been demonstrated to enrich leukocyte

from blood[109] (Figure 4.12b). At a sample throughput of 1 µL/min (0.02 µL/min whole blood) WBC were enriched ~9-times compared to the input sample.

4.2.2 Active cell separation methods

Cell separation methods, such as dielectrophoresis, magnetophoresis, optical tweezers, and acoustophoresis, take advantage of external force fields to manipulate cells in suspensions. Active cell separation methods are often preferred when high sorting efficiencies and purities are required.

Dielectrophoresis

Particles placed in a non-uniform electrical field can experience forces due to an induced or permanent dipole. If the particle is more polarizable than the medium, positive dielectrophoresis (pDEP) moves the particle towards the region of highest electrical field strength. Opposite, if the medium is more polarizable than the particle, negative dielectrophoresis (nDEP) moves the particle towards the electrical field region with the lowest intensity (Figure 4.13a). The magnitude of the DEP force is dependent on the particle volume and the dielectric properties and can be adjusted for example by optimizing the driving voltage, the electrode geometry, and the frequency. DEP has been applied for platelet separation from whole blood,[110] leukocyte enrichment,[111] separation of leukocyte subpopulations,[112] and isolation of circulating tumor cells.[113,114]

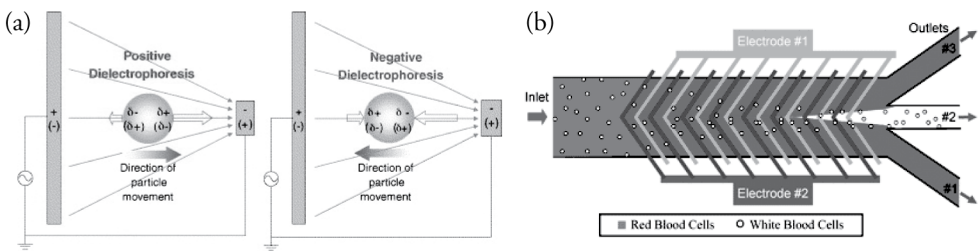

Figure 4.13: Dielectrophoresis (DEP). Particles placed in a non-uniform electrical field are exposed to forces due to an induced or permanent dipol. (a) Depending on the surrounding medium, particles are either moved towards the field maximum (positive DEP) or towards the field minimum (negative DEP). (b) Cells can be separated in DEP based on their size and polarizability as shown for the separation of WBC and RBC. Adopted and reprinted with permission from Doh and Cho,[115] ©2005, Elsevier B.V.; and Han and Frazier,[111] ©Royal Society of Chemistry (2008).

Yang et al.[112] designed a device exploiting the density and dielectric property differences of leukocyte subpopulations. Using a frequency sweep in the DEP field at different frequencies, cells were levitated from the channel wall and eluted from the chamber at different time points depending on the properties. For example, T-lymphocytes were eluted faster than monocytes and could be separated with 92% and 98% purity, respectively. In this case, 50 µL of cells were separated within 21 min (5 min preparation + 16 min separation), accounting for a sample

throughput of 2.3 µL/min and 4600 cells/min. The process is done in a batch process rather than in a continuous process due to the elution mode of the separation (Figure 4.4c).

Fractionation of whole blood into RBC and WBC using DEP was demonstrated by Han and Frazier.[111] RBC experience a higher DEP force and are driven away from WBC (Figure 4.13b). Separation was performed at 50 µL/h, i.e. 0.15 µL/min whole blood equivalent, and separation efficiency into the different outlets was 92.1% for WBC and 87% for RBC.

Piacentini et al.[110] showed the separation of platelets from blood using DEP forces which repels WBC and RBC from the sample fluid while platelets are not affected and can be collected in a separate outlet. A platelet purity of 98.8% and separation efficiency of 98% was achieved with a sample throughput of ~0.013 µL/min with ~2000 cells/min (~33 cells/s).

The label-free manner of DEP can be beneficial in blood cell fractionation. However, cells need to be suspended in specific buffers to achieve separation and sample flow rates are typically very low. The cell viability in these systems depends mainly on the electrical field strength and on the so-called Joule heating effect. Cell death can be induced when used improperly.[116, 117]

Magnetophoresis

Label-free separation of particles and cells can be done by employing their intrinsic magnetophoretic properties. Cells in a magnetic field will experience a force based on their magnetic susceptibility. Han and Frazer[118] showed that RBC can be moved away from a ferromagnetic wire by magnetic forces due to the iron in the hemoglobin found in RBCs. In whole blood WBC behave as diamagnetic particles, while RBC can behave either as paramagnetic or diamagnetic particles depending on their hemoglobin oxygenation. Separation of WBC and RBC from bovine whole blood was shown using a magnetophoretic microseparator[119] (Figure 4.14). Further development of the system enabled separation of WBC from WBC enriched bovine blood with 97.4% efficiency while 93.5% of the RBCs were deflected to the RBC outlet. Sample throughput was 5 µL/h, equivalent of processing 0.008 µL/min whole blood.[120] Jung and Han[121] increased the flow speed by a factor of 4 with similar efficiencies of RBC from 10x diluted whole blood but with decreased WBC efficiency (89.2%).

Seo et al.[122] was able to improve the sample throughput by combining hydrodynamic effects and magnetophoresis. Sample throughput of 1 mL/min was shown for a WBC spiked blood sample, however the high dilution of the blood accounts for an effective throughput of whole blood of ~6.6 µL/min with separation efficiencies of 86.8% and 29.1% for RBC and WBC, respectively.

Besides utilizing the intrinsic magnetic properties of cells, one can also use label-based approaches where magnetic particles are bound to cells of interest and separate them from unlabeled cells in a magnetic field.[123–125] Using beads with different magnetic properties targeting different cell types, isolation of more than one cell type is in principle possible.[126]

Label-free size-based separation of cells is furthermore possible using magnetic liquids in a process termed negative magnetophoresis.[127] When cells are suspended in magnetic liquids and exposed to a magnetic field, the magnetic media will be attracted by the magnetic field gradient and

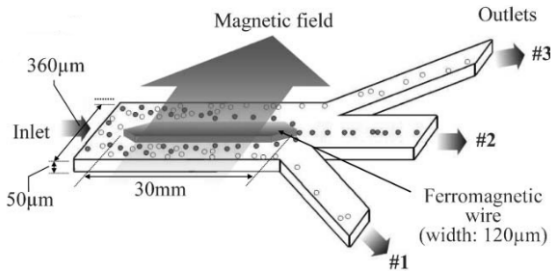

Figure 4.14: Magnetophoresis. In an magnetic field, RBCs can be separated from WBCs based on their intrinsic magnetophoretic properties. RBCs behave either as paramagnetic or diamagnetic particles while WBC display diamagnetic properties. Reprinted with permission from Han and Frazier,[120] ©Royal Society of Chemistry (2006)

pushes the cells away. The force acting on cells is proportional to their sizes, and separation of cells spiked into diluted whole blood has been demonstrated.[128,129] The reported sample throughput was ~0.02 µL/min with ~28 cells/s. For blood cell fractionation, magnetic liquids need to be carefully chosen based on their biocompatibility.

Optical methods

Dielectric particles can be manipulated by a focused laser beam in a method referred to as optical tweezers. Particles entering a beam of light will experience forces due to the optical gradient force as a result from the refraction of light when passing through a particle. Depending on the refractive index of a particle relative to the surrounding medium force is induced on the particle either towards or away from the beam waist i.e. the narrowest part of the focused beam. Optical tweezers are especially useful for single-cell handling and can manipulation objects in the micro-and nano-size.[25]

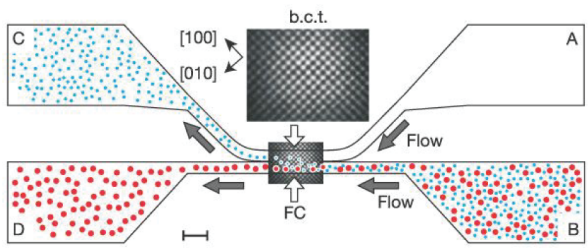

Figure 4.15: Optical tweezers. A microfluidic device with three-dimensional optical lattices can be used to manipulate cells in suspenstion in a continuous mode. A focused beam of laser will move particles based on their size and refrective index. Reprinted with permission from MacDonald et al.,[130] ©2003, Springer Nature.

MacDonald et al.[130] designed a microfluidic device with three-dimensional optical lattice and

demonstrated separation of different sized particles as well as particles with different refractive index (Figure 4.15). Separation efficiencies were >96% with a throughput of ~25 cells/s.

Optical induced dielectrophoresis (ODEP) was also introduced for continuous flow cell separation. Here, a light shining on a photosensitive material will change its' electrical impedance and create a nonuniform electrical field. In this way CTCs were separated from leukocytes based on their size difference.[131,132]

Acoustophoresis

Cells in an ultrasonic standing wave field will experience forces depending on their volume, density, and deformability in relation to their surrounding medium. A detailed description about the physics, practical considerations and applications will be given in the following Chapter 5.

4.3 Summary and conclusion

Passive and active cell separation methods at the microscale have their advantages and disadvantages. Passive methods do not require an external force field and are often simpler in their setup. On the other hand, active methods can employ separation not only on size, density, and deformability but also dependent on the cell's intrinsic properties such as polarizability, compressibility, magnetic properties etc. Furthermore, both active and passive methods can be used in a label-free or marker-based manner. Label-free separation is preferable, as it's independent of specific surface markers and is often cheaper and less time-consuming. Marker specific separation can increase the specificity of the separation methods. In general, different separation methods can be combined freely to achieve the best possible separation outcome. For example, Karabacak et al.[133] combined DLD, inertial focusing and magnetophoresis to isolate CTC from whole blood at a processing rate of 8 mL/h whole blood.

To summarize this chapter, Table 4.2 compares different microfluidic techniques for the separation of WBC and RBC from whole blood in terms of sample throughput and separation efficiency.

Table 4.2: Microfluidic separation methods to separate WBC and RBC from whole blood.

Method (reference)		Blood dilution	Sample processing		Separation performance	
			Flow rate (undiluted)	Cell throughput	RBC	WBC
Filtration	[3]	undiluted	5 µL/min	~4.2x10^5 cells/s *	50% recovery	>97% depletion†
	[38]	200x	20 µL/min (0.1 µL/min)	~8300 cells/s *	60-95% recovery	70-95% depletion†
	[40]	~100x	10 µL/min (0.1 µL/min)	~1666 cells/s	91.2% depletion†	27.4% recovery
Hydrodynamic filtration	[54]	~333x	0.33 µL/min (0.001 µL/min)	~84 cells/s *	~80%	n.a.
	[57]	10x	20 µL/min 2 µL/min	~1.7x10^5 cells/s *	n.a.	n.a.
	[59]	undiluted	0.06 µL/min	~5000 cells/s *	~99.975% depletion †	~98% efficiency ~50% recovery ~2000x enrichment
	[58]	20x	40 µL/min (2 µL/min)	~1.7x10^5 cells/s *	n.a.	~80% efficiency ~80% purity
DLD	[66]	undiluted	~0.017 µL/min	~1400 cells/s *	~99% depletion	99.6% efficiency ~110x enrichment
	[67]	undiluted	23 µL/min‡	~1.92x10^6 cells/s‡	n.a.	~7x enrichment$
Inertia	[89]	~80x	800 µL/min (10 µL/min)	~8.33x10^5 cell/s *	~95% depletion†	98.4% recovery
	[88]	500x	1.8 mL/min (3.6 µL/min)	~3x10^5 cell/s *	94% efficiency	95% efficiency
	[91]	20x	4.8 mL/min £ (240 µL/min)	~2x10^7 cells/s £*	n.a.	n.a.
Bio-mimetic	[96]	undiluted	9.6x10^{-4} µL/min (WBC outlet flow)	n.a.	n.a.	10x increase in WBC concentration 34x enrichment
DEP	[111]	5x diluted	~0.83 µL/min (~0.17 µL/min)	4x10^4 cells/s	87% efficiency	92.1% efficiency
Magnetophoresis	[120]	10x diluted **	~0.083 µL/min (~0.008 µL/min)	~666 cells/s *	93.5% efficiency	97.4% efficiency
	[121]	10x diluted	~0.33 µL/min (~0.033 µL/min)	~2.78x10^5 cells/s *	93.9% efficiency	89.2% efficiency
	[122]	WBC spiked blood	1 mL/min (~6.6 µL/min)	~5.6x10^5 cells/s *	86.8% efficiency	29.1% efficiency
Acousto-phoresis	[152]	Buffy coat	40 µL/min	~5.3x10^6 cells/s	~44% depletion	92% efficiency
	[201]	20x	100 µL/min (5 µL/min)	~1.7x10^5 cells/s	99.95% depletion	87% MNC efficiency 53% MNC purity

* throughput calculated based on flow rate and cell concentration of 5x10^9 cells/mL in whole blood

† compared to input

‡ 6 parallel devices

$ Enrichment in WBC concentration compared to input

** Bovine blood

5

Acoustofluidics

Acoustophoresis is a technique that uses sound to move cells or particles. The interaction of particles in a sound field was already demonstrated in 1866 by Kundt.[134] A pipe filled with cork dust showed specific patterns in the dust when exposed to an acoustic standing wave depending on the applied frequency. The use of sound to move microparticles in combination with microfluidics is termed acoustofluidics. This field has evolved rapidly over the past years and has enabled the development of new approaches for label-free and gentle cell separation methods. This chapter describes the fundamentals of acoustophoresis relevant for the papers included in this thesis.

5.1 Acoustic forces

Sound is a vibration propagating as a wave of pressure through a medium such as gas, liquid, or solid. Humans are able to hear sound in the frequency range of 20Hz to 20kHz. Frequencies below the hearing range are called infrasound and frequencies above are termed ultrasound.

Acoustic waves are longitudinal waves, i.e. they travel in the same direction as the vibration. Two sound waves traveling at the same frequency and amplitude, but opposite direction, create a standing wave when superimposed. The standing wave is not moving in any direction, however nodes with a pressure minimum and anti-nodes with a pressure maximum are formed (Figure 5.1).

Forces in the acoustic standing wave field will induce a movement of particles. The fundamental theory of the acoustic radiation forces has been described throughout the history[135–138] and is summarized more recently by Bruus.[139,140]

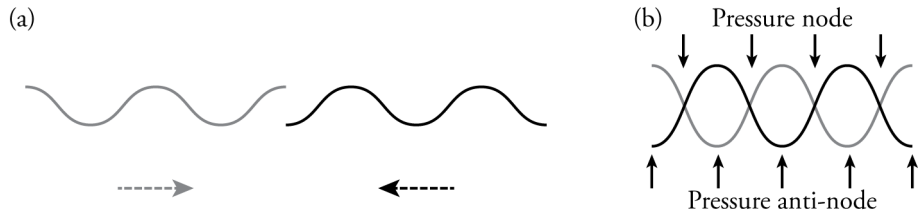

Figure 5.1: Ultrasonic standing wave. (a) Two acoustic waves are traveling at the same frequency and amplitude but in the opposite direction. (b) When superimposed, they form a standing wave with pressure minimum (node) and pressure maximum (anti-node).

Primary acoustic radiation force

Within an acoustic standing wave field, acoustic radiation forces will act on suspended particles. The primary axial radiation force F_y^{rad} for particles with considerably smaller radius than the wavelength can be described by the following equation, assuming a 1-dimensional planar half-standing wave field:

$$F_y^{rad} = 4\pi\phi(\tilde{\kappa},\tilde{\rho})ka^3E_{ac}sin(2ky)$$

$$E_{ac} = \frac{p_a^2}{4\rho_o c_o^2}$$

$$\phi(\tilde{\kappa},\tilde{\rho}) = \frac{1}{3}f_1(\tilde{\kappa}) + \frac{1}{2}f_2(\tilde{\rho}) = \frac{1}{3}\left[\frac{5\tilde{\rho}-2}{2\tilde{\rho}+1} - \tilde{\kappa}\right]$$

$$f_1(\tilde{\kappa}) = 1-\tilde{\kappa} \text{ and } \tilde{\kappa} = \frac{\kappa_p}{\kappa_o}$$

$$f_2(\tilde{\rho}) = \frac{2(\tilde{\rho}-1)}{2\tilde{\rho}+1} \text{ and } \tilde{\rho} = \frac{\rho_p}{\rho_o}$$

Where a is the particle radius, E_{ac} is the acoustic energy density, k is the wave number ($2\pi/\lambda$), y is the particle position in the direction of the wave propagation, ϕ is the acoustic contrast factor (ACF), p_a is the pressure amplitude, c_0 is the speed of sound in the medium, κ_o, ρ_o, κ_p, and ρ_p are the compressibility and density of the fluid and particle, respectively.[139] The primary acoustic radiation force is strongly dependent on the particle size, but also on the density and compressibility of the particle in relation to the surrounding medium. In general, larger and denser particles move faster in the acoustic field while smaller and less dense particles move slower. Based on the sign of the ACF, which is depending on the density and compressibility of the particle in relation to the medium, particles move either to the node or anti-node in the standing wave field (Figure 5.2).

A particle moved by the primary acoustic radiation force will experience a drag force F_d (Stokes' drag) in the opposite direction of the movement. By balancing the two forces, the particle velocity u_{rad} relative to the dynamic viscosity η of the fluid can be derived:

$$F_y^{rad} = F_d = 6\pi\eta a u_{rad}$$

$$u_{rad} = \frac{2\phi}{3\eta} a^2 k E_{ac} sin(2ky)$$

It should be noted from the equation that the particle velocity u_{rad} scales with the square of the particle radius. Therefore, particles can be acoustically discriminated in size-based separations.

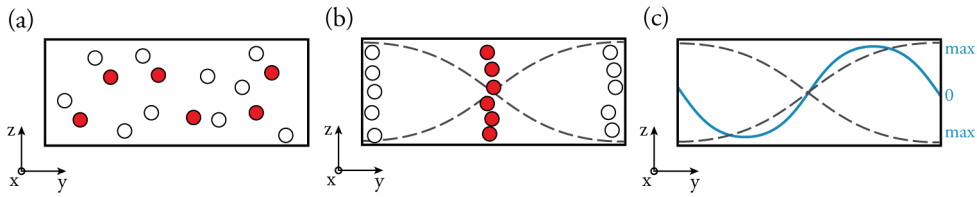

Figure 5.2: Primary acoustic radiation force. (a) Particles randomly distributed within the cross-section of a microfluidic device will experience forces when exposed to an ultrasonic standing wave field. (b) Depending on the acoustic contrast factor (ACF), particles will either move to the pressure node (positive ACF, red particles) or pressure anti-node (negative ACF, white particles). (c) The blue line indicates the strength of the primary acoustic radiation force at different places within the cross-section, where the force is zero at the node and anti-node.

Secondary acoustic radiation force

Within an ultrasonic standing wave field, a secondary acoustic radiation force, the so called Bjerknes force,[141] can occur between particles due to interactions of waves scattered by the suspended particles. For two particles with the same size the secondary acoustic radiation force F_{sec} can be described in a simplified way as:

$$F_{sec} = 4\pi a^6 \left[\frac{(\rho_p - \rho_o)^2 (3cos^2\theta - 1)}{6\rho_o d^4} v^2(y) - \frac{\omega^2 \rho_o (\kappa_p - \kappa_o)^2}{9d^2} p^2(y) \right]$$

where θ is the angle between the center line of the two particles and the direction of the propagation of the acoustic wave, d is the distance between the particles, v is the velocity field, and p is the pressure field[142] (Figure 5.3). Depending on the sign of the force, there is either an attractive interparticle force (F_{sec}<0) or a repulsive force (F_{sec}>0). The force is highly dependent on the distance between particles and is typically much weaker than the primary acoustic radiation force. Only when working with high particle concentrations, as in acoustophoretic whole blood applications, the force needs to be taken into consideration.

Acoustic streaming

Acoustic actuation of a microfluidic device will induce vortices within the fluid known as acoustic streaming. Acoustic streaming can be classified into Eckart streaming, Schlichting streaming, and Rayleigh streaming based on the scale of the induced vortices in relation to the wave length.[144]

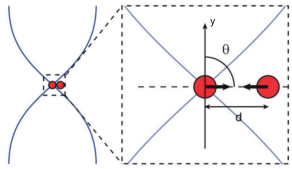

Figure 5.3: Secondary acoustic radiation force. Particles in an ultrasonic standing wave field can experience secondary acoustic radiation forces, so called Bjerknes forces. The force is highly dependent on the distance between particles and can be either attractive ($F_{sec}<0$) or repulsive ($F_{sec}>0$). Reprinted with permission from Hammarström et al.[143] ©Royal Society of Chemistry (2012).

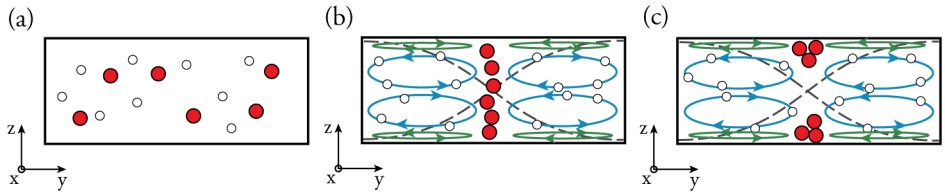

Figure 5.4: Acoustic streaming. The attenuation of an acoustic wave in the viscous boundary layer of the fluid along the channel wall will induce Schlichting streaming (green line) which generates counter vortices in the bulk of the fluid called Rayleigh vortices (blue line). (a) Randomly distributed particles in a microfluidic device will experience forces due to radiation force and the acoustic streaming in an ultrasonic standing wave field. (b) Large particles (red) will move towards the pressure node in the wave field (dashed line) due to the strong acoustic radiation force. For small particles (white) the drag force of the acoustic streaming dominates over the radiation force and they will follow the streamlines of the vortices. (c) Large particles (red) focused at the node will, to some extent, also experience drag forces from the acoustic streaming and will move to the top and bottom of the microchannel within the pressure node.

Eckart streaming occurs due to the dissipation of acoustic energy into the bulk of a liquid along the traveling wave direction. The vortex length scale is of much larger scale than the acoustic wavelength and can be neglected in the herein presented papers. The Schlichting streaming or inner boundary layer streaming is driven by the attenuation of an acoustic wave in the viscous boundary layer of the fluid along the channel wall, parallel to the wave propagation.[145] It occurs within the viscous boundary layer and is <1µm for the acoustofluidic devices presented in this thesis. The powerful Schlichting streaming generates counter vortices in the bulk of the fluid named after Lord Rayleigh[146] (Figure 5.4b). The fluid vortices of the Rayleigh streaming will induce drag forces on particles suspended in the microchannel. For small particles, typically <1µm , the drag force is stronger than the acoustic radiation force, moving the particles within the streaming roles rather than focusing them to the pressure node or anti-node of the standing wave field (Figure 5.4b).[147,148] Larger particles, acoustically focused in the center of a microfluidic device, will also experience drag forces from the acoustic streaming and will move to the top and bottom of the device over time (Figure 5.4c). The diameter of human blood cells is >>1µm and therefore acoustic streaming can be neglected in the applications presented in the papers of this thesis.

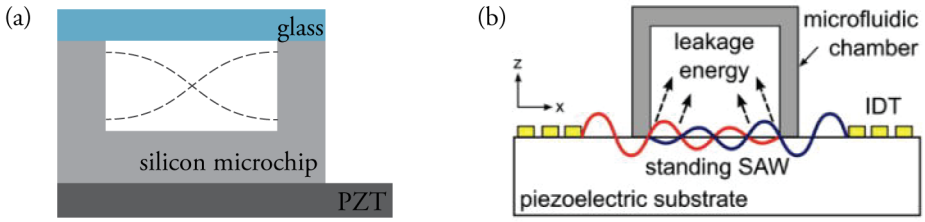

Figure 5.5: Acoustofluidic devices. (a) A bulk acoustic wave (BAW) device is often made of silicon sealed by a glass lid or all in glass and is actuated by a piezoceramic transducer (PZT) attached to the device. (b) Surface acoustic wave (SAW) devices often use soft materials, such as PDMS, and are actuated by integrated interdigitated transducers (IDT) placed on a piezoelectric substrate. Reprinted with permission from Lin et al.,[149] ©Royal Society of Chemistry (2012).

5.2 Types of acoustofluidic devices

Generally, the microscale acoustofluidic community differentiates between bulk acoustic waves (BAW) and surface acoustic waves (SAW). Both techniques manipulate particles with acoustic forces, but the main difference is in the actuation method and the device material (Figure 5.5).

Throughout this thesis, BAW devices were used for the fractionation of blood cells. Devices for BAW are typically fabricated in hard materials such as silicon and/or glass. The microchannel is fabricated to match half a wavelength and the device is actuated using a piezoelectric transducer.

In contrast, SAW devices are often manufactured in soft materials such as PDMS and are actuated by integrated interdigitated transducers (IDT) placed on a piezoelectric substrate. The sound waves travel along the surface of the substrate (traveling surface acoustic wave, TSAW) and can also form standing surface acoustic waves (SSAW) when using two opposing TSAW. SAW devices can be operated at very high frequencies (>9 MHz),[150] making them suitable for precise control of particles. However, due to the nature of SAW dissipating their energy from the substrate surface, commonly less acoustic energy is delivered in the depth of the microchannel as compared to BAW. Therefore, SAW devices for cell separation are often operated at higher voltages and lower flow rate.

5.3 Practical considerations

There are many factors influencing the magnitude of the acoustic radiation force as well as the outcome of the cell and particle manipulation using ultrasonic standing wave fields. Some of the common practical considerations, when designing an acoustic experiment, are described below.

Microchip material

For BAW devices it is desirable to have materials with high acoustic impedance, i.e. density multiplied by speed of sound. A large difference in acoustic impedance between the liquid/solid

interface of the device will allow accumulation of acoustic energy in the acoustic standing wave inside the channel as compared to impedance matched materials. For some common materials, Table 5.1 shows the acoustic impedance and the corresponding reflection coefficient vs. water. Both silicon and glass display a high acoustic impedance and a low acoustic attenuation and are generally considered good materials for BAW devices. Furthermore, silicon microfabrication processes enable precision manufacturing of microchannels, serving as efficient acoustic resonators and integration in flow-through components. Therefore, silicon has been used widely within acoustic cell separation applications.[151–156] Another material used for BAW is glass. Depending on the microfabrication process, channel walls in glass devices can either be rounded[157,158] or straight.[159]

Table 5.1: Acoustic device material properties.[160]

	Density [kg/m^3]	**Speed of sound [m/s]**	**Acoustic Impedance [10^6 kg·s/m^2]**	**Reflection coefficienct vs. water**
Silicon	2331	8490	19.79	0.74
Aluminum	2700	6420	17.33	0.71
Glass (Pyrex)	2230	5647	12.59	0.62
Polystyrene	1050	1700	1.79	0.01
Water (25℃)	997	1497	1.49	

To reduce cost of the microchip devices, other materials such as aluminum[161] and plastic[162–164] are gaining more attention. Micromachine drilling in aluminum and polystyrene reduces the production costs. Aluminum has, similar to silicon, a high acoustic impedance. Polystyrene, on the other hand, has a low acoustic impedance, requiring high voltages and low flow rates[163,164] and separation outcomes are not as good as in silicon devices.[165]

Pre-alignment of cells

Randomly distributed cells within a microfluidic channel will travel at different flow velocities due to the parabolic flow profile (Figure 4.2). Particles flowing close to the top, bottom and side wall of the channel will travel at very low flow speed and will spend more time in the acoustic standing wave field than particles further away from the channel structures, reducing the efficiency and purity of a particle separation. For this reason, Augustsson et al.[156] introduced a pre-alignment step before the acoustic separation of two different sized particles. Using an acoustic standing wave field with two pressure nodes in the horizontal and one pressure node in the vertical plane (Figure 5.6), particles are pre-aligned both in width and height and enter the main separation area at the same starting position and flow velocity. In this way the separation is purely based on the acoustophysical properties of the particles and independent from the starting position. The importance of pre-alignment was shown in several applications[156,166,167] and is used in all the devices presented in the paper of this thesis.

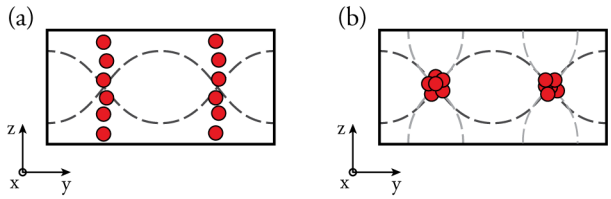

Figure 5.6: Acoustophoretic pre-alignment. (a) Particles within an 1D ultrasonic standing wave field are focused towards the pressure node in the horizontal plane but not vertical plane. (b) Adding a second standing wave field from top to bottom allows to 2D focus particles at the same position and flow velocity.

Particle concentration

At high particle concentrations both the secondary acoustic radiation force and the hydrodynamic particle-particle interactions become more prominent. Particles with lower acoustophoretic mobility are hydrodynamical coupled to faster moving particles and are thus dragged along to the acoustic pressure node, reducing the separation efficiency. Furthermore, it should be noted that the particle mobility within the acoustic standing wave field decreases with increasing particle concentration. Experimental data monitoring the washing efficiency, i.e. the acoustophoretic transport of particles from one liquid into a clean wash fluid, showed a threshold of 10^7-10^8 particles/mL depending on the particle size.[168–170] Ley et al.[171] estimated the theoretical threshold for hydrodynamic coupling in acoustophoresis systems to be at volume fractions of 0.01.

Human undiluted blood has a volume fraction ~0.4 ($5x10^9$ cells/mL) indicating a dominant effect of the hydrodynamic coupling for the separation outcome when processing undiluted whole blood. Paper III shows that the dilution of the blood had a significant impact on the separation outcome. Between 5% blood and 10% blood with volume fractions of ~0.008 and ~0.04, respectively, there was a large drop in the separation performance.

Temperature

A stable temperature is crucial for the separation performance of acoustofluidic devices. Augustsson et al.[172] demonstrated that the acoustic resonance peak shifted by ~1 kHz/°C and that a temperature change of 5 °C completely changed the resonance mode of the device. Actuation of the piezoceramic transducers (PZT) and energy losses withing the PZT material as well as the coupling material of the PZT to the device will induce heating in the system. Therefore, cooling units, using a Peltier element and a feedback loop from a temperature sensor, are typically implemented to stabilize the separation performance[156] and have been used in Paper III, IV and VI of this thesis. Paper V describes an air-cooling unit and a holder with a free-hanging chip to minimize acoustic power dissipation, still enabling effective cooling. High separation performance for sample flow rates of up to 500 µL/min was shown.

Fluid relocation

Not only particles are influenced by the acoustic standing wave field but also liquids with differences in their acoustic impedance laminated next to each other or fluid containing gradients in acoustic impedance. Deshmukh et al.[173] showed that a liquid with higher acoustic impedance will move towards the pressure node (Figure 5.7a). A difference in the impedance of two liquids as low as 0.1% can induce relocation of liquids or stabilize the interface between them. The underlying physics of this phenomena have been described by Karlsen et al.[174]

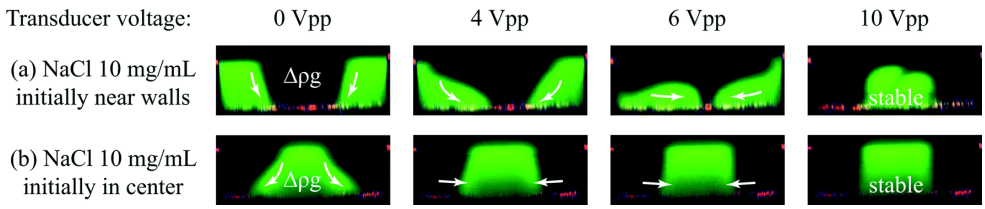

Figure 5.7: Fluid relocation. (a) A liquid with higher acoustic impedance close to the channel walls (green) will relocate with a liquid with lower acoustic impedance in the center of a channel (black) when the ultrasonic standing wave field is turned on. (b) In the reversed case, without ultrasound turned on, the liquid with higher acoustic impedance in the center of the channel will sink due to gravity forces. When the ultrasound is turned on, acoustic radiation forces will stabilize the liquid with higher acoustic impedance in the channel center. Reprinted with permission from Deshmukh et al.,[173] ©Royal Society of Chemistry (2014).

Whole blood has an acoustic impedance of ~1.64×10^6 Pa·s/m while standard saline buffer has ~1.52×10^6 Pa·s/m. If laminated next to each other, the entire whole blood fluid volume will move towards the pressure node without any separation of the different blood cells. Therefore, it is important to adjust the buffer conditions to suppress fluid relocation when working with high concentration of whole blood.[165]

Cell viability and functional capacity

When working with biological samples, the separation method of choice should be as mild as possible without introducing cell death or changing the functional capacity of the cells of interest. Microscale acoustofluidics has been shown to be a gentle method for cell handling.[175] Several studies concluded that acoustophoresis does not influence cell viability,[154,156,176] nor the functional capacity of separated cells[156,176–178] or the colony-forming ability of hematopoietic stem and progenitor cells.[154,177,179] When processing blood components, the concern of platelet activation has also been addressed, however, activation was low and in the range of standard centrifugal processes.[154,178,180]

5.4 Applications

Acoustofluidics at the microscale has been shown useful for a variety of applications. Amongst others, acoustophoresis has been used to focus,[157,181–183] wash,[157,170,180,184,185] concentrate,[186,187] separate,[151,154,156,188] sort,[166,189] and trap[190–193] cells/particles in microfluidic environments.

If two cells differ in their acoustic properties it is possible to separate them. Often size is the main separation criteria, but also density and compressibility related separation has been shown.[194] The acoustophoretic mobility of cells is related to the surrounding medium, so by adjusting the medium properties, cells can change their behavior in acoustic fields. Examples of how acoustophoresis has been explored for the preparation of whole blood components using BAW are given below.

Plasmapheresis

Extraction of plasma from undiluted whole blood using acoustophoresis was first shown by Lenshof et al.[153] Blood cells were acoustically focused towards the centre of the microchannel and sequentially removed at sample flow rates of 80 µL/min producing plasma at 10 µL/min which fulfills the standard requirements from the Council of Europe (Figure 5.8a).

Later on, Tajudin et al.[188] presented a device to produce high quality plasma at a flow rate of 50 µL/min undiluted whole blood and showed an integrated detection of prostate specific antigen on a protein microarray.

Platelet separation

Platelets are smaller and less dense than other blood cells, displaying a lower acoustophoretic mobility, and can thus be acoustically separated from whole blood. Petersson et al.[152] adjusted the medium properties to enable separation of platelets from RBC with efficiencies of 92% and 99% for RBC and platelet, respectively.

Platelets are often accumulated in the centrifugation-based collection of peripheral blood progenitor cell products leading to a significant depletion of donor platelets. Dykes et al.[154] used acoustophoresis to remove excessive platelets (89%) with 98% WBC efficiency at 20 µL/min sample flow (~1 x10^8 cells/mL), see Figure 5.8b.

High-throughput acoustic separation of platelets from undiluted whole blood was demonstrated by Chen et al.[197] At 5 mL/min sample flow 88.4% of the RBC/WBC were removed while recovering 86.2% of the platelets. In a similar device design, Gu et al.[198] increased the sample throughput to 20 ml/min of undiluted whole blood with comparable efficiency and RBC/WBC removal.

Ohlsson et al.[165] showed platelet separation in acoustic impedance matched buffers at 400 µL/min sample flow, equivalent to 4 µL/min whole blood. Platelets were separated with 95% efficiency from 1% whole blood, while removing 99.9% of the blood cells.

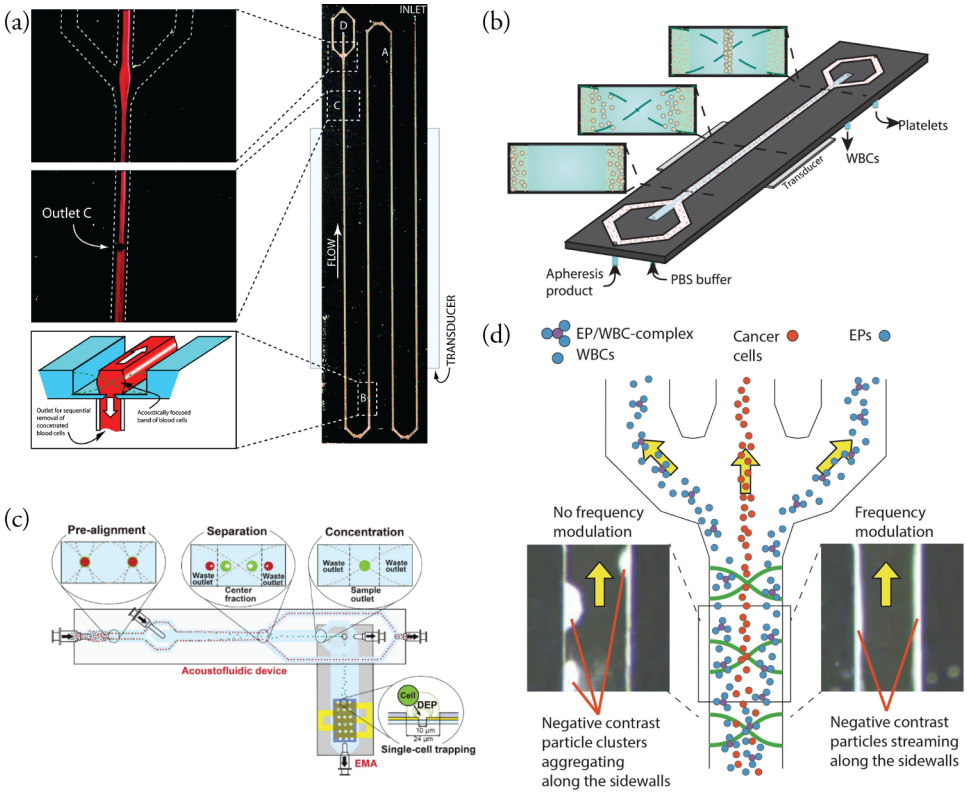

Figure 5.8: Applications for microfluidic acoustofluidics. Examples for blood fractionation using acoustophoresis are: (a) plasmapheresis, i.e. the removal of all cellular components from blood, (b) platelet removal, (c) combined acoustic pre-alignment, separation, and concentration of CTC combined with DEP trapping, and (d) CTC enrichment from WBC using negative contrast particles. Adapted and reprinted with permisson from Lenshof et al.,[153] ©2009, American Chemical Society; Dykes et al.[154] ©2011 Dykes et al.; Antfolk et al.,[195] ©2017, Springer Nature Publishing AG; and Cushing et al.[196] ©2017 Elsevier B.V.

Separation of bacteria

Bacteria detection in whole blood is important in sepsis diagnostic to rapidly identify the pathogen. Ohlsson et al.[199] developed an integrated device for acoustophoretic separation and enrichment of bacteria. The time for bacteria detection in sepsis patients was reduced from 5-6h to <2h. Later on, Ohlsson et al.[165] showed the use of acoustic impedance matched buffers to enable the processing of higher cell concentrations. Bacteria spiked in 5x diluted blood was separated at 400 µL/min sample flow (80 µL/min whole blood equivalent) with 89% bacteria recovery and >99% RBC removal efficiency.

Similar, Dow et al.[163] separated bacteria from 5x diluted blood using a acoustofluidic device made of polystyrene. However, the device performance was modest, only removing 85% of the RBCs while retaining 45-60% of the bacteria, at a 8x lower whole blood throughput as compared to Ohlsson et al.[165]

Gautam et al.[200] took advantage of the relocation of two liquids with different acoustic impedance, where a high density buffer was laminated along the sides and blood/bacteria in the centre stream. As the acoustically induced relocation occurred the bacteria were relocated with the fluid while the blood cells were retained in the channel centre by the acoustic radiation force. Less voltage was necessary to introduce relocation of the fluids and to separate particles from each other as compared to regular acoustophoretic separation; however, the outcome in terms of purity and efficiency is not comparable to what Ohlsson et al.[165] achieved in their system.

Whole blood fractionation

Separation of RBC and WBC is more challenging due to the distinct properties of the cells in the acoustic field. As shown by Urbansky et al.[201] (Paper III) the acoustophoretic mobility of RBC and WBC overlap largely in standard saline solution and separation is therefore not possible under such conditions. Early work by Petersson et al.[152] showed that medium manipulation can indeed change the acoustic behavior of WBC, RBC, and platelets in a buffy coat (WBC enriched blood). Paper III, Urbansky et al.,[201] includes a more extended comparison and theoretical calculations of how medium manipulation changes the acoustophoretic mobility of WBC and RBC. Under optimized medium conditions, mononuclear cells (MNC), i.e. lymphocytes and monocytes, displayed sufficiently reduced acoustophoretic mobility in comparison to RBC and granulocytes, enabling separation. An ~2800x enrichment of MNC/RBC was achieved at 100 µL/min sample flow (5 µL/min whole blood), with MNC purity and recovery of 53% and >60%, respectively.

Circulating tumor cell enrichment

Enrichment of circulating tumor cells (CTC) from blood helps to provide guidance in the prognosis of cancer patients and to further characterize the cancer cells. Based on size differences, Augustsson et al.[156] could isolate CTC spiked into WBC with an efficiency of 97% while depleting 96.1% of the WBC. The sample throughput was 70 µL/min and worked well for concentrations up to 3.25×10^6 cells/mL.

Iranmanesh et al[202] showed separation, isolation, up-concentration and trapping of cells within the same microchip using acoustophoresis at different frequencies. Cancer cells spiked into RBCs where separated with 92.4% efficiency at flow rates of 4.5 µL/min. Anfolk et al.[195] combined pre-alignment, separation and concentration of CTC spiked into peripheral blood mononuclear cells (PBMC) using acoustophoresis and in-line single-cell trapping with DEP to stain for CTCs on chip (Figure 5.8c). The combined device could trap 76% of the initial tumor cells with 0.12% contamination of the PBMC at 80 µL/min sample flow rate.

Another approach was proposed by Cushing et al.[196] using negative acoustic contrast particles (Figure 5.8d). By binding elastomeric particles to WBC and focus them towards the anti-node, tumor cells were simultaneously enriched in the center fraction with efficiencies of >98% and recoveries >85% while reducing the WBC background 52 to 86-fold.

Separation of WBC subsets

Specific WBC subpopulations such as T cells show similar acoustic properties to other WBCs and are therefore difficult to acoustically separate. Using beads which target cells of interest and make them more acoustic mobile as compared to unbound cells, they can be separated from unbound cells. This was successfully shown for CD4 T helper cells[177] and CD8 cytotoxic T cells[179] (Paper I and Paper II).

The main WBC subsets, i.e. lymphocytes, monocytes, and granulocytes, differ slightly in their size and density. Grenvall et al.[203] showed the concurrent isolation of lymphocytes and granulocytes from fixed, non-viable WBC. Monocytes displayed similar acoustic properties as lymphocytes and granulocytes and were therefore harder to separate. Paper V, Urbansky et al.,[204] describes the separation of viable WBC subsets with higher sample throughput, 300 µL/min compared to 8 µL/min for fixed cells by Grenvall et al.,[203] and similar separation outcome.

Lissandrello et al.[205] claimed to purify lymphocytes from diluted whole blood by acoustic separation in a plastic microchannel. Enrichment for the lymphocytes was shown with recoveries <40% while still containing a large fraction of RBC at sample flow rates <35 µL/min.

6

Acoustofluidic device fabrication, assembly and setup

All acoustophoretic microfluidic devices used in this thesis were made of silicon and sealed by a glass lid. Channel structures in silicon can be manufactured precisely in the desired size range with straight vertical channel walls. The significantly higher acoustic impedance of silicon as compared to water allows the generation of an effective acoustic standing wave field for acoustophoretic separation. The microfluidic devices used in Paper I, II, IV, and VI were fabricated in-house by anisotropic wet etching as described below (Figure 6.1), while the devices in Paper III and V were fabricated by Micronit Microtechnologies (Enschede, Netherlands) using Deep Reactive Ion Etching.

6.1 Microfabrication

Mask

A positive photoresist and chromium-covered glass is used as a mask substrate. The channel structure is drawn on a computer, saved in a CAD-file and transferred to the mask using an UV-laser only exposing the channel structures defined in the CAD-file. The UV-exposed photoresist, e.g. the channel structure, is removed by a developer uncovering the chromium underneath which in a next step is etched away.

Oxidation of silicon

Thermal oxidation is used to produce a thin layer (~1µm) of silicon dioxide on the surface of a ⟨100⟩ silicon wafer to protect the silicon and allow etching of the desired channel pattern (Figure 6.1-2). The silicon wafer is heated for 6-8 hours at high temperatures of ~1000℃ in combination with oxygen or water vapour.

Photoresist patterning and oxide etching

After thermal oxidation the silicon wafer is spin coated on one side with a thin layer of positive photoresist (Figure 6.1-3). To reduce stickiness and to harden the photoresist layer the wafer is baked at 80℃ for 25min. Next, the pattern from the mask is transferred by UV light exposure (Figure 6.1-4), the photoresist is developed, a second baking step (120℃ for 30min) hardens the developed photoresist pattern (Figure 6.1-5), the uncovered silicon dioxide is etched away using hydrofluoric acid (HF) (Figure 6.1-6) and the remaining photoresist is removed (Figure 6.1-7).

Anisotropic wet etching

The exposed silicon is etched for a few hours using potassium hydroxide (KOH) at 80℃, transferring the channel structure of desired depth from the silicon oxide layer into the silicon (Figure 6.1-8). The remaining silicon dioxide on the wafer is afterwards removed by HF (Figure 6.1-9). Inlet and outlet holes to the microfluidic channel on the backside of the silicon wafer can be done either in a second process of oxide patterning and anisotropic wet etching or by drilling in the silicon.

Anodic bonding

Finally, the channel structures from the silicon wafer and fitting glass lids are diced and cleaned thoroughly. The glass is anodically bound to the silicon by placing the silicon on a heated plate (450℃), working as one electrode, and placing another electrode on the glass placed on top of the silicon substrate. When high voltage (1000V) is applied, a charge displacement between the silicon and glass will form an electrostatic bond between the substrates, bonding the two pieces together and thereby sealing the channel structure (Figure 6.1-10).

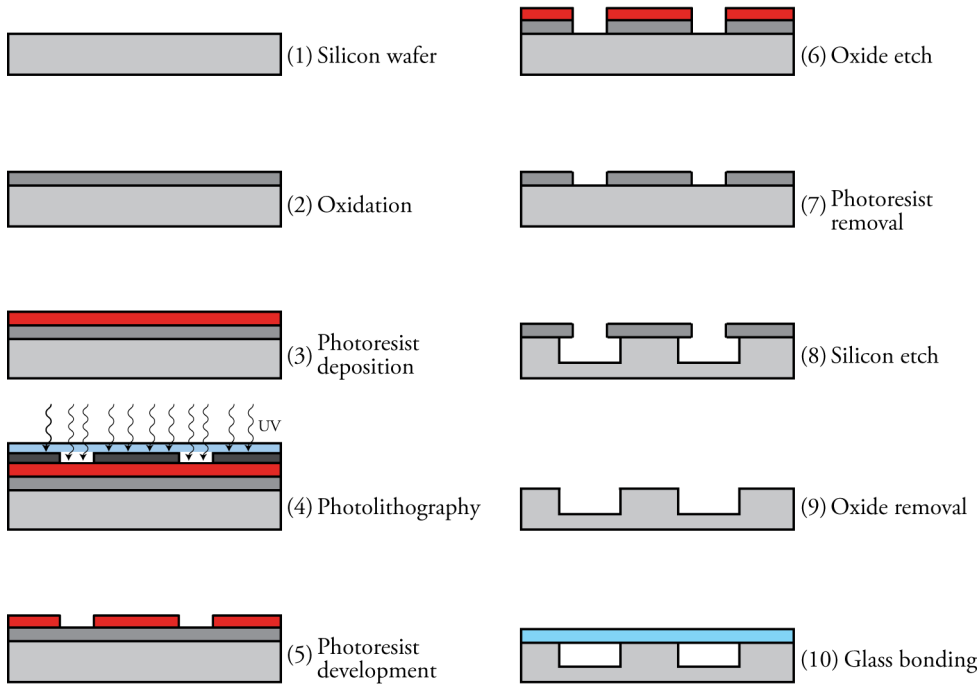

Figure 6.1: Fabrication steps for a silicon microfluidic device using anisotropic wet etching. The channel structure is drawn on a computer and transferred to a mask. A silicon wafer is oxidized, spin-coated with a photoresist and the channel structure is transferred from the mask to the photoresist using UV-light. After oxid etching and removal of the photoresist the actual silicon is etched to create the desired channel structure. Last, the oxide layer is removed and the channel is sealed by a glass lid using anodic bonding.

6.2 Device assembly and experimental setup

Throughout this thesis the device assembly and experimental setup was only slightly modified. A simplified schematic of the setup is shown in Figure 6.2. In general, piezoelectric ceramics (PZT) with resonance frequencies of 2 MHz (main separation channel) and 5 MHz (pre-focusing channel) are glued to the backside of the microfluidic device using superglue. A function generator connected to signal amplifiers is used to drive the PZTs using an oscilloscope to measure the voltage over each transducer. A feedback loop consisting of a Pt1000 resistance temperature detector attached to the PZT at the main separation channel and a Peltier element attached to the acoustophoretic system is used for temperature regulation (Paper III, IV, VI). In Paper V an air-cooling based unit is implemented for equal temperature distribution and removal of excess heat instead of the temperature feed-back loop using a Peltier element. The fluidic setup is either controlled by syringe pumps (Paper I and II) or through an in-hose build pressure-driven system with feedback regulation monitored by flow sensors (Paper III-VI). For visual inspection of the

separation procedure the setup is equipped with a microscope and a camera.

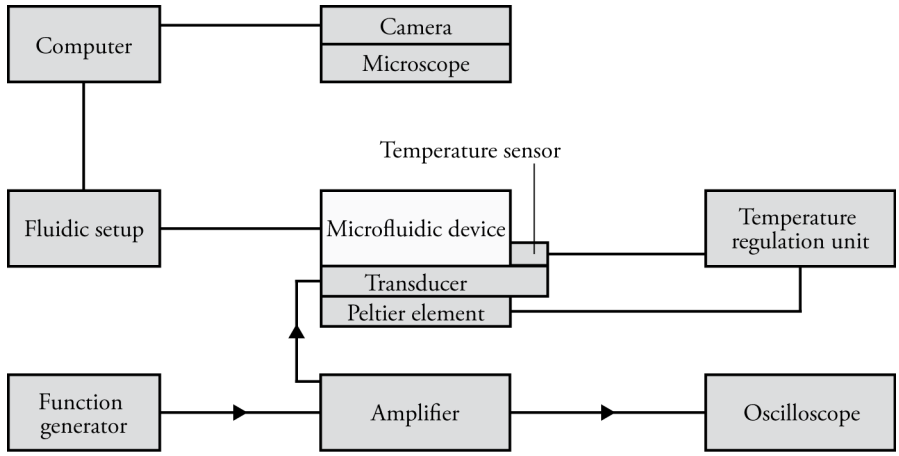

Figure 6.2: Schematic of the experimental setup for acoustophoretic separation as used in this thesis.

7

Summary of included papers

The aim of this thesis was to investigate the use of acoustophoresis for the preparation of blood components and the outcome is summarized within this chapter. To address the challenge of separating specific cell populations from complex samples, different strategies were developed such as changing the acoustophoretic mobility of the cell samples (Paper I-III). Potential use for clinical applications is shown in Paper IV for tumor cell purging in stem cell transplants. Furthermore, our technical developments lead to a system for high throughput separation of three different cell populations simultaneously (Paper V). And finally, Paper VI describes a statistical method to retrieve biomechanical cell properties important for designing the conditions forf acoustophoretic separations.

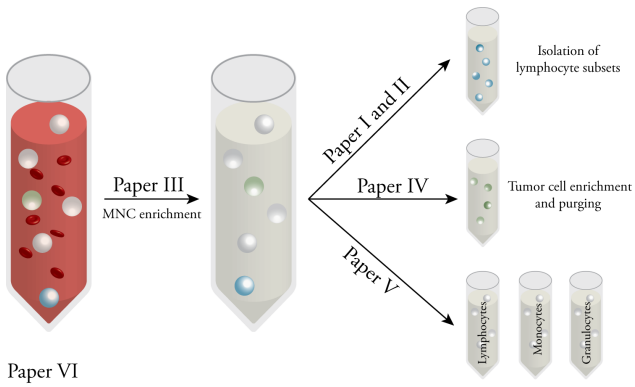

Paper I: Efficient purification of CD4+ lymphocytes from peripheral blood progenitor cell products using affinity bead acoustophoresis

Label-free separation of a specific cell population from a complex biological sample is challenging due to the similar acoustophoretic properties such as cell size and density. Paper I describes the use of affinity beads to target cells of interest and increase the acoustophoretic mobility of the bead/cell complex in relation to unbound cells. The use of a high-density wash buffer allowed bead-bound cells to move to the pressure node in the acoustic standing wave field while creating a barrier for unbound cells (Figure 7.1). In this way, CD4+ T-helper cells were successfully separated from peripheral blood mononuclear cells with high purity (87 $\pm$ 12%) and efficiency (65 $\pm$ 22%). The separation results were comparable to standard magnetic cell sorting. Furthermore, acoustophoresis did not affect cell viability, T cell proliferation and cytokine production, nor the colony forming ability of hematopoietic stem and progenitor cells of non-target cells post separation.

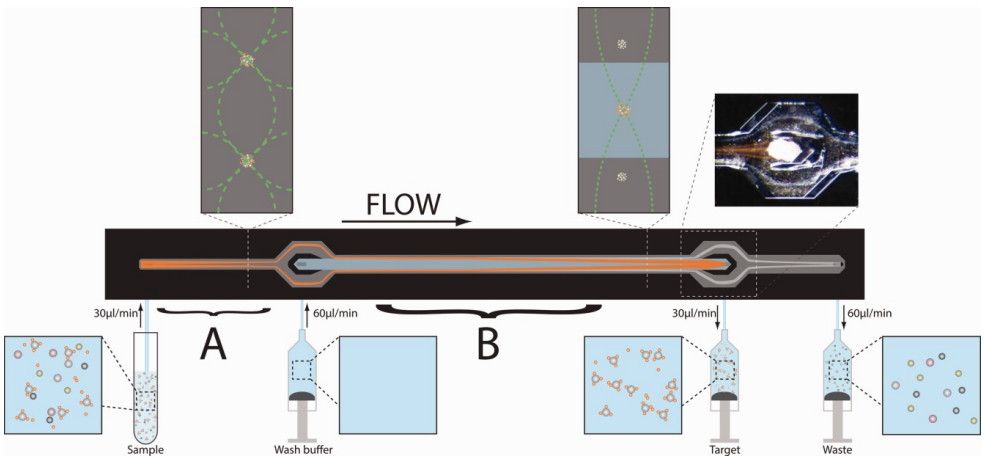

Figure 7.1: Affinity-bead-mediated acoustophoretic separation. Cells with overlapping acoustophoretic mobilities can be separated from each other via affinity bead acoustophoresis. Cells of interest are labeled with beads (orange) and create large and dense bead-cell complexes. These complexes move faster in the acoustic field than unbound cells (white). Using a high-density wash buffer creates an additional barrier for unbound cells, so that only the bead-cell complexes can cross this barrier with the acoustic radiation force moving them to the center of the microchannel. Unbound cells stay close in the original buffer stream and are collected through the waste outlet.

Paper II: Affinity-bead-mediated enrichment of CD8+ lymphocytes from peripheral blood progenitor cell products using acoustophoresis

Paper II is a continuation of Paper I, describing the use of affinity-bead-mediated acoustophoresis for the enrichment of CD8+ lymphocytes from peripheral blood mononuclear cells. The device was able to separate less frequent cell populations at a two-times increased sample throughput (600,000 cells/min and 60 µL/min) compared to Paper I, with preserved separation performance in terms of purity and efficiency of 91 ± 8% and 63%, respectively. Again, no influence of the acoustophoretic separation was observed for cell viability, T cell proliferation capacity and clonogenic capacity of hematopoietic progenitor cells. Furthermore, a more detailed description of the need of high-density wash buffer for the separation outcome is included (Figure 7.2).

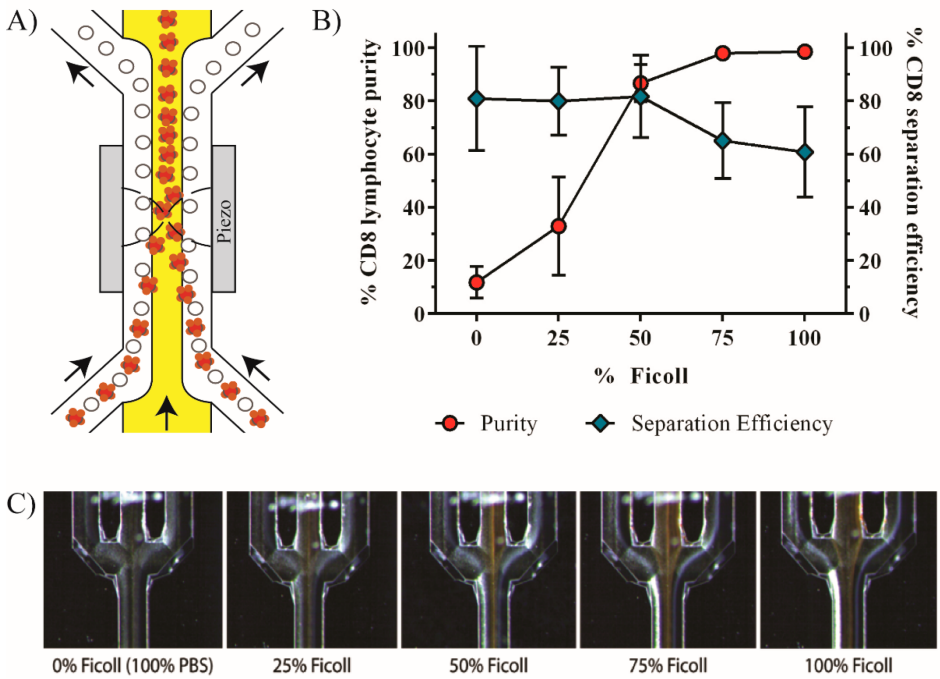

Figure 7.2: Acoustophoretic separation of bead-labeled cells. (a) Cells of interest are labeled with beads to create large bead-cell complexes (red). Due to their higher acoustophoretic mobility they are able to cross a high-density barrier (yellow) and can be acoustically focused towards the center of the microchannel and are separated from unbound cells (white). (b) The separation efficiency and purity of targeted CD8+ lymphocytes are shown for different wash buffer densities with (c) corresponding microscopic images from the separation process at the outlet bifurcation where the orange/brown stream comprise the cell bead complex and the white stream line the unbound cells.

Paper III: Rapid and effective enrichment of mononuclear cells from blood using acoustophoresis

Mononuclear cells (MNC), i.e. monocytes and lymphocytes, are routinely isolated from whole blood for clinical and research applications. Acoustophoreitc separation of MNC from red blood cells (RBC) is challenging due to their overlapping acoustophoretic mobility in standard saline buffer. Paper III shows the use of density modified buffers to change the acoustophoretic mobilities of the cells and enable acoustic separation (Figure 7.4). At optimized buffer conditions, MNC were enriched 2800x in relation to RBCs with >60% recovery, and 53.3 ± 14.5% MNC purity. Acoustophoresis has been shown to be a label-free and continuous microfluidic approach as an alternative to the labor-intensive and time-consuming standard techniques with a sample throughput of 10^5 cells/s, equivalent to 5 µL/min undiluted whole blood.

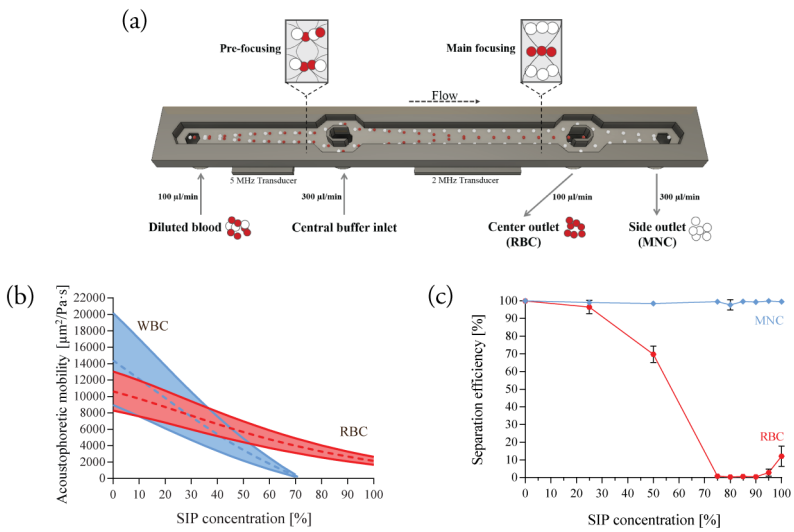

Figure 7.3: Enrichment of mononuclear cells (MNC) from red blood cells (RBC). (a) Schematic of the acoustophoretic separation of MNC from RBC using a microfluidic device with a pre-alignment step and a main-focusing channel. (b) Theoretical calculations of the mobility of white blood cells (WBC) and RBC in medium with varying stock isotonic Percoll (SIP) concentration. (c) Experimental data showing the successful separation of MNC and RBC at increased SIP concentrations.

Paper IV: Label-free neuroblastoma cell separation from hematopoietic progenitor cell products using acoustophoresis - towards cell processing of complex biological samples

Circulating tumor cells in stem cell collections provide important diagnostic and prognostic information and have been associated to contribute to relapse after stem cell transplantation. A model system of peripheral blood and progenitor cell (PBPC) products spiked with cultured neuroblastoma cells (NBC) demonstrated the possibility for label-free acoustophoretic enrichment of viable NBC (Figure 7.4). The separation could be aimed for high tumor cell separation efficiency (60-97%) or high NBC purities of up to 90% depending on the downstream application. Purging of PBPC products was able with 1.5-2.3 log depletion of NBC, however, with a low PBPC efficiency (>43%). A sample throughput of 100 µL/min was used, and separation efficiencies were stable up to cell concentrations of 10^6 cells/mL (~1700 cells/s). Proliferation capacities and viability were not compromised after acoustic separation demonstrating a promising step forward to label-free, non-contact cell separation of complex cell products.

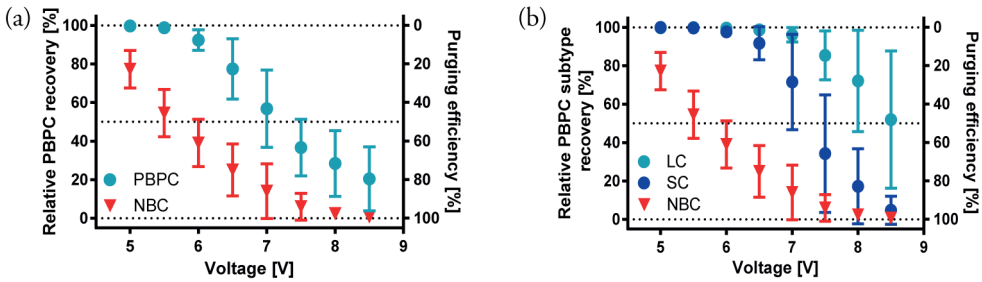

Figure 7.4: Acoustophoretic enrichment of tumor cells. Neuroblastoma cells (NBC) spiked in peripheral blood and progenitor cell (PBPC) products could be acoustically enriched in a label-free, continuous way. (a) Shown are the purging efficiency of NBC and separation efficiency for PBPC at increasing amplitude of the acoustic standing wave. (b) A more detailed graph shows the separation efficiency for different subpopulations of interest, namely lymphocytes (LC) and stem cells (SC), at different voltages in relation to the purging efficiency of NBC.

Paper V: Label-free separation of leukocyte subpopulations using high throughput multiplex acoustophoresis

Temperature variations in the acoustofluidic device are known to influence the separation performance. Paper V describes the design of a chip holder with air cooling and a free hanging chip for optimal thermal distribution and minimal chip clamping for reduced acoustic power dissipation, yielding an improved acoustophoresis performance. Concurrent separation of three distinct particle populations (Figure 7.5) was possible for sample flow rates up to 500 µL/min (~$4.2x10^5$ beads/s) with high efficiencies (>95.4%) and purities (>96.3%). Also, fractionation of viable white blood cells (WBC) was shown for sample flow rates up to 300 µL/min (5000 cells/s) with high purities (>90%) for lymphocytes and granulocytes. Due to the overlapping acoustophoretic mobility of monocytes their purity was compromised by the high sample flow rate from 71.8 ± 10.1% at 100 µL/min to 20.9 ± 10% at 300 µL/min.

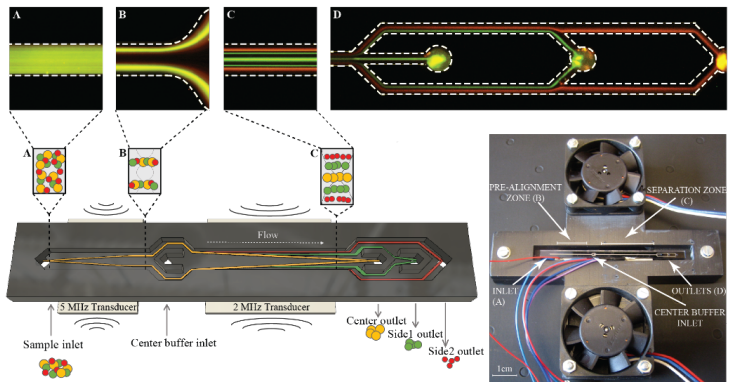

Figure 7.5: High throughput, label-free separation in multiplex acoustophoresis. The schematic illustrates the multiplex separation in an acoustofluidic device. Randomly distributed cells (A) are pre-aligned in width and height (B) before entering the main separation channel (C) where they are separated from each other based on their acoustophysical properties. Fluorescence images on the top illustrate the separation process of 2, 4, and 7 µmpolystyrene beads throughout the microchip while the photograph on the lower right corner shows the design of the cooling unit using fans for optimal thermal distribution.

Paper VI: Statistic Estimation of Biomechanical Cell Compressibility Based on Acoustophoretic Separation Data

Acoustofluidic separation of different cell types is known to be based on the cells' properties such as size, density, and compressibility in relation to their surrounding medium. However, in practice it is not always straight forward to predict the acoustophoretic mobility of different cell types in different medium conditions as e.g. compressibility data scarcely is available whereas density data is more often so. In Paper VI a theoretical approach is presented to estimate cell properties, such as the compressibility, based on acoustophoretic separation data. Cells with unknown acoustic properties were run through an acoustofluidic microchannel together with reference beads at varying amplitudes (Figure 7.7). Based on the separation behavior of the cells in relation to the reference beads with known acoustic properties, an estimation of the cells' compressibility was possible. The data is comparable to previously published estimations while requiring considerably less cells for the experiments than macroscopic methods, enabling the acoustophoretic characterization of rare cells. The theoretical model takes into account the distribution of cell properties and the system parameters such as hydrodynamics, acoustic radiation force, drag enhancement, and acoustic streaming. Compressibility measurements of three tumor cell lines as well as WBC as a population, and the WBC subpopulations: lymphocytes, granulocytes and monocytes and finally a head and neck squamous cell line were made using the new method.

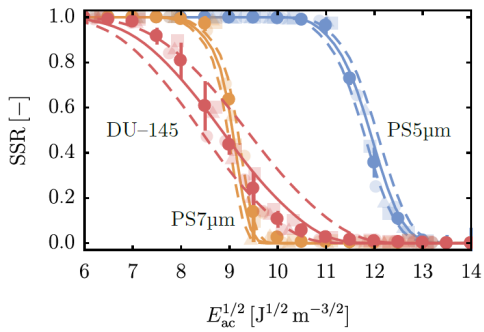

Figure 7.6: Acoustophoretic separation data for statistic estimation of a cell's compressibility. Cells with unknown acoustic properties were run through an acoustofluidic microdevice together with reference beads at varying applied voltages, which is proportional to the acoustic energy density Eac1/2. SSR describes the side-stream recovery for the different beads and cells. Polystyrene (PS) microbeads at 5 and 7µm with known properties were used to calibrate the acoustophoretic device and experimental data (dots) was fit with the theoretical data (lines) using compressibility for the cells of interest as the fitting parameter.

8

Conclusion and Outlook

Preparation of whole blood components is routinely done for various clinical and research related applications, such as in diagnostics, blood transfusion, stem cell transplantation, and immunotherapy. Separation methods are available both at the macroscale and microscale, all having their advantages and disadvantages. In comparison to macroscale cell handling methods, microfluidic system can handle small sample volumes and, due to the controlled fluid behaviour in small volumes, flow patterns can be predicted and cells within liquids can be precisely control by external forces.

This thesis showed the use of microscale acoustofluidics for preparation of whole blood components. Microscale acoustofluidics has gained increasing attention over the last decades, describing the fundamentals and physics of the method as well as showing technical improvements of typical device setups. This knowledge has been implemented and further extended in the applications presented in the papers of this thesis. In general, microscale acoustofluidics is a gentle and continuous method for handling of biological samples. In this thesis both affinity-based and label-free acoustophoretic implementations were demonstrated successfully for blood cell fractionation. In agreement to theoretical calculations, separation of cells with similar acoustophoretic mobility was enabled by buffer density modulation. Furthermore, a way to statistically estimate unknown acoustic properties of particles based on experimental data is provided in the thesis. This allows to better predict the behaviour of cells within an acoustic sound field and enables a more straightforward way to optimize experimental conditions for cell separation.

Upscaling of sample throughput is a common challenge when working at the microscale. A way of increasing sample throughput in acoustophoretic devices was shown by integrating an air cooling system, allowing to operate the device isothermally at an increased acoustic energy. Further research needs to be done to provide clinically relevant sample throughputs in the range of millilitres per min of whole blood

As shown in this thesis, microscale acoustofluidics is a promising technology for blood cell fractionation. Integration with other microfluidic devices for sample preparation or analysis could further improve the impact of acoustophoretic cell separation in clinical and research related applications.

9

Populärvetenskaplig sammanfattning

Celler är byggstenar för alla levande organismer. De bygger människokroppens struktur, tar upp näring frå n mat, hämtar syre från luften och omvandlar detta till energi för kroppen. Människokroppen består av trillioner celler och varje cell behöver sin egen energiförsörjning. Blod är vätskan som cirkulerar genom kroppen för att ta med sig alla viktiga näringskomponenter till cellerna och ta bort avfallsprodukter. Blod består av en bärvätska som kallas plasma samt olika blodkroppar. De olika blodkroppar som ingår i helblod är röda blodkroppar, vita blodkroppar och blodplättar. Alla har sina egna viktiga funktioner. Röda blodkroppar tar hand om syretillförseln i kroppen genom att transportera syre från lungorna till cellerna och ta med sig koldioxid tillbaka från cellerna till lungorna. Vita blodkroppar har hand om kroppens immunförsvar när bakterier, virus eller annat främmande material tar sig in i kroppen. Blodplättar hjälper till att stoppa blödningar i kroppens blodkärl genom att klumpa ihop sig (aggregera) och täcka det öppna såret.

Blod innehåller också viktig information om människors välbefinnande. Till exempel kan antalet vita blodkroppar berätta om en person är sjuk medan mängden av röda blodkroppar kan vara ett tecken på järnbrist eller olika sjukdomar. För att få information från blodet och även kunna bedriva forskning på de olika blodkropparna för att förstå deras funktion eller använda dem i kliniska tillämpningar är det nödvändigt att separera de olika blodkomponenterna från varandra.

Denna avhandling undersöker användningen av en teknik som kallas akustofores för att dela upp blod i sina komponenter. Akustofores kommer från engelska acoustophoresis som betyder att flytta (migrera) med ljud. Man använder ultraljud vilket är ljud med frekvenser högre än gränsen för människans hörsel. Celler i ett ultraljudsfält migrerar till olika platser i ljudfältet beroende på deras fysikaliska egenskaper såsom storlek, densitet och kompressibilitet, men också

beroende på den omgivande vätskans egenskaper. Akustofores görs ofta i en liten kanal som kallas mikrokanal som vanligen är mindre än tjockleken av ett kreditkort och så tunn som ett blyertsstift. Fördelen med att använda en sådan liten kanal är att mängden blod som behövs minskar markant, men även att flödet i kanalen är mer förutsägbart, lättare att hantera och att cellerna förflyttar sig huvudsakligen på grund av krafterna i det akustiska fältet. Figure 9.1 visar förenklat hur akustofores fungerar.

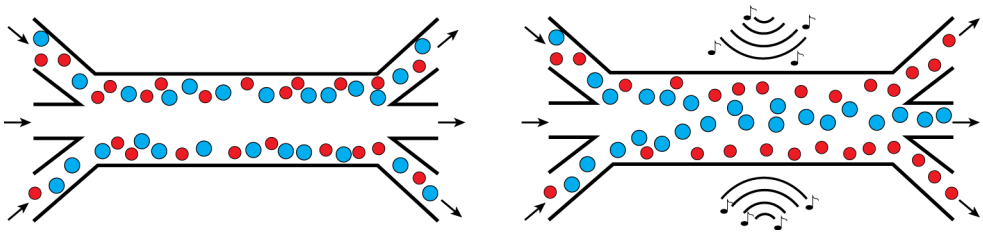

Figure 9.1: Principen för akustofores. Bilderna visar hur olika celler flödar genom en mikrokanal. Flödesriktining är från vänster till höger och visas med pilarna. På den vänstra bilden finns inget ultraljud närvarande och cellerna håller sig nära kanalväggarna, dvs. ingen separation av de olika cellerna är möjlig. Den högra bilden visar hur partiklar beter sig i ett akustiskt fält. De stora, blåa cellerna är mer påverkade av den akustiska kraften och flyttas snabbare till mitten av mikrokanalen medan de små, röda cellerna inte är lika mycket påverkade och håller sig nära kanalväggarna. I slutet av kanalen går cellerna till olika utlopp och därmed separeras de från varandra.

En del av avhandlingen fokuserar på cellerna som kan användas för att behandla cancerpatienter. Människor med blodcancer är i behov av stamcellstransplantationer. Om det är möjligt används patientens eget blod och man behöver isolera en specifik celltyp som kallas stamceller som hjälper patienten att återhämta sig efter cancerbehandlingen. Stamcellerna är mycket sällsynta i blodet och deras akustiska egenskaper liknar andra celler i blodet, därför behöver man justera blodprovet för att kunna använda akustofores för att separera stamcellerna. Avhandlingen beskriver en metod för att använda små sfäriska partiklar som fäster vid cellerna man är intresserad av för att göra dem större och förändra deras akustika egenskaper. Det blir därmed möjligt att isolera cell-partikel-komplexen från andra celler utan att påverka cellernas livskraft och funktionalitet. Systemet har testats att fungerar på att separera specifika vita blodkroppar från stamcellspreparationer och visar därmed möjligheten att isolera stamceller från andra blodkroppar i framtiden. Akustofores kan även användas att separera tumörceller som cirkulerar i blodet av cancerpatienter. I detta avseendet visar avhandlingen principen för hur man kan använda akustofores för att isolera tumörceller från stamcellspreparationer i syfte att minska risken för att återge tumörceller till patienten. De separerade tumörcellerna kan användas för att karaktärisera tumören. Separationen fungerar utan att förändra cellerna eller den omgivande vätskan då den är baserad på skillnaden i akustiska storleksmässiga egenskaper mellan tumörceller och andra vita blodkroppar.

Som tidigare beskrivits spelar vita blodkroppar en viktig roll i immunförsvaret. Att isolera dem från blod är inte så lätt eftersom det finns betydligt färre vita blodkroppar än röda blodkroppar, bara en av tusen blodkroppar är en vit blodkropp. Dessa skiljer sig inte heller nämnvärt i deras

akustiska egenskaper från röda blodkroppar. Avhandlingen analyserar hur man kan använda olika vätskor som omger blodcellerna för att ändra deras rörlighet i ett akustiskt fält. När man byter den omgivande vätskan till en med högre densitet sänks rörelsehastigheten på vita blodkroppar så att de inte rör sig så fort som de röda blodkropparna och därmed kan dessa separeras från varandra. Nästa del av avhandlingen visar hur man kan skala upp processhastigheten och separera flera olika grupper av vita blodkroppar från varandra samtidigt vid relativt höga flödeshastigheter. Detta öppnar på sikt möjligheter för kliniska tillämpningar som kräver hantering av större blodvolymer.

Den sista delen av avhandlingen visar ett sätt att estimera cellernas olika akustiska egenskaper med hjälp av separationsdata och statistiska beräkningar. Om man känner till cellernas akustiska egenskaper blir det lättare att förutsäga deras beteende i ett akustiskt fält och därmed hur man bästa skall anpassa sitt akustoforessystem för att utföra separationer av olika celltyper. Alla metoder som visas i denna avhandling ger en uppfattning om hur man kan använda akustofores för att separera olika blodkomponenter. Metodens mångsidighet demonstreras i det flertalet användbara tillämpningar inom kliniska eller forskningsrelaterade ämnen som redovisas. Akustofores kan hjälpa till att minimera blodvolymen som behövs för en cellseparation. Tekniken kan automatiseras och göras användarvänlig och den kan enkelt integreras med andra analystekniker. Sammantaget har akustofores en stor potential inom kliniska och bioanalytiska tillämpningar.

10

Acknowledgements

Time is flying when you have fun and it's hard to believe that my time as a PhD student already comes to an end. It all started back in 2012 when I needed to find a place to do my diploma thesis. For some time, I had the idea to come to Sweden and luckily, there was a position for me. One thing led to another…

There are so many people to thank and so many opportunities to be grateful for. First of all, I would like to express my deepest gratitude towards my supervisor Thomas Laurell. Thank you for giving me the opportunity to join your research group, giving me the freedom to explore while always having an open ear for questions and concerns. Thanks to my co-supervisor Andreas Lenshof, introducing me to the acoustic setup and guiding me through all the time from a master student to a PhD student. Without my co-supervisor Stefan Scheding I wouldn't even be here in Lund. I started my journey in his group, before he passed me on to "the dark side".

Thanks to all my current and former colleagues for making the working environment so enjoyable! Thanks to my first master student, office colleague and friend Franziska Olm for the endless hours of coffee time and discussions; thanks to Eva Undvall for the lovely office time together and your friendship; to Cecilia Magnusson for the positive lab spirit, the great fika and lunch company and all the baby talk; Klara Petersson, for the great office time together; Valentina, Axel and Lee, our newest members at BMC.

I would also like to thank all the people at the department: Johan Nilsson for heading the department and welcoming everyone to the BME group; Per Augustsson and Pelle Ohlsson for great discussions, all your enthusiasm about acoustics and for being stubborn talking Swedish to me; the biomechanics group for Monday fikas and lunches; Maria Antfolk for interesting discussions and warning me to stay away from CTCs; Ola Jakobsson for your great humor; Axel Tojo, Linus Jonsson and Matthias Ohlin for helping me with the device manufacturing, holder designs and

last minute fixes; Fabio Garofalo for magically bringing more equations in our life; Désirée Jarebrant, Ulrika Westerdahl, Ammi Lindgren, Eva Everitt, and Malgo Luczak for all the help with administration; Anna Fornell and Carl Johanesson for planning the acoustofluidics course; and everyone else from the acoustofluidics group for great discussions.

All my current and former colleagues at Stefan's lab for all the cell related advice: Dimitra, Hongzhe, Roshanak, Hooi Ching, Marie, Sandro, Pauline, Hanne. Thanks to Anna and Helen at the hematology department for the bloody work.

To the people at AcouSort introducing me to the "real" world in a company!

A special thanks to the people from LAPASO, for great meetings and collaborations, creating a perfect environment to exchange knowledge and to think outside the box: Stefan, Bao, Kushagr, Elisabeth, Miguel, Carlos, Clément, Walter, Vitor, Geneviève, Laura, Simone, Jason, Ewan and all the other LAPASO partners and fellows.

Outside work I would like to thank my friends for their support and all the fun time together: Aneta, Ingvi, Pamela, Johan, Evelyn, Filip, Marc, Arian, Besar, Lisa, Raul, Vy, Louis, Dimitra, Vykis, Roula, Victor, Barbara, and Marina. And my friends in Germany, who are still part of my journey after such a long time: Verena, Dani, Claudia, Jana, Steffi, and Matze.

Lastly and most importantly, a special thanks to my family: my parents for their unlimited support, my brother Björn for all the fights and always being there for me when needed, to my extended family in Germany and Lebanon, to Paul for always being on my side and to our lovely daughter Emma, the most wonderful thing that has ever happened to me.

References

[1] John F. Dailey. *Dailey's Notes on blood*. Medical Consulting Group, 2002.

[2] Kathleen Deska Pagana and Timothy J. Pagana. *Mosby's Diagnostic and Laboratory Test Reference - eBook*. Elsevier Health Sciences, 10 edition, 2010.

[3] Palaniappan Sethu, Aaron Sin, and Mehmet Toner. Microfluidic diffusive filter for apheresis (leukapheresis). *Lab on a Chip*, 6(1):83–89, 2006.

[4] Blausen.com staff. Medical gallery of Blausen Medical 2014. *WikiJournal of Medicine*, 1(2), 2014.

[5] HK Walker, WD Hall, and JW Hurst, editors. *Clinical Methods: The History, Physical, and Laboratory Examinations*. Butterworth Publishers, 3 edition, 1990.

[6] Kevin W. Cushing, Fabio Garofalo, Cecilia Magnusson, Lars Ekblad, Henrik Bruus, and Thomas Laurell. Ultrasound Characterization of Microbead and Cell Suspensions by Speed of Sound Measurements of Neutrally Buoyant Samples. *Analytical Chemistry*, 89(17):8917–8923, 2017.

[7] Sally V. Rudmann. *Textbook of Blood Banking and Transfusion Medicine*. Elsevier Health Sciences, 2 edition, 2005.

[8] Gerard J. Tortora and Bryan Derrickson. *Principles of Anatomy & Physiology*. Wiley, 14 edition, 2014.

[9] Kara Rogers, editor. *Blood: Physiology and Circulation*. The Rosen Publishing Group, 2010.

[10] Barbara H. Estridge and Anna P. Reynolds. *Basic Clinical Laboratory Techniques*. Cengage Learning, 6 edition, 2011.

[11] Matthew G Krebs, Jian-Mei Hou, Tim H Ward, Fiona H Blackhall, and Caroline Dive. Circulating tumour cells: their utility in cancer management and predicting outcomes. *Therapeutic advances in medical oncology*, 2(6):351–65, 2010.

[12] T. Felzmann, V. Witt, D. Wimmer, G. Ressmann, D. Wagner, P. Paul, K. Hiittner, and G. Fritsch. Monocyte enrichment from leukapharesis products for the generation of DCs by plastic adherence, or by positive or negative selection. *Cytotherapy*, 5(5):391–398, 2003.

[13] Anthony A Marfin and Thomas H Price. Granulocyte Transfusion Therapy. *Journal of Intensive Care Medicine*, 30(2):79–88, 2015.

[14] Bruce L. Levine, James Miskin, Keith Wonnacott, and Christopher Keir. Global Manufacturing of CAR T Cell Therapy. *Molecular Therapy - Methods & Clinical Development*, 4:92–101, 2017.

[15] Marc J Shapiro. To filter blood or universal leukoreduction: what is the answer? *Critical Care*, 8(Suppl 2):S27–S30, 2004.

[16] A D Sharma, G Sreeram, T Erb, H P Grocott, and T F Slaughter. Leukocyte-reduced blood transfusions: perioperative indications, adverse effects, and cost analysis. *Anesthesia and analgesia*, 90(6):1315–23, 2000.

[17] S T Baksaas, V Videm, T E Mollnes, T Pedersen, H Karlsen, and J L Svennevig. Effects on complement, granulocytes and platelets of a leukocyte-depletion filter during in vitro extracorporeal circulation. *Scandinavian cardiovascular journal : SCJ*, 31(2):73–7, 1997.

[18] Jin-Hee Cho, Ju Hee Choi, Mina Hur, Hee-Won Moon, Chul Min Park, and Yeo-Min Yun. Comparison of two leukocyte reduction filters for whole blood derived platelets. *Transfusion and Apheresis Science*, 47(1):21–25, 2012.

[19] Susan R. Mikkelsen and Eduardo Cortón. *Bioanalytical Chemistry*. John Wiley & Sons, 2004.

[20] A. Bøyum. Isolation of Lymphocytes, Granulocytes and Macrophages. *Scandinavian Journal of Immunology*, 5:9–15, 1976.

[21] J. Lundahl, G. Halldén, M. Hallgren, C.M. Sköld, and J. Hed. Altered expression of CD11b/CD18 and CD62L on human monocytes after cell preparation procedures. *Journal of Immunological Methods*, 180(1):93–100, 1995.

[22] Stefan Zahler, Christian Kowalski, Andreas Brosig, Christian Kupatt, Bernhard F. Becker, and Eckehart Gerlach. The function of neutrophils isolated by a magnetic antibody cell separation technique is not altered in comparison to a density gradient centrifugation method. *Journal of Immunological Methods*, 200(1-2):173–179, 1997.

[23] Anna C. Söderström, Mads Nybo, Christian Nielsen, and Pernille J. Vinholt. The effect of centrifugation speed and time on pre-analytical platelet activation. *Clinical Chemistry and Laboratory Medicine (CCLM)*, 54(12):1913–1920, 2016.

[24] Kiho Son, Manali Mukherjee, Brendan A.S. McIntyre, Jose C. Eguez, Katherine Radford, Nicola LaVigne, Caroline Ethier, Francis Davoine, Luke Janssen, Paige Lacy, and Parameswaran Nair. Improved recovery of functionally active eosinophils and neutrophils using novel immunomagnetic technology. *Journal of Immunological Methods*, 449:44–55, 2017.

[25] Wonhee Lee, Peter Tseng, and Dino Di Carlo. *Microtechnology for Cell Manipulation and Sorting*. Springer, 2016.

[26] Leon W.M.M. Terstappen, Heidi Meiners, and Michael R. Loken. A rapid sample preparation technique for flow cytometric analysis of immunofluorescence allowing absolute enumeration of cell subpopulations. *Journal of Immunological Methods*, 123(1):103–112, 1989.

[27] Desmond A. McCarthy and Marion G. Macey. *Cytometric Analysis of Cell Phenotype and Function*. Cambridge University Press, 2001.

[28] Qingjun Pan, Ling Ye, Zhenzhen Deng, Lu Li, and Huafeng Liu. Effects of Red Blood Cell Lysing Solutions on the Detection of Peripheral Basophils of Healthy Normals and Sle Patients by Flow Cytometry. *Journal of Immunoassay and Immunochemistry*, 35(4):368–377, 2014.

[29] Anthony D. Ho, Rainer Haas, and Richard E. Champlin, editors. *Hematopoietic Stem Cell Transplantation*. CRC Press, 2000.

[30] Kerry Atkinson, Richard Champlin, Jerome Ritz, Willem E. Fibbe, Per Ljungman, and Malcom K. Brenner. *Clinical Bone Marrow and Blood Stem Cell Transplantation*. Cambridge University Press, 2004.

[31] Brian D Plouffe, Shashi K Murthy, and Laura H Lewis. Fundamentals and application of magnetic particles in cell isolation and enrichment: a review. *Reports on progress in physics. Physical Society (Great Britain)*, 78(1):016601, 2015.

[32] Sim Siong Leong, Swee Pin Yeap, and JitKang Lim. Working principle and application of magnetic separation for biomedical diagnostic at high- and low-field gradients. *Interface focus*, 6(6):20160048, 2016.

[33] Julien Picot, Coralie L Guerin, Caroline Le Van Kim, and Chantal M Boulanger. Flow cytometry: retrospective, fundamentals and recent instrumentation. *Cytotechnology*, 64(2):109, 2012.

[34] Andreas Radbruch. *Flow Cytometry and Cell Sorting*. Springer Science & Business Media, 2013.

[35] Albert Folch. *Introduction to BioMEMS*. CRC Press, 2012.

[36] Daniel R. Gossett, Westbrook M. Weaver, Albert J. Mach, Soojung Claire Hur, Henry Tat Kwong Tse, Wonhee Lee, Hamed Amini, and Dino Di Carlo. Label-free cell separation and sorting in microfluidic systems. *Analytical and Bioanalytical Chemistry*, 397(8):3249–3267, 2010.

[37] Mehmet Toner and Daniel Irimia. Blood-on-a-chip. *Annual Review of Biomedical Engineering*, 7:77–103, 2005.

[38] Hong Miao Ji, Victor Samper, Yu Chen, Chew Kiat Heng, Tit Meng Lim, and Levent Yobas. Silicon-based microfilters for whole blood cell separation. *Biomedical Microdevices*, 10(2):251–257, 2008.

[39] Peter Wilding, Larry J. Kricka, Jing Cheng, Gia Hvichia, Mann A. Shoffner, and Paolo Fortina. Integrated Cell Isolation and Polymerase Chain Reaction Analysis Using Silicon Microfilter Chambers. *Analytical Biochemistry*, 257(2):95–100, 1998.

[40] Xing Chen, Da Fu Cui, Chang Chun Liu, and Hui Li. Microfluidic chip for blood cell separation and collection based on crossflow filtration. *Sensors and Actuators B: Chemical*, 130(1):216–221, 2008.

[41] Xiang Li, Weiqiang Chen, Guangyu Liu, Wei Lu, and Jianping Fu. Continuous-flow microfluidic blood cell sorting for unprocessed whole blood using surfacemicromachined microfiltration membranes. *Lab on a Chip*, 14(14):2565–2575, 2014.

[42] Sara Thorslund, Oliver Klett, Fredrik Nikolajeff, Karin Markides, and Jonas Bergquist. A hybrid poly(dimethylsiloxane) microsystem for on-chip whole blood filtration optimized for steroid screening. *Biomedical Microdevices*, 8(1):73–79, 2006.

[43] Kiana Aran, Alex Fok, Lawrence A. Sasso, Neal Kamdar, Yulong Guan, Qi Sun, Akif Ündar, and Jeffrey D. Zahn. Microfiltration platform for continuous blood plasma protein extraction from whole blood during cardiac surgery. *Lab on a Chip*, 11(17):2858, 2011.

[44] Max M Gong, Brendan D Macdonald, Trung Vu Nguyen, Kinh Van Nguyen, and David Sinton. Field tested milliliter-scale blood filtration device for point-of-care applications. *Biomicrofluidics*, 7(4):44111, 2013.

[45] Pin-Chuan Chen, Chih-Chun Chen, and Kung-Chia Young. Characterization of thermoplastic microfiltration chip for the separation of blood plasma from human blood. *Biomicrofluidics*, 10(5):054112, 2016.

[46] Yousang Yoon, Seonil Kim, Jusin Lee, Jaewoong Choi, Rae-Kwon Kim, Su-Jae Lee, Onejae Sul, and Seung-Beck Lee. Clogging-free microfluidics for continuous size-based separation of microparticles. *Scientific Reports*, 6(1):26531, 2016.

[47] Yong Tae Kim, Kyun Joo Park, Seyl Kim, Soon Ae Kim, Seok Jae Lee, Do Hyun Kim, Tae Jae Lee, and Kyoung G. Lee. Portable vibration-assisted filtration device for on-site isolation of blood cells or pathogenic bacteria from whole human blood. *Talanta*, 179:207–212, 2018.

[48] Y Miyazaki, S Nomura, T Miyake, H Kagawa, C Kitada, H Taniguchi, Y Komiyama, Y Fujimura, Y Ikeda, and S Fukuhara. High shear stress can initiate both platelet aggregation and shedding of procoagulant containing microparticles. *Blood*, 88(9):3456–3464, 1996.

[49] Jawaad Sheriff, João Silva Soares, Michalis Xenos, Jolyon Jesty, and Danny Bluestein. Evaluation of Shear-Induced Platelet Activation Models Under Constant and Dynamic Shear Stress Loading Conditions Relevant to Devices. *Annals of Biomedical Engineering*, 41(6):1279–1296, 2013.

[50] Yasuhiko Iwasaki, Asako Mikami, Kimio Kurita, Nobuhiko Yui, Kazuhiko Ishihara, and Nobuo Nakabayashi. Reduction of surface-induced platelet activation on phospholipid polymer. *Journal of Biomedical Materials Research*, 36(4):508–515, 1997.

[51] Sang Ho Ye, Junji Watanabe, Yasuhiko Iwasaki, and Kazuhiko Ishihara. Antifouling blood purification membrane composed of cellulose acetate and phospholipid polymer. *Biomaterials*, 24(23):4143–4152, 2003.

[52] Timothy A. Crowley and Vincent Pizziconi. Isolation of plasma from whole blood using planar microfilters for lab-on-a-chip applications. *Lab on a Chip*, 5(9):922, 2005.

[53] Masumi Yamada, Megumi Nakashima, and Minoru Seki. Pinched Flow Fractionation: Continuous Size Separation of Particles Utilizing a Laminar Flow Profile in a Pinched Microchannel. *Analytical chemistry*, 76:5465–5471, 2004.

[54] Junya Takagi, Masumi Yamada, Masahiro Yasuda, and Minoru Seki. Continuous particle separation in a microchannel having asymmetrically arranged multiple branches. *Lab on a Chip*, 2005.

[55] Asger Laurberg Vig and Anders Kristensen. Separation enhancement in pinched flow fractionation. *Applied Physics Letters*, 93(20):203507, 2008.

[56] Tomoki Morijiri, Satoshi Sunahiro, Masashi Senaha, Masumi Yamada, and Minoru Seki. Sedimentation pinched-flow fractionation for size-and density-based particle sorting in microchannels. *Microfluidics and Nanofluidics*, 11(1):105–110, 2011.

[57] Masumi Yamada and Minoru Seki. Hydrodynamic filtration for on-chip particle concentration and classification utilizing microfluidics. *Lab on a Chip*, 5(11):1233–1239, jun 2005.

[58] Masumi Yamada, Wataru Seko, Takuma Yanai, Kasumi Ninomiya, and Minoru Seki. Slanted, asymmetric microfluidic lattices as size-selective sieves for continuous particle/cell sorting. *Lab on a Chip*, 17(2):304–314, 2017.

[59] Virginia VanDelinder and Alex Groisman. Perfusion in Microfluidic Cross-Flow: Separation of White Blood Cells from Whole Blood and Exchange of Medium in a Continuous Flow. *Analytical Chemistry*, 79(5):2023–2030, 2007.

[60] Lotien Richard Huang, Edward C. Cox, Robert H. Austin, and James C. Sturm. Continuous Particle Separation Through Deterministic Lateral Displacement. *Science*, 304(5673):987–990, 2004.

[61] Stefan H Holm, Jason P Beech, Michael P Barrett, and Jonas O Tegenfeldt. Separation of parasites from human blood using deterministic lateral displacement. *Lab on a Chip*, 11(7):1326–1332, 2011.

[62] Raymond Quek, Vinh Le, and K.-H Chiam. Separation of deformable particles in deterministic lateral displacement devices. *PHYSICAL REVIEW E*, 83:56301, 2011.

[63] Jason P Beech, Stefan H Holm, Karl Adolfsson, and Jonas O Tegenfeldt. Sorting cells by size, shape and deformability. *Lab on a Chip*, 12(6):1048–1051, 2012.

[64] David Holmes, Graeme Whyte, Joe Bailey, Nuria Vergara-Irigaray, Andrew Ekpenyong, Jochen Guck, and Tom Duke. Separation of blood cells with differing deformability using deterministic lateral displacement. *Interface Focus*, 4(6):20140011, 2014.

[65] Mingliang Jiang, Kostyantyn Budzan, and German Drazer. Fractionation by shape in deterministic lateral displacement microfluidic devices. *Microfluidics and Nanofluidics*, 19(2):427–434, 2015.

[66] John A Davis, David W Inglis, Keith J Morton, David A Lawrence, Lotien R Huang, Stephen Y Chou, James C Sturm, and Robert H Austin. Deterministic hydrodynamics: taking blood apart. *Proceedings of the National Academy of Sciences of the United States of America*, 103(40):14779–14784, 2006.

[67] David W Inglis, Megan Lord, and Robert E Nordon. Scaling deterministic lateral displacement arrays for high throughput and dilution-free enrichment of leukocytes. *Journal of Micromechanics and Microengineering*, 21(5):054024, 2011.

[68] Fabio Fachin, Philipp Spuhler, Joseph M. Martel-Foley, Jon F. Edd, Thomas A. Barber, John Walsh, Murat Karabacak, Vincent Pai, Melissa Yu, Kyle Smith, Henry Hwang, Jennifer Yang, Sahil Shah, Ruby Yarmush, Lecia V. Sequist, Shannon L. Stott, Shyamala Maheswaran, Daniel A. Haber, Ravi Kapur, and Mehmet Toner. Monolithic Chip for High-throughput Blood Cell Depletion to Sort Rare Circulating Tumor Cells. *Scientific Reports*, 7(1):10936, 2017.

[69] L B Leverett, J D Hellums, C P Alfrey, and E C Lynch. Red blood cell damage by shear stress. *Biophysical journal*, 12(3):257–73, 1972.

[70] Jiaming Hua, Larry E. Erickson, Tian-Yih Yiin, and Larry A. Glasgow. A Review of the Effects of Shear and Interfacial Phenomena on Cell Viability. *Critical Reviews in Biotechnology*, 13(4):305–328, 1993.

[71] Kevin Loutherback, Joseph D'Silva, Liyu Liu, Amy Wu, Robert H. Austin, and James C. Sturm. Deterministic separation of cancer cells from blood at 10 mL/min. *AIP Advances*, 2(4):042107, 2012.

[72] Trung S. H. Tran, Bao D. Ho, Jason P. Beech, and Jonas O. Tegenfeldt. Open channel deterministic lateral displacement for particle and cell sorting. *Lab Chip*, 17(21):3592–3600, 2017.

[73] Zongbin Liu, Rui Chen, Ying Li, Jianqiao Liu, Ping Wang, Xuefeng Xia, and Lidong Qin. Integrated Microfluidic Chip for Efficient Isolation and Deformability Analysis of Circulating Tumor Cells. *Advanced Biosystems*, 2(10):1800200, 2018.

[74] Joseph D'Silva, Robert H. Austin, and James C. Sturm. Inhibition of clot formation in deterministic lateral displacement arrays for processing large volumes of blood for rare cell capture. *Lab on a Chip*, 15(10):2240–2247, 2015.

[75] Kevin Loutherback, Kevin S. Chou, Jonathan Newman, Jason Puchalla, Robert H. Austin, and James C. Sturm. Improved performance of deterministic lateral displacement arrays with triangular posts. *Microfluidics and Nanofluidics*, 9(6):1143–1149, 2010.

[76] Ji-chul Hyun, Jaeyub Hyun, Semyung Wang, and Sung Yang. Improved pillar shape for deterministic lateral displacement separation method to maintain separation efficiency over a long period of time. *Separation and Purification Technology*, 172:258–267, 2017.

[77] G. Segré and A. Silberberg. Radial Particle Displacements in Poiseuille Flow of Suspensions. *Nature*, 189(4760):209–210, 1961.

[78] Dino Di Carlo. Inertial microfluidics. *Lab on a Chip*, 9(21):3038–3046, 2009.

[79] Jian Zhou and Ian Papautsky. Fundamentals of inertial focusing in microchannels. *Lab on a Chip*, 13(6):1121–1132, 2013.

[80] Joseph M. Martel and Mehmet Toner. Inertial Focusing in Microfluidics. *Annual Review of Biomedical Engineering*, 16(1):371–396, 2014.

[81] Ga-Yeong Kim, Jong-In Han, and Je-Kyun Park. Inertial Microfluidics-Based Cell Sorting. *BioChip Journal*, 12(4):257–267, 2018.

[82] Sathyakumar S. Kuntaegowdanahalli, Ali Asgar S. Bhagat, Girish Kumar, and Ian Papautsky. Inertial microfluidics for continuous particle separation in spiral microchannels. *Lab on a Chip*, 9(20):2973–2980, 2009.

[83] S A Berger, L Talbot, and L. S Yao. FLOW IN CURVED PIPES. Technical report, 1983.

[84] Ali Asgar, S Bhagat, Sathyakumar S Kuntaegowdanahalli, and Ian Papautsky. Continuous particle separation in spiral microchannels using dean flows and differential migration. 2008.

[85] Soojung Claire Hur, Sung-Eun Choi, Sunghoon Kwon, and Dino Di Carlo. Inertial focusing of non-spherical microparticles. *Applied Physics Letters*, 99(4):044101, 2011.

[86] Mahdokht Masaeli, Elodie Sollier, Hamed Amini, Wenbin Mao, Kathryn Camacho, Nishit Doshi, Samir Mitragotri, Alexander Alexeev, and Dino Di Carlo. Continuous Inertial Focusing and Separation of Particles by Shape. *Physical Review X*, 2(3):031017, 2012.

[87] Soojung Claire Hur, Nicole K. Henderson-MacLennan, Edward R. B. McCabe, and Dino Di Carlo. Deformability-based cell classification and enrichment using inertial microfluidics. *Lab on a Chip*, 11(5):912–920, 2011.

[88] Nivedita Nivedita and Ian Papautsky. Continuous separation of blood cells in spiral microfluidic devices. *Biomicrofluidics*, 7(5):54101, 2013.

[89] Lidan Wu, Guofeng Guan, Han Wei Hou, Ali Asgar. S. Bhagat, and Jongyoon Han. Separation of Leukocytes from Blood Using Spiral Channel with Trapezoid Cross-Section. *Analytical Chemistry*, 84(21):9324–9331, 2012.

[90] Zhenlong Wu, Yu Chen, Moran Wang, and Aram J. Chung. Continuous inertial microparticle and blood cell separation in straight channels with local microstructures. *Lab on a Chip*, 16(3):532–542, 2016.

[91] Jun Zhang, Dan Yuan, Ronald Sluyter, Sheng Yan, Qianbin Zhao, Huanming Xia, Say Hwa Tan, Nam Trung Nguyen, and Weihua Li. High-Throughput Separation of White Blood Cells From Whole Blood Using Inertial Microfluidics. *IEEE Transactions on Biomedical Circuits and Systems*, 11(6):1422–1430, 2017.

[92] Han Wei Hou, Chayakorn Petchakup, Hui Min Tay, Zhi Yang Tam, Rinkoo Dalan, Daniel Ek Kwang Chew, King Ho Holden Li, and Bernhard O. Boehm. Rapid and label-free microfluidic neutrophil purification and phenotyping in diabetes mellitus. *Scientific Reports*, 6:29410, 2016.

[93] Harisha Ramachandraiah, Helene A. Svahn, and Aman Russom. Inertial microfluidics combined with selective cell lysis for high throughput separation of nucleated cells from whole blood. *RSC Advances*, 7(47):29505–29514, 2017.

[94] Albert J Mach, Jae Hyun Kim, Armin Arshi, Soojung Claire Hur, and Dino Di Carlo. Automated cellular sample preparation using a Centrifuge-on-a-Chip. *Lab on a Chip*, 11(17):2827–2834, jan 2011.

[95] H L Goldsmith, G R Cokelet, and P Gaehtgens. Robin Fåhraeus: evolution of his concepts in cardiovascular physiology. *The American journal of physiology*, 257(3 Pt 2):H1005–15, 1989.

[96] Sergey S Shevkoplyas, Tatsuro Yoshida, Lance L Munn, and Mark W Bitensky. Biomimetic Autoseparation of Leukocytes from Whole Blood in a Microfluidic Device. *Analytical Chemistry*, 77(3):933–937, 2005.

[97] Hui Min Tay, Rinkoo Dalan, King Ho Holden Li, Bernhard O. Boehm, and Han Wei Hou. A Novel Microdevice for Rapid Neutrophil Purification and Phenotyping in Type 2 Diabetes Mellitus. *Small*, 14(6):1702832, 2018.

[98] Han Wei Hou, Lidan Wu, Diana P. Amador-Munoz, Miguel Pinilla Vera, Anna Coronata, Joshua A. Englert, Bruce D. Levy, Rebecca M. Baron, and Jongyoon Han. Broad spectrum immunomodulation using biomimetic blood cell margination for sepsis therapy. *Lab on a Chip*, 16(4):688–699, 2016.

[99] Han Wei Hou, Hiong Yap Gan, Ali Asgar S. Bhagat, Leon D. Li, Chwee Teck Lim, and Jongyoon Han. A microfluidics approach towards high-throughput pathogen removal from blood using margination. *Biomicrofluidics*, 6(2):024115, 2012.

[100] Abraham D. Stroock, Stephan K.W. Dertinger, Armand Ajdari, Igor Mezic, Howard A. Stone, and George M. Whitesides. Chaotic Mixer for Microchannels. *Science*, 295(5555):647–651, 2002.

[101] Peter B. Howell, Jr., David R. Mott, Stephanie Fertig, Carolyn R. Kaplan, Joel P. Golden, Elaine S. Oran, and Frances S. Ligler. A microfluidic mixer with grooves placed on the top and bottom of the channel. *Lab on a Chip*, 5(5):524, 2005.

[102] T.M. Floyd-Smith, J.P. Golden, P.B. Howell, and F.S. Ligler. Characterization of passive microfluidic mixers fabricated using soft lithography. *Microfluidics and Nanofluidics*, 2(2):180–183, 2006.

[103] Sungyoung Choi and Je-Kyun Park. Continuous hydrophoretic separation and sizing of microparticles using slanted obstacles in a microchannel. *Lab on a Chip*, 7(7):890, 2007.

[104] Chia-Hsien Hsu, Dino Di Carlo, Chihchen Chen, Daniel Irimia, and Mehmet Toner. Microvortex for focusing, guiding and sorting of particles. *Lab on a Chip*, 8(12):2128, 2008.

[105] Sungyoung Choi, Seungjeong Song, Chulhee Choi, and Je-Kyun Park. Microfluidic Self-Sorting of Mammalian Cells to Achieve Cell Cycle Synchrony by Hydrophoresis. *Analytical Chemistry*, 81(5):1964–1968, 2009.

[106] Sungyoung Choi, Seungjeong Song, Chulhee Choi, and Je-Kyun Park. Continuous blood cell separation by hydrophoretic filtration. *Lab on a Chip*, 7(11):1532–1538, jan 2007.

[107] Sungyoung Choi, Taeyun Ku, Seungjeong Song, Chulhee Choi, and Je-Kyun Park. Hydrophoretic high-throughput selection of platelets in physiological shear-stress range. *Lab on a Chip*, 11(3):413–418, 2011.

[108] Dong-Hyun Kang, Kyongtae Kim, and Yong-Jun Kim. Plasma extraction rate enhancement scheme for a real-time and continuous blood plasma separation device using a sheathless cell concentrator. *Journal of Micromechanics and Microengineering*, 28(2):025008, 2018.

[109] Jeffrey R. SooHoo and Glenn M. Walker. Microfluidic aqueous two phase system for leukocyte concentration from whole blood. *Biomedical Microdevices*, 11(2):323–329, 2009.

[110] Niccolò Piacentini, Guillaume Mernier, Raphaël Tornay, and Philippe Renaud. Separation of platelets from other blood cells in continuous-flow by dielectrophoresis field-flow-fractionation. *Biomicrofluidics*, 5(3):34122–341228, 2011.

[111] Ki-Ho Han and A Bruno Frazier. Lateral-driven continuous dielectrophoretic microseparators for blood cells suspended in a highly conductive medium. *Lab on a Chip*, 8(7):1079–1086, 2008.

[112] Jun Yang, Ying Huang, Xiao-Bo Wang, Frederick F Becker, and Peter R C Gascoyne. Differential Analysis of Human Leukocytes by Dielectrophoretic Field-Flow-Fractionation. *Biophysical Journal*, 78(5):2680–2689, 2000.

[113] F F Becker, X B Wang, Y Huang, R Pethig, J Vykoukal, and P R Gascoyne. Separation of human breast cancer cells from blood by differential dielectric affinity. *Proceedings of the National Academy of Sciences of the United States of America*, 92(3):860–4, 1995.

[114] Waqas Waheed, Anas Alazzam, Bobby Mathew, Nicolas Christoforou, and Eiyad Abu-Nada. Lateral fluid flow fractionation using dielectrophoresis (LFFF-DEP) for size-independent, label-free isolation of circulating tumor cells. *Journal of Chromatography B*, 1087-1088:133–137, 2018.

[115] Il Doh and Young-Ho Cho. A continuous cell separation chip using hydrodynamic dielectrophoresis (DEP) process. *Sensors and Actuators A: Physical*, 121(1):59–65, 2005.

[116] Darren S. Gray, John L. Tan, Joel Voldman, and Christopher S. Chen. Dielectrophoretic registration of living cells to a microelectrode array. *Biosensors and Bioelectronics*, 19(7):771–780, 2004.

[117] Cheng Qian, Haibo Huang, Liguo Chen, Xiangpeng Li, Zunbiao Ge, Tao Chen, Zhan Yang, Lining Sun, Cheng Qian, Haibo Huang, Liguo Chen, Xiangpeng Li, Zunbiao Ge, Tao Chen, Zhan Yang, and Lining Sun. Dielectrophoresis for Bioparticle Manipulation. *International Journal of Molecular Sciences*, 15(10):18281–18309, 2014.

[118] Ki-Ho Han and A Bruno Frazier. Continuous magnetophoretic separation of blood cells in microdevice format. *Journal of Applied Physics*, 96(10):5797–5802, 2004.

[119] Ki-Ho Han and A B Frazier. Diamagnetic capture mode magnetophoretic microseparator for blood cells. *Journal of Microelectromechanical Systems*, 14(6):1422–1431, 2005.

[120] Ki-Ho Han and A Bruno Frazier. Paramagnetic capture mode magnetophoretic microseparator for high efficiency blood cell separations. *Lab on a Chip*, 6(2):265–273, 2006.

[121] Jinhee Jung and Ki-Ho Han. Lateral-driven continuous magnetophoretic separation of blood cells. *Applied Physics Letters*, 93(22):223902, 2008.

[122] Hye-Kyoung Seo, Yong-Ho Kim, Hyun-Ok Kim, and Yong-Jun Kim. Hybrid cell sorters for on-chip cell separation by hydrodynamics and magnetophoresis. *Journal of Micromechanics and Microengineering*, 20(9):095019, sep 2010.

[123] Brian D. Plouffe, Madhumita Mahalanabis, Laura H. Lewis, Catherine M. Klapperich, and Shashi K. Murthy. Clinically Relevant Microfluidic Magnetophoretic Isolation of Rare-Cell Populations for Diagnostic and Therapeutic Monitoring Applications. *Analytical Chemistry*, 84(3):1336–1344, 2012.

[124] Jeong Won Park, Nae-Rym Lee, Sung Mok Cho, Moon Youn Jung, Chunhwa Ihm, and Dae-Sik Lee. Microdevice for Separation of Circulating Tumor Cells using Embedded Magnetophoresis with V-shaped Ni-Co Nanowires and Immuno-nanomagnetic Beads. *ETRI Journal*, 37(2):233–240, 2015.

[125] Hyungseok Cho, Jinho Kim, Chang-Wan Jeon, and Ki-Ho Han. A disposable microfluidic device with a reusable magnetophoretic functional substrate for isolation of circulating tumor cells. *Lab on a Chip*, 17(23):4113–4123, 2017.

[126] Nicole Pamme, Jan C.T. Eijkel, and Andreas Manz. On-chip free-flow magnetophoresis: Separation and detection of mixtures of magnetic particles in continuous flow. *Journal of Magnetism and Magnetic Materials*, 307(2):237–244, 2006.

[127] Wujun Zhao, Rui Cheng, Joshua R. Miller, and Leidong Mao. Label-Free Microfluidic Manipulation of Particles and Cells in Magnetic Liquids. *Advanced Functional Materials*, 26(22):3916–3932, 2016.

[128] Fengshan Shen, Hyundoo Hwang, Young Ki Hahn, and Je-Kyun Park. Label-Free Cell Separation Using a Tunable Magnetophoretic Repulsion Force. *Analytical Chemistry*, 84(7):3075–3081, 2012.

[129] Wujun Zhao, Taotao Zhu, Rui Cheng, Yufei Liu, Jian He, Hong Qiu, Lianchun Wang, Tamas Nagy, Troy D. Querec, Elizabeth R. Unger, and Leidong Mao. Label-Free and Continuous-Flow Ferrohydrodynamic Separation of HeLa Cells and Blood Cells in Biocompatible Ferrofluids. *Advanced Functional Materials*, 26(22):3990–3998, jun 2016.

[130] M. P. MacDonald, G. C. Spalding, and K. Dholakia. Microfluidic sorting in an optical lattice. *Nature*, 426(6965):421–424, 2003.

[131] Wen-Pin Chou, Hung-Ming Wang, Jyun-Huan Chang, Tzu-Keng Chiu, Chia-Hsun Hsieh, Chia-Jung Liao, and Min-Hsien Wu. The utilization of optically-induced-dielectrophoresis (ODEP)-based virtual cell filters in a microfluidic system for continuous isolation and purification of circulating tumour cells (CTCs) based on their size characteristics. *Sensors and Actuators B: Chemical*, 241:245–254, 2017.

[132] Tzu-Keng Chiu, A-Ching Chao, Wen-Pin Chou, Chia-Jung Liao, Hung-Ming Wang, Jyun-Huan Chang, Ping-Hei Chen, and Min-Hsien Wu. Optically-induced-dielectrophoresis (ODEP)-based cell manipulation in a microfluidic system for high-purity isolation of integral circulating tumor cell (CTC) clusters based on their size characteristics. *Sensors and Actuators B: Chemical*, 258:1161–1173, 2018.

[133] Nezihi Murat Karabacak, Philipp S Spuhler, Fabio Fachin, Eugene J Lim, Vincent Pai, Emre Ozkumur, Joseph M Martel, Nikola Kojic, Kyle Smith, Pin-i Chen, Jennifer Yang, Henry Hwang, Bailey Morgan, Julie Trautwein, Thomas A Barber, Shannon L Stott, Shyamala Maheswaran, Ravi Kapur, Daniel A Haber, and Mehmet Toner. Microfluidic, marker-free isolation of circulating tumor cells from blood samples. *Nature protocols*, 9(3):694–710, 2014.

[134] August Kundt. Über eine neue Art akustischer Staubfiguren und über die Anwendung derselben zur Bestimmung der Schallgeschwindigkeit in festen Körpern und Gasen. *Annalen der Physik und Chemie*, 203(4):497–523, jan 1866.

[135] Louis Vessot King. On the acoustic radiation pressure on spheres. *Proceedings of the Royal Society of London. Series A - Mathematical and Physical Sciences*, 147(861):212–240, 1934.

[136] K. Yosioka and Y. Kawasima. Acoustic radiation pressure on a compressible sphere. *Acustica*, 5(3):167–173, 1955.

[137] L. P. Gor'kov. On the Forces Acting on a Small Particle in an Acoustical Field in an Ideal Fluid. *Soviet Physics Doklady*, 6(9):773–775, 1962.

[138] Wesley L. Nyborg. Radiation Pressure on a Small Rigid Sphere. *The Journal of the Acoustical Society of America*, 42(5):947–952, 1967.

[139] Henrik Bruus. Acoustofluidics 7: The acoustic radiation force on small particles. *Lab on a Chip*, 12(6):1014, 2012.

[140] Thomas Laurell and Andreas Lenshof. *Microscale Acoustofluidics*. Royal Society of Chemistry, 2014.

[141] V Bjerknes. *Die Kraftfelder*. F. Vieweg, Braunschweig, braunschwe edition, 1909.

[142] Thomas Laurell, Filip Petersson, and Andreas Nilsson. Chip integrated strategies for acoustic separation and manipulation of cells and particles. *Chemical Society reviews*, 36(3):492–506, 2007.

[143] Björn Hammarström, Thomas Laurell, and Johan Nilsson. Seed particle-enabled acoustic trapping of bacteria and nanoparticles in continuous flow systems. *Lab on a Chip*, 12(21):429–4304, 2012.

[144] Martin Wiklund, Roy Green, and Mathias Ohlin. Acoustofluidics 14: Applications of acoustic streaming in microfluidic devices. *Lab on a chip*, 12(14):2438–2451, 2012.

[145] H. Schlichting. Berechnung ebener periodischer Grenzschichtströmungen. *Physkal. Z.*, 33:327–335, 1932.

[146] Lord Rayleigh. On the Circulation of Air Observed in Kundt's Tubes, and on Some Allied Acoustical Problems. *Philosophical Transactions of the Royal Society of London*, 175:1–21, 1884.

[147] S. M. Hagsäter, A. Lenshof, P. Skafte-Pedersen, J. P. Kutter, T. Laurell, and H. Bruus. Acoustic resonances in straight micro channels: beyond the 1D-approximation. *Lab on a chip*, 8(7):1178–1184, 2008.

[148] Rune Barnkob, Per Augustsson, Thomas Laurell, and Henrik Bruus. Acoustic radiation- and streaming-induced microparticle velocities determined by microparticle image velocimetry in an ultrasound symmetry plane. *Physical Review. E, Statistical, Nonlinear, and Soft Matter Physics*, 86(5 Pt 2):56307, 2012.

[149] Sz-Chin Steven Lin, Xiaole Mao, and Tony Jun Huang. Surface acoustic wave (SAW) acoustophoresis: now and beyond. *Lab on a chip*, 12(16):2766–2770, 2012.

[150] Itziar González, Julie Earl, Luis Fernández, Bruno Sainz, Alberto Pinto, Rosa Monge, Sonia Alcalá, Adela Castillejo, Jose Soto, Alfredo Carrato, Itziar González, Julie Earl, Luis J. Fernández, Bruno Sainz, Alberto Pinto, Rosa Monge, Sonia Alcalá, Adela Castillejo, Jose L. Soto, and Alfredo Carrato. A Label Free Disposable Device for Rapid Isolation of Rare Tumor Cells from Blood by Ultrasounds. *Micromachines*, 9(3):129, mar 2018.

[151] Henrik Jönsson, Cecilia Holm, Andreas Nilsson, Filip Petersson, Per Johnsson, and Thomas Laurell. Particle separation using ultrasound can radically reduce embolic load to brain after cardiac surgery. *The Annals of Thoracic Surgery*, 78(5):1572–1577, 2004.

[152] Filip Petersson, Lena Aberg, Ann-Margret Swärd-Nilsson, and Thomas Laurell. Free flow acoustophoresis: microfluidic-based mode of particle and cell separation. *Analytical chemistry*, 79(14):5117–5123, 2007.

[153] Andreas Lenshof, Asilah Ahmad-Tajudin, Kerstin Järås, Ann-Margret Swärd-Nilsson, Lena Aberg, György Marko-Varga, Johan Malm, Hans Lilja, and Thomas Laurell. Acoustic whole blood plasmapheresis chip for prostate specific antigen microarray diagnostics. *Analytical chemistry*, 81(15):6030–6037, 2009.

[154] Josefina Dykes, Andreas Lenshof, Ing-Britt Åstrand-Grundström, Thomas Laurell, and Stefan Scheding. Efficient removal of platelets from peripheral blood progenitor cell products using a novel micro-chip based acoustophoretic platform. *PloS one*, 6(8):e23074, 2011.

[155] Allen H J Yang and H Tom Soh. Acoustophoretic sorting of viable mammalian cells in a microfluidic device. *Analytical chemistry*, 84(24):10756–10762, 2012.

[156] Per Augustsson, Cecilia Magnusson, Maria Nordin, Hans Lilja, and Thomas Laurell. Microfluidic, label-free enrichment of prostate cancer cells in blood based on acoustophoresis. *Analytical chemistry*, 84(18):7954–7962, 2012.

[157] Mikael Evander, Andreas Lenshof, Thomas Laurell, and Johan Nilsson. Acoustophoresis in wet-etched glass chips. *Analytical chemistry*, 80(13):5178–5185, 2008.

[158] Bongkot Ngamsom, Maria J. Lopez-Martinez, Jean-Claude Raymond, Patrick Broyer, Pradip Patel, and Nicole Pamme. On-chip acoustophoretic isolation of microflora including S. typhimurium from raw chicken, beef and blood samples. *Journal of Microbiological Methods*, 123:79–86, 2016.

[159] Hyungjun Jang, Muhammad Haq, Jonghyun Ju, Youngkyu Kim, Seok-min Kim, Jiseok Lim, Hyungjun Jang, Muhammad Refatul Haq, Jonghyun Ju, Youngkyu Kim, Seok-min Kim, and Jiseok Lim. Fabrication of All Glass Bifurcation Microfluidic Chip for Blood Plasma Separation. *Micromachines*, 8(3):67, 2017.

[160] A Lenshof, M Evander, T Laurell, and J Nilsson. Acoustofluidics 5: Building microfluidic acoustic resonators. *Lab on a chip*, 12(4):684–695, 2012.

[161] Gayatri P. Gautam, Tobias Burger, Andrew Wilcox, Michael J. Cumbo, Steven W. Graves, and Menake E. Piyasena. Simple and inexpensive micromachined aluminum microfluidic devices for acoustic focusing of particles and cells. *Analytical and Bioanalytical Chemistry*, 410(14):3385–3394, 2018.

[162] A Mueller, A Lever, T V Nguyen, J Comolli, and J Fiering. Continuous acoustic separation in a thermoplastic microchannel. *Journal of Micromechanics and Microengineering*, 23(12):125006, 2013.

[163] P. Dow, K. Kotz, S. Gruszka, J. Holder, and J. Fiering. Acoustic separation in plastic microfluidics for rapid detection of bacteria in blood using engineered bacteriophage. *Lab on a Chip*, 2018.

[164] R. Silva, P. Dow, R. Dubay, C. Lissandrello, J. Holder, D. Densmore, and J. Fiering. Rapid prototyping and parametric optimization of plastic acoustofluidic devices for blood–bacteria separation. *Biomedical Microdevices*, 19(3):70, 2017.

[165] Pelle Ohlsson, Klara Petersson, Per Augustsson, and Thomas Laurell. Acoustic impedance matched buffers enable separation of bacteria from blood cells at high cell concentrations. *Scientific Reports*, 8(1):9156, 2018.

[166] Ola Jakobsson, Carl Grenvall, Maria Nordin, Mikael Evander, and Thomas Laurell. Acoustic actuated fluorescence activated sorting of microparticles. *Lab Chip*, 14(11):1943–1950, 2014.

[167] Carl Grenvall, Christian Antfolk, Christer Zoffmann Bisgaard, and Thomas Laurell. Two-dimensional acoustic particle focusing enables sheathless chip Coulter counter with planar electrode configuration. *Lab Chip*, 14(24):4629–4637, 2014.

[168] Jeremy J Hawkes, Robert W Barber, David R Emerson, and W Terence Coakley. Continuous cell washing and mixing driven by an ultrasound standing wave within a microfluidic channel. *Lab on a Chip*, 4(5):446–452, 2004.

[169] Filip Petersson, Andreas Nilsson, Henrik Jönsson, and Thomas Laurell. Carrier medium exchange through ultrasonic particle switching in microfluidic channels. *Analytical chemistry*, 77(5):1216–1221, 2005.

[170] Per Augustsson, Lena B Åberg, Ann-Margret K Swärd-Nilsson, and Thomas Laurell. Buffer medium exchange in continuous cell and particle streams using ultrasonic standing wave focusing. *Microchimica Acta*, 164(3-4):269–277, 2009.

[171] Mikkel W. H. Ley and Henrik Bruus. Continuum modeling of hydrodynamic particle–particle interactions in microfluidic high- concentration suspensions. *Lab on a Chip*, pages 1178–1188, 2016.

[172] Per Augustsson, Rune Barnkob, Steven T Wereley, Henrik Bruus, and Thomas Laurell. Automated and temperature-controlled micro-PIV measurements enabling long-term-stable microchannel acoustophoresis characterization. *Lab on a chip*, 11(24):4152–4164, 2011.

[173] Sameer Deshmukh, Zbigniew Brzozka, Thomas Laurell, and Per Augustsson. Acoustic radiation forces at liquid interfaces impact the performance of acoustophoresis. *Lab on a Chip*, 14(17):3394–3400, mar 2014.

[174] Jonas T Karlsen, Per Augustsson, and Henrik Bruus. Acoustic Force Density Acting on Inhomogeneous Fluids in Acoustic Fields. *Physical Review Letters*, 117(11):114504, 2016.

[175] Martin Wiklund. Acoustofluidics 12: Biocompatibility and cell viability in microfluidic acoustic resonators. *Lab on a Chip*, 12(11):2018–2028, 2012.

[176] J Hultström, O Manneberg, K Dopf, H M Hertz, H Brismar, and M Wiklund. Proliferation and viability of adherent cells manipulated by standing-wave ultrasound in a microfluidic chip. *Ultrasound in Medicine & Biology*, 33(1):145–151, 2007.

[177] A. Lenshof, A. Jamal, J. Dykes, A. Urbansky, I. Åstrand-Grundström, T. Laurell, and S. Scheding. Efficient purification of CD4+ lymphocytes from peripheral blood progenitor cell products using affinity bead acoustophoresis. *Cytometry Part A*, 85(11):933–941, 2014.

[178] Pierre Bohec, Jérémie Gachelin, Véronique Ollivier, Thibaut Mutin, Xavier Télot, Benoît Ho-Tin-Noé, and Sandra Sanfilippo. Acoustophoretic purification of platelets: Feasibility and impact on platelet activation and function. *Platelets*, pages 1–7, 2017.

[179] A. Urbansky, A. Lenshof, J. Dykes, T. Laurell, and S. Scheding. Affinity-bead-mediated enrichment of CD8+ lymphocytes from peripheral blood progenitor cell products using acoustophoresis. *Micromachines*, 7(6):101, 2016.

[180] Jonathan D Adams, Christian L Ebbesen, Rune Barnkob, Allen H J Yang, H Tom Soh, and Henrik Bruus. High-throughput, temperature-controlled microchannel acoustophoresis device made with rapid prototyping. *Journal of Micromechanics and Microengineering*, 22(7):075017, 2012.

[181] Andreas Nilsson, Filip Petersson, Henrik Jönsson, and Thomas Laurell. Acoustic control of suspended particles in micro fluidic chips. *Lab on a chip*, 4(2):131–135, 2004.

[182] Klara Petersson, Ola Jakobsson, Pelle Ohlsson, Per Augustsson, Stefan Scheding, Johan Malm, and Thomas Laurell. Acoustofluidic hematocrit determination. *Analytica Chimica Acta*, 1000:199–204, 2018.

[183] Menake E Piyasena, Pearlson P Austin Suthanthiraraj, Robert W Applegate, Andrew M Goumas, Travis A Woods, Gabriel P López, and Steven W Graves. Multinode Acoustic Focusing for Parallel Flow Cytometry. *Analytical Chemistry*, 84(4):1831–1839, 2012.

[184] Sixing Li, Xiaoyun Ding, Zhangming Mao, Yuchao Chen, Nitesh Nama, Feng Guo, Peng Li, Lin Wang, Craig E Cameron, and Tony Jun Huang. Standing surface acoustic wave (SSAW)-based cell washing. *Lab on a Chip*, 15(1):331–338, 2015.

[185] Per Augustsson, Jonas Persson, Simon Ekström, Mats Ohlin, and Thomas Laurell. Decomplexing biofluids using microchip based acoustophoresis. *Lab on a chip*, 9(6):810–818, 2009.

[186] Maria Nordin and Thomas Laurell. Two-hundredfold volume concentration of dilute cell and particle suspensions using chip integrated multistage acoustophoresis. *Lab on a Chip*, 12(22):4610–4616, 2012.

[187] Ola Jakobsson, Seung Soo Oh, Maria Antfolk, Michael Eisenstein, Thomas Laurell, and H Tom Soh. Thousand-Fold Volumetric Concentration of Live Cells with a Recirculating Acoustofluidic Device. *Analytical Chemistry*, 87(16):8497–8502, 2015.

[188] A Ahmad Tajudin, K Petersson, A Lenshof, A.-M. Swärd-Nilsson, L Aberg, G Marko-Varga, J Malm, H Lilja, and T Laurell. Integrated acoustic immunoaffinity-capture (IAI) platform for detection of PSA from whole blood samples. *Lab on a Chip*, 13(9):1790–1796, 2013.

[189] Linda Johansson, Fredrik Nikolajeff, Stefan Johansson, and Sara Thorslund. On-chip fluorescence-activated cell sorting by an integrated miniaturized ultrasonic transducer. *Analytical Chemistry*, 81(13):5188–5196, 2009.

[190] Mikael Evander, Linda Johansson, Tobias Lilliehorn, Jure Piskur, Magnus Lindvall, Stefan Johansson, Monica Almqvist, Thomas Laurell, and Johan Nilsson. Noninvasive acoustic cell trapping in a microfluidic perfusion system for online bioassays. *Analytical chemistry*, 79(7):2984–2991, 2007.

[191] Björn Hammarström, Mikael Evander, Herve Barbeau, Mattias Bruzelius, Jörgen Larsson, Thomas Laurell, and Johan Nilsson. Non-contact acoustic cell trapping in disposable glass capillaries. *Lab on a Chip*, 10(17):2251–2257, 2010.

[192] Melinda Rezeli, Olof Gidlöf, Mikael Evander, Paulina Bryl-Górecka, Ramasri Sathanoori, Patrik Gilje, Krzysztof Pawłowski, Péter Horvatovich, David Erlinge, György Marko-Varga, and Thomas Laurell. Comparative Proteomic Analysis of Extracellular Vesicles Isolated by Acoustic Trapping or Differential Centrifugation. *Analytical Chemistry*, 88(17):8577–8586, 2016.

[193] Anson Ku, Hooi Ching Lim, Mikael Evander, Hans Lilja, Thomas Laurell, Stefan Scheding, and Yvonne Ceder. Acoustic Enrichment of Extracellular Vesicles from Biological Fluids. *Analytical Chemistry*, 90(13):8011–8019, 2018.

[194] Sanjay Gupta, Donald L. Feke, and Ica Manas-Zloczower. Fractionation of mixed particulate solids according to compressibility using ultrasonic standing wave fields. *Chemical Engineering Science*, 50(20):3275–3284, 1995.

[195] Maria Antfolk, Soo Hyeon Kim, Saori Koizumi, Teruo Fujii, and Thomas Laurell. Label-free single-cell separation and imaging of cancer cells using an integrated microfluidic system. *Scientific Reports*, 7:46507, 2017.

[196] Kevin Cushing, Eva Undvall, Yvonne Ceder, Hans Lilja, and Thomas Laurell. Reducing WBC background in cancer cell separation products by negative acoustic contrast particle immuno-acoustophoresis. *Analytica Chimica Acta*, 1000:256–264, 2018.

[197] Yuchao Chen, Mengxi Wu, Liqiang Ren, Jiayang Liu, Pamela H. Whitley, Lin Wang, and Tony Jun Huang. High-throughput acoustic separation of platelets from whole blood. *Lab on a Chip*, 16(18), 2016.

[198] Yuyang Gu, Chuyi Chen, Zeyu Wang, Po-Hsun Huang, Hai Fu, Lin Wang, Mengxi Wu, Yuchao Chen, Tieyu Gao, Jianying Gong, Jean Kwun, Gowthami M. Arepally, and Tony Jun Huang. Plastic-based acoustofluidic devices for high-throughput, biocompatible platelet separation. *Lab on a Chip*, 19(3):394–402, jan 2019.

[199] Pelle Ohlsson, Mikael Evander, Klara Petersson, Lisa Mellhammar, Ari Lehmusvuori, Ulla Karhunen, Minna Soikkeli, Titta Seppä, Emilia Tuunainen, Anni Spangar, Piia von Lode, Kaisu Rantakokko-Jalava, Gisela Otto, Stefan Scheding, Tero Soukka, Saara Wittfooth, and Thomas Laurell. Integrated Acoustic Separation, Enrichment, and Microchip Polymerase Chain Reaction Detection of Bacteria from Blood for Rapid Sepsis Diagnostics. *Analytical Chemistry*, 88(19):9403–9411, 2016.

[200] Gayatri P. Gautam, Rubi Gurung, Frank A. Fencl, and Menake E. Piyasena. Separation of sub-micron particles from micron particles using acoustic fluid relocation combined with acoustophoresis. *Analytical and Bioanalytical Chemistry*, 410(25):6561–6571, oct 2018.

[201] Anke Urbansky, Pelle Ohlsson, Andreas Lenshof, Fabio Garofalo, Stefan Scheding, and Thomas Laurell. Rapid and effective enrichment of mononuclear cells from blood using acoustophoresis. *Scientific Reports*, 7(1), 2017.

[202] Ida Iranmanesh, Harisha Ramachandraiah, Aman Russom, and Martin Wiklund. On-chip ultrasonic sample preparation for cell based assays. *Rsc Advances*, 5(91):74304–74311, 2015.

[203] Carl Grenvall, Cecilia Magnusson, Hans Lilja, and Thomas Laurell. Concurrent Isolation of Lymphocytes and Granulocytes Using Prefocused Free Flow Acoustophoresis. *Analytical Chemistry*, 87(11):5596–5604, 2015.

[204] Anke Urbansky, Franziska Olm, Stefan Scheding, Thomas Laurell, and Andreas Lenshof. Label-free separation of leukocyte subpopulations using high throughput multiplex acoustophoresis. *Lab on a Chip*, 2019.

[205] Charles Lissandrello, Ryan Dubay, Kenneth T. Kotz, and Jason Fiering. Purification of Lymphocytes by Acoustic Separation in Plastic Microchannels. *SLAS TECHNOLOGY*, 23(4):352–363, 2018.

Paper I

Cytometry
PART A
Journal of the International Society for Advancement of Cytometry

Efficient Purification of CD4+ Lymphocytes from Peripheral Blood Progenitor Cell Products Using Affinity Bead Acoustophoresis

Andreas Lenshof,[1†*] Arshad Jamal,[2†] Josefina Dykes,[2,3] Anke Urbansky,[1,2] Ingbritt Åstrand-Grundström,[2] Thomas Laurell,[1,4] Stefan Scheding[2,5]

[1]Department of Biomedical Engineering, Lund University, Lund, Sweden

[2]Department of Laboratory Medicine, Lund Stem Cell Center, Lund University, Lund, Sweden

[3]Department of Clinical Immunology and Transfusion Medicine, University and Regional Laboratories, Lund, Sweden

[4]Department of Biomedical Engineering, Dongguk University, Seoul, South Korea

[5]Department of Hematology, University Hospital Skane, Lund, Sweden

[†]These authors contributed equally to the work.

Received 12 December 2013; Revised 30 April 2014; Accepted 30 June 2014

Grant sponsors: Vinnova (Swedish Governmental Agency for Innovation Systems), Innovations for Future Health – CellCARE, The Royal Physiographic Society in Lund, the Georg Danielssons Foundation, John Persson Foundation, Skåne University Hospital Fonds, ALF (Government Public Health Grant), Skåne County Councils Research Foundation

Additional Supporting Information may be found in the online version of this article.

*Correspondence to: Andreas Lenshof, Biomedical Engineering, Lund University, Lund, Sweden. E-mail: andreas.lenshof@bme.lth.se

Published online 22 July 2014 in Wiley Online Library (wileyonlinelibrary.com)

DOI: 10.1002/cyto.22507

ISAC
International Society for Advancement of Cytometry

Abstract

Processing of peripheral blood progenitor cells (PBPC) for clinical transplantation or research applications aims to effectively isolate or deplete specific cell populations, utilizing primarily magnetic or fluorescence activated sorting methods. Here, we investigated the performance of microfluidic acoustophoresis for the separation of lymphocyte subsets from PBPC, and present a novel method for affinity-bead-mediated acoustic separation of cells which can otherwise not be acoustically discriminated. As the acoustic force on a particle depends on particle size, density and compressibility, targeting of cells by affinity specific beads will generate cell-bead complexes that exhibit distinct acoustic properties relative to nontargeted cells and are, thus, possible to isolate. To demonstrate this, PBPC samples (n = 22) were obtained from patients and healthy donors. Following density gradient centrifugation, cells were labeled with anti-CD4-coated magnetic beads (Dynal) and isolated by acoustophoresis and, for comparison, standard magnetic cell sorting technique in parallel. Targeted CD4+ lymphocytes were acoustically isolated with a mean (±SD) purity of 87 ± 12%, compared with 96 ± 3% for control magnetic sorting. Viability of sorted cells was 95 ± 4% (acoustic) and 97 ± 3% (magnetic), respectively. The mean acoustic separation efficiency of CD4+ lymphocytes to the target fraction was 65 ± 22%, compared with a mean CD4+ lymphocyte recovery of 56 ± 15% for magnetic sorting. Functional testing of targeted CD4+ lymphocytes demonstrated unimpaired mitogen-mediated proliferation capacity and cytokine production. Hematopoietic progenitor cell assays revealed a preserved colony forming ability of nontarget cells post sorting. We conclude that the acoustophoresis platform can be utilized to efficiently isolate bead-labeled CD4+ lymphocytes from PBPC samples in a continuous flow format, with preserved functional capacity of both target and nontarget cells. These results open up for simultaneous affinity-bead-mediated separation of multiple cell populations, something which is not possible with current standard magnetic cell separation technology. © 2014 International Society for Advancement of Cytometry

Key terms

peripheral blood progenitor cells; PBPC; lymphocytes; magnetic beads; acoustophoresis; ultrasound; cell sorting

CELL separation technologies are essential tools in the processing of hematopoietic cells for therapeutic administration, diagnostic purposes or research applications. Separation by centrifugal force is generally employed for primary extraction of leukocytes from whole blood or bone marrow (1), followed by selective affinity methods, such as magnetic activated cell sorting (MACS) (2), or fluorescence activated cell sorting (FACS) (3), for isolation or depletion of specific cell populations. Depending on sample characteristics and the specific cell sorting application, the currently available techniques have distinct advantages as well as disadvantages in terms of recovery, purity, and throughput (1).

Hematopoietic stem cell transplantation using PBPC apheresis products from healthy donors is a well-established therapy for hematological malignancies. Transplanted cells include stem/progenitor cells, which will restore bone marrow function in the recipient, but also different lymphocyte cell populations, such as CD4+ T-helper cells, which are capable of mounting immunological anti-leukemic effects. This reaction can, however, develop into a potentially lethal condition involving a response against nonmalignant recipient cells; graft-versus-host disease. Processing of PBPC for clinical transplantation aims to effectively isolate or deplete specific stem cell or lymphocyte cell populations, to provide the best possible graft for the patient (4).

In the last decade, acoustophoretic sorting which is primarily based on size, density, and compressibility (5) has emerged as a simple, cost-effective and continuous flow based separation technique with minimal impact on survival and function of cells (6–8). In the light of recently reported applications in cell biology and clinical settings (9–11), acoustophoresis presents an interesting alternative to current cell separation techniques. Moreover, the flow-through sorting approach makes it suitable for lab-on-a-chip designs and for integration into existing separation and analysis systems (12,13). Continuous flow acoustophoresis utilizes a standing wave field perpendicular to a laminar flow of suspended particles to induce particle movement across the width of a micro-channel (14). The acoustic forces, which are proportional to the particle radius to the 3rd power, move most particle types to the acoustic pressure node at the centre of the channel while laminar flow maintains the central positioning of the particles (5). By ending the channel in a trifurcation, the acoustically focused fraction in the center can be separated from the acoustically unaffected or less affected particles located closer to the channel side walls. The direction of migration in an acoustic field is also dependent on the acoustic properties of the particle relative to the surrounding media. In aqueous systems, most rigid particles migrate to the pressure node, while lipid particles (15) and recently developed polydimethylsioxane (PDMS) micro spheres (16) are moved to the pressure anti-node of the standing wave. Modification of the chip design with an increased number of outlets for simultaneously sorting of multiple targets, or adjustment of medium density for efficient separation of cells or particles which would otherwise behave similarly in an acoustic field, have been demonstrated (17). Recently reported improvements of the separation efficiency of such systems include the use of a two dimensional acoustic prealignment procedure, in which particles are focused in a tight band with uniform flow velocity before entering the separation channel ensuring that the acoustophoretic migration of all particles across the channel will start from identical positions as well as have the same retention time in the separation zone (9). Further improvement comprises constant temperature regulation to ensure unperturbed acoustic standing wave conditions (18). Exploiting the acoustic properties of affinity specific micro beads has further extended the field of applying acoustophoresis. Very small particles (<1 μm) which are not affected by the primary acoustic radiation force, such as peptides or viruses, can be extracted by the use of affinity micro beads which bind selectively to the particle of interest. The acoustic properties of the micro beads will thus enable target purification, as demonstrated by Augustsson et al. utilizing antigen (grass pollen allergen Phl p5) coated micro beads in a microfluidic phage display selection process to selectively enrich and extract antigen specific phages from a phage library (19). Phage particles are too small to be influenced by the acoustic standing wave field when operated in the standard 2 MHz range. However, the use of target specific microbeads enabled acoustic extraction of phages, expressing antibodies specific for the grass pollen allergen. Specific extraction of molecular compounds from complex samples for in proteomic sample preparation has also been demonstrated using metal oxide affinity microbeads (MOAC) to enrich and purify phosphopeptides prior to MALDI MS analysis (20).

Although bead-mediated extraction of larger targets, such as cells, proved to be a much more complex challenge in terms of controlling the acoustic and fluidic parameters, we demonstrate in the current study the feasibility of utilizing affinity micro beads to allow separation of cells with otherwise similar acoustic properties. Dynabeads (diameter 4.5 μm, density 1.6 g/cm^3) were chosen primarily for their ability to alter the acoustic properties, i.e., size and density, of bead labeled cells versus nonlabeled cells, thus enabling acoustophoretic isolation of targeted lymphocytes. Secondarily, the choice of commercially available magnetic micro beads for labeling allowed for a direct comparison of the acoustic cell separation system to a standard magnetic cell sorting technique. Magnetic beads were previously used by Adams et al. to simultaneously separate three different particles by combining acoustic and magnetic forces in a microfluidics system (21). Neither of the micro beads were however used to perform affinity based cell separation.

Choosing lymphocytes targeted with anti-CD4-coated beads as a prototype for investigating bead-mediated acoustic cell separation, we demonstrate for the first time that affinity acoustophoresis can be utilized to efficiently isolate specific cell populations, with preserved functional capacity of both targeted and nontargeted cells. These results open up for simultaneous bead-mediated separation of multiple cell populations, utilizing affinity micro beads with different acoustic properties, something which is not possible with current standard magnetic cell separation technology.

Materials and Methods

Collection of PBPC Samples

Samples were obtained from peripheral blood progenitor cell (PBPC) apheresis products collected after standard mobilization treatment of healthy donors (granulocyte colony-stimulating factor (G-CSF), Neupogen; Amgen, Thousand Oaks, CA) and patients (protocol specific chemotherapy + G-CSF). Large volume leukapheresis was performed with a Cobe Spectra (Cobe, Lakewood, CO), using the MNC program, version 7.0. On the day of the leukapheresis, or after a maximum

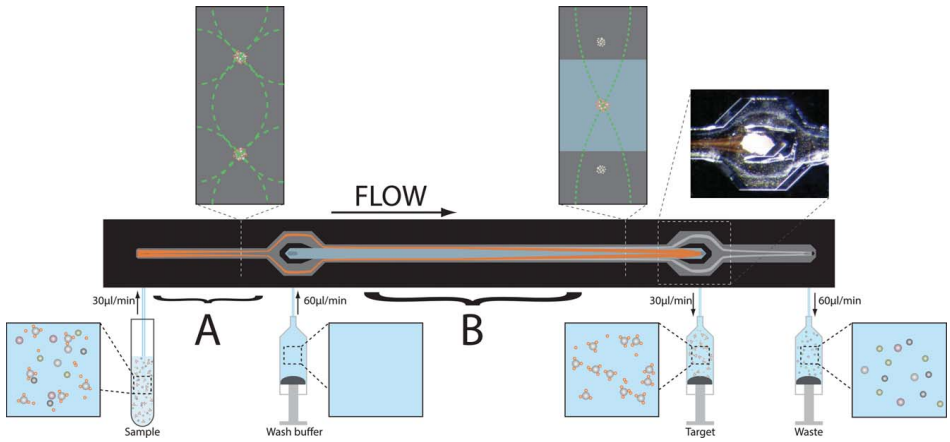

Figure 1. Overview of the acoustophoresis chip. **A**: Prefocusing zone. Sample (bead-labeled cells, nonlabeled cells, and unbound beads) is entered into the prefocusing channel where particles are subjected to acoustic standing waves in two dimensions. The prefocusing channel is designed to support a single node resonance from top to bottom at the same time as a double node resonance is generated across the width of the channel. Thereby, the particles are focused in two parallel bands, which are oriented along the direction of the flow and subsequently bifurcated to each side of a central inlet buffer flow, such that the particles are laminated towards the channel walls as they enter the separation region (**B**). The pre-focusing step will ensure that the transfer of all particles across the separation channel starts from identical positions, thereby eliminating loss in separation efficiency due to the laminar flow profile. **B**: Separation. In the separation zone, bead-labeled cells are transferred into the Ficoll wash buffer in the center of the channel by a one dimensional acoustic standing wave and collected through the central outlet (target fraction), whereas nonlabeled cells are less acoustically affected and exit through the side branches (nontarget fraction).

of 24 h storage, 1 mL of PBPC sample was removed from the collection bag for quality control, using a standard automated hematology analyzer (Sysmex KX-21N, Sysmex, Kungsbacka, Sweden). Surplus cells were separated by Ficoll density gradient centrifugation (LSM 1077 Lymphocyte, PAA, Pasching, Austria) and the isolated mononuclear cell (MNC) fraction was used for further experiments. Sampling of patient and donor PBPC products for use in the current study was approved by the Regional Ethical Review Board. Written informed consent was obtained from all participants involved in the study.

Targeting of CD4+ Lymphocytes with Magnetic Beads

Dynabeads (Invitrogen-Life Technologies, Carlsbad CA, Dynal CD4 positive isolation kit, cat. # 11331D, superparamagnetic polystyrene beads 4.5 µm in diameter), coated with primary monoclonal anti-CD4 antibody were used to label CD4+ cells. Briefly, 25 µl Dynabeads were added per 10^7 MNC. The cell-bead mixture was incubated at 2–8°C for 20 min under continuous agitation, and split in two equally sized portions of 10^7 MNC in 1 mL for sorting in parallel on the Dynal magnetic cell separation system and the acoustophoresis micro-chip.

Following magnetic and acoustic sorting, respectively, the isolated cells were released from bound beads by incubation with DETACHaBEAD (10 µl/10^7cells) at room temperature for 45 min under continuous agitation. The cell-bead mixture was then exposed to a Dynal magnet for removal of detached beads, and washed twice with 1 mL PBS + 2% fetal bovine serum (FBS) (Gibco) and 0.6% acid-citrate-dextrose (ACDA) (Terumo BCT. Inc.) such that released cells could be collected from the wash buffer. Collected cells were washed twice by 5 min centrifugation at 400*g*, stained with trypan blue (Gibco-Life Technologies Carlsbad CA) for exclusion of nonviable cells and counted using a Neubauer chamber.

Magnetic Cell Separation

Magnetic separation was performed with the Dynal system according to the manufacturer's protocol. During magnetic isolation of bead-labeled cells, nonlabeled cells were eliminated by washing three times with 1 mL PBS (2% FBS, 0.6% ACDA). Subsequently, bead-labeled cells were released from the magnet and resuspended in buffer (100 µl/10^7 cells).

Acoustophoresis Chip Design

The chip design and fabrication process is described in more detail by Augustsson et al. (9). In brief, the chip was designed to consist of a sample inlet leading to a prefocusing channel, a bifurcation that diverts the flow to each side of a central wash buffer inlet, and a separation channel ending in a trifurcation equipped with one central outlet and a common outlet for the two lateral branches (Fig. 1). The silicon acoustophoresis channel was made by anisotropic wet etching using Potassium hydroxide (220 g KOH in 550 MilliQ H_2O) and sealed with a glass lid using anodic bonding. The prefocusing

channel width was set to 300 μm to match a wave length resonance of 5 MHz, whereas the width of the separation channel was set to 375 μm to match half a wavelength resonance of 2 MHz. Silicon tubing with an inner diameter of 1/16 inch was glued to the inlets and outlets, to act as docking ports for fluidic tubing.

Acoustophoresis Set Up

The chip was connected to three syringe pumps (neMESYS, Cetoni GmbH, Germany). Two pumps were set in withdrawal mode and connected to 1 mL plastic syringes (BD Plastipak, Franklin Lakes, NJ, USA) to control the flow through the chip. The third pump was connected to the chip central inlet, infusing Ficoll wash buffer (Histopaque-1077, Sigma-Aldrich) from a 5 mL glass syringe (1005 TLL, Hamilton Bonaduz AG, Bonaduz, Switzerland). All pumps were connected via Teflon tubing (VWR Intnl. O.d. 1.54 mm, I.d. 0.05 mm) to the chip outlets. The PBPC sample was connected to the chip pre-focusing channel inlet at a net flow rate set by the three pumps. The ultrasonic standing waves were generated by two piezoelectric transducers (PZ26, Ferroperm Piezoceramics, Kvistgard, Denmark), at a resonance frequency of 5 and 2 MHz, respectively, for the prefocusing and the separation transducer. Both transducers were driven by Agilent waveform generators (Agilent 33220A, Hewlett-Packard, Palo Alto, CA) equipped with different signal amplifiers for the pre-focus (Amplifier Research 75A250, Southerton, PA) and the separation transducer (in-house build amplifier). Transducer driving voltage was monitored with an oscilloscope (TDS 1002, Tektronix, Beaverton, OR) and visual monitoring of the fluidics was performed using a Nikon SMZ800 microscope.

Fluidics and Sampling Procedure

Before sample processing, the flow system was pre-filled with PBS to evacuate air. The two pumps in withdrawal mode were set to provide a flow rate through each of the three exit branches of 30 μL/min. The Ficoll wash buffer was infused at a flow rate of 60 μL/min, leaving a net flow rate of 30 μL/min (15 μL/min in each side inlet branch) for the PBPC sample (10^7 MNC in 1 mL). The operational parameters were tuned by visual inspection of the outlet trifurcation and set when bead-labeled cells were optimally focused into the central outlet and nonlabeled cells were distributed to the lateral branches (Fig. 1). Processed sample was collected directly into the syringes as target (labeled cells) and nontarget (nonlabeled cells) fractions.

Flow Cytometric Analysis

PBPC samples as well as magnetic target fractions and acoustic target and nontarget fractions, respectively, were analyzed for CD4+ helper T cell contents by flow cytometry (Supporting Information Fig. S1), using a four-color flow cytometer (FACSCalibur, BD Biosciences, San Diego, CA). PBSC samples and acoustic nontarget fractions were also analyzed for cytotoxic T cell, hematopoietic stem/progenitor cell, monocyte, NK cell and B cell contents. Cells were spun down at 400*g*, 4°C for 10 min, resuspended in blocking buffer (PBS with 2% Gammanorm (Octapharm AG, Lachen-Switzerland), and 1% FBS (Gibco)) and incubated with monoclonal antibodies at 4°C in the dark for 35 min. Directly conjugated antibodies were used in different combinations as follows: anti-CD3 fluorescein isothiocyanate (FITC) (clone HIT3a), anti-CD4 allophycocyanin (APC) (clone RPA-T4), anti-CD8 phycoerythrin (PE) (clone RPA-T8), anti-CD45 APC (clone HI30), anti-CD34 FITC (clone 581), anti-CD14 PE (clone M5E2), anti-CD19 PE (clone HIB19), and anti-CD56 APC (clone B159) (all from Becton Dickinson, BD, San Jose, CA). For isotype controls IgG1 (FITC), IgG1 (PE) and IgG1 (APC) were used (BD). Cells were washed by adding 1 mL FACS buffer (PBS, 1% BSA, 0.1% sodium azide, Sigma-Aldrich, St. Louis, MO) followed by centrifugation at 3,000 rpm for 5 min. 7-amino-actinomycin D (7-AAD, 200 μg/mL, Sigma-Aldrich) was used for dead cell exclusion. 10,000 events were acquired with the CellQuest software (BD Biosciences, San Diego, CA) and data were analyzed by FlowJo software (Tree Star Inc., Ashland, OR).

Hematopoietic Progenitor Cell Assays

PBPC samples and acoustic nontarget fractions were evaluated for hematopoietic progenitor cell content in standard colony-forming cell assays using standard methylcellulose culture (MACS HSC-CFU media complete with EPO, Miltenyi Biotec GmbH, Bergisch Gladbach, Germany, cat # 130-091-280). Cells were plated at a concentration of 3,000 cells/mL and incubated for 14 days (Thermo Forma Steri incubator, 37°C, 5% CO2). Colony forming units (CFU) were enumerated based on standard criteria using an Olympus IX70 microscope.

Lymphocyte Proliferation Assays

Proliferation of isolated CD4+ T cells was assessed by carboxyfluorescein succinimidyl ester (CFSE)-based lymphocyte proliferation assays. Briefly, 1×10^6 CD4+ target cells were suspended in 1 mL PBS (0.1% BSA, Sigma Aldrich) and CFSE solution (Invitrogen-Life Technologies Carlsbad CA, cat # C34554) at a final concentration of 0.5 μM, and incubated at 37°C for 7 min. The staining was quenched by addition of 2 volumes of pre warmed FBS and incubation at room temperature for 10 min, followed by three washing steps with culture media and centrifugation at 400*g* for 5 min. CFSE labeled CD4+ cells were cultured at 25×10^3 cells per well in a 96-well flat bottom plate (TRP) in final volume of 200 μL RPMI 1640 medium (Gibco Life Technologies, Carlsbad, CA), with 10% human AB serum (PAA) and 50 ng/mL of IL-2 (Miltenyi Biotec). Cells were stimulated either with PMA (10 μg/mL) and Ionomycin (100 ng/mL)(Sigma-Aldrich), or with anti-CD3 (5 μg/mL) and anti-CD28 (2 μg/mL) (eBioscience, San Diego, CA). On Days 1-6 of culture, cell proliferation, as determined by successive halving of CFSE fluorescence intensity, was analyzed by flow cytometry (FACSCalibur, CellQuest and FlowJo software).

Lymphocyte Cytokine Secretion Assays

On day six of the CFSE-assay, the culture plate was centrifuged and the supernatants were collected for cytokine analysis.

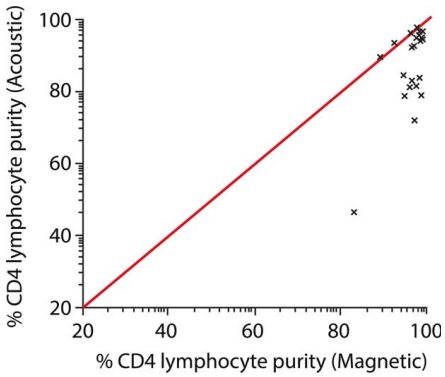

Figure 2. Purity of acoustic and magnetic sorted CD4+ T lymphocytes. Comparison of CD4+ lymphocyte purities obtained with parallel magnetic and acoustic separations ($n = 22$). Results from the magnetic enrichments are plotted against results obtained from the corresponding acoustic enrichments. The red line indicates the diagonal isoeffective line. [Color figure can be viewed in the online issue, which is available at wileyonlinelibrary.com.]

Cytokine concentrations were measured using the Cytometric Bead Array (CBA) Human Th1/Th2 Cytokine Kit (BD) according to manufacturer's instructions. For assay preparations, Human Th1/Th2 Cytokines Standards were reconstituted in 2 mL Assay Diluent (top standard) and serially diluted: 1:2, 1:4, 1:8, 1:16, 1:32, 1:64, and 1:128, a pool of Human Th1/Th2 Cytokine Capture Beads was prepared by mixing equal volumes of each Capture Bead solution in a single tube, and the sample (CFSE-assay supernatants) was diluted 1:2 in Assay Diluent. To perform the assay, 50 µL of pooled Capture Beads was added to each test tube, followed by 50 µL of the Human Th1/Th2 PE Detection Reagent, and finally 50 µL of either supernatant sample, standard dilutions, or negative control. Tubes were incubated for 3 h at room temperature in the dark, and washed with1 mL of Wash Buffer followed by centrifugation at 200*g* for 5 min. The bead pellets were resuspended in 300 μL of Wash Buffer and analyzed by flow cytometry (FACSCalibur, CellQuest, and FlowJo software).

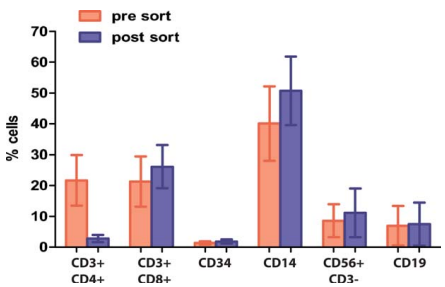

Figure 3. Leukocyte subset distribution. Comparison of the mean (±SD) relative distribution between CD3+/4+ CD3+/8+, CD34+, C14+, CD19+, and CD56+/3- cells in the presort (PBPC) versus postsort (nontarget fraction) samples ($n = 6$). As expected, the selective separation of CD4+ cells to the target fraction was coupled to a relative increase of nontargeted lymphocyte subpopulations in the nontarget fractions, as compared with the PBSC samples. [Color figure can be viewed in the online issue, which is available at wileyonlinelibrary.com.]

Statistical Analyses

Statistical analyses were performed using Prism 5.0 (Graphpad San Diego, CA). Data are presented as mean ± standard deviation (SD). Statistical significance was determined by using unpaired Student's *t*-tests.

Results

Acoustophoretic Enrichment of Bead-labeled CD4+ T Lymphocytes

PBPC samples were obtained from seven healthy donors and 15 patients (multiple myeloma, $n = 11$ or lymphoma, $n = 4$) to evaluate the performance of Dynabead-mediated acoustophoretic cell separation in comparison to standard magnetic sorting (Fig. 2). Targeted CD4+ lymphocytes were acoustically isolated with a mean (±SD) purity of 87 ± 12%, as compared with 96 ± 3% for magnetic enrichment. The purity of CD4+ lymphocytes in the acoustic target fraction was ≥80% in all but two separations (sample no. 6 and 12) in which however the frequency of CD4+ lymphocytes in the corresponding presort PBPC samples was relatively low, 0.9% and 3.0%, respectively. The purity of individual PBPC samples is presented in Supporting Information Table 1. The mean separation efficiency of CD4+ lymphocytes to the target fraction was 65 ± 22% of the total number of CD4+ lymphocytes obtained in both target and nontarget fractions, compared to a mean recovery of magnetically sorted CD4+ lymphocytes of 56 ± 15%. Regarding the mean viability of sorted cells, acoustophoresis (95 ± 4%) and magnetic separation were comparable (97 ± 3%).

Leukocyte Subpopulation Distribution

Flow cytometry analysis following acoustophoretic separation ($n = 6$) revealed changes in the composition of leukocyte subpopulations in pre- versus postsort samples (Fig. 3). As expected, the selective separation of CD4+ cells to the target fraction was coupled to a relative increase of nontargeted leukocyte subpopulations in the nontarget fraction, as compared with the PBPC samples. The mean (±SD) relative distribution between mononuclear cell populations in the presort (PBSC) versus postsort (nontarget fraction) samples changed as follows: CD3+/4+ cells, 22 (±8.2)% versus 2.8 (±1.1)%; CD3+/8+ cells, 22 (±8.9)% versus 27 (±7.4)%; CD34+ cells, 1.3 (±0.6)% versus 1.8(±0.8)%; CD14+ cells, 37 (±9.2)% versus 48 (±9.5)%; CD56+/3-cells, 9.4 (±5.4)% versus 13 (±7.8)%, and CD19+ cells, 8.0 (±6.3)% versus 8.7 (±6.8)%. For individual cell populations, the mean relative increase in the postsorted (nontarget fraction) compared with the presorted (PBPC samples) was 19% for CD3+/8+ cells, 27% for CD34+ cells, 24% for CD14+ cells, 25% for CD56+/3- cells and 8% for CD19+ cells.

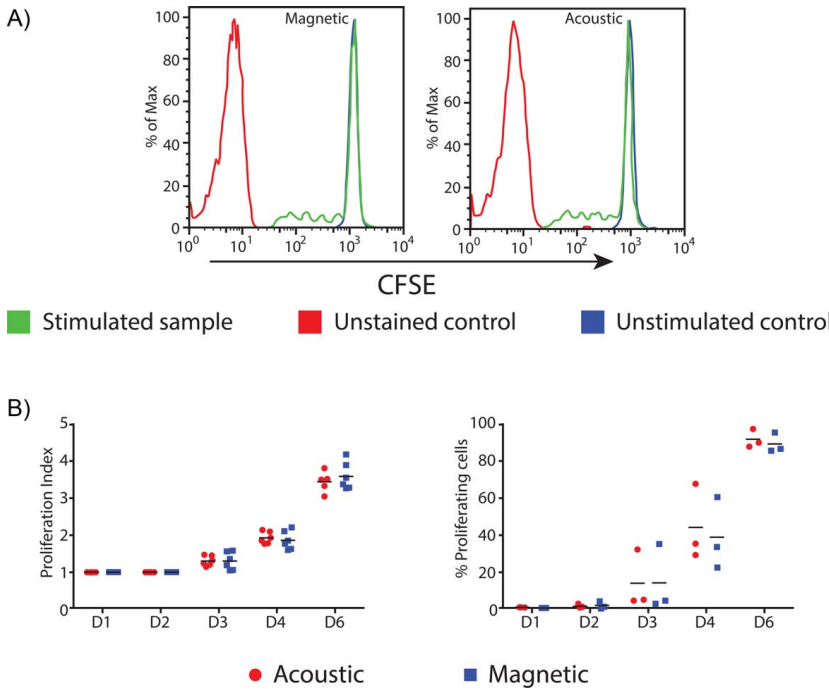

Figure 4. CD4+ T lymphocyte proliferation. Induced proliferation capacity of sorted CD4+ cells as measured by cell division (CFSE), following 6 days of cultivation in the presence of activating PMA/Ionomycin or anti CD3/CD28. Representative histograms from one of three samples at Day 4 are shown (**A**). Acoustic sorted CD4+ cells were evaluated each day of culture in the presence of anti CD3/CD28. The proliferation index, i.e., the ratio of the total number of dividing cells to the number of original parent cells, as well as the relative numbers of proliferating cells in culture each day, are given (**B**).

Progenitor Cell Function Is Not Affected by Acoustophoresis

Cells from PBPC samples ($n = 5$) were plated in methylcellulose before and after acoustophoresis separation and evaluated for colony-forming ability (Supporting Information Fig. S2). Results were comparable ($P = 0.9344$) in pre- and postsort samples indicating a preserved clonogenic capacity postsorting, with a mean (±SD) number of granulocyte macrophage colony-forming units (CFU-GM)/3,000 plated cells of 11 ± 2.2 in the presort (PBPC) and 12 ± 1.4 in the postsort (nontarget fraction) samples, respectively. Similarly, a mean (±SD) number of erythroid burst-forming units (BFU-E)/3,000 plated cells of 7.0 ± 0.8 were yielded in postsort samples compared with 7.7 ± 1.6 in presort samples ($P = 0.4071$).

CD4+ T-Lymphocyte Function Is Not Affected by Acoustophoresis

Isolated CD4+ cells ($n = 4$) were cultured for six days in the presence of activating PMA/Ionomycin or CD3/CD28 antibodies, to evaluate their functional capacity in terms of proliferation and cytokine production following acoustic and magnetic separation, respectively (Figs. 4 and 5). The results of in vitro activation indicated that acoustically isolated CD4+ cells were equally responsive to stimulation with anti-CD3/CD28 as were magnetically sorted cells ($P = 0.9367$), with a mean (±SD) relative number of proliferating isolated cells of 75 ± 16% (acoustic) versus 74 ± 5.9% (magnetic) Following PMA/Ionomycin stimulation, however, cell proliferation levels were slightly higher in magnetically (87 ± 6.5%) compared with acoustically sorted cells (75 ± 9.4%), although the difference was not statistically significant ($P = 0.0808$). Another three samples of sorted CD4+ cells were evaluated at Days 1, 2, 3, 4, and 6 of culture in the presence of anti CD3/CD28. The proliferation index, i.e., the ratio of the total number of dividing cells to the number of original parent cells, showed no significant difference in the immediate proliferative capacity of acoustically versus magnetically sorted CD4+ cells, indicating a lack of stress induced on the cells by either of the two sorting techniques. The proliferation index for acoustically versus magnetically isolated cells was at Days 1 and 2 (1.00 ± 0.00 versus 1.00 ± 0.00), at Day 3 (1.30 ± 0.24

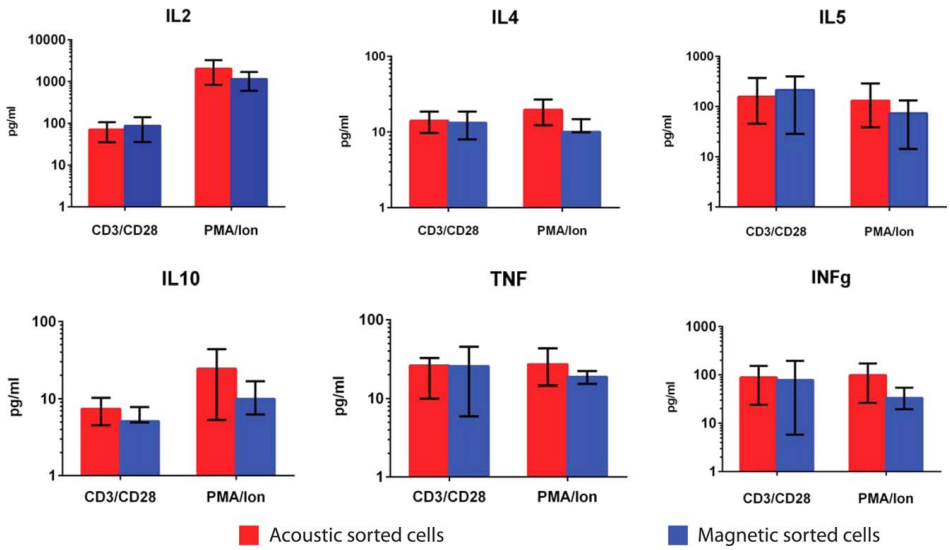

Figure 5. CD4+ T lymphocyte Cytokine Production. Cytokine production of proliferating sorted CD4+ cells as quantified by the CBA Human Th1/Th2 Cytokine Kit. Cytokine (IL-2, IL-4, IL-5, IL-10, TNF, IFNγ) secretion levels of proliferating acoustic and magnetic sorted CD4+ cells, respectively, are given as the mean (±SD) of four individual samples. No significant difference in the cytokine production levels between acoustically and magnetically isolated cells could be detected.

versus 1.30 ± 0.14), at Day 4 (1.86 ± 0.25 versus 1.93 ± 0.16), and at Day 6 (3.59 ± 0.37 versus 3.44 ± 0.28) (Fig. 4B).

Moreover, there was no significant difference in cytokine production levels between acoustically and magnetically isolated cells (Fig. 5), as quantified by the CBA Human Th1/Th2 Cytokine Kit. Following PMA/Ionomycin stimulation of acoustically and magnetically isolated cells, respectively, the secretion levels (mean ± SD pg/mL) were similar for interleukin (IL)-2 (1,150 ± 554 versus 2,029 ± 1,203), IL-4 (11 ± 2.4 versus 20 ± 7.3), IL-5 (73 ± 59 versus 148 ± 105), IL-10 (11 ± 4.5 versus 24 ± 19), tumor necrosis factor (TNF, 19 ± 3.4 versus 28 ± 13) and interferon gamma (INFg, 35 ± 15 versus 99 ± 73). Following CD3/CD28 stimulation, the secretion levels (mean ± SD pg/mL) for acoustic versus magnetic isolation were as follows: IL-2 (88 ± 52 versus 71 ± 36); IL-4 (13 ± 5.2 versus 14 ± 4.4); IL-5 (214 ± 186 versus 183 ± 138); IL-10 (5.8 ± 1.4 versus 7.4 ± 2.9); TNF (26 ± 20 versus 24 ± 9.7), and INFg (89 ± 80 versus 89 ±65).

Discussion

Acoustophoresis provides a gentle method for continuous flow separation primarily based on biophysical properties of the cells or particles to be separated, i.e., size, density, and compressibility (5). Recently, size-dependent acoustophoretic separation with integrated prefocusing was demonstrated to enable a highly discriminative separation of polystyrene microbeads (5 and 7 μm in diameter) as well as tumor cells from white blood cells (9). Acoustic fractionation of more complex cell or particle suspensions, that display partly overlapping acoustic properties in an aqueous system, can be successfully addressed by altering the density of the suspending medium (17), whereas the acoustic properties of affinity micro beads can be exploited for selective extraction of targets like bioanalytes (20) and phages (19), which would otherwise be difficult to acoustically discriminate due to their small size.

On the basis of these principles, we investigated a microfluidic acoustophoresis platform for the selective extraction of a specific lymphocyte subset from a suspension of PBPC-derived MNC, by utilizing affinity micro beads to alter the acoustic properties of targeted cells. CD4+ lymphocytes were chosen as a prototype to be labeled with commercially available magnetic micro beads (Dynabeads), thus enabling acoustophoretic separation and control magnetic sorting in parallel. Given the relatively small size of the micro beads (4.5 μm) compared with the targeted lymphocytes (7–10 μm) (22) and the variable number of beads that bind to each cell, the resulting size distribution of labeled CD4+ cells will partly overlap with nonlabeled MNC (7–20 μm). Consequently, labeled and nonlabeled cells display similar acoustic properties and cannot be adequately separated by standard size-dependent acoustophoresis (9,10,12). However, the radiation force responsible for particle migration in an acoustic field is also dependent on density and compressibility of the particle relative to the

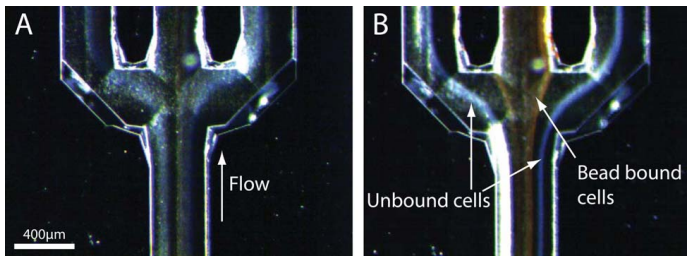

Figure 6. The effect of wash buffer density adjustment. **A**: When PBS is used as wash buffer, labeled, and nonlabeled cells are both affected by the acoustic forces in a similar way and distributed to both the central and lateral exit branches. Thus, separation is not achieved. **B**: With the use of the denser Ficoll wash buffer, bead-labeled cells are successfully isolated through the central outlet (brown streak in central outlet), while nonlabeled cells (white streaks) exit laterally.

surrounding media (5). With a wash buffer of equal composition to the original sample buffer, e.g., PBS, labeled cells cannot be isolated from nonlabeled cells of overlapping size (see Fig. 6A). By utilizing a wash buffer of a denser medium, such as Ficoll (density 1.077 g/mL), the nonlabeled MNC (density 1.062–1.070 g/mL) (23) and the cells labeled with the dense magnetic micro beads (1.6 g/cm^3)will, however, display a significantly different acoustic contrast factor in the central wash buffer. The denser Ficoll wash buffer will, thus, provide an acoustic impedance barrier preventing the unlabeled cells from entering the Ficoll buffer in the center of the channel when exposed to acoustic forces. This is seen in Fig. 6B where the unbound cells are confined to a distinct band at the buffer interface, exiting the side outlet, and the bead bound cells are focused to the centre outlet. Accordingly, with the use of Ficoll wash buffer the acoustic power could be tuned such that the labeled CD4+ lymphocytes were efficiently separated (65%) into the center of the channel at a high purity (87%), whereas nonlabeled cells remained at the lateral walls (Fig. 1). The selective separation of CD4+ lymphocytes to the target fraction was coupled to a relative increase of CD8+ cells, CD34+ cells, CD14+ cells, CD56+ cell, and CD19+ cells, in the postsort (nontarget fraction) compared with the presort (PBPC) samples. The observed changes in the distribution of nontargeted lymphocyte subpopulations were found to be within the expected range. A negative influence of acoustophoresis on cell viability could be ruled out, thus confirming previously reported studies (7,12). Also, in agreement with our previous experience (12), the functional capacity of early hematopoietic progenitor cells was not affected by the acoustophoresis procedure. G-CSF treatment for PBPC mobilization may alter CD4+ T helper (Th) cell function, as indicated by a reduced proliferative response to in vitro stimulation and a shift in cytokine secretion profile from a Th1 to a Th2 phenotype (24,25). Notwithstanding, CD4+ T lymphocytes isolated from PBPC grafts were similar in proliferative capacity and cytokine production levels following acoustic and magnetic separation, respectively.

The performance of the acoustic separation (separation efficiency 65%, purity 87%), compared well to the control magnetic sorting (recovery 56%, purity 96%), and also to what can be obtained using current standard technology for large scale, clinical grade MACS (recovery 60%, purity 95%) (26,27). However, technical improvements of the current acoustophoretic setup, such as optimization of the resonance frequency, wash buffer modification or adjustment of the relative flow rates at the inlets and outlets, may further increase separation efficiency, target cell purity and sample throughput. Moreover, automated temperature control of the acoustophoresis device may be employed to enhance separation stability, as previously reported by Augustsson et al. (18). In terms of sample throughput, large scale MACS for clinical cell separation performs at a sample processing rate of 3–5 mL/min (28). Operating multiple acoustic separation channels in parallel would be a possible approach to increase sample throughput, as was previously described for microchip-based blood washing utilizing a device comprising eight separation channels in a bifurcation tree at a flow rate of 0.5 mL/min (29). Ultimately, an acoustic chip designed to enable targeted micro beads with different acoustic properties to be sequentially extracted would realize simultaneous affinity sorting of multiple cell populations, which is not possible with current magnetic separation technology.

Cell separation technologies are essential in processing of PBPC for clinical transplantation or research applications. The performance of cell separation techniques is characterized by target cell recovery and purity, but should also include low mechanical stress and minimal interference such that separated cells maintain viability and biological function. Large-scale separation, such as in PBPC graft engineering, additionally demands high capacity and throughput. Also, processing of cells for therapeutic use must be carried out in closed systems or, otherwise, under controlled environmental conditions in conformity with Good Manufacturing Practice standards (30). Acoustophoresis has recently emerged as an efficient and gentle method for closed environment continuous flow cell separation with potential applications in the field of PBPC graft engineering. Acoustic transfer of intact target cells to a clean suspension medium (20,31) with concomitant platelet depletion (12) is certainly an attractive alternative to the manual centrifugation

steps currently applied for cell wash (32), with accumulating mechanical stress on target cells and risk of cell loss. Today, advanced processing such as CD34+ progenitor cell selection or T-cell depletion requires a complete switch to a second platform, i.e., MACS, which is restricted to one-parameter sorting (1). With the potential application of multitarget affinity-acoustophoresis (i.e., the use of targeted microbeads), for discriminative separation of multiple cell populations (T-cells, B-cells, NK-cells, etc.), acoustophoresis has the potential to offer a single platform technique for multiparameter cell separation in PBPC graft engineering.

Conclusions

We demonstrate the efficient purification of CD4+ lymphocytes from a heterogeneous suspension of hematopoietic cells without impairing lymphocyte or progenitor cell function, by combining affinity-bead-mediated acoustophoresis and buffer density adjustment. Affinity-assisted acoustophoresis is, thus, an interesting technology for PBPC processing, which has furthermore the potential to offer a single platform technique for multiparameter cell separation.

Acknowledgments

The authors would like to thank Dr. Per Augustsson at the Department of Biomedical Engineering, Lund University, Lund, Sweden, for his help with designing and manufacturing the acoustophoretic silicon chip.

Literature Cited

1. Dainiak MB, Kumar A, Galaev IY, Mattiasson B. Methods in cell separations. Cell separation: Fundamentals, analytical and preparative methods. Adv Biochem Eng Biotechnol 2007;106:1–18.
2. Miltenyi S, Muller W, Weichel W, Radbruch A. High gradient magnetic cell separation with MACS. Cytometry 1990;11:231–238.
3. Ibrahim SF, van den Engh G. Flow cytometry and cell sorting. Cell separation: Fundamentals, analytical and preparative methods. Adv Biochem Eng-Biotechnol 2007; 106:19–39.
4. Ljungman P, Bregni M, Brune M, Cornelissen J, de Witte T, Dini G, Einsele H, Gaspar HB, Gratwohl A, Passweg J, et al. Allogeneic and autologous transplantation for haematological diseases, solid tumours and immune disorders: Current practice in Europe 2009. Bone Marrow Transplant 2010;45:219–234.
5. Laurell T, Petersson F, Nilsson A. Chip integrated strategies for acoustic separation and manipulation of cells and particles. Chem Soc Rev 2007;36:492–506.
6. Jonsson H, Nilsson A, Petersson F, Allers M, Laurell T. Particle separation using ultrasound can be used with human shed mediastinal blood. Perfusion-UK 2005;20: 39–43.
7. Burguillos MA, Magnusson C, Nordin M, Lenshof A, Augustsson P, Hansson MJ, Elmer E, Lilja H, Brundin P, Laurell T, et al. Microchannel acoustophoresis does not impact survival or function of microglia, leukocytes or tumor cells. PLOS ONE 2013;8:e64233.
8. Hultstrom J, Manneberg O, Dopf K, Hertz HM, Brismar H, Wiklund M. Proliferation and viability of adherent cells manipulated by standing-wave ultrasound in a microfluidic chip. Ultrasound Med Biol 2007;33:145–151.
9. Augustsson P, Magnusson C, Nordin M, Lilja H, Laurell T. Microfluidic, label-free enrichment of prostate cancer cells in blood based on acoustophoresis. Anal Chem 2012;84:7954–7962.
10. Thevoz P, Adams JD, Shea H, Bruus H, Soh HT. Acoustophoretic synchronization of mammalian cells in microchannels. Anal Chem 2010;82:3094–3098.
11. Lenshof A, Laurell T. Emerging clinical applications of microchip-based acoustophoresis. JALA 2011;16:443–449.
12. Dykes J, Lenshof A, Astrand-Grundstrom IB, Laurell T, Scheding S. Efficient removal of platelets from peripheral blood progenitor cell products using a novel micro-chip based acoustophoretic platform. PLoS One 2011;6:e23074.
13. Tajudin AA, Petersson K, Lenshof A, Sward-Nilsson AM, Aberg L, Marko-Varga G, Malm J, Lilja H, Laurell T. Integrated acoustic immunoaffinity-capture (IAI) platform for detection of PSA from whole blood samples. Lab Chip 2013;13:1790–1796.
14. Nilsson A, Petersson F, Jonsson H, Laurell T. Acoustic control of suspended particles in micro fluidic chips. Lab Chip 2004;4:131–135.
15. Petersson F, Nilsson A, Holm C, Jonsson H, Laurell T. Separation of lipids from blood utilizing ultrasonic standing waves in microfluidic channels. Analyst 2004;129: 938–943.
16. Cushing KW, Piyasena ME, Carroll NJ, Maestas GC, Lopez BA, Edwards BS, Graves SW, Lopez GP. Elastomeric negative acoustic contrast particles for affinity capture assays. Anal Chem 2013;85:2208–2215.
17. Petersson F, Aberg L, Sward-Nilsson AM, Laurell T. Free flow acoustophoresis: Microfluidic-based mode of particle and cell separation. Anal Chem 2007;79:5117–5123.
18. Augustsson P, Barnkob R, Wereley ST, Bruus H, Laurell T. Automated and temperature-controlled micro-PIV measurements enabling long-term-stable microchannel acoustophoresis characterization. Lab Chip 2011:4152–4164.
19. Persson J, Augustsson P, Laurell T, Ohlin M. Acoustic microfluidic chip technology to facilitate automation of phage display selection. FEBS J 2008;275:5657–5666.
20. Augustsson P, Persson J, Ekstrom S, Ohlin M, Laurell T. Decomplexing biofluids using microchip based acoustophoresis. Lab Chip 2009;9:810–818.
21. Adams JD, Thevoz P, Bruus H, Soh HT. Integrated acoustic and magnetic separation in microfluidic channels. Appl Phys Lett 2009;95:254103.
22. Dailey JF. Blood. Manley JE, editor. Arlington, MA 02474, U.S.A.: Medical Consulting Group; 1998.
23. Guide to the preparation, use and quality assurance of blood components, 13th ed.; Council of Europe publishing: Strasbourg, 2007.
24. Sloand EM, Kim S, Maciejewski JP, Van Rhee F, Chaudhuri A, Barrett J, Young NS. Pharmacologic doses of granulocyte colony-stimulating factor affect cytokine production by lymphocytes in vitro and in vivo. Blood 2000;95:2269–2274.
25. Jun HX, Jun CY, Yu ZX. In vivo induction of T-cell hyporesponsiveness and alteration of immunological cells of bone marrow grafts using granulocyte colony-stimulating factor. Haematologica 2004;89:1517–1524.
26. Schumm M, Lang P, Taylor G, Kuci S, Klingebiel T, Buhring HJ, Geiselhart A, Niethammer D, Handgretinger R. Isolation of highly purified autologous and allogeneic peripheral CD34(+) cells using the CliniMACS device. J Hematotherapy 1999; 8:209–218.
27. Lang P, Handgretinger R, Niethammer D, Schlegel PG, Schumm M, Greil J, Bader P, Engel C, Scheel-Walter H, Eyrich M, et al. Transplantation of highly purified CD34(+) progenitor cells from unrelated donors in pediatric leukemia. Blood 2003; 101:1630–1636.
28. Dykes JH, Hult A, Toporski J, Lenhoff S, Scheding S, Turkiewicz D. Effective TcR alpha/beta plus cell depletion using the CliniMACS (R) system to produce peripheral blood progenitor cell products for haploidentical transplantation. Bone Marrow Transplant 2013;48:S187–S187.
29. Jonsson H, Holm C, Nilsson A, Petersson F, Johnsson P, Laurell T. Particle separation using ultrasound can radically reduce embolic load to brain after cardiac surgery. Annals Thoracic Surg 2004;78:1572–1578.
30. DIRECTIVE 2004/23/EC OF THE EUROPEAN PARLIAMENT AND OF THE COUNCIL of 31 March 2004 on setting standards of quality and safety for the donation p, testing, processing, preservation, storage and distribution of human tissues and cells: Official Journal of the European Union.
31. Lenshof A, Magnusson C, Laurell T. Acoustofluidics 8: Applications of acoustophoresis in continuous flow microsystems. Lab Chip 2012;12:1210–1223.
32. Dykes JH, Toporski J, Juliusson G, Bekassy AN, Lenhoff S, Lindmark A, Scheding S. Rapid and effective CD3 T-cell depletion with a magnetic cell sorting program to produce peripheral blood progenitor cell products for haploidentical transplantation in children and adults. Transfusion 2007;47:2134–2142.

SUPPLEMENTARY INFORMATION

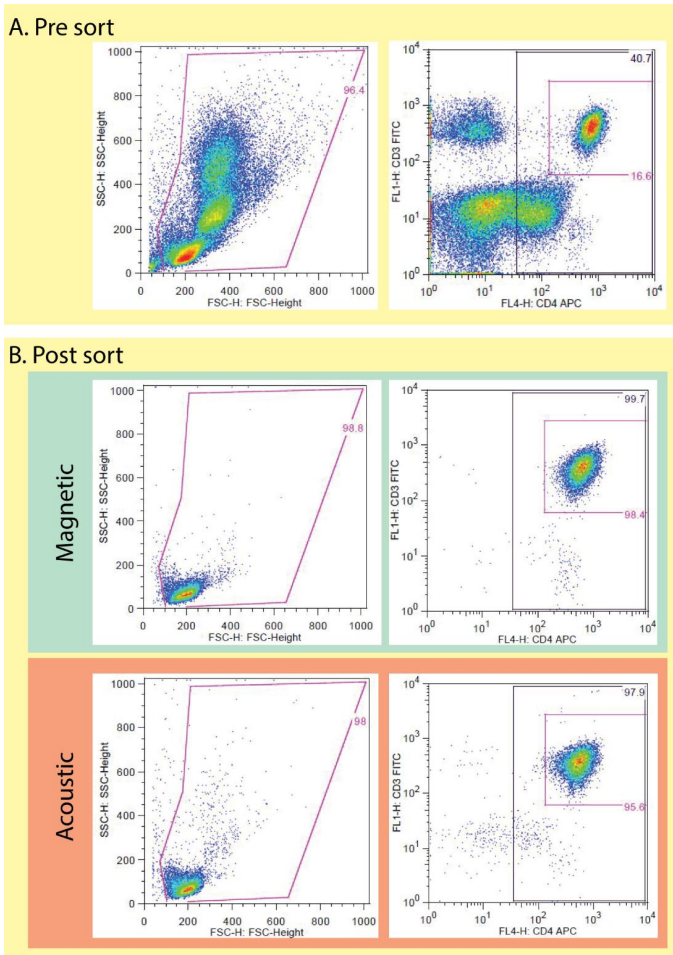

Supplementary Figure S1. Flow cytometry analysis of a representative PBPC sample before cell sorting (A) and following parallel enrichment of CD4+ cells by magnetic and acoustic separation, respectively (B). CD4+ cells and CD3+/4+ T lymphocytes are gated after exclusion of debris and dead cells (7AAD positive).

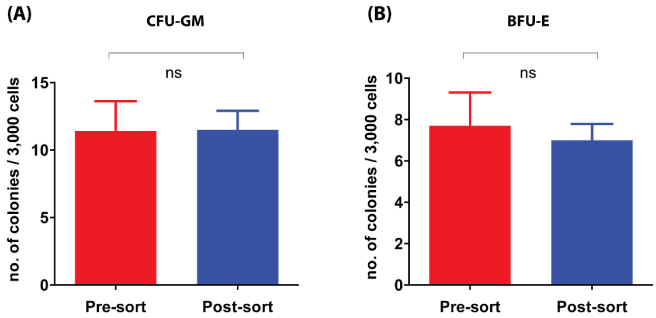

Figure S2.Clonogenic capacity. The mean (± SD) numbers of white (A) and red (B) colonies, respectively, per 3,000 plated cells from five different PBPC samples (pre-sort) and their corresponding non-target fractions (post-sort) are presented. (ns = non-significant).

Supplementary Table S1. The purity of CD4+ T lymphocytes in the acoustic target fractions isolated from individual PBPC samples.

sample no.	sample	CD3+CD4+ cells purity %
1	Myeloma	89.6
2	Myeloma	92.5
3	Lymphoma	93.7
4	Myeloma	93.6
5	Healthy	94.6
6	Myeloma	46.4
7	Myeloma	81.3
8	Myeloma	79.0
9	Healthy	93.1
10	Healthy	96.7
11	Healthy	96.6
12	Myeloma	72.1
13	Myeloma	84.6
14	Healthy	92.3
15	Myeloma	92.7
16	Lymphoma	78.8
17	Myeloma	83.6
18	Lymphoma	81.6
19	Myeloma	82.9
20	Lymphoma	94.1
21	Healthy	94.8
22	Healthy	97.4

Paper II

micromachines

MDPI

Article

Affinity-Bead-Mediated Enrichment of CD8+ Lymphocytes from Peripheral Blood Progenitor Cell Products Using Acoustophoresis

Anke Urbansky [1,*], Andreas Lenshof [1], Josefina Dykes [2,3], Thomas Laurell [1,4,*] and Stefan Scheding [2,5]

1 Department of Biomedical Engineering, Lund University, 221 00 Lund, Sweden; andreas.lenshof@bme.lth.se
2 Department of Laboratory Medicine, Lund Stem Cell Center, Lund University, 221 00 Lund, Sweden; josefina.dykes@med.lu.se (J.D.); stefan.scheding@med.lu.se (S.S.)
3 Department of Clinical Immunology and Tranfusion medicine, University and Regional Laboratories, 221 85 Lund, Sweden
4 Department of Biomedical Engineering, Dongguk University, 04620 Seoul, Korea
5 Department of Hematology, University Hospital Skåne, 222 41 Lund, Sweden
* Correspondence: anke.urbansky@bme.lth.se (A.U.); thomas.laurell@bme.lth.se (T.L.); Tel.: +46-722-810-566 (A.U.); +46-706-667-540 (T.L.)

Academic Editor: Nam-Trung Nguyen
Received: 14 March 2016; Accepted: 2 June 2016; Published: 9 June 2016

Abstract: Acoustophoresis is a technique that applies ultrasonic standing wave forces in a microchannel to sort cells depending on their physical properties in relation to the surrounding media. Cell handling and separation for research and clinical applications aims to efficiently separate specific cell populations. Here, we investigated the sorting of CD8 lymphocytes from peripheral blood progenitor cell (PBPC) products by affinity-bead-mediated acoustophoresis. PBPC samples were obtained from healthy donors (n = 4) and patients (n = 18). Mononuclear cells were labeled with anti-CD8-coated magnetic beads and sorted on an acoustophoretic microfluidic device and by standard magnetic cell sorting as a reference method. CD8 lymphocytes were acoustically sorted with a mean purity of 91% $\pm$ 8% and a median separation efficiency of 63% (range 15.1%–90.5%) as compared to magnetic sorting (purity 91% $\pm$ 14%, recovery 29% (range 5.1%–47.3%)). The viability as well as the proliferation capacity of sorted lymphocytes in the target fraction were unimpaired and, furthermore, hematopoietic progenitor cell assay revealed a preserved clonogenic capacity post-sorting. Bead-mediated acoustophoresis can, therefore, be utilized to efficiently sort less frequent CD8+ lymphocytes from PBPC products in a continuous flow mode while maintaining cell viability and functional capacity of both target and non-target fractions.

Keywords: acoustophoresis; ultrasound; CD8 lymphocytes; magnetic-beads; cell sorting; PBPC; peripheral blood progenitor cells

1. Introduction

Hematopoietic stem cell transplantation (HSCT) is an established therapy for hematological malignancies and other diseases. Potential stem cell sources are bone marrow, peripheral blood and umbilical cord blood. Over the last two decades peripheral blood progenitor cells (PBPC), which are collected after mobilization treatment, have replaced bone marrow as the main stem cell source for transplantations [1].

A standard transplant contains a variety of different cells including stem and progenitor cells as well as different lymphocyte populations [2–4], and it has been shown that an optimal graft composition of the transplant is crucial for the transplantation outcome [5]. For example, CD8 depletion

in nonmyeloablative allogeneic stem cell transplantation decreased graft-*versus*-host disease (GVHD) while preserving engraftment and the graft-*versus*-leukemia (GVL) effect [6]. Other groups have shown that a higher CD8+ cell dose in myeloablative as well as nonmyeloablative allogeneic HSCT correlates with better T cell engraftment, improved freedom from disease progression and overall survival [7,8]. Therefore, graft processing methods have been developed aiming to provide an optimized transplant by enrichment or depletion of certain cell types. Following collection of chemotherapy- and/or hematopoietic growth factor–mobilized peripheral blood stem cells by large-volume leukapheresis [9], further processing of PBPC products is nowadays usually performed by large-scale magnetic cell sorting (MACS) [10,11]. Microfluidic approaches to separate lymphocyte subpopulations from clinical samples in continuous flow-based magnetic separations have not been reported. However, studies investigating the isolation of tumor cell lines spiked in blood have demonstrated high recoveries as well as reasonable purities [12]. Fluorescence-activated cell sorting (FACS) is also an option which, however, is limited by extensive processing times when sorting clinically relevant cell numbers and difficulties in complying with current good manufacturing practices (GMP) regulations [13,14].

As an alternative cell handling and sorting tool, acoustophoresis has gained increased attention for preclinical-scale cell sorting with a strong developmental potential towards later clinical applications [15,16]. Acoustophoresis utilizes an ultrasonic standing wave generated in a microchannel commonly of a width corresponding to half a wavelength [17]. The standing wave generates a pressure node in the center of the channel and a pressure anti-node at the sidewall, and consequently, the acoustic radiation forces will induce a movement of suspended particles either to the pressure node or the anti-node, depending on physical properties such as size, density and compressibility in relation to the suspending medium. Typically, denser particles such as cells or beads move to the pressure node in aqueous systems while less dense particles such as lipid particles are focused towards the pressure anti-node [18]. The magnitude of the radiation force increases with the cube of the particle radius and, therefore, larger particles move faster compared to smaller particles with the same acoustic properties [19]. Acoustophoresis, as a continuous laminar flow-based and easy-to-handle separation method, has been shown not to affect cell viability or functional capacity [20–22], and thus might offer an alternative for cell handling in clinical settings [15,23–26].

Recently, label-free separation of lymphocytes and granulocytes as well as platelets was demonstrated using microchip-based free-flow acoustophoresis [25,27]. Based on these results we developed a system to acoustically sort bead-labeled CD4 lymphocytes from peripheral stem cell products [28]. Bead-labeling was introduced to form bead-target cell complexes which have a higher net acoustic mobility than unbound cells and thus enable acoustophoretic discrimination of the target lymphocytes from the general lymphocyte population. Label-free acoustic separation of lymphocyte subpopulations is not possible due to the minute differences in acoustic properties, specifically in size.

In the current work, we investigated the performance of affinity-bead-mediated acoustophoresis to separate CD8+ cytotoxic T cells from PBPC products and optimized the sorting for this cell population, which is less frequent in the starting material compared to CD4+ cells. Following system optimization, we were able to increase the processing speed by a factor of two, as compared to our earlier work on acoustic separation of CD4+ cells [28], while still obtaining efficient separation with fully preserved functional capacity of sorted cells. Affinity-bead-mediated acoustophoresis can therefore be used to target and enrich specific cell populations in a continuously perfused microfluidic device. Furthermore, these data represent a step forward towards acoustic sorting of even rarer cell populations, such as peripheral blood stem cells and also open up the potential for simultaneous acoustic separation of multiple cell populations.

2. Materials and Methods

2.1. Ethical Statement

The use of patient and donor PBPC products in the current study was approved by the Regional Ethical Review Board at Lund University. Written informed consent was obtained from all participants involved in the study.

2.2. Sample Collection

Peripheral blood progenitor cell products were obtained by large volume leukapheresis performed with a Cobe Spectra (Terumo BCT, Lakewood, CO, USA), using the MNC program, version 7.0. Samples were collected after standard mobilization treatment of healthy donors (granulocyte colony-stimulating factor (G-CSF), Filgrastim, Sandoz, Novartis, Basel, Switzerland) and patients (protocol specific chemotherapy + G-CSF). On the day of leukapheresis, 1 mL of PBPC sample was removed from the collection bag and the mononuclear cell (MNC) fraction was isolated by Ficoll density gradient centrifugation for subsequent use in the experiments.

2.3. Labeling of CD8+ Cells with Affinity Beads

Superparamagnetic 4.5 μm polystyrene Dynabeads (Invitrogen Life Technologies, Thermo Fisher Scientific, Waltham, MA, USA) coated with primary monoclonal anti-CD8 antibody were used to label CD8+ cells in the MNC fraction. Magnetic beads used in this study were chosen for acoustic separation due to their commercial availability as well as to have a positive control of the separation procedure using a standard method, in this case magnetic sorting. In general, affinity-bead-mediated acoustophoresis can be performed with any kind of bead, as long as it has proper acoustic properties to distinguish bead-bound cells from unbound cells in the acoustic field.

In brief, 25 μL Dynabeads were added per 10^7 cells/mL and incubated at 4 °C for 20 min under continuous agitation. The sample was split equally for tube-based magnetic separation on a DynaMag^{TM}-15 magnet (Thermo Fisher Scientific) and acoustic separation on an acoustophoresis micro-chip in parallel (see below).

Following magnetic and acoustic separation, the isolated cells were incubated with DETACHaBEAD (10 μL per 10^7 cells) at room temperature for 45 min under continuous agitation to release bound beads. The cell-bead mixture was exposed to a DynaMag^{TM}-15 magnet and the supernatant containing released cells was transferred to a fresh tube. The beads were washed twice in 1 mL PBS + 2% fetal bovine serum (FBS) (Gibco Life Technologies, Thermo Fisher Scientific) and 0.6% acid-citrate-dextrose (ACDA) (Terumo BCT) to recover residual cells. Collected cells were washed by centrifugation at 400× *g* for 5 min, stained with Trypan blue (Gibco Life Technologies) for dead cell exclusion and counted using a Neubauer chamber.

2.4. Magnetic Cell Separation

Magnetic separation was performed according to manufacturer's instructions (Dynabeads CD8 Positive Isolation Kit, Invitrogen Life Technologies). Bead-labeled cells were isolated using a DynaMag^{TM}-15 magnet while non-labeled cells were removed by washing three times with 1 mL wash buffer (PBS with 2% FBS and 0.6% ACDA). Isolated cells were released from the magnet and re-suspended in wash buffer (100 μL/10^7 cells).

2.5. Acoustophoresis Chip

A detailed description of the acoustophoresis chip design and fabrication process can be found in Augustsson *et al*. [26]. In brief, the structure of the microchannel was made by anisotropic wet etching in a silicon wafer using standard photolithography and anisotropic KOH etching, and sealed with a glass lid using anodic bonding. The chip consists of a sample inlet, leading to a pre-focusing channel

(10 mm × 300 µm × 150 µm), a flow splitter that directs the flow to each side of a central fluid inlet, and a main separation channel (20 mm × 375 µm × 150 µm) ending in a trifurcation with one central outlet and a common outlet for the two side branches (Figure 1). Docking ports for fluidic tubing were glued to the inlets and outlets in form of silicon tubing with an inner diameter of one-sixteenth of an inch.

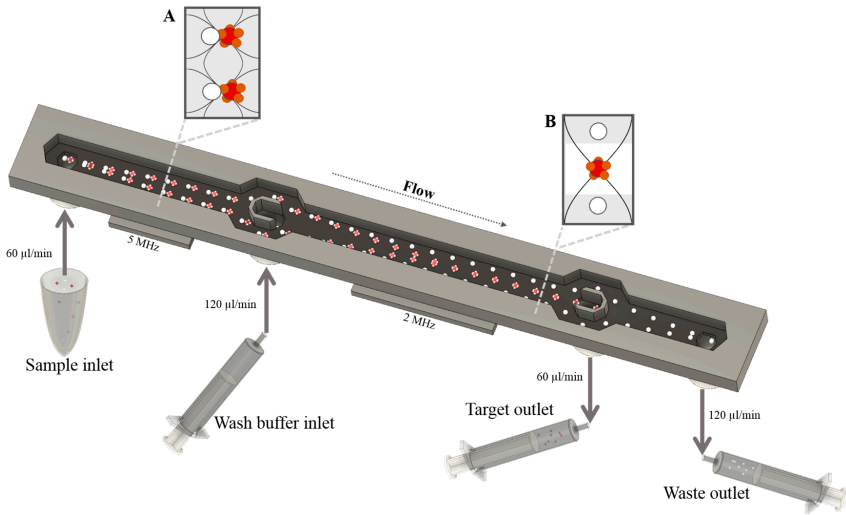

Figure 1. Schematic picture of the acoustophoretic chip design. The sample consisting of a mixture of bead-bound cells (red) and unbound cells (white) is injected into the pre-focusing channel through the sample inlet. In a first step particles are pre-focused into two parallel bands (**A**) using a 5 MHz piezoceramic transducer that drives a full wavelength resonance across the channel width, with two pressure nodes that superimpose with a half-wavelength resonance in the vertical direction. Following the flow direction, the particles are then bifurcated to each side of the wash buffer inlet where Ficoll is infused. Due to the pre-focusing step, cells enter the separation channel close to the channel walls and are prealigned in the width and height dimension of the channel, ensuring an identical starting position for the separation procedure and thereby maximizing the resolution of the separation. In the main separation channel, acoustic forces in an ultrasonic standing wave field with a pressure node in the center of the channel induce movement of cells and particles depending on their acoustophysical properties. Bead-bound cells are forced into the Ficoll buffer (**B**) and can be collected through the target outlet while unbound cells stay close to the channel wall and can be collected through the waste outlet.

A piezoceramic transducer resonant at 5 MHz was glued underneath the pre-focusing channel, while a second piezoceramic transducer resonant at 2 MHz was attached underneath the main separation channel. Both transducers were driven by a dual channel function generator (AFG3022B, Tektronix, Beaverton, OR, USA), equipped with signal amplifiers (in-house build), and the voltage over each transducer was measured via a two-channel digital oscilloscope (TDS 1002, Tektronix). For visualization of the separation procedure a Nikon SMZ800 microscope (Nikon, Tokyo, Japan) was used.

2.6. Fluidic Setup and Sample Procedure

The flow through the chip was controlled by three syringe pumps (neMESYS, Cetoni GmbH, Korbußen, Germany). Two of the pumps were coupled to the chip outlets in withdrawal mode and connected to 1 mL plastic syringes (BD Plastipak, Becton Dickinson, Franklin Lakes, NJ, USA). The third pump was used to infuse Ficoll wash buffer (Histopaque-1077, Sigma-Aldrich, St. Louis, MI, USA) via a 5 mL glass syringe (Hamilton Bonaduz, Bonaduz, Switzerland) to the chip central inlet.

Before sample processing, the system was flushed with PBS to evacuate air. The flow rate on each of the three exit branches was set to 60 μL/min and the wash buffer was infused at a flow rate of 120 μL/min. The bead-labeled PBPC sample (1×10^7 MNC in 1 mL) was connected to the chip side inlet and entered into the pre-focusing channel at a net flow rate of 60 μL/min. Due to the pre-focusing step, cells are prealigned in the width and height dimension and enter the separation channel laminated towards the channel walls ensuring an identical starting position for the separation procedure and thereby enhancing the resolution of the separation [26]. The operational parameters such as frequency and voltage were set by visual inspection of the outlet trifurcation, showing an optimal focus of the bead-labeled cells into the central outlet while non-labeled cells were distributed to the side branches. Labeled cells in the center outlet (target fraction) and non-labeled cells in the side outlet (non-target fraction) were collected directly in the syringes.

2.7. Flow Cytometric Analysis

A four-color flow cytometer (FACSCalibur, BD Biosciences, Becton Dickinson) was used to analyze the PBPC samples before and after magnetic and acoustic processing. Cells were spun down at 400× *g*, 4 °C for 5 min, re-suspended in PBS + 2% Gammanorm (Octapharma AG, Lachen, Switzerland) + 1% FBS and incubated with monoclonal antibodies for 35 min at 4 °C in the dark. Directly conjugated monoclonal antibodies used in different combinations in this study were: anti-CD3 fluorescein isothiocyanate (FITC) (clone SK7), anti-CD4 allophycocyanin (APC) (clone SK3), anti-CD8 phycoerythrin (PE) (clone SK1), anti-CD19 APC (clone HIB19), anti-CD34 PE (clone 581), anti-CD45 FITC (clone 2D1), anti-CD45 peridinin-chlorophyll protein (PerCP) (clone 2D1), and anti-CD56 PE (clone MY31), as well as corresponding isotype controls (all from BD Bioscience). Cells were washed by adding 1 mL FACS buffer (PBS, 1% BSA, 0.1% sodium azide (Sigma-Aldrich)), spun down for 5 min at 3000 rpm and re-suspended in FACS buffer. For dead cell exclusion 7-amino-actinomycin D (7-AAD, 200 μg/mL, Sigma-Aldrich) or propidium iodide (PI, 1 μg/mL, Sigma-Aldrich) was added to the cells. Data acquisition on the FACSCalibur was performed using the CellQuest software (BD Biosciences), recording 10,000 events and analyzing the data with FlowJo software (Tree Star Inc., Ashland, OR, USA).

2.8. In Vitro Cell Proliferation Assay

The proliferation capacity of isolated CD8+ cells in response to anti-CD3/anti-CD28 stimulation was evaluated by flow cytometry utilizing carboxyfluorescein diacetate succinimidyl ester (CFSE) staining. In brief, 1×10^6 target cells were suspended in 1 mL pre-warmed PBS/0.1% BSA) and CellTrace CFSE-solution (Invitrogen Life Technologies) at a final concentration of 0.5 μM. Following 10 min of incubation at 37 °C, the staining was quenched by addition of five volumes of ice-cold culture medium (RPMI-1640 (Gibco Life Technologies), 10% human AB serum (Thermo Fisher Scientific)). Following 5 min incubation on ice, cells were washed three times by centrifugation at 400× *g* for 5 min. CFSE labeled CD8+ cells were cultured in duplicates at 15,000 cells per well in a 96-well flat bottom plate (TPP Techno Plastic Products) in a final volume of 200 μL culture medium. Cells were stimulated with anti-CD3 (5 μg/mL) and anti-CD28 (2 μg/mL) (eBioscience) in presence of 50 ng/mL IL-2 (Miltenyi Biotech) and incubated for up to four days (Thermo Forma Steri incubator, 37 °C, 5% CO_2). At indicated time points CFSE fluorescence intensity distributions were measured by flow cytometry (FACSCalibur, CellQuest and FlowJo software) to analyze cell proliferation.

2.9. Hematopoietic Progenitor Cell Assay

Standard colony-forming cell assay using methylcellulose culture (MethoCult H4435 Enriched, Stemcell Technologies Inc., Vancouver, BC, Canada) was used to evaluate the hematopoietic progenitor cell content in PBPC samples and acoustic non-target fractions. Cells were plated at a concentration of 5000 cells/mL and incubated for 14 days at 37 °C and 5% CO_2. Colony-forming units (CFU) were examined using a CK2 inverted microscope (Olympus, Tokyo, Japan) and counted based on standard criteria.

2.10. Statistical Analysis

Statistical tests were performed using GraphPad Prism 5.0 (GraphPad Software, San Diego, CA, USA). Using the paired or unpaired *t*-test, statistical significance was determined for p values $\leqslant 0.05$.

3. Results

3.1. Enrichment of CD8+ Lymphocytes Using Affinity Bead Acoustophoresis

The performance of affinity-bead-mediated enrichment of CD8+ lymphocytes from PBPC products using acoustophoresis was evaluated in comparison to standard magnetic cell sorting (Figure 2). Results from 22 samples (healthy donor $n = 4$, lymphoma $n = 7$, myeloma $n = 8$, multiple sclerosis $n = 3$) showed an efficient separation of targeted cells with a mean purity (±SD) of 90.9% ± 8.3% for acoustic sorting as compared to 90.9% ± 13.8% for magnetic sorting. In the magnetic separation, two samples had a purity of less than 65%, whereas for the corresponding acoustically-sorted samples purities of 94.5% and 97.2%, respectively, were reached.

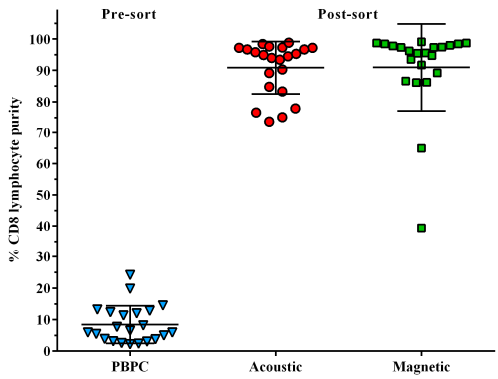

Figure 2. Frequency of CD8+ cytotoxic T cells in pre-sorted peripheral blood progenitor cell (PBPC) products and CD8+ purities following acoustic and magnetic separation post-sorted samples are shown. Both, acoustic and magnetic separation allowed effective enrichment of CD8+ cells. Data are presented as individual data points (triangles, circles, and quadrants) and corresponding means ± SD, $n = 22$.

The median separation efficiency for acoustically sorted samples, as calculated by the ratio of CD8 cells in the target and non-target fraction, was 63.2% (15.1%–90.5%) in comparison to a median recovery of 28.6% (5.1%–47.3%) for standard magnetic separation as defined by the ratio of post-sorted and pre-sorted CD8 cells. Furthermore, the viability of sorted cells, as obtained with 7-AAD staining, was 97.6% ± 1.8% in acoustically sorted samples as compared to 98.3% ± 1.4% for magnetic sorting.

3.2. Distribution of Leukocyte Subpopulations

Flow cytometry analysis was chosen to reveal changes in the distribution of leukocyte subpopulations ($n = 3$) in pre-sorted PBPC samples compared to the non-target fraction after acoustic sorting (post-sort). As expected, the selective removal of CD8+ cells into the target fractions led to a relative increase of non-CD8+ cells in the non-target fraction as compared with the pre-sorted samples (Figure 3).

Comparison of the mean (±SD) relative distribution between leukocyte subsets in the pre-sort *versus* post-sort sample showed the following changes: CD3+/CD4+ T helper cells, 10.15% ± 4.13% *versus* 13.81% ± 6.38%; CD3+/CD8+ cytotoxic T cells, 8.61% ± 8.42% *versus* 3.20% ± 4.14%; CD19+/CD3− B cells, 0.26% ± 0.15% *versus* 0.28% ± 0.11%; CD34+ hematopoietic stem and progenitor

cells, 2.65% ± 0.76% *versus* 2.85% ± 0.92%; and CD56+/CD3− natural killer cells, 2.45% ± 2.46% *versus* 2.64% ± 2.50%.

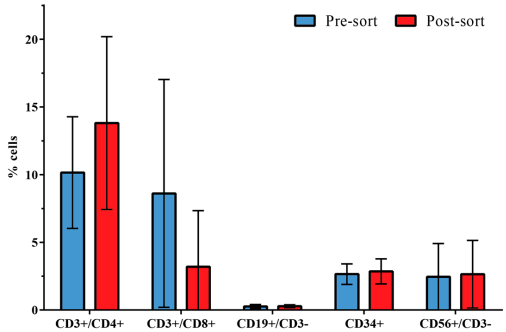

Figure 3. Flow cytometry analysis of the distribution of leukocyte subpopulations in the non-target fraction (side outlet) of acoustically sorted samples. Comparison of the mean (±SD) percentages of CD3+/CD4+, CD3+/CD8+, CD19+/CD3−, CD34+ and CD56+/CD3− cells in pre-sorted PBPC and post-sorted non-target samples (n = 3). Due to the removal of CD8+ cells from the sample and collection in the target fraction, a relative decrease of CD3+/CD8+ cells is observed in the non-target fraction compared to the input PBPC sample.

The low CD19+/CD3− B cell count is due to the fact that all three samples used for the leukocyte subset analysis were from patients with multiple myeloma, for whom a statistically significant decrease of the percentage of total CD19+ cells is observed compared with healthy controls [29].

3.3. CD3/CD28-Mediated T Cell Proliferation Capacity of Acoustically Sorted Cells Is Unimpaired

The proliferative response of acoustically and magnetically sorted CD8+ cytotoxic T cells stimulated with anti CD3/CD28 was evaluated after two, three and four days of culture (n = 3). The results show similar proliferation capacities of acoustically sorted cells compared to the magnetically sorted cells (Figure 4). The mean (±SD) relative number of proliferating cells for acoustically sorted cells *versus* magnetically sorted cells was: 10.7% ± 8% *versus* 12.3% ± 17.2% on day 2, 52.1% ± 18.7% *versus* 55.2% ± 23.8% on day 3, and 84.9% ± 7.7% *versus* 88.0% ± 7.6% on day 4.

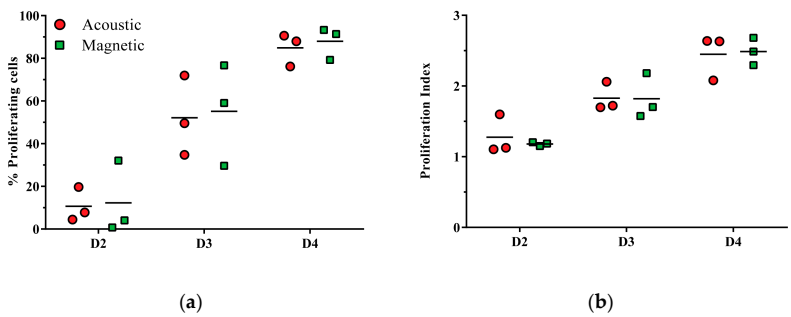

Figure 4. CD3/CD28-mediated T cell proliferation of acoustically and magnetically sorted CD8+ cytotoxic T cells. Cells were stimulated in the presence of anti-CD3/CD28 and proliferation was measured on days 2, 3 and 4 of culture using CFSE staining (n = 3). For each day the relative number of proliferating cells (**a**) as well as the proliferation index, *i.e.*, the average number of cell divisions all responding cells have undergone, are presented (**b**).

In addition to the relative number of proliferating cells, the proliferation index, *i.e.*, the average number of cell divisions all responding cells have undergone, indicated no significant differences between acoustically and magnetically sorted cells. The proliferation index for acoustically *versus* magnetically sorted cells was 1.28% ± 0.28% *versus* 1.18% ± 0.03% on day 2, 1.83% ± 0.20% *versus* 1.82% ± 0.32% on day 3, and 2.45% ± 0.32% *versus* 2.49% ± 0.19% on day 4.

3.4. Hematopoietic Progenitor Cell Colony-Forming Ability Is Unaffected by Acoustophoresis

Colony-forming ability of hematopoietic progenitor cells as evaluated by standard methylcellulose assay revealed a preserved clonogenic capacity post-sorting (Figure 5). The mean (±SD) number of granulocyte macrophage colony-forming units (CFU-GM)/5000 cells was 14.6 ± 6.5 for PBPC samples (pre-sort) as compared to 11.3 ± 5.9 in the corresponding acoustic non-target fraction (post-sort). Correspondingly, there was no significant difference between the mean (±SD) number of erythroid burst-forming units (BFU-E)/5000 cells in the pre-sort (12.6 ± 6.5) *versus* post-sort samples (15.6 ± 5.1).

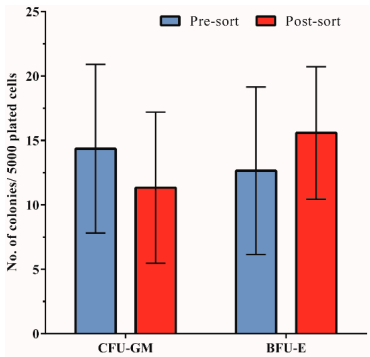

Figure 5. Hematopoietic progenitor cell colony-forming ability. The mean (±SD) number of granulocyte macrophage colony-forming units (CFU-GM) as well as erythroid burst-forming units (BFU-E) is shown for cells from pre-sorted (PBPC) and acoustically post-sorted (non-target) fractions (n = 4).

4. Discussion

Acoustophoresis, as a gentle microfluidic separation method, is based on acoustophysical properties such as size, density and compressibility of the particles in relation to the suspending medium. Previously, acoustophoretic label-free cell separations based on significant size differences have been shown for tumor cell enrichment from white blood cell samples [26], for blood lymphocyte and granulocyte separation [27], as well as for the removal of platelets from PBPC products [25].

In the current study, separation of lymphocyte populations from PBPC products was investigated. Similar acoustic properties of the different lymphocyte subpopulations make it impossible to realize a label-free sorting strategy using acoustic forces. Therefore, we used 4.5 µm affinity beads to label the cells of interest, thereby increasing the size as well as changing the acoustic contrast factor such that the bead-cell complex obtains an increased acoustic mobility as compared to non-labeled cells. However, due to the large variety in the cell diameter of lymphocytes (6–20 µm) [30–32] and the variable number of beads that can bind to a target cell, is it likely that the size of the bead-cell complexes partly overlaps with the non-labeled lymphocytes. We therefore also modified the medium properties of the central buffer to adjust the acoustic forces on the different particles to improve the discrimination of bead-bound cells *versus* non-bead-bound cells. This was performed by adjusting the density of the medium in the central inlet of the acoustophoresis chip, utilizing the known fact that the acoustic contrast factor and hence the resulting acoustic radiation force on a cell is dependent on the density difference *versus* the surrounding medium. The option to tune the net acoustic force on different

cells in a sample was previously demonstrated by Peterson *et al*. by adjusting the density of the cell suspension buffer with cesium chloride [19].

The beads used in our experiments have a density of 1.6 g/mL, whereas unbound cells have a lower density of 1.055–1.085 g/mL [33]. Using Ficoll with a density of 1.078 g/mL as a central buffer, an acoustophoretic barrier is created across which the bead-cell complex is able to migrate. Unbound cells, having a mean lower density than the central buffer, either cannot overcome this barrier or migrate very slowly in the higher density buffer. They can thus be isolated from the bead-cell population and collected at the side outlet of the acoustic chip (Figure 6). By optimizing the central buffer medium properties it became possible to sort CD8+ lymphocytes from mononuclear cells with high purity (90.9%) and efficiency (63.2%) into the center outlet. Analysis of lymphocyte subpopulations in the non-target fraction of the acoustically sorted sample showed a slight relative increase of CD4, CD19, CD34 as well as CD56 cells, which was due to removal of CD8 cells into the target fraction (Figure 3). The distribution of the populations is thus in the expected range. The viability and proliferation capacity of sorted cells were unimpaired, as was the colony-forming ability of hematopoietic stem and progenitor cells in the non-target fraction. These results are in good agreement with previously published data [15,22] and show that acoustophoresis is a promising sorting technology also for possible clinical applications where optimizing the cell composition is of importance.

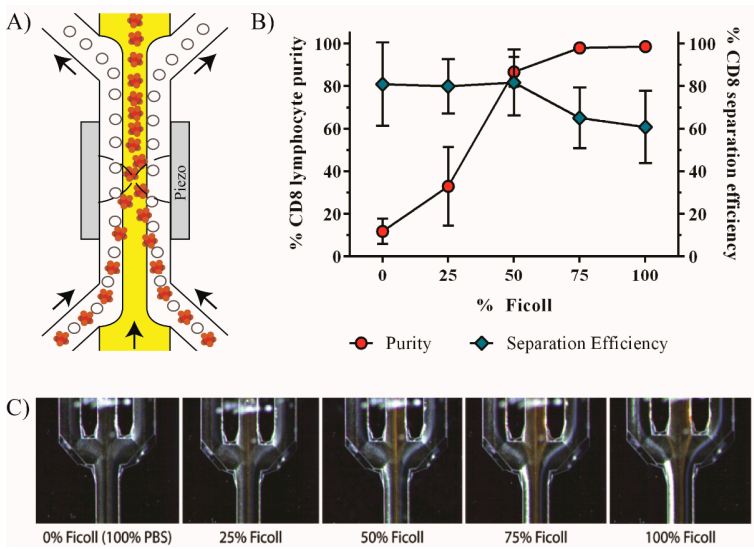

Figure 6. Purity and separation efficiency of acoustically sorted CD8+ cells in relation to the central buffer density. (**A**) Schematic drawing of the microfluidic device showing the effect of the high density central buffer. Bead-labeled cells (orange) and unlabeled cells (white) enter into the main separation channel. High density buffer infused in the central inlet (yellow) creates a barrier across which bead-labeled cells can be acoustically moved into the center stream and collected in the central outlet while unlabeled cells are not able to move into the high density buffer and thus exit the separation channel through the side outlet. Arrows indicate the flow direction; (**B**) Ficoll was diluted in PBS in different concentrations and used as central buffer. The purity of the acoustic separation as well as the separation efficiency was determined (n = 3); (**C**) The image sequence of the central outlet illustrates the effect on the acoustic separation at increasing levels of Ficoll in the central buffer. The increase of the central buffer density creates a barrier through which bead-labeled cells (orange) are able to move whereas unlabeled cells (white) are not and remain at the sidewall to be collected through the side outlet.

The use of affinity microbeads in acoustophoretic applications has previously been shown to allow the capture of phage viral particles [34] and also to sort CD4 lymphocytes from PBPC products [28]. In this paper, we show the ability to sort a lymphocyte population which is considerably less abundant in the starting material as compared to CD4 cells, and our data clearly show that optimized acoustic sorting as described herein can be successfully applied also to the sorting of less frequent cell populations. Also, we were able to increase the throughput of the sample by a factor of two (600,000 cells/min, 60 µL/min sample flow), as compared to acoustic sorting of CD4 cells (300,000 cells/min, 30 µL/min sample flow), while maintaining high purity of the sorted sample and preserving functional capacity of both the target and non-target cells. Affinity-bead-mediated acoustophoresis can therefore be used to target and enrich specific cell populations in a continuously perfused microfluidic device. Furthermore, this is a promising step towards the sorting of rare CD34+ hematopoietic stem and progenitor cells, which make up around only 1% to 2% of the MNC collected from peripheral blood after mobilization treatment [35], as compared to 8.4% $\pm$ 5.8% CD8+ cells (own data).

Processing of PBPC products for clinical use is nowadays usually performed by large-scale magnetic cell sorting using the Miltenyi CliniMACS system (Miltenyi Biotec, Bergisch Gladbach, Germany). Here, the cells of interest are labeled with 50-nm-sized magnetic particles and are either depleted or positively selected using a magnetic field in an automated device. Magnetic sorting with the CliniMACS can be performed with high purities and recoveries of usually 95%–99% and 60%–70%, respectively [36–38], as well as high throughput of sample. The CliniMACS sorting process is a batch process and the separation is limited by the loading capacity of the magnetic column [39], whereas acoustophoresis offers a continuous flow-based separation procedure without limitation of the processed sample volume. However, processing of clinical-scale samples by acoustophoresis would require a substantial upscale of the throughput. When compared to the CliniMACS system, which is able to process samples at a speed of 1 mL/min [40], the throughput of the acoustophoresis microchip is much slower and would have to be increased by a factor of 10 to process PBPC at a clinical scale. Likely, this can be achieved by increasing the length of the separation channel and/or by using several microchannels in parallel [23]. However, the scope of the current work has been to show a proof of concept that matches the performance of clinical practice and an up-scaled system having clinical capacity is a next step in the technical development.

Our data show that the performance of acoustic separation is in the range of what is reported for other systems and was even superior compared to the control sorting experiments performed in parallel with the Dynabead system. Nevertheless, further improvements of the acoustic cell sorting system are of course desirable, and could be realized by optimization of the experimental setup, for example enhancing the separation stability of the acoustic setup, such as wash buffer modification, maximizing flow rates and acoustic energy in the channel, temperature and frequency control and implementation of a more stable pressure-driven flow control system as compared to syringe pumps. Augustsson *et al*. [41] reported a temperature dependence of the resonance frequency and acoustic energy in the microchannel and later implemented a thermostabilized system to enable long-term stable operation at a fixed resonance frequency [26]. Moreover, the beads used in the experiments were not optimized for acoustophoresis but rather chosen because they allowed a direct comparison with magnetic sorting. Different bead materials and sizes as well as optimization of the binding capacity therefore represent additional ways to potentially increase performance.

Acoustophoresis is an easy-to-handle separation technology and it provides an interesting alternative in the handling of PBPC products for research purposes, pre-clinical as well as clinical applications. The microfluidic device can easily be combined in line with additional up- and down-stream applications, for example combining the separation of target cells with direct preparation and analysis of the separated cells [24]. Also, the separation of multiple target fractions using different-sized beads in a suitable microfluidic chip design [19] is possible and offers the opportunity

for simultaneous sorting of two or more cell types, a feature which cannot be realized with current magnetic sorting devices.

5. Conclusions

In this study we show that acoustophoresis of bead-labeled cells can be utilized to efficiently sort the CD8+ lymphocyte population from peripheral blood progenitor cell products. Optimization of the system substantially increased the performance, allowing us to double the processing speed compared to previously reported acoustic CD4 separation while still facilitating an efficient separation with fully preserved functional capacity of the sorted cells. Bead-mediated acoustophoresis can therefore be used to target and separate specific cell populations from a complex sample in a continuously perfused microfluidic device. Furthermore, the technology opens up the potential for simultaneous acoustic separation of several cell populations on a single device.

Acknowledgments: The research leading to these results has received funding from the People Programme (Marie Curie Actions) of the European Union's Seventh Framework Programme FP7/2007-2013/ under REA grant agreement n° 607350 and was supported as well by funds from Vinnova (Swedish Innovation Agency) under the program Innovations for Further Health—CellCARE. Furthermore, the project was funded by the University Hospital of Lund Funds, and ALF (Governmental Public Health Grant) as well as by the Knut and Alice Wallenberg Foundation (Grant No. KAW 2012.0023). In addition, Scheding is a fellow of the Swedish Cancer Foundation (Cancerfonden).

Author Contributions: Anke Urbansky, Andreas Lenshof and Stefan Scheding conceived and designed the experiments; Anke Urbansky performed the experiments and analyzed the data; Anke Urbansky wrote the paper and Andreas Lenshof, Josefina Dykes, Thomas Laurell and Stefan Scheding contributed to the evaluation and the manuscript writing.

Conflicts of Interest: Thomas Laurell and Stefan Scheding are board members, founders and shareholders of AcouSort AB which develops acoustophoresis technology. The work presented in the current paper is not biased by commercial interest from AcouSort AB.

References

1. Gratwohl, A.; Baldomero, H.; Horisberger, B.; Schmid, C.; Passweg, J.; Urbano-Ispizua, A. Accreditation Committee of the European Group for Blood and Marrow Transplantation (EBMT) Current trends in hematopoietic stem cell transplantation in Europe. *Blood* **2002**, *100*, 2374–2386. [CrossRef] [PubMed]
2. Dreger, P.; Haferlach, T.; Eckstein, V.; Jacobs, S.; Suttorp, M.; Löffler, H.; Müller-Ruchholtz, W.; Schmitz, N. G-CSF-mobilized peripheral blood progenitor cells for allogeneic transplantation: Safety, kinetics of mobilization, and composition of the graft. *Br. J. Haematol.* **1994**, *87*, 609–613. [CrossRef] [PubMed]
3. Theilgaard-Mönch, K.; Raaschou-Jensen, K.; Palm, H.; Schjødt, K.; Heilmann, C.; Vindeløv, L.; Jacobsen, N.; Dickmeiss, E. Flow cytometric assessment of lymphocyte subsets, lymphoid progenitors, and hematopoietic stem cells in allogeneic stem cell grafts. *Bone Marrow Transplant.* **2001**, *28*, 1073–1082. [CrossRef] [PubMed]
4. Saraceni, F.; Shem-Tov, N.; Olivieri, A.; Nagler, A. Mobilized peripheral blood grafts include more than hematopoietic stem cells: The immunological perspective. *Bone Marrow Transplant.* **2015**, *50*, 886–891. [CrossRef] [PubMed]
5. Schmitz, N.; Barrett, J. Optimizing engraftment—Source and dose of stem cells. *Semin. Hematol.* **2002**, *39*, 3–14. [CrossRef] [PubMed]
6. Baron, F.; Baudoux, E.; Frère, P.; Tourqui, S.; Schaaf-Lafontaine, N.; Greimers, R.; Herens, C.; Fillet, G.; Beguin, Y. Nonmyeloablative stem cell transplantation with CD8-depleted or CD34-selected peripheral blood stem cells. *J. Hematother. Stem Cell Res.* **2002**, *11*, 301–314. [CrossRef] [PubMed]
7. Cao, T.M.; Shizuru, J.A.; Wong, R.M.; Sheehan, K.; Laport, G.G.; Stockerl-Goldstein, K.E.; Johnston, L.J.; Stuart, M.J.; Grumet, F.C.; Negrin, R.S.; *et al.* Engraftment and survival following reduced-intensity allogeneic peripheral blood hematopoietic cell transplantation is affected by CD8+ T-cell dose. *Blood* **2005**, *105*, 2300–2306. [CrossRef] [PubMed]
8. Kim, D.H.; Won, D.I.; Lee, N.Y.; Sohn, S.K.; Suh, J.S.; Lee, K.B. Non-CD34+ cells, especially CD8+ cytotoxic T cells and CD56+ natural killer cells, rather than CD34 cells, predict early engraftment and better transplantation outcomes in patients with hematologic malignancies after allogeneic peripheral stem cell transplantation. *Biol. Blood Marrow Transplant. J. Am. Soc. Blood Marrow Transplant.* **2006**, *12*, 719–728.

9. Van Hoef, M.E. Guidelines for efficient peripheral blood progenitor cell collection. *Neth. J. Med.* **1996**, *48*, 29–37. [CrossRef]
10. Miltenyi, S.; Müller, W.; Weichel, W.; Radbruch, A. High gradient magnetic cell separation with MACS. *Cytometry* **1990**, *11*, 231–238. [CrossRef] [PubMed]
11. Brinchmann, J. E.; Vartdal, F.; Gaudernack, G.; Markussen, G.; Funderud, S.; Ugelstad, J.; Thorsby, E. Direct immunomagnetic quantification of lymphocyte subsets in blood. *Clin. Exp. Immunol.* **1988**, *71*, 182–186. [PubMed]
12. Ozkumur, E.; Shah, A.M.; Ciciliano, J.C.; Emmink, B.L.; Miyamoto, D.T.; Brachtel, E.; Yu, M.; Chen, P.; Morgan, B.; Trautwein, J.; *et al.* Inertial Focusing for Tumor Antigen–Dependent and –Independent Sorting of Rare Circulating Tumor Cells. *Sci. Transl. Med.* **2013**, *5*, 179ra47. [CrossRef] [PubMed]
13. Bonner, W.A.; Hulett, H.R.; Sweet, R.G.; Herzenberg, L.A. Fluorescence activated cell sorting. *Rev. Sci. Instrum.* **1972**, *43*, 404–409. [CrossRef] [PubMed]
14. Kirby, M.R.; Donahue, R.E. Rare event sorting of CD34+ hematopoietic cells. *Ann. N. Y. Acad. Sci.* **1993**, *677*, 413–416. [CrossRef] [PubMed]
15. Lenshof, A.; Laurell, T. Emerging clinical applications of microchip-based acoustophoresis. *J. Lab. Autom.* **2011**, *16*, 443–449. [CrossRef] [PubMed]
16. Tenje, M.; Lundgren, M.N.; Swärd-Nilsson, A.-M.; Kjeldsen-Kragh, J.; Lyxe, L.; Lenshof, A. Acoustophoretic removal of proteins from blood components. *Biomed. Microdevices* **2015**, *17*, 95. [CrossRef] [PubMed]
17. Laurell, T.; Petersson, F.; Nilsson, A. Chip integrated strategies for acoustic separation and manipulation of cells and particles. *Chem. Soc. Rev.* **2007**, *36*, 492–506. [CrossRef] [PubMed]
18. Petersson, F.; Nilsson, A.; Holm, C.; Jonsson, H.; Laurell, T. Separation of lipids from blood utilizing ultrasonic standing waves in microfluidic channels. *Analyst* **2004**, *129*, 938–943. [CrossRef] [PubMed]
19. Petersson, F.; Aberg, L.; Swärd-Nilsson, A.-M.; Laurell, T. Free flow acoustophoresis: microfluidic-based mode of particle and cell separation. *Anal. Chem.* **2007**, *79*, 5117–5123. [CrossRef] [PubMed]
20. Yasuda, K.; Haupt, S. S.; Umemura, S.; Yagi, T.; Nishida, M.; Shibata, Y. Using acoustic radiation force as a concentration method for erythrocytes. *J. Acoust. Soc. Am.* **1997**, *102*, 642–645. [CrossRef] [PubMed]
21. Hultström, J.; Manneberg, O.; Dopf, K.; Hertz, H. M.; Brismar, H.; Wiklund, M. Proliferation and viability of adherent cells manipulated by standing-wave ultrasound in a microfluidic chip. *Ultrasound Med. Biol.* **2007**, *33*, 145–151. [CrossRef] [PubMed]
22. Burguillos, M.A.; Magnusson, C.; Nordin, M.; Lenshof, A.; Augustsson, P.; Hansson, M.J.; Elmér, E.; Lilja, H.; Brundin, P.; Laurell, T.; Deierborg, T. Microchannel acoustophoresis does not impact survival or function of microglia, leukocytes or tumor cells. *PLoS ONE* **2013**, *8*, e64233. [CrossRef] [PubMed]
23. Jönsson, H.; Holm, C.; Nilsson, A.; Petersson, F.; Johnsson, P.; Laurell, T. Particle separation using ultrasound can radically reduce embolic load to brain after cardiac surgery. *Ann. Thorac. Surg.* **2004**, *78*, 1572–1577. [CrossRef] [PubMed]
24. Lenshof, A.; Ahmad-Tajudin, A.; Järås, K.; Swärd-Nilsson, A.-M.; Aberg, L.; Marko-Varga, G.; Malm, J.; Lilja, H.; Laurell, T. Acoustic whole blood plasmapheresis chip for prostate specific antigen microarray diagnostics. *Anal. Chem.* **2009**, *81*, 6030–6037. [CrossRef] [PubMed]
25. Dykes, J.; Lenshof, A.; Åstrand-Grundström, I.-B.; Laurell, T.; Scheding, S. Efficient removal of platelets from peripheral blood progenitor cell products using a novel micro-chip based acoustophoretic platform. *PLoS ONE* **2011**, *6*, e23074. [CrossRef] [PubMed]
26. Augustsson, P.; Magnusson, C.; Nordin, M.; Lilja, H.; Laurell, T. Microfluidic, label-free enrichment of prostate cancer cells in blood based on acoustophoresis. *Anal. Chem.* **2012**, *84*, 7954–7962. [CrossRef] [PubMed]
27. Grenvall, C.; Magnusson, C.; Lilja, H.; Laurell, T. Concurrent Isolation of Lymphocytes and Granulocytes Using Prefocused Free Flow Acoustophoresis. *Anal. Chem.* **2015**, *87*, 5596–604. [CrossRef] [PubMed]
28. Lenshof, A.; Jamal, A.; Dykes, J.; Urbansky, A.; Astrand-Grundström, I.; Laurell, T.; Scheding, S. Efficient purification of CD4+ lymphocytes from peripheral blood progenitor cell products using affinity bead acoustophoresis. *Cytom. Part J. Int. Soc. Anal. Cytol.* **2014**, *85*, 933–941. [CrossRef] [PubMed]
29. Všianská, P.; Říhová, L.; Varmužová, T.; Suská, R.; Kryukov, F.; Mikulášová, A.; Kupská, R.; Penka, M.; Pour, L.; Adam, Z.; *et al.* Analysis of B-cell subpopulations in monoclonal gammopathies. *Clin. Lymphoma Myeloma Leuk.* **2015**, *15*, e61–e71. [CrossRef] [PubMed]
30. Henrikson, R.C.; Mazurkiewicz, J.E. *Histology*; Lippincott Williams & Wilkins: Philadelphia, PA, USA, 1997.

31. Turgeon, M.L. *Clinical Hematology: Theory and Procedures*; Lippincott Williams & Wilkins: Philadelphia, PA, USA, 2005.
32. McClatchey, K.D. *Clinical Laboratory Medicine*; Lippincott Williams & Wilkins: Philadelphia, PA, USA, 2002.
33. Sethu, P.; Sin, A.; Toner, M. Microfluidic diffusive filter for apheresis (leukapheresis). *Lab. Chip* **2006**, *6*, 83–89. [CrossRef] [PubMed]
34. Augustsson, P.; Persson, J.; Ekström, S.; Ohlin, M.; Laurell, T. Decomplexing biofluids using microchip based acoustophoresis. *Lab. Chip* **2009**, *9*, 810–818. [CrossRef] [PubMed]
35. Feller, N.; Schuurhuis, G.J.; van der Pol, M.A.; Westra, G.; Weijers, G.W.D.; van Stijn, A.; Huijgens, P.C.; Ossenkoppele, G.J. High percentage of CD34-positive cells in autologous AML peripheral blood stem cell products reflects inadequate in vivo purging and low chemotherapeutic toxicity in a subgroup of patients with poor clinical outcome. *Leukemia* **2003**, *17*, 68–75. [CrossRef] [PubMed]
36. Elmaagacli, A.H.; Peceny, R.; Steckel, N.; Trenschel, R.; Ottinger, H.; Grosse-Wilde, H.; Schaefer, U.W.; Beelen, D.W. Outcome of transplantation of highly purified peripheral blood CD34+ cells with T-cell add-back compared with unmanipulated bone marrow or peripheral blood stem cells from HLA-identical sibling donors in patients with first chronic phase chronic myeloid leukemia. *Blood* **2003**, *101*, 446–453. [PubMed]
37. Handgretinger, R.; Klingebiel, T.; Lang, P.; Gordon, P.; Niethammer, D. Megadose transplantation of highly purified haploidentical stem cells: Current results and future prospects. *Pediatr. Transplant.* **2003**, *7*, 51–55. [PubMed]
38. Després, D.; Flohr, T.; Uppenkamp, M.; Baldus, M.; Hoffmann, M.; Huber, C.; Derigs, H. G. CD34+ cell enrichment for autologous peripheral blood stem cell transplantation by use of the CliniMACs device. *J. Hematother. Stem Cell Res.* **2000**, *9*, 557–564. [CrossRef] [PubMed]
39. Perseghin, P.; Gaipa, G.; Dassi, M.; Belotti, D.; Pogliani, E.M.; Pioltelli, P.; Balduzzi, A.; Rovelli, A.; Uderzo, C.; Biondi, A. CD34+ stem cell recovery after positive selection of "overloaded" immunomagnetic columns. *Stem Cells Dev.* **2005**, *14*, 740–743. [CrossRef] [PubMed]
40. Dykes, J.H.; Toporski, J.; Juliusson, G.; Békássy, A.N.; Lenhoff, S.; Lindmark, A.; Scheding, S. Rapid and effective CD3 T-cell depletion with a magnetic cell sorting program to produce peripheral blood progenitor cell products for haploidentical transplantation in children and adults. *Transfusion* **2007**, *47*, 2134–2142. [CrossRef] [PubMed]
41. Augustsson, P.; Barnkob, R.; Wereley, S.T.; Bruus, H.; Laurell, T. Automated and temperature-controlled micro-PIV measurements enabling long-term-stable microchannel acoustophoresis characterization. *Lab. Chip* **2011**, *11*, 4152–4164. [CrossRef] [PubMed]

Paper III

SCIENTIFIC REPORTS

OPEN

Rapid and effective enrichment of mononuclear cells from blood using acoustophoresis

Received: 16 June 2017
Accepted: 22 November 2017
Published online: 07 December 2017

Anke Urbansky[1], Pelle Ohlsson[1,2], Andreas Lenshof[1], Fabio Garofalo[1], Stefan Scheding[3,4,5] & Thomas Laurell[1,6]

Effective separation methods for fractionating blood components are needed for numerous diagnostic and research applications. This paper presents the use of acoustophoresis, an ultrasound based microfluidic separation technology, for label-free, gentle and continuous separation of mononuclear cells (MNCs) from diluted whole blood. Red blood cells (RBCs) and MNCs behave similar in an acoustic standing wave field, compromising acoustic separation of MNC from RBC in standard buffer systems. However, by optimizing the buffer conditions and thereby changing the acoustophoretic mobility of the cells, we were able to enrich MNCs relative to RBCs by a factor of 2,800 with MNC recoveries up to 88%. The acoustophoretic microchip can perform cell separation at a processing rate of more than 1×10^5 cells/s, corresponding to 5 µl/min undiluted whole blood equivalent. Thus, acoustophoresis can be easily integrated with further down-stream applications such as flow cytometry, making it a superior alternative to existing MNC isolation techniques.

Mononuclear cells (MNCs), i.e. lymphocytes and monocytes, as part of the white blood cell population (WBC), play a critical role in the human immune system and are important in a variety of clinical and research applications. Working with MNCs often requires enrichment or isolation of the cells which can be challenging due to their low abundance of less than 0.06% of all blood cells[1].

Separation of MNCs is commonly performed in batch processes either by density gradient centrifugation or red blood cell (RBC) lysis and centrifugation, both involving several manual handling steps. Alternatives to replace these labor-intensive methods are intensely researched within the microfluidics field. Miniaturized and automated fluid handling holds great promise of reducing several of the shortcomings encountered in macroscale handling of cell samples[2]. The deterministic behavior of fluids governed by the laminar flow conditions in microscale devices has driven the development of a wide range of modalities for separating cells, in which separation performances take advantages of physical scaling laws, but many times at the expense of system throughput[3–9].

A key area of interest has been to develop methods that can differentiate cells solely based on their intrinsic parameters, which would enable a label free separation of the target cells and thereby reduce manual handling steps and costs. To achieve this goal, the microfluidic systems have to be designed to utilize differences in physical properties of the cells such as size, shape, density, electrical charge and deformability[2]. The benefits of these microfluidic concepts can then be fully realized by integration with downstream unit operations or other lab-on-a chip devices[5,10,11].

When addressing label-free and continuous WBC separation from blood using microfluidics, different working principles have been proposed including cross-flow filtration[8,12], hydrodynamic filtration[13,14], hydrophoretic filtration[15], deterministic lateral displacement[9], inertial focusing[16–19], dielectrophoresis[20,21], leukocyte margination[22], and erythrocyte lysis[23,24]. However, most of the microfluidic devices reported thus far are either not sufficiently efficient in terms of separation performance or operate at low throughput rates ranging from 0.018 µl/min to 2 µl/min of undiluted blood[8,9,13] (Table 1). Furthermore, to our understanding, none of the described methods allows for direct separation of MNCs from whole blood with acceptable purities of the MNC fraction.

[1]Division of Nanobiotechnology, Department of Biomedical Engineering, Lund University, 221 00, Lund, Sweden. [2]AcouSort AB, Medicon Village, 223 81, Lund, Sweden. [3]Lund Stem Cell Center, Lund University, 221 00, Lund, Sweden. [4]Division of Molecular Hematology, Department of Laboratory Medicine, Lund University, 221 00, Lund, Sweden. [5]Department of Hematology, Skåne University Hospital, 222 41, Lund, Sweden. [6]Department of Biomedical Engineering, Dongguk University, 04620, Seoul, South Korea. Correspondence and requests for materials should be addressed to A.U. (email: anke.urbansky@bme.lth.se)

Method		Dilution factor	WBC Separation efficiency	RBC depletion	Purity		WBC Enrichment	Sample throughput**
					WBC	MNC		
Cross-Flow filter	8	Undiluted	~98%	~99.975%	~70.5%	~28%*	~2000	0.06 µl/min
	12	Undiluted	~97.2%	NA	~96.9%	~39%*	NA	0.33 µl/min
Hydrodynamic filtration	13	10x	NA	NA	~3.6%	~1.4%*	~29	2 µl/min
Hydrophoretic filtration	15	20x (rat blood)	NA	NA	~58%	~23.2%*	~210	0.05 µl/min
Deterministic lateral displacement	9	Undiluted	~96% (WBC) ~95% (MNC)	~99.1%	~9%	~5.5%	~110	0.018 µl/min
Microfiltration using ranchets	26	Undiluted	~98% (WBC)	~100%	~100%	~40%*	NA	0.083 µl/min
Inertial focusing	16	500x	~95%	~94%	NA	NA	NA	3.6 µl/min
	18	400x	~89.7%	~99.8%	~91%	~36.4%*	NA	0.375 µl/min
	19	20x	NA	NA	~48%	~19.2%*	NA	240 µl/min (30 µl/min per channel)
Dielectrophoresis	21	5x	~92.1%	~87%	NA	NA	NA	0.16 µl/min
Leukocyte margination	22	Undiluted	NA	NA	NA	NA	~34	NA
Continuous erythrocyte lysis	23	Undiluted	~100%	>99.5%	NA	NA	NA	0.5 µl/min
	24	10x	~99%	NA	NA	NA	NA	100 µl/min
Slanted hydrodynamic filtration	27	20x	~85%	NA	~80%	~32%*	NA	2 µl/min
Acoustophoresis	This work	20x	>43% (WBC) >87% (MNC)	>99.95%	~54%	~53%	~1000 (WBC) ~2800 (MNC)	5 µl/min

Table 1. Label-free, continuous separation of WBC from blood using microfluidics. *Calculated based on assumption that ~40% of WBC are MNCs[25] **Whole blood equivalent.

Acoustophoresis, as an alternative microfluidic cell handling technique, offers a label-free and continuous cell separation that provides both high throughput and good separation performance for bioanalytical and medical applications[28–31]. Typically, an ultrasonic standing half wave is generated across a microchannel, in which acoustic radiation forces induce a movement of suspended cells or particles either towards the pressure node in the center of the channel or towards the pressure anti-node at the sidewalls. The magnitude and direction of the radiation force is dependent on the physical properties of the cells such as size, density and compressibility in relation to the surrounding medium[32]. In an aqueous system, denser particles, such as cells, are typically focused towards the pressure node while less dense particles, such as lipids, move to the pressure anti-node[33,34]. Particles with the same acoustic properties can be separated based on their size, as the acoustic radiation force scales with the particle volume and hence larger particles move faster than smaller particles[35]. Size based separation was successfully shown for a variety of clinical relevant applications such as separation of lymphocytes from granulocytes[36], isolation of tumor cells[37], separation of WBCs from platelets[38], cell cycle phase synchronization in mammalian cells[39] and isolation of bacteria in blood from sepsis patients[10]. Furthermore, acoustophoresis has been shown to be a gentle method that does not affect the viability and proliferative capacity of acoustically-separated cells[38,40–43].

There is a clear unmet need for a rapid, simple and efficient method to separate MNC from blood, with at least a 3-log reduction of the RBC fraction and high MNC recovery above 80%, as an alternative to current labor-intensive density gradient centrifugation or RBC lysis and centrifugation[44]. Acoustophoresis based cell separation holds promise of addressing this shortcoming in view of the significant size differences between the two cell types. However, acoustophoretic WBC isolation experiments indicated that WBC and RBC displayed to a large extent overlapping acoustophoretic mobilities when diluted in the most commonly used buffer systems, such as phosphate buffered saline (PBS)[35], which has so far prevented the use of acoustophoresis to generate pure MNC populations from blood for bioanalytical and diagnostic purposes.

In this paper, we report the development of an acoustophoresis protocol that enables the efficient and rapid separation of MNCs from diluted whole blood. The acoustophoresis chip was based on the earlier reported design by Augustsson[37] with a 2-dimensional pre-alignment zone preceding the separation zone but was modified by increasing the channel length (both pre-focusing channel, from 10 mm to 26 mm and separation channel, from 20 mm to 43 mm) in order to enable an increased sample flow rate. Separation was realized by optimizing the acoustic properties of the suspending medium, thereby changing the acoustophoretic mobility of MNCs versus RBCs. This method has a much higher separation efficiency combined with higher throughput than previous reports on the label-free microfluidic separation of WBC components from blood[8,9,13,16,21]. The gentle, label-free and continuous acoustophoresis separation protocol developed herein presents an important step towards integration of downstream diagnostic applications such as direct analysis of MNCs in flow cytometry.

Results and discussion

Optimizing the acoustic properties of the suspending medium. The acoustic radiation force acting on a particle in a one-dimensional ultrasonic standing wave field is dependent on particle properties such as size, density and compressibility, and scales with the particle radius to the third power (Supplementary Equation 1). In human whole blood, the cell volumes and densities differ between various populations. Mononuclear cells are larger but less dense (diameter 6–20 µm, volume 160–450 μm^3, density 1.055–1.070 g/cm^3) as compared to red blood cells (7–8 µm, 80–100 μm^3, 1.089–1.100 g/cm^3)[25,45–47]. Calculations of the acoustophoretic mobility showed

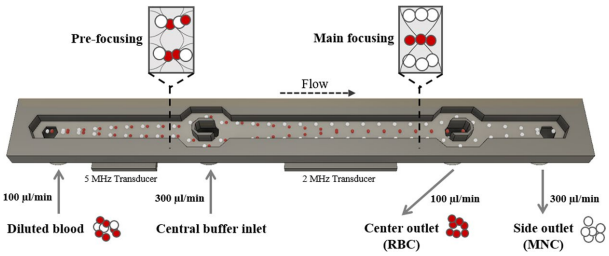

Figure 1. Microfluidic chip design. Diluted blood is injected into the pre-focusing channel where cells are pre-aligned using a 5 MHz transducer. The transducer generates an acoustic pressure node from top to bottom as well as a double node across the width of the channel, aligning the cells in height and width into two parallel bands. Pre-aligned blood is bifurcated at the v-shaped flow splitter around the central buffer inlet and enters the main focusing channel close to the channel wall. Due to the pre-alignment, cells are starting at identical positions and at the same flow speed, enhancing the resolution of the separation. In the main focusing channel, a 2 MHz transducer creates an acoustic standing wave field with a pressure node in the center of the channel, inducing movement of the cells depending on their acoustophysical properties. Cells with high acoustic mobility are moved faster to the channel center and can be collected in the center outlet while cells with low acoustic mobility stay close to the channel wall and are collected at the side outlet.

an overlap between WBCs and RBCs in PBS (Supplementary Figure 1a), indicating difficulties to acoustophoretically separate WBC or MNC from RBC under these conditions, which was confirmed experimentally. When increasing the magnitude of the acoustic radiation force, both MNC and RBC started to move from the side wall of the acoustophoresis channel (Fig. 1) towards the pressure node in the center fraction, revealing similar separation profiles under standard buffer conditions (Fig. 2a). However, the acoustic radiation force on a cell is also coupled to the acoustophysical properties of the surrounding medium. Changes of the medium properties can thus alter the acoustic forces acting on a cell[35,42,43,48] as expressed by the acoustic contrast factor[49]. Usually, particles that are denser than the suspending medium display a positive acoustic contrast factor and migrate towards the pressure node in the acoustic field. By increasing the density and decreasing the compressibility of the medium, the acoustic contrast factor of the cell decreases resulting in a reduction of the cell's acoustophoretic mobility[48]. Ultimately, a movement towards the pressure anti-node can be accomplished if the acoustic contrast factor becomes negative[50].

By calculating the acoustophoretic mobility for WBC and RBC for modified buffer compositions using increasing concentrations of Stock Isotonic Percoll (SIP) solution, a standard buffer density modifier, we anticipated that the mobility of WBC should approach zero at a concentration of 70% SIP while the corresponding average mobility value for RBC should be about 4000 $\mu m^2/Pa{\cdot}s$ (Supplementary Figure 1a). Based on these calculations, it thus could be expected that MNC would display similar discrimination properties with respect to their acoustophoretic mobility in separation experiments.

We therefore investigated the acoustophoretic mobility of MNC and RBC, as measured by the obtained separation efficiency, in buffer compositions with different SIP concentrations. Dilution of SIP decreases the density of the medium as well as the speed of sound and increases the compressibility (Supplementary Figure 1b,d). For the separation experiments, blood was diluted 100 times in SIP (at indicated concentrations), 500 µl of sample were processed through the acoustic chip, and both outlet fractions were analyzed for their cell content.

For optimum separation, it was critical that the central inlet buffer had the same SIP composition as the buffer used for the cell sample dilution. The acoustic impedance differences between the central buffer and the diluted sample entering through the side inlets, would have otherwise led to an acoustic radiation force-induced translocation of the two fluids, compromising the separation efficiency[51].

Figure 2b summarizes the outcome of our measurements, showing the separation efficiency for MNC and RBC at different SIP concentrations. The amplitude settings on the 2 MHz transducer were adjusted to the different acoustophoretic conditions as follows: 0% SIP (equivalent to PBS) $2V_{pp}$, 25% SIP $4V_{pp}$, 50% SIP $6V_{pp}$, 75–85% SIP $25V_{pp}$, and 90–100% SIP $30V_{pp}$. Based on the theoretical calculations (Supplemental Figure 1A) both MNCs and RBCs displayed a lower acoustophoretic mobility at increased SIP concentrations. Therefore, voltage settings had to be increased in order to achieve suitable pressure amplitudes, to move the RBCs equivalently into the center fraction at higher SIP concentrations. Scanning of the optimal voltage range was done for the different buffer conditions (Supplementary Figure 2). For 0–25% SIP, no separation was possible regardless of the voltage, which is due to the similar acoustophoretic mobility of MNCs and RBCs under these conditions (Supplementary Figure 2). At a concentration of 50% SIP, the acoustophoretic mobility of the MNCs was reduced in relation to RBCs, resulting in a mean separation efficiency ($\pm$SD) of $98.4 \pm 1.2\%$ of MNCs while $30.3 \pm 4.7\%$ of the RBCs were depleted. Optimal separation was achieved between 75–100% SIP, with RBC contamination rates of only $0.8 \pm 0.6\%$ and MNC separation efficiencies of $99.4 \pm 0.4\%$ at 75% SIP. Increasing the SIP concentration to 100% also reduced the mobility of RBCs which was reflected by a decreased RBC depletion rate to $88.0 \pm 6.7\%$ (Fig. 2b).

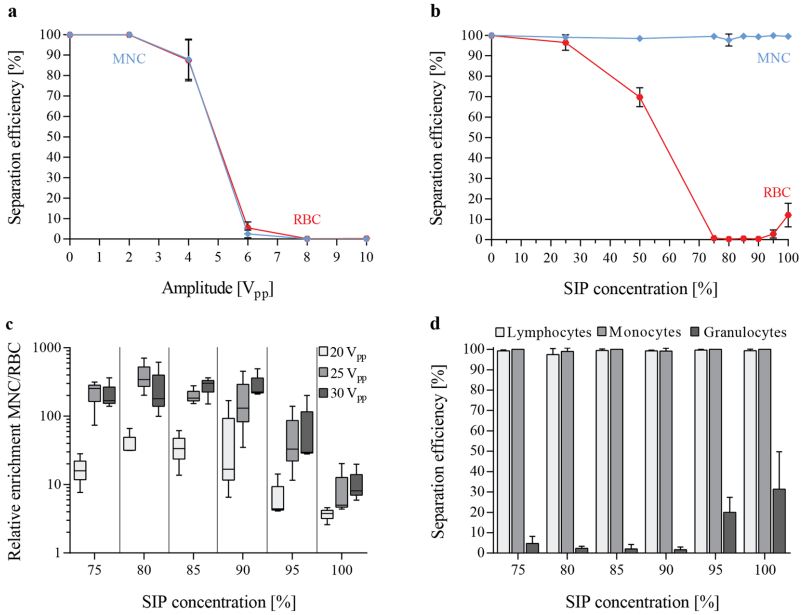

Figure 2. Optimizing buffer condition changes acoustic mobility of blood cells and enables separation of mononuclear cells (MNC) from red blood cells (RBC). (**a**) Separation efficiencies, defined as the ratio of cells in the side outlet as compared to both outlets, are shown for MNCs and RBCs in PBS with increasing strength of the acoustic field, peak-to-peak voltage, V_{pp} (**b**) as well as for varying buffer conditions by increasing the percentage of Stock Isotonic Percoll solution (SIP). A range of 75–100% SIP changes the acoustic mobility of MNCs and RBCs sufficiently to enable separation of the two cell populations. (**c**) The relative enrichment, calculated by the ratio of MNCs to RBCs after the separation compared to the input ratio, MNCs at different SIP concentrations ranging from 75–100% and at different actuation voltages. (**d**) The separation efficiency for different white blood cell populations is shown in the same SIP range for 25 V_{pp}. (mean ± SD, n = 3).

For SIP concentrations above 90%, RBCs did not have sufficient time to migrate into the center fraction before reaching the outlets, resulting in a decreased RBC depletion rate. Theoretically, this decrease in RBC depletion could be compensated by decreasing the flow rate, which however would also decrease the throughput. Alternatively, increasing the length of the main separation channel would enable the RBCs to reach the center fraction even at SIP concentrations >90%. Accordingly, design-modified chips, as well as increased amplitude of the acoustic field could further decrease the RBC contamination when using high SIP concentrations. However, increasing the amplitude significantly increases temperature losses in the piezoelectric actuator, causing a temperature drift of the system, and ultimately leading to a drift in the resonance frequency of the acoustophoresis channel[52].

The acoustic separation outcome can be expressed as the relative enrichment of MNC to RBC, calculated by MNC to RBC cell ratio after the separation divided by the corresponding input ratio. Figure 2c illustrates the results for SIP concentrations between 75–100% for three different actuation voltages. The highest enrichment was achieved at 80% SIP, 25V_{pp} with a mean (±SD) of 390.6 ± 169.8-fold enrichment. Under these conditions, increasing the voltage to 30V_{pp} resulted in a higher fraction of MNCs that was translocated to the center, thus resulting in a decreased relative enrichment. In comparison, for higher SIP concentrations, more RBCs contaminated the side outlet fraction leading to a lower relative enrichment.

Lymphocytes and monocytes, as part of the MNCs, together with granulocytes are subpopulations of white blood cells. Both lymphocytes and monocytes show a similar behavior in the acoustic field and can be collected in the side outlet with high separation efficiencies at SIP concentrations ranging between 75–100% SIP and 25V_{pp} actuation (Fig. 2d). In contrast, granulocytes display acoustophysical properties similar to RBCs and are therefore moved towards the acoustic pressure node in the microchannel center. At SIP concentration of 75–90% less than 5% of all granulocytes are collected in the side outlet fraction, resulting in a less contaminated and more purified MNC sample.

Blood concentration influences separation efficiency. When using external force fields in microfluidic separations, the particle concentration becomes a critical factor for the separation outcome, as also confirmed by theoretical modeling of hydrodynamic particle-particle interactions[53,54]. At high particle concentrations, the hydrodynamic interaction between particles increases, which causes the suspension to move as a whole. For

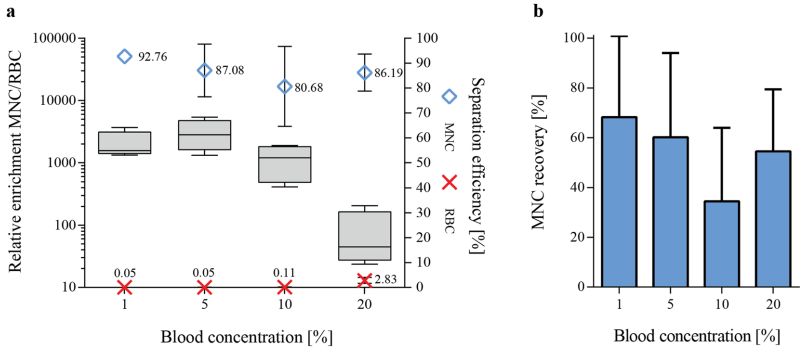

Figure 3. Whole blood dilution rates influenced separation outcome. (**a**) The separation efficiencies of MNC (blue) and RBC (red) in the side outlet fraction as well as the relative enrichment of MNC to RBC as compared to the input blood sample (boxplot) for different blood concentrations are shown (n = 4). (**b**) The recovery of MNC for the different blood concentrations was calculated as the percentage of cells in the output to the input sample. Blood was diluted in 80% SIP and separated at 25 V_{pp} (mean ± SD, n = 4).

a given particle, the migration velocity towards the pressure node is lowered at higher particle concentrations at the same time as other particles with lower acoustophoretic mobility are hydrodynamical coupled to faster moving particles. The threshold for hydrodynamic coupling, estimated by monitoring the washing efficiency of beads or cells, has experimentally been shown to range to between 10^7–10^8 particles/mL[55–57] depending on the particle size used. The theoretical estimates by Ley *et al.*[54] on the threshold values for hydrodynamic coupling in acoustophoresis systems indicate that volume fractions above 0.01 significantly impact the separation. Human undiluted blood has an average of about 5×10^9 cells/ml (volume fraction ≈0,4) which is clearly above the threshold for hydrodynamic coupling. Therefore, the influence of different starting blood concentrations diluted in 80% SIP on the acoustophoretic separation outcome was investigated. A 200 µl sample was separated at 25V_{pp} and the separation efficiencies of MNCs and RBCs for the side outlet fraction, as well as the relative enrichment of MNCs to RBCs as compared to the input sample were recorded. Dilution of blood decreased the average cell concentration to about 5×10^8 cells/ml (10% blood, volume fraction ≈0,04) and 5×10^7 cells/ml (1% blood, volume fraction ≈0,004). As shown in Fig. 3a, an increase in the final blood concentration led to a decrease in mean separation efficiency (±SD) of MNC from 92.8 ± 1.3% at a blood concentration of 1% to 80.7 ± 16.1% at 10% blood concentration, in agreement with the theoretical threshold for hydrodynamic coupling. Interestingly, increasing the starting blood concentration further to 20% resulted in a slightly higher mean MNC separation efficiency (86.2 ± 7.4%) compared to 10%. However, in this case also more RBCs were recovered in the side outlet due to an overload of the central outlet, an effect which has been reported previously for washing of blood cells[33]. Overall, the best results with a median relative enrichment of MNC to RBCs of 2806-fold (range 1318–5398) were achieved for a starting blood concentration of 5% (Fig. 3a).

Acoustophoretic separation of blood cells outperforms other previously reported continuous and label-free microfluidic separation devices, both in relative enrichment as well as sample throughput. The published literature reports sample flow rates between 0.018 µl/min and 3.6 µl/min undiluted whole blood equivalent, however, relative enrichment rates of WBCs versus RBCs are often as low as 15–110 fold[8,9,13,16,21,23] compared to 2,800-fold of MNC enrichment with our system. The most promising enrichment results obtained with other systems were reported for a microfluidic cross-flow device[8], which enabled to increase the ratio of WBC to RBC 2,000-fold as compared to the initial sample with ~98% separation efficiency while recovering ~52% of the WBC. However, the overall throughput of this system reached only 0.06 µl/min of undiluted whole blood equivalent, which is more than 80 times lower compared to the acoustophoretic system reported herein. Unfortunately, many studies in the field only report separation results for the whole WBC population[8,13,16,21,22] without considering that different WBC subtypes might respond differently to the separation process and thus introduce a possible bias. This makes a direct comparison of the published methods to acoustophoretic MNC separation difficult. Nevertheless, in our study, a sample throughput of 5 µl/min whole blood equivalent ($>10^5$ cells/s) was achieved when using a 5% blood concentration.

When calculating the overall enrichment of WBC (accounting for the depletion of granulocytes of 82.1 ± 11.5%) a median 1,013-fold enrichment of WBCs to RBCs was accomplished, which is considerably higher than most other reported microfluidic systems.

The total MNC recovery, as calculated by the percentage of mononuclear cells in the side outlet compared to the input cell amount, was lower than the measured separation efficiency (Fig. 3b). However, this can be explained by the residual volume of the microfluidic system, such as connecting tubings and the microfluidic chip, in which a significant fraction of the sample volume remains after processing. Obviously, this problem becomes less relevant when higher volumes are processed and can easily be solved by introducing a final flushing step. This is illustrated by running 200 µl sample of 1% blood which produced a total MNC recovery of 68% whereas MNC recovery was increased to 88% by increasing the volume to 500 µl, which resulted in separation efficiency of 92%.

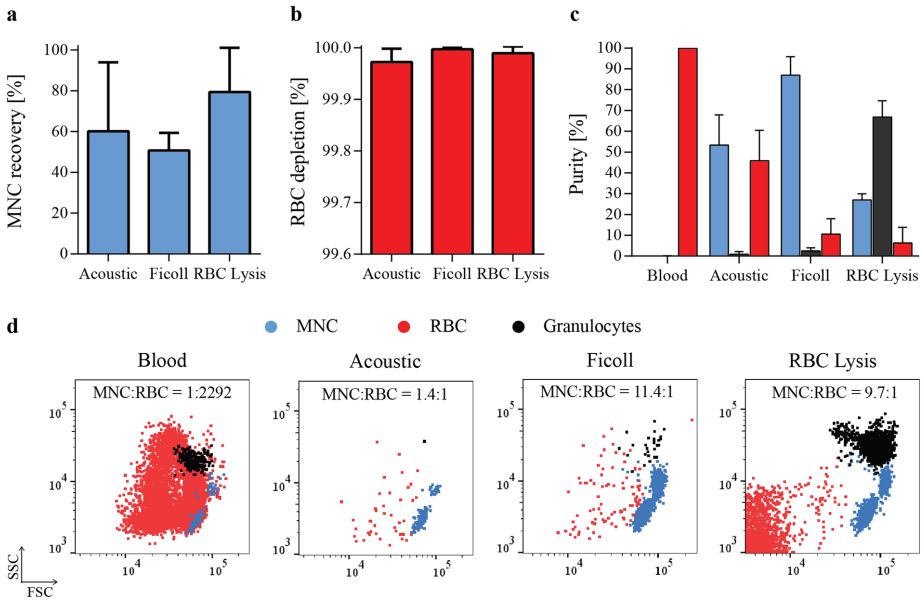

Figure 4. Comparison of acoustophoresis and standard separation methods. (**a**) Recovery of MNCs, calculated as the percentage of cells in the output compared to the input cell amount, and (**b**) depletion of RBCs are shown for acoustic separation as well as for density gradient centrifugation (Ficoll) and RBC lysis (mean ± SD, n = 3). (**c**) Purities of the different populations as obtained by each separation method were calculated as the ratio of MNCs (blue), granulocytes (black) and RBCs (red) respectively to the total number of cells in the separated sample (mean ± SD, n = 3). (**d**) Representative FACS plots show the distribution of the different cell types in the starting blood sample (left) as well as after the different separation methods.

Acoustic separation in comparison to standard separation methods. Separation of MNCs can be performed by various methods, all of them having their benefits and disadvantages. Here, we compared the acoustophoretic separation to two standard methods, Ficoll separation and RBC Lysis. Isolation of MNCs using Ficoll is based on differences in cell density using density gradient centrifugation, whereas RBC Lysis selectively disrupts RBCs in the blood sample followed by washing and enrichment of MNCs by sequential centrifugation steps. MNC recovery and RBC depletion are shown for the different separation methods in Fig. 4a and b, respectively. All three methods reached comparable RBC depletion rates of over 99.97%. The lowest mean (±SD) recovery of MNCs of 50.7 ± 8.7% was achieved using Ficoll separation, which also required the largest volume of blood (5 mL). The highest recovery was obtained using RBC lysis with 79.4 ± 21.7%. As described previously, MNC recovery for acoustic separation is dependent on the starting blood concentration as well as on the processed sample volume and was highest for 500 µl of 1% starting blood concentration (88.5 ± 15.6%). Figure 4 shows the results for acoustic separation of blood at 5% starting concentration, 200 µl sample volume, run with 80% SIP at $25V_{pp}$ which gave the highest relative enrichment of MNCs to RBCs (Fig. 3a).

Sample purities (Fig. 4c) as well as representative FACS plots (Fig. 4d) show the different distributions of cell types in the input and output samples. Starting blood samples consisted to 99.86 ± 0.03% of RBCs, to 0.1 ± 0.03% of granulocytes and only to 0.044 ± 0.005% of MNCs, which corresponded to a MNC to RBC ratio of 1 to 2292. Acoustic separation considerably reduced the number of RBCs leading to a MNC to RBC ratio of 1.4 to 1, with a MNC purity of 53.3 ± 14.5%. In comparison, Ficoll density gradient centrifugation resulted in the highest ratio in MNC to RBCs of 11.5 to 1 and a MNC purity of 87 ± 8.9%. RBC lysis had the highest granulocyte contamination and gave the lowest purity of MNCs of 27 ± 3% but also the lowest RBC contamination with a MNC to RBC ratio of 9.7 to 1. Furthermore, RBC lysis increased the amount of cell debris in the sample as indicated in the flow cytometry data (Fig. 4d).

Based on our results, acoustophoresis offers an alternative to standard MNC separation methods, and can also be applied to separate other cell types which show overlapping acoustic mobilities in standard buffer conditions. Furthermore, due to the continuous acoustic separation of MNC from blood, the device can be easily integrated with downstream applications, such as direct analysis of MNC in a flow cytometer. Counting MNC from whole blood with cell concentrations of ~5.000.000 cells/µl is not possible with current flow cytometer systems (flow speed of 10.000–200.000 events/s, cell concentrations 5.000–1.000.000 cells/µl)[58]. Acoustophoresis can decomplex blood samples sufficiently from ~115.000 cells/s to ~560 cells/s and thus enable analysis of a purified MNC fraction directly in the flow cytometer without increasing the number of manual steps such as pipetting or centrifugation.

Conclusion

We have shown that acoustophoresis can be used to enrich mononuclear cells from red blood cells with high efficiency and recovery. In agreement with theoretical calculations we demonstrate experimentally that the acoustophoretic mobilities of MNC and RBC can be differentially affected by modifying the acoustophysical properties of the buffer, thereby enabling efficient separation of the two cell types with otherwise overlapping acoustophoretic mobilities.

Materials and Methods

Ethical statement. The collection of blood samples from healthy volunteers was approved by the Regional Ethical Review Board at Lund University. All experiments were performed in accordance with relevant guidelines and regulations.

Sample collection. Blood samples were obtained from healthy volunteers after informed consent at Lund University Hospital, Lund, Sweden and collected in vacutainer tubes (BD Bioscience, San Jose, CA, USA), containing ethylenediaminetetraacetic acid (EDTA) as anticoagulant.

Central inlet buffer preparation. Percoll density medium (Sigma-Aldrich, St. Louis, MI, USA) was used as central inlet buffer as well as to prepare dilutions of blood for the acoustophoretic separation. To adjust the osmolality of undiluted Percoll, 1 part (v/v) of 1.5 M NaCl (Sigma-Aldrich) was added to 9 parts (v/v) of Percoll to make a stock isotonic percoll (SIP) solution. Adjustments of the density of SIP were done by further dilution of SIP in 0.15 M NaCl.

Sample preparation, immunostaining and flow cytometric analysis. Blood samples were processed within 10 hours after collection, stained with monoclonal antibodies for 15 min at room temperature in the dark and further diluted in central inlet buffer. The following directly conjugated monoclonal antibodies were used in this study: CD3-APC (clone HIT3a), CD14-PE (clone MφP9), CD19 FITC (clone HIB19), CD45-PerCP (clone 2D1), CD61-PE (clone VI-PL2), CD66b FITC (clone G10F5) and CD235a APC (clone GA-R2), as well as matched isotype controls (all from BD Bioscience, San Jose, CA, USA). Stained samples were analyzed before and after separation on a FACSCanto II flow cytometer (BD Bioscience) and acquired data was further analyzed using the FlowJo software (Tree Star Inc., Ashland, OR, USA).

Standard methods for mononuclear cell separation. Mononuclear cells (MNC) were isolated by Ficoll density gradient centrifugation using Ficoll-Paque Premium (1.078 g/ml, GE Healthcare Life Sciences, Little Chalfont, UK). In brief, 5 mL blood was diluted four times and layered over 15 mL of Ficoll-Paque Premium. After 40 min of centrifugation at 400 × g the mononuclear cell layer was removed and washed twice at 200 × g, for 10 min.

For comparison, selective lysis of red blood cells (RBCs) to enrich the MNC fractions was performed using BD Pharm Lyse (BD Bioscience, San Jose, CA, US). A total of 200 µL blood was lysed by adding 2 mL of 1x lysing solution, incubated for 15 min at room temperature in the dark and washed twice at 200 × g for 5 minutes.

Acoustophoretic setup. *Microfluidic chip design.* The acoustophoretic chip was manufactured by Micronit (Enschede, Netherlands) using Deep Reactive Ion Etching and sealed with a glass lid. The channel structure was etched into silicon and consists of a sample inlet, a pre-focusing zone (26 mm × 300 µm × 150 µm), a v-shaped flow splitter around the central buffer inlet, a main separation channel (43 mm × 375 µm × 150 µm) and a trifurcation with a central outlet and a common side outlet for the two lateral branches (Fig. 1).

Acoustic actuation. The standing wave field was created using piezoceramic transducers glued underneath the pre-focusing channel as well as underneath the main separation channel. Frequencies were set to 4.831 MHz for the pre-focusing channel with 5 V_{pp} amplitude and 1.956 MHz for the main separation channel. A dual channel function generator (AFG3022B, Tektronix, Beaverton, OR, USA), connected to signal amplifiers (in-house build) was used to drive both transducers while the voltage over each transducer was measured via a two-channel digital oscilloscope (TDS 1002, Tektronix). Temperature regulation was achieved using a Peltier element and a PT100 resistance temperature detector attached to the acoustophoretic system.

Fluidic setup and sample procedur. An in-house designed pressure driven system with feedback regulation was used for controlling the fluids to and from the chip monitored by SLI-1000 Liquid Flow Meters (Sensirion AG, Switzerland)[59]. A total volume of 200–500 µl diluted blood was infused through the sample inlet at 100 µl/min and pre-aligned in width and height into two parallel bands in the pre-focusing channel. Pre-aligned blood entered the main-separation channel, with a central inlet buffer flow rate set to 300 µl/min, and cells were separated in the acoustic standing wave field, based on their acoustophysical properties into the center outlet fraction (100 µl/min) or the side outlet fraction (300 µl/min). Samples of both outlet fractions were collected in 5 ml tubes and analyzed for their cell content.

Data availability. The authors declare that all data supporting the findings of this study are provided in the paper and it's Supplementary Information. Raw data is available on request.

References

1. Henrikson, R. C. & Mazurkiewicz, J. E. *Histology*. (Lippincott Williams & Wilkins, 1997).
2. Lee, W., Tseng, P. & Carlo, D. D. *Microtechnology for Cell Manipulation and Sorting*. (Springer, 2016).
3. Pamme, N. Continuous flow separations in microfluidic devices. *Lab. Chip* **7**, 1644–1659 (2007).
4. Bhagat, A. A. S. *et al.* Microfluidics for cell separation. *Med. Biol. Eng. Comput.* **48**, 999–1014 (2010).

5. Toner, M. & Irimia, D. Blood-on-a-chip. *Annu. Rev. Biomed. Eng.* **7**, 77–103 (2005).
6. Hou, H. W. *et al*. Microfluidic Devices for Blood Fractionation. *Micromachines* **2**, 319–343 (2011).
7. Antfolk, M. & Laurell, T. Continuous flow microfluidic separation and processing of rare cells and bioparticles found in blood – A review. *Anal. Chim. Acta* **965**, 9–35 (2017).
8. VanDelinder, V. & Groisman, A. Perfusion in Microfluidic Cross-Flow: Separation of White Blood Cells from Whole Blood and Exchange of Medium in a Continuous Flow. *Anal. Chem.* **79**, 2023–2030 (2007).
9. Davis, J. A. *et al*. Deterministic hydrodynamics: taking blood apart. *Proc. Natl. Acad. Sci. USA* **103**, 14779–14784 (2006).
10. Ohlsson, P. *et al*. Integrated Acoustic Separation, Enrichment, and Microchip Polymerase Chain Reaction Detection of Bacteria from Blood for Rapid Sepsis Diagnostics. *Anal. Chem*. **88**, 9403–9411 (2016).
11. Tajudin, A. A. *et al*. Integrated acoustic immunoaffinity-capture (IAI) platform for detection of PSA from whole blood samples. *Lab. Chip* **13**, 1790–1796 (2013).
12. Kim, M., Mo Jung, S., Lee, K.-H., Jun Kang, Y. & Yang, S. A Microfluidic Device for Continuous White Blood Cell Separation and Lysis From Whole Blood. *Artif. Organs* **34**, 996–1002 (2010).
13. Yamada, M. & Seki, M. Hydrodynamic filtration for on-chip particle concentration and classification utilizing microfluidics. *Lab. Chip* **5**, 1233–1239 (2005).
14. Matsuda, M., Yamada, M. & Seki, M. Blood cell classification utilizing hydrodynamic filtration. *Electron. Commun. Jpn.* **94**, 1–6 (2011).
15. Choi, S., Song, S., Choi, C. & Park, J.-K. Continuous blood cell separation by hydrophoretic filtration. *Lab. Chip* **7**, 1532–1538 (2007).
16. Nivedita, N. & Papautsky, I. Continuous separation of blood cells in spiral microfluidic devices. *Biomicrofluidics* **7**, 054101 (2013).
17. Wu, L., Guan, G., Hou, H. W., Bhagat, A. A. S. & Han, J. Separation of Leukocytes from Blood Using Spiral Channel with Trapezoid Cross-Section. *Anal. Chem*. **84**, 9324–9331 (2012).
18. Wu, Z., Chen, Y., Wang, M. & Chung, J. A. Continuous inertial microparticle and blood cell separation in straight channels with local microstructures. *Lab. Chip* **16**, 532–542 (2016).
19. Zhang, J. *et al*. High-Throughput Separation of White Blood Cells From Whole Blood Using Inertial Microfluidics. *IEEE Trans. Biomed. Circuits Syst.* **PP**, 1–9 (2017).
20. Huang, Y. *et al*. Electric Manipulation of Bioparticles and Macromolecules on Microfabricated Electrodes. *Anal. Chem.* **73**, 1549–1559 (2001).
21. Han, K.-H. & Frazier, A. B. Lateral-driven continuous dielectrophoretic microseparators for blood cells suspended in a highly conductive medium. *Lab. Chip* **8**, 1079–1086 (2008).
22. Shevkoplyas, S. S., Yoshida, T., Munn, L. L. & Bitensky, M. W. Biomimetic Autoseparation of Leukocytes from Whole Blood in a Microfluidic Device. *Anal. Chem.* **77**, 933–937 (2005).
23. Sethu, P., Anahtar, M., Moldawer, L. L., Tompkins, R. G. & Toner, M. Continuous flow microfluidic device for rapid erythrocyte lysis. *Anal. Chem.* **76**, 6247–6253 (2004).
24. Ramachandraiah, H., A. Svahn, H. & Russom, A. Inertial microfluidics combined with selective cell lysis for high throughput separation of nucleated cells from whole blood. *RSC Adv.* **7**, 29505–29514 (2017).
25. Turgeon, M. L. *Clinical Hematology: Theory and Procedures*. (Lippincott Williams & Wilkins, 2005).
26. Guo, Q., Duffy, S. P., Matthews, K., Islamzada, E. & Ma, H. Deformability based Cell Sorting using Microfluidic Ratchets Enabling Phenotypic Separation of Leukocytes Directly from Whole Blood. *Sci. Rep*. **7** (2017).
27. Yamada, M., Seko, W., Yanai, T., Ninomiya, K. & Seki, M. Slanted, asymmetric microfluidic lattices as size-selective sieves for continuous particle/cell sorting. *Lab. Chip* **17**, 304–314 (2017).
28. Lenshof, A. & Laurell, T. Emerging clinical applications of microchip-based acoustophoresis. *J. Lab. Autom.* **16**, 443–449 (2011).
29. Augustsson, P., Malm, J. & Ekström, S. Acoustophoretic microfluidic chip for sequential elution of surface bound molecules from beads or cells. *Biomicrofluidics* **6**, 34115 (2012).
30. Tenje, M. *et al*. Acoustophoretic removal of proteins from blood components. *Biomed. Microdevices* **17**, 95 (2015).
31. Li, P. *et al*. Acoustic separation of circulating tumor cells. *Proc. Natl. Acad. Sci.* **112**, 4970–4975 (2015).
32. Barnkob, R., Augustsson, P., Laurell, T. & Bruus, H. Measuring the local pressure amplitude in microchannel acoustophoresis. *Lab. Chip* **10**, 563–570 (2010).
33. Petersson, F., Nilsson, A., Holm, C., Jonsson, H. & Laurell, T. Separation of lipids from blood utilizing ultrasonic standing waves in microfluidic channels. *The Analyst* **129**, 938–943 (2004).
34. Grenvall, C., Folkenberg, J. R., Augustsson, P. & Laurell, T. Label-free somatic cell cytometry in raw milk using acoustophoresis. *Cytometry A* **81A**, 1076–1083 (2012).
35. Petersson, F., Aberg, L., Swärd-Nilsson, A.-M. & Laurell, T. Free flow acoustophoresis: microfluidic-based mode of particle and cell separation. *Anal. Chem*. **79**, 5117–5123 (2007).
36. Grenvall, C., Magnusson, C., Lilja, H. & Laurell, T. Concurrent Isolation of Lymphocytes and Granulocytes Using Prefocused Free Flow Acoustophoresis. *Anal. Chem*. (2015).
37. Augustsson, P., Magnusson, C., Nordin, M., Lilja, H. & Laurell, T. Microfluidic, label-free enrichment of prostate cancer cells in blood based on acoustophoresis. *Anal. Chem*. **84**, 7954–7962 (2012).
38. Dykes, J., Lenshof, A., Åstrand-Grundström, I.-B., Laurell, T. & Scheding, S. Efficient removal of platelets from peripheral blood progenitor cell products using a novel micro-chip based acoustophoretic platform. *PloS One* **6**, e23074 (2011).
39. Thévoz, P., Adams, J. D., Shea, H., Bruus, H. & Soh, H. T. Acoustophoretic synchronization of mammalian cells in microchannels. *Anal. Chem.* **82**, 3094–3098 (2010).
40. Evander, M. *et al*. Noninvasive acoustic cell trapping in a microfluidic perfusion system for online bioassays. *Anal. Chem*. **79**, 2984–2991 (2007).
41. Hultström, J. *et al*. Proliferation and viability of adherent cells manipulated by standing-wave ultrasound in a microfluidic chip. *Ultrasound Med. Biol*. **33**, 145–151 (2007).
42. Lenshof, A. *et al*. Efficient purification of CD4+ lymphocytes from peripheral blood progenitor cell products using affinity bead acoustophoresis. *Cytometry A* **85**, 933–941 (2014).
43. Urbansky, A., Lenshof, A., Dykes, J., Laurell, T. & Scheding, S. Affinity-Bead-Mediated Enrichment of CD8+ Lymphocytes from Peripheral Blood Progenitor Cell Products Using Acoustophoresis. *Micromachines* **7**, 101 (2016).
44. European Directorate for the Quality of Medicines & Healthcare. *Guide for the Preparation, Use and Quality Assurance of Blood Components: Recommendation No. R (95) 15*. (Council of Europe Publishing, 2015).
45. Chapman, E. H., Kurec, A. S. & Davey, F. R. Cell volumes of normal and malignant mononuclear cells. *J. Clin. Pathol.* **34**, 1083–1090 (1981).
46. McClatchey, K. D. *Clinical Laboratory Medicine*. (Lippincott Williams & Wilkins, 2002).
47. Sethu, P., Sin, A. & Toner, M. Microfluidic diffusive filter for apheresis (leukapheresis). *Lab. Chip* **6**, 83–89 (2006).
48. Augustsson, P., Karlsen, J. T., Su, H.-W., Bruus, H. & Voldman, J. Iso-acoustic focusing of cells for size-insensitive acousto-mechanical phenotyping. *Nat. Commun.* **7**, 11556 (2016).
49. Laurell, T. & Lenshof, A. *Microscale Acoustofluidics*. (Royal Society of Chemistry, 2014).
50. Cushing, K. W. *et al*. Elastomeric negative acoustic contrast particles for affinity capture assays. *Anal. Chem.* **85**, 2208–2215 (2013).
51. Deshmukh, S., Brzozka, Z., Laurell, T. & Augustsson, P. Acoustic radiation forces at liquid interfaces impact the performance of acoustophoresis. *Lab. Chip* **14**, 3394–3400 (2014).

52. Augustsson, P., Barnkob, R., Wereley, S. T., Bruus, H. & Laurell, T. Automated and temperature-controlled micro-PIV measurements enabling long-term-stable microchannel acoustophoresis characterization. *Lab. Chip* **11**, 4152–4164 (2011).
53. Mikkelsen, C. & Bruus, H. Microfluidic capturing-dynamics of paramagnetic bead suspensions. *Lab. Chip* **5**, 1293–1297 (2005).
54. H. Ley, M. W. & Bruus, H. Continuum modeling of hydrodynamic particle–particle interactions in microfluidic high-concentration suspensions. *Lab. Chip* **16**, 1178–1188 (2016).
55. Hawkes, J. J., Barber, R. W., Emerson, D. R. & Coakley, W. T. Continuous cell washing and mixing driven by an ultrasound standing wave within a microfluidic channel. *Lab. Chip* **4**, 446–452 (2004).
56. Petersson, F., Nilsson, A., Jönsson, H. & Laurell, T. Carrier medium exchange through ultrasonic particle switching in microfluidic channels. *Anal. Chem.* **77**, 1216–1221 (2005).
57. Augustsson, P., Åberg, L. B., Swärd-Nilsson, A.-M. K. & Laurell, T. Buffer medium exchange in continuous cell and particle streams using ultrasonic standing wave focusing. *Microchim. Acta* **164**, 269–277 (2009).
58. Picot, J., Guerin, C. L., Kim, C. L. V. & Boulanger, C. M. Flow cytometry: retrospective, fundamentals and recent instrumentation. *Cytotechnology* **64**, 109 (2012).
59. Augustsson, P., Magnusson, C., Lilja, H. & Laurell, T. Acoustophoresis in Tumor Cell Enrichment. in *Circulating Tumor Cells* (ed. Fan, Z. H.) 227–248, https://doi.org/10.1002/9781119244554.ch10 (John Wiley & Sons, Inc, 2016).

Acknowledgements

This work was supported by the People Programme (Marie Curie Actions) of the European Union's Seventh Framework Programme FP7/2007-2013/ under REA grant agreement n° 607350; the Knut Alice Wallenberg Foundation (Grant No. KAW 2012.0023); the Swedish Research Council (Grant No. 621-2014-6273); VINNOVA, CellCARE, (Grant No. 2009-00236); the University Hospital of Lund Funds; the ALF grant from the Medical Faculty at Lund University; the Carl Trygger Foundation (13:254) and the SSF Strategic Research Centre. In addition, Scheding is a fellow of the Swedish Cancer Foundation (Cancerfonden).

Author Contributions

A.U., P.O., A.L., S.S. and T.L conceived and discussed the method and experiments. A.U. designed and performed the experiments, analyzed data and wrote the manuscript. F.G. performed viscosity measurements and the theoretical calculations. T.L. and S.S. supervised the project and all authors edited the manuscript.

Additional Information

Supplementary information accompanies this paper at https://doi.org/10.1038/s41598-017-17200-9.

Competing Interests: T.L. and S.S. are board members and T.L., P.O., A.L., S.S. and A.U. are shareholders in AcouSort AB.

Publisher's note: Springer Nature remains neutral with regard to jurisdictional claims in published maps and institutional affiliations.

Rapid and effective enrichment of mononuclear cells from blood using acoustophoresis

Anke Urbansky[1,*], Pelle Ohlsson[1,2], Andreas Lenshof[1], Fabio Garofalo[1], Stefan Scheding[3,4,5] and Thomas Laurell[1,6]

[1]Department of Biomedical Engineering, Lund University, 221 00 Lund, Sweden. [2]AcouSort AB, BMC D10, 221 84 Lund, Sweden. [3]Lund Stem Cell Center, Lund University, 221 00 Lund, Sweden. [4]Division of Molecular Hematology, Department of Laboratory Medicine, Lund University, 221 00 Lund, Sweden [5]Department of Hematology, Skåne University Hospital, 222 41 Lund, Sweden. [6]Department of Biomedical Engineering, Dongguk University, 04620 Seoul, Korea. *e-mail: anke.urbansky@bme.lth.se

Supplementary

$$F_z^{rad} = \frac{4}{3}\pi\phi(\tilde{\kappa},\tilde{\rho})ka^3E_{ac}\sin(2kz)$$

$$E_{ac} = \frac{p_a^2}{4\rho_0 c_0^2};\ \ \phi(\tilde{\kappa},\tilde{\rho}) = \frac{5\tilde{\rho}-2}{2\tilde{\rho}+1} - \tilde{\kappa};\qquad \tilde{\kappa} = \frac{\kappa_p}{\kappa_0};\qquad \tilde{\rho} = \frac{\rho_p}{\rho_0}$$

Supplementary Equation 1. Acoustic radiation force F_z^{rad} acting on a particle in an acoustic standing wave field where κ_0, ρ_0, κ_p and ρ_p are the compressibility and density of the fluid and particle, $\phi(\tilde{\kappa},\tilde{\rho})$ is the acoustic contrast factor, k is the wave number ($2\pi/\lambda$), E_{ac} is the acoustic energy density, z is the position of the particle along the wave propagation axis, p_a is the pressure amplitude, c_0 is the speed of sound in the medium[1].

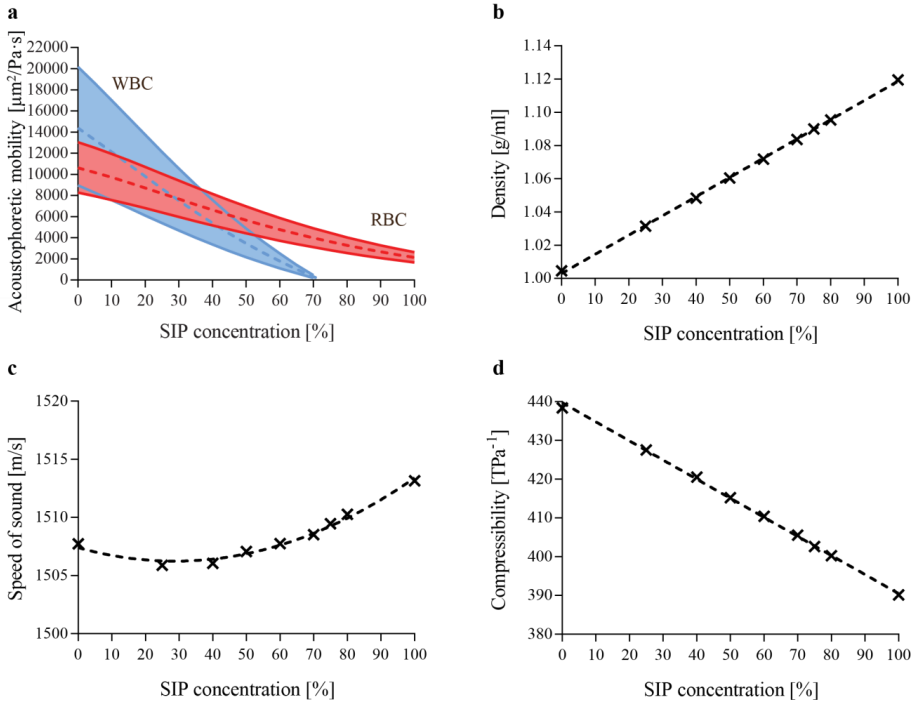

Supplementary Figure 1. (**a**) Acoustophoretic mobility, calculated as the radius squared times the acoustic contrast factor divided by the viscosity of the medium, $a^2\Phi/\eta$, is shown for WBC (blue) and RBC (red) at different concentrations of stock isotonic percoll solution (SIP) with the colored area showing the variance associated with the size variability of the population and the dashed line indicating the average mobility value (calculations are based on values obtained by Cushing et al.[2]). (**b**) Both the density ρ and (**c**) speed of sound c at 25°C of SIP (black) as a function of the SIP concentration were determined using a density and sound velocity meter (DSA 5000M, Anton Paar GmbH). (**d**) The compressibility κ was calculated from the obtained values as $1/(\rho c^2)$.

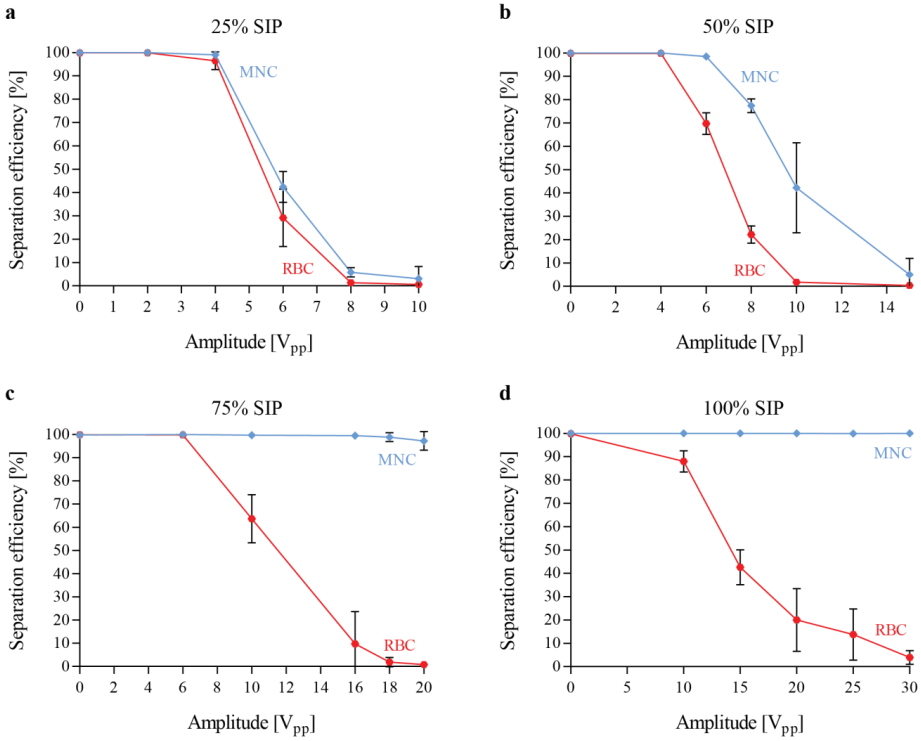

Supplementary Figure 2. Increasing concentrations of SIP enabled the acoustic separation of MNC and RBC. Blood was diluted in increasing concentrations of stock isotonic percoll solution (SIP) of (**a**) 25%, (**b**) 50%, (**c**) 75%, and (**d**) 100%, and perfused through the acoustophoretic chip at varying amplitudes of the acoustic field. Separation efficiency, defined as the ratio of cells in the side outlet as compared to both outlets, is shown for mononuclear cells (MNC) and red blood cells (RBC). (n=3)

References

1. Laurell, T. & Lenshof, A. *Microscale Acoustofluidics*. (Royal Society of Chemistry, 2014).

2. Cushing, K. W. *et al.* Ultrasound Characterization of Microbead and Cell Suspensions by Speed of Sound Measurements of Neutrally Buoyant Samples. *Anal. Chem.* **89,** 8917–8923 (2017).

Paper V

Lab on a Chip

PAPER

View Article Online
View Journal

Cite this: DOI: 10.1039/c9lc00181f

Label-free separation of leukocyte subpopulations using high throughput multiplex acoustophoresis†

Anke Urbansky, [a] Franziska Olm, [b] Stefan Scheding,[bc] Thomas Laurell*[a] and Andreas Lenshof *[a]

Received 20th February 2019,
Accepted 6th March 2019

DOI: 10.1039/c9lc00181f

rsc.li/loc

Multiplex separation of mixed cell samples is required in a variety of clinical and research applications. Herein, we present an acoustic microchip with multiple outlets and integrated pre-alignment channel to enable high performance and label-free separation of three different cell or particle fractions simultaneously at high sample throughput. By implementing a new cooling system for rigorous temperature control and minimal acoustic energy losses, we were able to operate the system isothermally and sort suspensions of 3, 5 and 7 μm beads with high efficiencies (>95.4%) and purities (>96.3%) at flow rates up to 500 μL min^{-1} corresponding to a throughput of ~2.5×10^6 beads per min. Also, human viable white blood cells were successfully fractionated into lymphocytes, monocytes and granulocytes with high purities of 96.5 ± 1.6%, 71.8 ± 10.1% and 98.8 ± 0.5%, respectively, as well as high efficiencies (96.8 ± 3.3%, 66.7 ± 3.2% and 99.0 ± 0.7%) at flow rates up to 100 μL min^{-1} (~100 000 cells per min). By increasing the flow rate up to 300 μL min^{-1} (~300 000 cells per min) both lymphocytes and granulocytes were still recovered with high purities (92.8 ± 1.9%, 98.2 ± 1 .0%), whereas the monocyte purity decreased to 20.9 ± 10.3%. The proposed isothermal multiplex acoustophoresis platform offers efficient fractionation of complex samples in a label-free and continuous manner at thus far unreached high sample throughput rates.

Introduction

White blood cells (WBC), leukocytes, play an important role in the human immune system and can be divided into three main subpopulations: lymphocytes, monocytes, and granulocytes. Immediate and individual access to these WBC subtypes holds significant value in research as well as clinical applications, such as lymphocyte purification for diagnostic purposes, or widely-applied standard lymphocyte function tests and gene expression analysis. In clinical cell processing WBC subtypes are used for manufacturing chimeric antigen receptor T cells in immunotherapy,[1] for monocyte enrichment to generate dendritic cells used in immunotherapy,[2] and for separation of granulocytes for transfusion.[3,4] However, methods that offer rapid, simultaneous and label-free separation of the three blood cell subsets, in limited sample volumes, still pose an unmet need.

Common separation methods such as fluorescence activated cell sorting (FACS) and magnetic activated cell sorting (MACS) require labeling of the cells, they are time consuming, expensive and require trained personnel. Microfluidic systems offer an alternative to label-based and/or affinity-based separation methods and can be used for multiplex separation of cells based on their physical properties such as size, density, shape, deformability, compressibility, charge, polarizability and magnetic susceptibility. Multiplex separation of different particle types with high efficiency and purity has been shown for several microfluidic devices such as deterministic lateral displacement (DLD),[5–8] inertial microfluidics,[9,10] dielectrophoresis (DEP),[11–13] acoustophoresis[14–16] or combinations of different forces and flow designs.[17,18] However, working with complex cell suspensions is often more difficult due to larger variation and overlaps in the biophysical cell properties. Previous reports on multiplex separation of lymphocytes, monocytes, and granulocytes at throughputs that meet bioanalytical or clinical needs have shown only limited success. Ramachandraiah *et al.*[10] used selective RBC lysis combined with inertial microfluidics to separate the three WBC subpopulations with fair purities (86% granulocytes, 43% monocytes, 91% lymphocytes) but only modest separation efficiencies (27% granulocytes, 90% monocytes, 53% lymphocytes) indicating a loss of especially granulocytes and lymphocytes in their system. Grenvall *et al.*[15] has demonstrated separation of WBC using pre-aligned free flow acoustophoresis. While this system showed sufficient

[a] *Department of Biomedical Engineering, Lund University, Lund, Sweden. E-mail: thomas.laurell@bme.lth.se, andreas.lenshof@bme.lth.se*
[b] *Department of Laboratory Medicine, Lund Stem Cell Center & Molecular Hematology, Lund University, Lund, Sweden*
[c] *Department of Hematology, University Hospital Skåne, Lund, Sweden*
† Electronic supplementary information (ESI) available. See DOI: 10.1039/c9lc00181f

separation efficiencies for lymphocytes and granulocytes but low monocyte purity, the maximum throughput was only 8 μL min^{-1} sample flow at a cell concentration of 10^6 cells per mL, *i.e.* 8000 cells per min.

In acoustophoresis, commonly a half-standing wave field is generated across a microchannel with a pressure node in the center of the channel and a pressure anti-node along the channel walls. The standing wave-induced acoustic radiation force moves cells or particles based on their size, density and compressibility in relation to their surrounding medium.[19] Typically, larger and denser particles experience higher acoustic forces and move faster towards the pressure node as compared to smaller and less dense particles. Based on the differences in the acoustophoretic mobility the various particles will end up in different lateral positions (stream lines) at the end of the microchannel and can there be collected into different outlets.

At higher throughput, the retention time for each particle in the sound field is reduced and thus the acoustic force has shorter time to act on the particle. To compensate for this, an increased channel length or higher actuation voltage can be employed. However, at higher voltages power dissipation in the electro-mechanical conversion in the transducer may result in elevated temperatures that require temperature control of the system.

In this paper, we describe multiplex separation in a multi-outlet acoustofluidic microchannel integrated with an acoustic pre-alignment channel. To allow operation of the piezoceramic actuator at elevated voltages a new air-cooling unit has been realized which alleviates thermal limitations in the system and thus enables a significantly increased sample throughput at unperturbed precision. In this study, we demonstrate high throughput multiplex acoustophoresis for particle mixtures as well as viable WBC.

Materials and methods

Acoustophoretic setup

The microfluidic structure was fabricated using deep reactive ion etching (Micronit, Enschede, Netherlands) and comprised a sample inlet, a pre-focusing channel (22 mm × 300 μm × 150 μm), a v-shaped flow splitter preceding the center buffer inlet and a main separation zone (30 mm × 375 μm × 150 μm) leading towards three outlets at the end of the channel (Fig. 1). The chip was sealed by anodic bonding of a glass lid and silicon tubings were glued to each inlet and outlet at the bottom of the microchannel as docking ports for the fluidic tubings. A pressure driven unit (VEMA-LS-8N3-9-D1-M5-22D9, Festo AB, Sweden) with flow sensor (SLI-1000 and SLI-2000 liquid flow meters, Sensirion AG, Switzerland) based

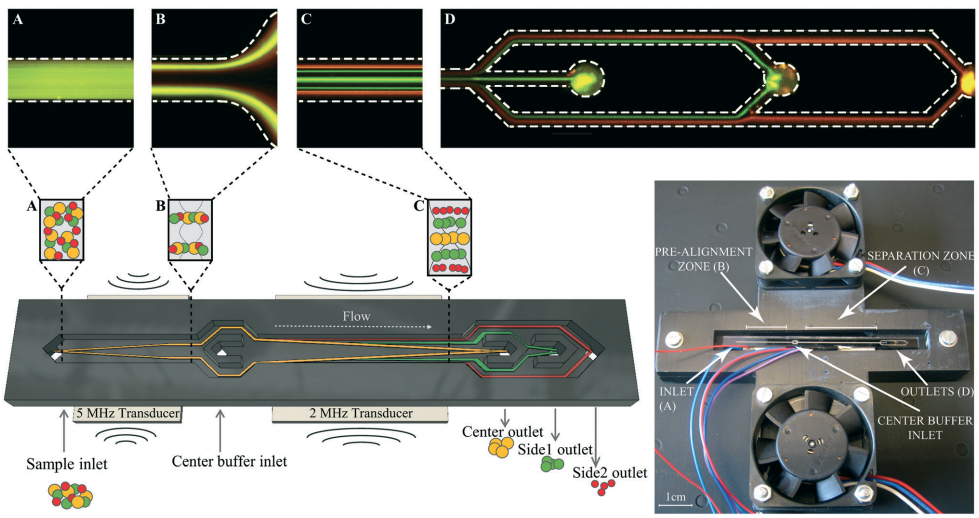

Fig. 1 Microfluidic chip and holder design. The schematic drawing shows the principle of multiplex acoustophoresis with acoustic pre-focusing as implemented in this study. A sample is injected into the microchannel (A) and the particle/cells are pre-aligned in width and height (B) before entering the main separation channel. Acoustic forces within the half-standing wave field in the separation channel will move the particles towards the pressure node in the center of the channel based on their acoustophysical properties (C and D). Larger and denser particles move faster in the sound field and can be collected into the center outlet (yellow) while medium sized particles move to side1 outlet (green) and the smallest particles are collected in side2 outlet (red). Fluorescence images (inserts in the top of the figure) were taken at different positions within the microchannel while acoustically separating 2 μm (red fluorescence), 4 μm (green fluorescence) and 6 μm (green fluorescence) beads, respectively, to support the schematic drawing. The picture on the lower right side shows the top view of the microfluidic chip holder with the positions of the inlets (A) and outlets (D) as well as the pre-alignment zone (B), the main separation zone (C), and the air-cooling fans.

feedback loop control (in-house build) was used to control the flow rates of the system. The flow rates at the different inlets and outlets for bead separation were set to 100 μL min^{-1} sample in, 300 μL min^{-1} center buffer in, 150 μL min^{-1} center out, 85 μL min^{-1} side1 out and 165 μL min^{-1} side2 out. Bead experiments at increased sample throughput were run by keeping the same split ratios at the inlets and outlets. Cell experiments were performed at 100 μL min^{-1} sample in, 300 μL min^{-1} center buffer in, 150 μL min^{-1} center out, 30 μL min^{-1} side1 out, and 220 μL min^{-1} side2 out. The acoustophoretic standing wave field was generated using piezoceramic transducers glued underneath the pre-focusing channel (resonant at 5 MHz) and main separation channel (resonant at 2 MHz). Both transducers were driven by a dual channel function generator (AFG3022B, Tektronix, Beaverton, OR, USA), connected to signal amplifiers (in-house build), and a two-channel digital oscilloscope (TDS 1002, Tektronix) was used to measure the voltage over each transducer. Temperature was monitored *via* PT1000 resistance temperature detectors attached to the side of the chip above the pre-alignment and main separation transducer. For visual inspection of the microchip and for taking fluorescence images a SZX10 stereo microscope equipped with a GFP filter, a XC10 camera (all Olympus, Tokyo, Japan), and a X-Cite 120Q excitation light source (Lumen Dynamics, Excelitas Technologies, Waltham, MA, USA) was used.

Holder design

The chip holder was designed in a 3D-CAD software (Autodesk Fusion 360) and 3D-printed (Ultimaker2, Ultimaker, Netherlands) in two pieces; the bottom piece contained air flow channels, the top piece had two open air conduits where two axial fans (Papst 412F2H, Elfa Distrelec, Sweden) were mounted, see supporting Fig. S1A.† The acoustofluidic chip was placed in the center slit of the chip holder. Besides four supportive regions where the tubings exit the chip, the chip is free hanging with open air vents above and below the chip. The fans push air through the manifold that exits through the top and bottom center slits where the chip is placed, see supporting Fig. S1B.†

Beads

Polystyrene beads in sizes 3, 5 and 7 μm (Sigma-Aldrich, St. Louis, MO, USA) were mixed equally in MilliQ + 0.01% Triton-X-100 (Sigma-Aldrich) and used as reference validation of the separation performance of the multiplex acoustophoresis chip.

For fluorescence images, Fig. 1, FITC-marked melamine resin micro particles in sizes 4 and 6 μm (Fluka, Sigma-Aldrich) and 2 μm Fluoro-Max red fluorescence polymer microspheres (Thermo Fisher Scientific, Waltham, MA, USA) were used.

Blood sample collection

Sample collection was approved by the Regional Ethical Review Board at Lund University, Sweden. Blood samples were obtained from healthy volunteers after informed consent at Lund University Hospital, Lund, Sweden and collected in vacutainer tubes (BD Bioscience, San Jose, CA, USA), containing ethylenediaminetetraacetic acid (EDTA) as anticoagulant.

White blood cell preparation and flow cytometric analysis

White blood cells (WBC) were obtained by selective lysis of red bloods cells using either BD Pharm Lyse lysing solution (BD Bioscience) for viable, non-fixed WBC samples, or BD FACS lysing solution (BD Bioscience) for fixed WBC preparation according to manufacture instructions. Cells were stained with monoclonal antibodies for 15 min at room temperature in the dark and adjusted to 1×10^6 cells per ml in 1× PBS + 2 mM EDTA + 0.01% BSA (Sigma-Aldrich). The following directly conjugated monoclonal antibodies were used: CD3-APC (clone HIT3a), CD14-PE (clone MφP9), CD19 FITC (clone HIB19), CD45-PerCP (clone 2D1), and CD66b FITC (clone G10F5), as well as matched isotype controls (all from BD Bioscience). Propidium iodide (Sigma-Aldrich) was used as a dead cell marker in viable WBC experiments. Immunofluorescent labeled samples were analyzed before and after acoustic separation on a FACSCanto II flow cytometer (BD Bioscience) and the acquired data were analyzed using FlowJo software (Tree Star Inc., Ashland, OR, USA).

Cell property measurements

Lymphocyte, monocyte and granulocyte populations were separated using acoustophoresis and purities were determined using a flow cytometer (all >90%). The size distribution of each cell fraction was measured with a Multisizer 3 Coulter Counter (Beckman Coulter, Brea, CA, USA), see Fig. S2.†

Statistics

If not otherwise stated, data are presented as mean ± standard deviation (SD) with $n = 3$ biological replicates and three technical repeats each.

Separation performance parameters

Separation performance parameters are reported as separation efficiency linked to the purity of that same collected fraction, where separation efficiency is calculated as the ratio of the number of desired particles per cells in a target outlet to the total number of desired particles per cells found in all outlets. Purity is defined as the ratio of the number of desired particles/cells to the total number of particles in a collected fraction. Furthermore, to also disclose system throughput in an unbiased manner we report the sample input volumetric flow rate and the particle/cell concentration of that same input sample. Mixing ratio of bead suspensions is given and for blood cell samples the initial sample as well as each collected fraction is presented with full FACS data.

Results and discussion

1. Thermal characterization of the cooling unit

Temperature stability is of importance in acoustofluidic systems as temperature drift alters the speed of sound of the

processed liquid, which in turn affects the resonance of the acoustophoresis channel. That is, a change in temperature causes a resonance frequency drift which results in a decrease in acoustic energy in the channel and thus the acoustic force acting on the particles is altered. Augustsson *et al.*[20] observed the shift in the acoustic resonance peak to be ~1 kHz °C^{-1} and a complete change of the resonance mode at temperature changes of 5 °C.

An increase of system temperature may originate from several sources. However, most prominently from losses in the piezo-mechanical coupling, where an increased voltage level will cause mechanical losses in the piezo ceramic that give rise to elevated temperatures. To counteract this temperature drift and maintain a constant level is thus very important.[20] Previously reported ways of cooling the chip have included the use of an aluminum chip holder with a Peltier element in proximity to the chip and a temperature sensor mounted on the piezo ceramic element linked to a feedback-loop control.[21] Although this design provided a successful temperature control, the clamping of the chip to the holder dissipated acoustic energy from the chip and thus the full potential of the acoustic energy input was not utilized. Work by Fong *et al.*[22] also reported the use of a fan located 2 cm from the chip to cool their acoustophoresis chips when driving the piezo actuator in the range of 1.4–1.8 MHz at voltages up to 23 V_{pp} and a 2 °C temperature variation. Without the fan, temperatures up to 70 °C were reported.

To alleviate the shortcomings of 1) a gradually rising temperature of the acoustophoresis system (red trace, Fig. 2A) causing a drift in optimal resonance frequency and 2) the acoustic power dissipation through the peltier/aluminium manifold, we have designed a 3D-printed air cooling manifold where the chip is free-hanging, suspended only in the connecting tubings. Furthermore, since the chip is positioned in an ambient air-flow path, the chip temperature stabilises a few degrees above ambient conditions (purple trace) within ~30 seconds. Two features transport heat from the acoustofluidic chip in operation: a) the liquid flowing through the chip and b) the fan driven convective transport of room tempered air across the chip (Fig. S1B†). Fig. 2A shows the impact of these different cooling aspects. At stop flow and no air cooling (red line), the temperature has not reached steady state even after four minutes of operation. With fluid flow active and no air cooling (blue line) the temperature levels out after 60 seconds at a five degree elevated temperature. Once the air fans are in operation the cooling effect is rapid, reaching steady state after 30 seconds at about two degree elevated chip temperature, and most notable the fluid flow at 800 μl min^{-1} through the chip does not significantly impact the system temperature, c.f. purple line *vs.* green line.

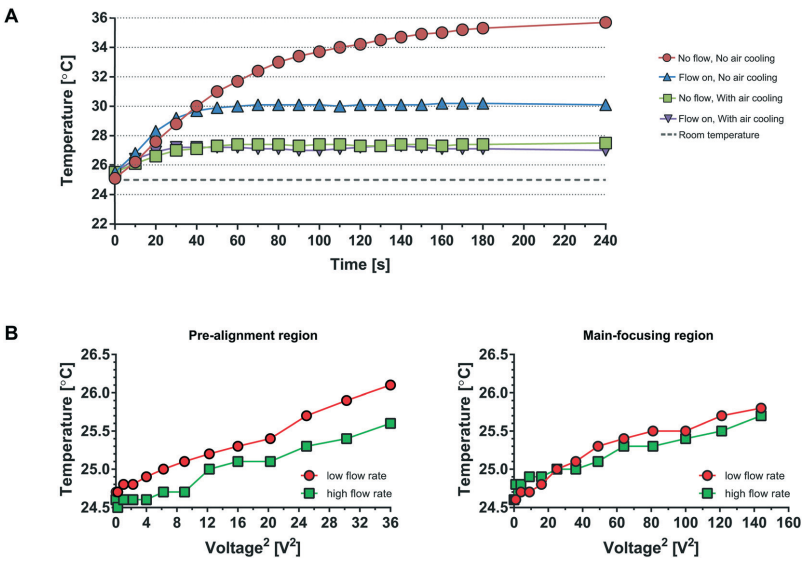

Fig. 2 Thermal characterization – (A) effects of cooling aspects at 800 μL min^{-1} total flow rate. Red: Without any cooling and no flow; blue: with flow and no air cooling; green: with air cooling and no flow; purple: both air cooling and flow. The pre-alignment transducer was driven at 4.3 V_{pp} and the main separation transducer at 4.6 V_{pp}. (B) The effect of an increase of amplitude on the temperature at the pre-focusing transducer (left) and main-focusing transducer (right) was investigated at total flow rates of 400 μL min^{-1} (low flow rate, red) and 2 mL min^{-1} (high flow rate, green) with air cooling turned on. The amplitude range was chosen based on the lowest and highest values used within the bead per cell experiments and temperature was measured 30 s after starting the system (n = 1).

Furthermore, experiments were conducted to analyze the effect on the temperature by applying different voltages at the pre-alignment transducer and main-separation transducer (Fig. 2B). The temperature is plotted against the voltage squared (V^2) as V^2 is proportional to the acoustic energy in the channel. The temperature increases less than 1.5 °C between 0 voltage applied and 6 V_{pp} (Fig. 2B, left) for the pre-alignment transducer and 12 V_{pp} (Fig. 2B, right) for the main-separation transducer, whereas when operating the system without the air cooling active the temperature rises ≈5 °C already at an operating voltage of 4.6 V_{pp} (Fig. 2A blue line). Going from 4.6 V_{pp} to 12 V_{pp} corresponds to a 7× increase in delivered acoustic energy. It should be noted that the higher temperature increase of ≈2 °C in Fig. 2A (purple line) is due to the additional heating of the microscope light source which was not activated in the experiments for Fig. 2B where a maximum of 1.5 °C temperature increase was seen. The free-hanging chip solution combined with the increased length of pre-alignment channel, allowed to operate the device at increased acoustic energy, resulting in a significantly increased sample throughput.

2. Effect of pre-alignment voltage

The simultaneous acoustophoretic fractionation of three different targets has been reported previously by Petersson *et al.*[14] Separation efficiencies of 76–96% were reported with samples containing 3, 7, and 10 μm polystyrene (PS) beads. The modest performance can be explained by the lack of a pre-alignment step which aligns all particles into the same flow vector and minimizes the influence of particles moving at different velocities in the Poiseuille flow. This ensures that the particles have the same retention time in the separation channel. The acoustophoretic pre-alignment, introduced by Augustsson *et al.*,[21] was later utilized by Grenvall *et al.*[15] in order to achieve separation of particles and cells based purely on acoustophysical properties, thereby minimizing influence of Poiseuille flow based dispersion. This resulted in significantly improved separation performance, 88–98%, for 3, 7, and 10 μm beads which also enabled WBC fractionation at recoveries of 86.5%, 83.1% and 68.4% for lymphocytes, monocytes and granulocytes, respectively.[15] This acoustic device was short with a pre-alignment length of only 10 mm and separation length of 22 mm. This translated to short retention times in the sound field, which required the use of very low flow rates (8 μL min^{-1}) to achieve a reasonable separation performance.

The design reported herein includes a pre-alignment channel of 22 mm length, a factor of 2.2 longer as compared to the original report on pre-alignment by Augustsson *et al.*[21] and later by Grenvall *et al.*[15] The longer pre-alignment channel enables a proportionally higher flow rate at unchanged pre-alignment performance. To show the influence and importance of the pre-alignment for multiplex acoustophoresis, an experiment was conducted in which the pre-alignment voltage initially was set to zero (pre-alignment off) and then gradually increased up to 18 Volts squared, see Fig. 3. At 0 Volts, *i.e.* no pre-alignment, a large fraction of 7 μm particles (yellow) ended up in side outlet 1 instead of the center outlet and 5 μm particles (green) were collected in side outlet 2 instead of side outlet 1. As the pre-alignment voltage increases and all particles end up in the same flow vector before the separation channel, the separation of the three particle sizes was greatly improved, now only depending on the acoustophysical properties of the particles.

3. Bead separation efficiency *versus* flow rate

Previous publications on acoustic multiplex particle separation reported maximum sample flow rates of 10 μL min^{-1} [15] and 40 μL min^{-1}.[14] To test the performance of the multiplex acoustic chip reported here, an equal mixture of 3, 5 and 7 μm polystyrene beads at a total bead concentration of 10^6 beads

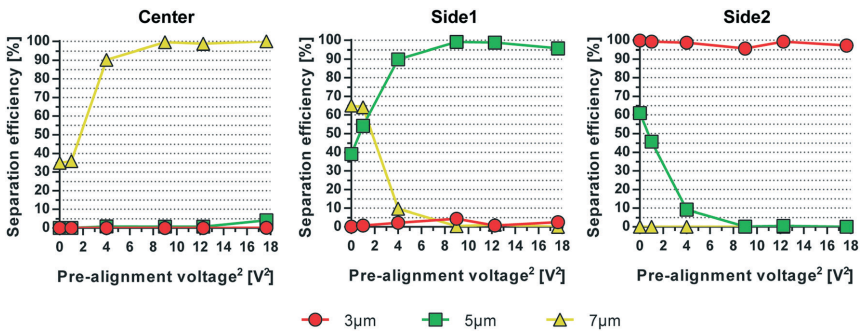

Fig. 3 Separation efficiency *vs.* pre-alignment voltage squared. At zero voltage, *i.e.* pre-alignment turned off, it is clearly visible that the separation efficiency is sub optimal with particle sizes ending up in several outlets. As the pre-alignment voltage is increased, all particles are effectively focused into the same flow vector with the same retention time in the main separation channel and thus the separation efficiency is purely determined by the acoustophysical properties of the particles. Note that the separation voltage controlling the one-dimensional standing wave was maintained constant at 4.5 V_{pp} and only the pre-alignment voltage was varied.

per mL was run through the chip at increasing sample flow rates. The split ratio of the inlets and outlets were fixed while the acoustic energy was increased such that the 7 μm beads exited through the center outlet, while the 5 μm beads were directed towards the side1 outlet and the 3 μm beads stayed along the channel wall and exited through the side2 outlet (Fig. 1). For sample flow rates up to 500 μL min^{-1} the mean separation efficiency, *e.g.* the number of desired beads in the target outlet compared to all three outlets, was >99.2% for 3 μm, >97.5% for 5 μm, and >99.9% for 7 μm, corresponding to mean purities of >98.7%, >99.3%, and >98.2% for 3, 5 and 7 μm, respectively (Fig. 4). At 600 μL min^{-1} a drop of system performance of up to 15% was observed mainly due to a contamination of 5 μm beads into the side2 outlet resulting in mean separation efficiencies (±SD) of 96.7 ± 2.6%, 82.4 ± 2.8% and 98.2 ± 0.1% and purities (±SD) of 83.5 ± 2.2%, 94.9 ± 2.4% and 98.5 ± 0.7% for 3, 5 and 7 μm, respectively. A possible explanation for the decrease in separation performance at higher flow rates is the increased flow instability due to the measuring range and accuracy of the flow sensors (SLI-1000: calibrated for ~80–1000 μl min^{-1} with 6% error, and SLI-2000: calibrated for ~200–5000 μl min^{-1} with 6.5% error) used to monitor the flow rate as well as the response time of the in-house built feed-back loop. Furthermore, at higher flow rates the beads may not have sufficient time in the pre-focusing channel to be pre-aligned in width and height before entering the main separation channel.

Recently, Wu *et al.*[23] combined acoustics and hydrodynamics to pre-align particles prior to multiplex particle separation using surface acoustic waves. Separation data on 10, 12 and 15 μm polystyrene beads showed purities around 90% for the different bead sizes in their target outlets. However, no data on bead concentration, flow rate, sample throughput and separation efficiency/recovery are given for the multiplex separation, which prevents a comparison of system throughput and performance to the system reported herein.

The acoustic radiation force acting on a particle scales with the particle radius to the third power (eqn (S1)†). Considering that previous multiplex acoustophoresis experiments were performed with bead sizes of 3, 7 and 10 μm, the separation shown in this paper with 3, 5 and 7 μm beads is more challenging due to the lower difference in acoustic mobility between the different bead sizes (eqn (S2)†). More precisely, in previous publications[14,15] the acoustic mobility of 3 and 7 μm polystyrene beads differed by a factor of ~5.44 and for 7 and 10 μm beads of ~2.04, while in this work the difference in mobility for 3 and 5 μm beads is only ~2.78, and for 5 and 7 μm beads ~1.96. Furthermore, compared to previous publications[14,15] an up to 60-fold increase in sample flow rate was achieved with comparable or even better separation performance.

4. Bead concentration influences separation efficiency

The initial sample concentration plays a crucial role for the separation outcome. Augustsson *et al.*[24] analyzed the washing efficiency, *i.e.* the transition of beads/cells from one laminated stream to another, for different particle concentrations and showed a constant drop of efficiencies at volume fractions >0.2%. This is in agreement with theoretical calculations from Ley and Bruus[25] which identified the threshold for the wash efficiency in acoustophoretic systems to be at around 1% particle volume fraction. At high particle concentrations the particle suspension starts to move as a whole due to hydrodynamic interactions between the particles. The migration velocity of a given particle towards the pressure node is lowered at higher particle concentrations while particles with lower acoustophoretic mobility are hydrodynamically coupled to faster moving particles. The effect of hydrodynamic interactions becomes even more crucial when trying to separate two different particle per cell types from each other. Magnusson *et al.*[26] reported a drop in performance when separating circulating tumor cells from white blood

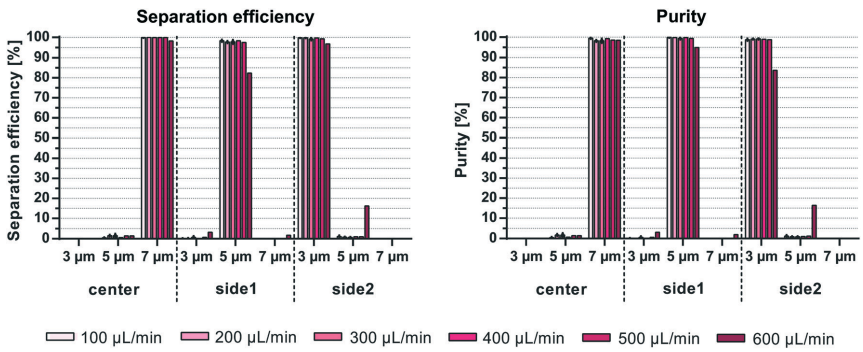

Fig. 4 Particle separation *vs.* flow rate. Acoustophoretic separation of an equal mixture of 3, 5 and 7 μm polystyrene beads at a total concentration of 10^6 beads per mL was performed at different sample flow rates varying the applied voltage squared from 25 to 130 at the main separation transducer. Shown are the separation efficiency, *i.e.* the number of particles collected in one outlet compared to all outlets, and the simultaneous purity of the targeted species at the three different outlets (n = 3, mean ± SD).

cells at an input concentration above 3.25×10^6 cells per mL, which corresponds to a volume fraction of ~0.2%.

Herein, system performance based on the initial sample concentration was investigated at 500 μL min^{-1} sample flow rate. Fig. 5 shows comparable separation efficiencies of >98.6% for 7 μm beads in the center outlet for sample concentrations up to 1.5×10^7 beads per mL (~0.13% volume fraction). However, the efficiency to separate 3 and 5 μm particles in side2 and side1 outlet, respectively, decreased with increasing sample concentrations from 99.3 ± 0.4% and 97.5 ± 0.5% at 1×10^6 beads per mL (~0.009% volume fraction) to 85.4 ± 0.8% and 89.1 ± 3% at 1.5×10^7 beads per mL (3 and 5 μm, respectively). Due to the carry-over of beads into non-target outlets the purity of 7 μm beads decreased from 98.5 ± 0.3% to 93.1 ± 2.2% with increasing sample concentrations, while the purity of 5 μm beads decreased from 99.3 ± 0.4% to 82.2 ± 6.9%. Only the purity of 3 μm beads remained between 99.8 ± 0.1% and 97.4 ± 1% in the side2 outlet. Similar to Magnusson *et al.*[26] the concentration limit for optimal separation is shown here to be below 0.2% volume fraction as compared to the 1% volume fraction in bead washing applications. Both Grenvall *et al.*[15] and Petersson *et al.*[14] used very high bead concentrations corresponding to 1.4 and 3.5–6% volume fraction, respectively, which could be one of the reasons for their lower separation outcome. Comparing the throughput of beads per min, we could reach up to 7.5×10^6 beads per min as compared to 1.5×10^6 beads per min[15] and 6×10^6–6.2×10^7 beads per min[14] with similar or better separation outcome despite working with a more challenging initial sample with small acoustic mobility differences between the beads (3, 5 and 7 μm beads used herein as compared to 3, 7 and 10 μm used previously).

5. Concurrent fractionation of white blood cells

Fractionation of white blood cells into lymphocytes, monocytes and granulocytes is of interest for various clinical and research applications. Acoustophoresis offers the possibility to simultaneously separate different particles and thus possibly also different blood cell types with high efficiencies and purities in limited sample volumes. Furthermore, acoustophoresis has been shown to be a gentle method which does not impact cell viability or functional capacity of the separated sample.[21,23,27–33]

There is a large size overlap between the different white blood cell populations with a median diameter (range) of 7.2 μm (5.5–10 μm) for lymphocytes, 9.5 μm (7.5–12 μm) for monocytes and 9.5 μm (8.5–11 μm) for granulocytes as determined by coulter counter measurements (Fig. S2†). The size differences are also reflected in corresponding scatter differences in fluorescent-activated flow cytometry analysis as shown in the histogram of the forward scatter signal (FSC) in Fig. 6A. The magnitude of the acoustic force acting on a particle is mainly depended on the particle size, which in this case would make it challenging to acoustically sort the three WBC subpopulations. However, also density and compressibility influence the acoustophoretic mobility of a particle. Typically, the density varies between 1.055–1.070 g cm^{-3} for monocytes and lymphocytes and 1.075–1.085 g cm^{-3} for granulocytes.[34] Based on these differences in the acoustic properties granulocytes show a higher acoustophoretic mobility in the acoustic standing wave field as compared to lymphocytes and move therefore faster towards the pressure node in the center of the microchannel where they can be collected in the center outlet. Lymphocytes on the other hand are less affected and stay close to the channel wall being directed to the side2 outlet. Monocytes show a more disperse acoustophoretic mobility and are mainly directed towards the side1 outlet.

Fractionation of viable WBC into lymphocytes, monocytes and granulocytes was shown successfully for different flow rates (Fig. 6B) without impairing the cell viability (98.4 ± 1.9% before and 98.2 ± 2.1% after separation). At 100 μL min^{-1} sample flow and a throughput of 100 000 cells per min 99 ± 0.7% of the granulocytes were translated to the center

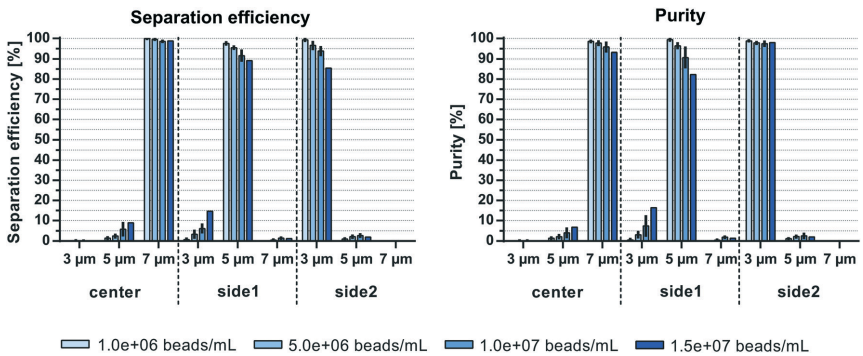

Fig. 5 Particle separation *vs.* sample bead concentration. Acoustophoretic separation of an equal mixture of 3, 5 and 7 μm polystyrene beads was performed at 500 μL min^{-1} sample flow while altering the initial sample concentrations. Shown are the separation efficiency and purity of the different beads in the three outlets (n = 3, mean ± SD).

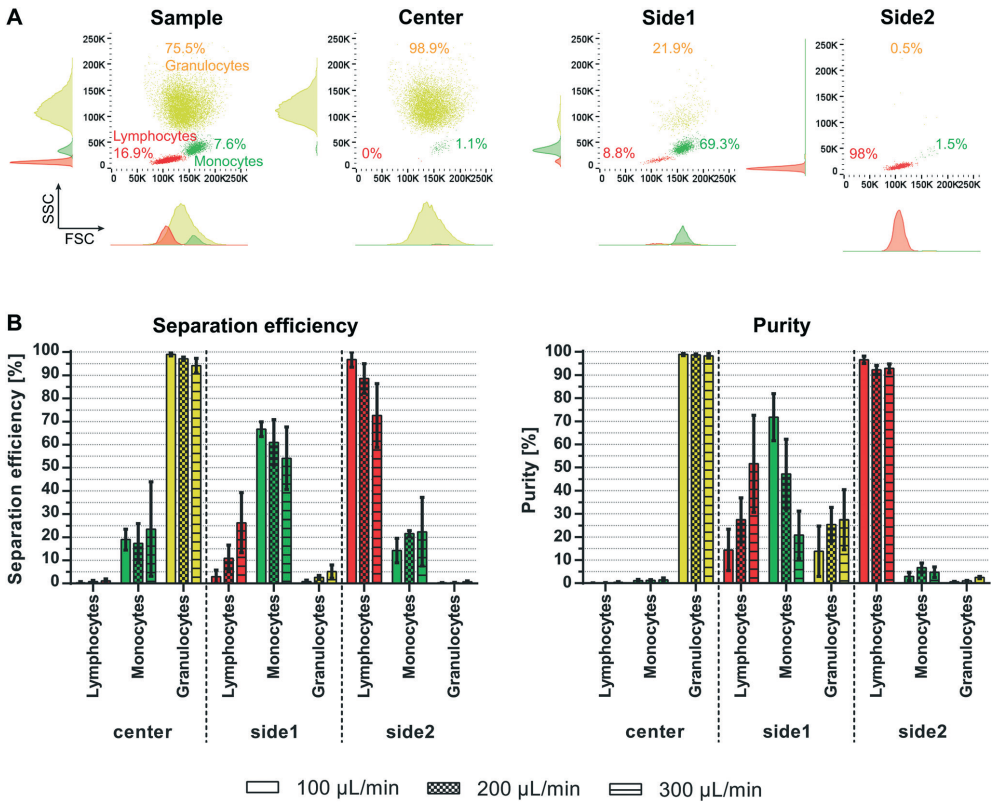

Fig. 6 Fractionation of viable white blood cell subpopulations. Simultaneous acoustophoretic separation of lymphocytes, monocytes and granulocytes from lysed whole blood at a starting concentration of 1×10^6 WBC per mL. (A) FACS plot analysis showing the forward scatter and side scatter plots of the input sample and the three different outlets for a typical run at 100 µL min^{-1} sample flow. (B) Shown are the separation efficiency and purity for varying sample flow rates (n = 3, mean ± SD).

outlet, 66.78 ± 3.2% of monocytes were directed towards the side1 outlet and 96.8 ± 3.3% of lymphocytes towards the side2 outlet. This corresponded to purities of 98.8 ± 0.5%, 71.8 ± 10.1% and 96.6 ± 1.6% for granulocytes, monocytes and lymphocytes, respectively. Increasing the sample flow rate, however, decreased the separation outcome. Especially lymphocytes tended to contaminate the side1 outlet resulting in a significantly lower purity of monocytes of 20.9 ± 10.3% and the larger drop in separation efficiency of lymphocytes to 72.6 ± 13.8% at 300 µL min^{-1} sample flow, maybe due to insufficient time for complete alignment in the pre-focusing channel before entering the main-separation channel. Ramachandraiah *et al.*[10] obtained similar purities of 91% for lymphocytes, 43% of monocytes and 86% of granulocytes using selective red blood cell lysis and inertial microfluidics. However, the reported separation efficiencies in their spiral microchannel indicated a considerable loss of granulocytes and lymphocytes in their system. We do see a shift in the WBC subpopulation ratio before and after the acoustic separation (Fig. S3†). However, this discrepancy is mainly seen at the lower sample flow rate of 100 µL min^{-1} (200 µL sample). Due to the considerably lower flow rate in the side1 outlet, *i.e.* the monocyte outlet, which is 30 µL min^{-1} out of 400 µL min^{-1} total flow and the dead volume in the sample tubing, not all monocytes are recovered into the side1 outlet tube. This effect will be evened out by running larger sample volumes, as seen for sample flow rates of 200 µL min^{-1} (400 µL sample) and 300 µL min^{-1} (600 µL sample), or by flushing the remaining cells in the tubing's after the acoustic run. Compared to previous acoustophoretic multiplex separation of leukocyte subpopulations, a higher separation efficiency for lymphocytes and granulocytes was achieved at high flow rates up to 200 µL min^{-1} (200 000 cells per min) with comparable purities for the two subpopulations as well as higher

purity for monocytes. Even at 300 μL min^{-1} (300 000 cells per min) comparable outcomes were achieved with separation efficiencies of 94.1 ± 3.2%, 54.1 ± 13.5% and 72.6 ± 13.8%, and purities of 98.2 ± 1%, 20.9 ± 10% and 92.8 ± 1.9% for granulocytes, monocytes and lymphocytes, respectively. This corresponds to flow rates that were 37.5 fold faster and a 37.5 fold faster cell throughput per minute than previously reported.[15]

However, it should be noted that Grenvall *et al.* used fixed cells in the experiments (8 μL min^{-1}, 8000 cells per min). This is important, as we can see a shift in the forward scatter and side scatter signal in the flow cytometer indicating a different size distribution as well as granularity distribution between the different subpopulations when comparing fixed and viable WBC (Fig. S4†). Density and speed of sound measurements by Cushing *et al.*[35] furthermore revealed an increase in the compressibility as well as a decrease in the density and the acoustophoretic contrast factor for fixed cells as compared to viable cells. Taken the reduced size distribution and acoustophoretic contrast factor of fixed WBC into account an overall lower acoustophoretic mobility of fixed WBC in the acoustic standing wave field is expected. These results are in agreement with Augustsson *et al.*[21] who reported a difference in separation performance between fixed and unfixed WBC. Lower acoustic energy was needed to move viable cells, which displayed a higher acoustophoretic contrast factor, however a better separation outcome was obtained using fixed cells due to changes in the acoustic properties of the cancer cells after fixation. As a result of the apparently bigger size overlap of fixed white blood cell subpopulations (Fig. S4,† Fig. 7A) and the decrease in the acoustophoretic contrast factor we expected a less promising separation performance in our multi-outlet chip using fixed cells. Separation data confirmed the assumption that we cannot discriminate equally well between the three subpopulations using fixed WBC (Fig. 7B). With a sample throughput of 100 μL min^{-1} (100 000 cells per min) we achieved a separation efficiency of only 76.1 ± 13.3% for granulocytes, 56.4 ± 13.8% for monocytes and 85 ± 3.5% for lymphocytes with purities of 98 ± 0.7%, 12.6 ± 5.3% and 85.6 ± 14.8% for granulocytes, monocytes and lymphocytes, respectively. Especially the monocytes are more disseminated between all three different outlets. The magnitude of the acoustic field needed to be increased in order to optimally pre-focus the cells which is in agreement with the observation of Augustsson *et al.*[21] and the measurements of Cushing *et al.*[35] Possibly, the magnitude of the acoustic force in the pre-alignment channel of the multi-outlet chip was not sufficiently strong to completely focus the cells before entering the main separation channel, which is indicated in the

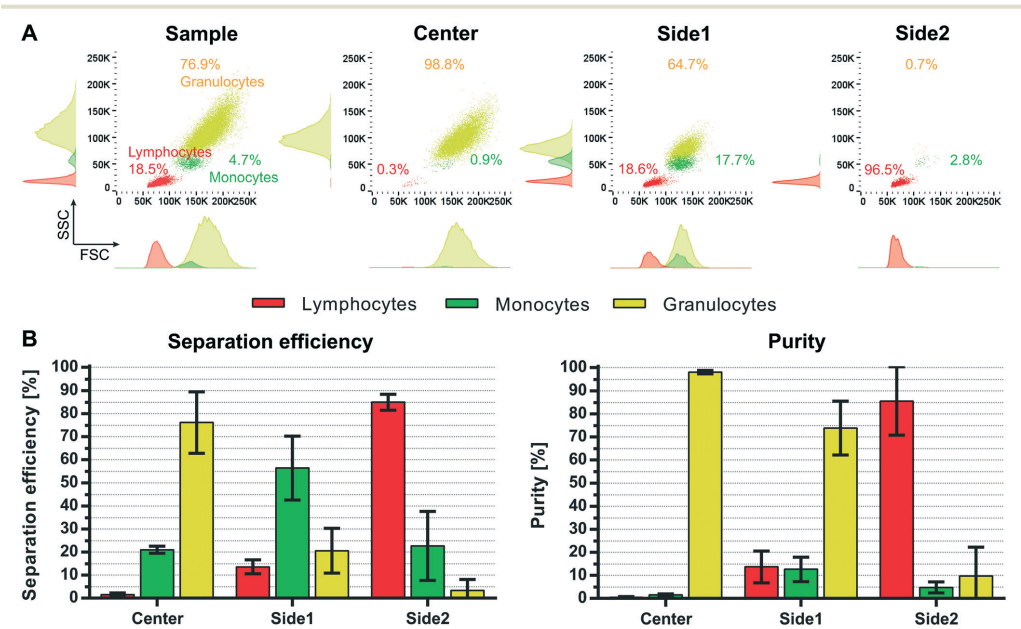

Fig. 7 Fractionation of fixed white blood cells. Acoustophoretic separation of lymphocytes, monocytes and granulocytes from lysed and fixed whole blood at a starting concentration of 1 × 10^6 WBC per mL. (A) FACS plot analysis showing the forward scatter and side scatter plots of the input sample and the three different outlets. (B) Shown are the separation efficiency and purity at 100 μL min^{-1} sample throughput (n = 3, mean ± SD).

increase of lymphocytes in the side1 outlet at elevated flow rates. Optimizing the running parameters such as flow rate, length of the pre-focusing channel and magnitude of the acoustic field may further increase the separation performance using fixed WBC.

Conclusion

We have demonstrated an acoustofluidic device with unsurpassed throughput for concurrent fractionation of WBC subpopulations. Sample flow rates were more than 10 times higher than in previously reported acoustofluidic devices for bead separation and more than 35 times higher for WBC fractionation (>35× higher cell throughput) at significantly better separation efficiency and purity. The novel design of the chip holder provided effective air cooling of the chip with minimal clamping of the acoustic device, which enabled more efficient utilization of the net input acoustic energy.

Author contributions

All authors conceived and discussed the method and experiments. A. U., F. O. and A. L. designed and performed the experiments and analyzed data. A. U. and A. L. wrote the manuscript and all authors edited the manuscript.

Conflicts of interest

There are no conflicts to declare.

Acknowledgements

This work was supported by the People Programme (Marie Curie Actions) of the European Union's Seventh Framework Programme FP7/2007-2013/under REA grant agreement no. 607350; the Knut Alice Wallenberg Foundation (Grant No. KAW 2012.0023); the Swedish Research Council (Grant No. 621-2014-6273); VINNOVA – CellCARE, (Grant No. 2009-00236); the University Hospital of Lund Funds; the ALF grant from the Medical Faculty at Lund University and the Carl Trygger Foundation (13:254). In addition, Scheding is a fellow of the Swedish Cancer Foundation (Cancerfonden).

References

1 B. L. Levine, J. Miskin, K. Wonnacott and C. Keir, *Mol. Ther.–Methods Clin. Dev.*, 2017, **4**, 92–101.
2 T. Felzmann, V. Witt, D. Wimmer, G. Ressmann, D. Wagner, P. Paul, K. Hiittner and G. Fritsch, *Cytotherapy*, 2003, **5**, 391–398.
3 A. A. Marfin and T. H. Price, *J. Intensive Care Med.*, 2015, **30**, 79–88.
4 D. Gurlek Gokcebay and S. Akpinar Tekgunduz, *Transfus. Apher. Sci.*, 2018, **57**, 16–19.
5 L. R. Huang, E. C. Cox, R. H. Austin and J. C. Sturm, *Science*, 2004, **304**, 987–990.
6 D. W. Inglis, J. A. Davis, T. J. Zieziulewicz, D. A. Lawrence, R. H. Austin and J. C. Sturm, *J. Immunol. Methods*, 2008, **329**, 151–156.
7 S. H. Holm, J. P. Beech, M. P. Barrett and J. O. Tegenfeldt, *Lab Chip*, 2011, **11**, 1326–1332.
8 D. Holmes, G. Whyte, J. Bailey, N. Vergara-Irigaray, A. Ekpenyong, J. Guck and T. Duke, *Interface Focus*, 2014, **4**, 20140011.
9 S. S. Kuntaegowdanahalli, A. A. S. Bhagat, G. Kumar and I. Papautsky, *Lab Chip*, 2009, **9**, 2973–2980.
10 H. Ramachandraiah, H. A. Svahn and A. Russom, *RSC Adv.*, 2017, **7**, 29505–29514.
11 K.-H. Han, S.-I. Han and A. B. Frazier, *Lab Chip*, 2009, **9**, 2958.
12 U. Kim, J. Qian, S. A. Kenrick, P. S. Daugherty and H. T. Soh, *Anal. Chem.*, 2008, **80**, 8656–8661.
13 N. Lewpiriyawong and C. Yang, *Electrophoresis*, 2014, **35**, 714–720.
14 F. Petersson, L. Aberg, A.-M. Swärd-Nilsson and T. Laurell, *Anal. Chem.*, 2007, **79**, 5117–5123.
15 C. Grenvall, C. Magnusson, H. Lilja and T. Laurell, *Anal. Chem.*, 2015, **87**, 5596–5604.
16 M. Wu, Y. Ouyang, Z. Wang, R. Zhang, P.-H. Huang, C. Chen, H. Li, P. Li, D. Quinn, M. Dao, S. Suresh, Y. Sadovsky and T. J. Huang, *Proc. Natl. Acad. Sci. U. S. A.*, 2017, **114**, 10584–10589.
17 J. D. Adams, P. Thévoz, H. Bruus and H. T. Soh, *Appl. Phys. Lett.*, 2009, **95**, 254103.
18 E. Ozkumur, A. M. Shah, J. C. Ciciliano, B. L. Emmink, D. T. Miyamoto, E. Brachtel, M. Yu, P. Chen, B. Morgan, J. Trautwein, A. Kimura, S. Sengupta, S. L. Stott, N. M. Karabacak, T. A. Barber, J. R. Walsh, K. Smith, P. S. Spuhler, J. P. Sullivan, R. J. Lee, D. T. Ting, X. Luo, A. T. Shaw, A. Bardia, L. V. Sequist, D. N. Louis, S. Maheswaran, R. Kapur, D. A. Haber and M. Toner, *Sci. Transl. Med.*, 2013, **5**, 179ra47–179ra47.
19 T. Laurell, F. Petersson and A. Nilsson, *Chem. Soc. Rev.*, 2007, **36**, 492–506.
20 P. Augustsson, R. Barnkob, S. T. Wereley, H. Bruus and T. Laurell, *Lab Chip*, 2011, **11**, 4152–4164.
21 P. Augustsson, C. Magnusson, M. Nordin, H. Lilja and T. Laurell, *Anal. Chem.*, 2012, **84**, 7954–7962.
22 E. J. Fong, A. C. Johnston, T. Notton, S.-Y. Jung, K. A. Rose, L. S. Weinberger and M. Shusteff, *Analyst*, 2014, **139**, 1192–1200.
23 M. Wu, K. Chen, S. Yang, Z. Wang, P.-H. Huang, J. Mai, Z.-Y. Li and T. J. Huang, *Lab Chip*, 2018, **18**, 3003–3010.
24 P. Augustsson, J. Persson, S. Ekström, M. Ohlin and T. Laurell, *Lab Chip*, 2009, **9**, 810–818.
25 M. W. H. Ley and H. Bruus, *Lab Chip*, 2016, **16**, 1178–1188.
26 C. Magnusson, P. Augustsson, A. Lenshof, Y. Ceder, T. Laurell and H. Lilja, *Anal. Chem.*, 2017, **89**, 11954–11961.
27 J. Dykes, A. Lenshof, I.-B. Åstrand-Grundström, T. Laurell and S. Scheding, *PLoS One*, 2011, **6**, e23074.

28 M. A. Burguillos, C. Magnusson, M. Nordin, A. Lenshof, P. Augustsson, M. J. Hansson, E. Elmér, H. Lilja, P. Brundin, T. Laurell and T. Deierborg, *PLoS One*, 2013, **8**, e64233.
29 A. Lenshof, A. Jamal, J. Dykes, A. Urbansky, I. Åstrand-Grundström, T. Laurell and S. Scheding, *Cytometry, Part A*, 2014, **85**, 933–941.
30 O. Jakobsson, S. S. Oh, M. Antfolk, M. Eisenstein, T. Laurell and H. T. Soh, *Anal. Chem.*, 2015, **87**, 8497–8502.
31 A. Urbansky, A. Lenshof, J. Dykes, T. Laurell and S. Scheding, *Micromachines*, 2016, **7**, 101.
32 C. Lissandrello, R. Dubay, K. T. Kotz and J. Fiering, *SLAS Technol.*, 2018, **23**, 352–363.
33 M. Wiklund, *Lab Chip*, 2012, **12**, 2018–2028.
34 P. Sethu, A. Sin and M. Toner, *Lab Chip*, 2006, **6**, 83–89.
35 K. W. Cushing, F. Garofalo, C. Magnusson, L. Ekblad, H. Bruus and T. Laurell, *Anal. Chem.*, 2017, **89**, 8917–8923.

Electronic Supplementary Material (ESI) for Lab on a Chip.

Supplementary information

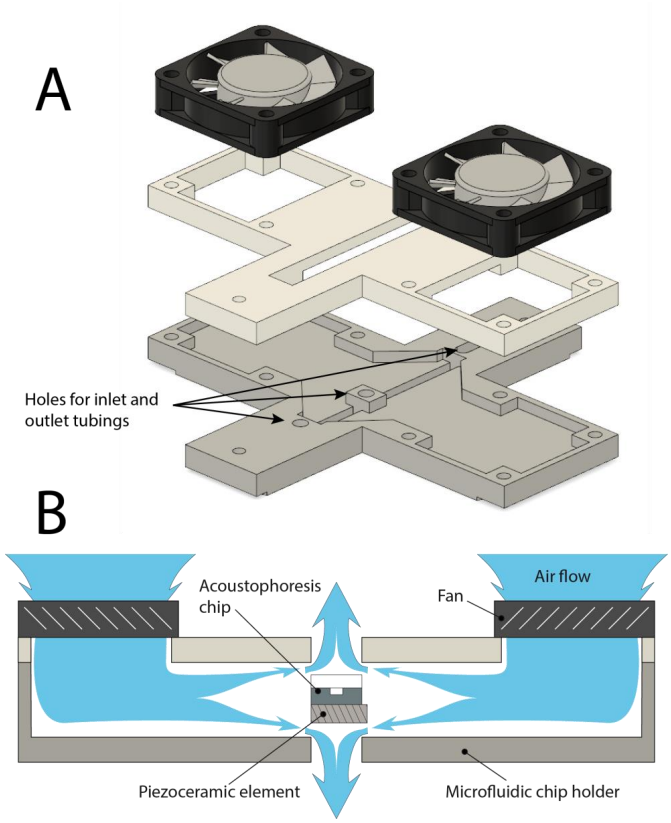

Figure S1. A) Exploded view of the microchip holder with air cooling. Dark grey bottom layer, white top layer and the two axial fans (black). B) Schematic cross section of the air flow inside the air-cooling manifold.

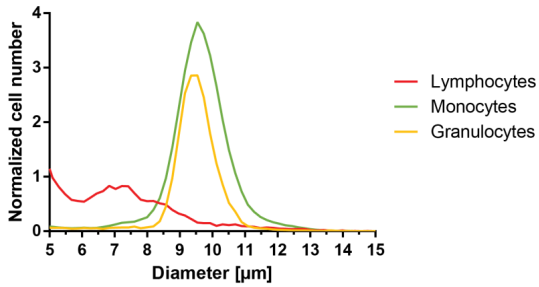

Figure S2. White blood cells were acoustically fractionated into lymphocytes (red), monocytes (green) and granulocytes (yellow) with purities >90% and cell sizes were determined using a Multisizer 3 Coulter Counter. Note, for the lymphocyte population the background of dead cell debris is relatively high leading to an increased signal in the diameter range of 5-6µm.

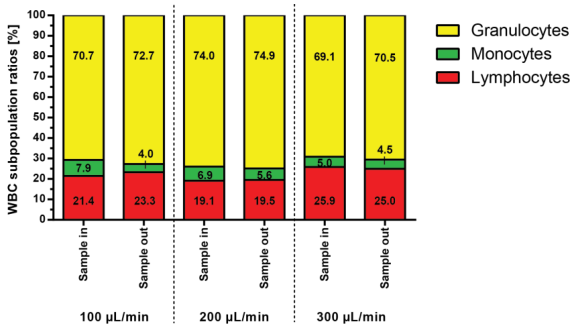

Figure S3. Ratio of WBC subpopulations before and after acoustic separation are shown at different sample flow rates. At low sample flow rate there is a discrepancy in the WBC subpopulation ratio. This is due to the considerably lower flow rate in the side1 outlet, i.e. monocyte outlet, and the dead volume in the sample tubing. By running larger sample volumes or by flushing the tubing's after the acoustic run the remaining cells can be recovered. The effect is less prominent at higher sample flow rates.

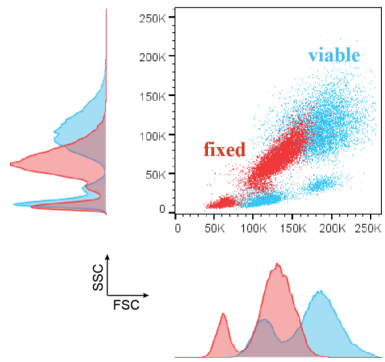

Figure S4. FACS plot with forward scatter (FSC) and side scatter (SSC) signal are shown for fixed (red) and viable (blue) white blood cells indicating a shift in the relative size and granularity of the WBC subpopulations due to fixation of the cells.

$$F_z^{rad} = \frac{4}{3}\pi\phi(\tilde{\kappa},\tilde{\rho})ka^3E_{ac}\sin(2kz)$$

$$E_{ac} = \frac{p_a^2}{4\rho_0 c_0^2};\ \ \phi(\tilde{\kappa},\tilde{\rho}) = \frac{5\tilde{\rho}-2}{2\tilde{\rho}+1} - \tilde{\kappa};\qquad \tilde{\kappa} = \frac{\kappa_p}{\kappa_0};\qquad \tilde{\rho} = \frac{\rho_p}{\rho_0}$$

Supplementary Equation 1. Acoustic radiation force F_z^{rad} acting on a particle with the radius α in an acoustic standing wave field where κ_0, ρ_0, κ_p and ρ_p are the compressibility and density of the fluid and particle, $\phi(\tilde{\kappa},\tilde{\rho})$ is the acoustic contrast factor, k is the wave number ($2\pi/\lambda$), E_{ac} is the acoustic energy density, z is the position of the particle along the wave propagation axis, p_a is the pressure amplitude, c_0 is the speed of sound in the medium[28].

$$Acoustophoretic\ mobility = \frac{a^2\phi}{\eta}$$

Supplementary Equation 2. Acoustophoretic mobility of a particle in an acoustic standing wave field where a is the radius and ϕ the acoustic contrast factor of the partice and η is the viscosity of the medium.